Infrared and Raman studies of thin polymer films

Jonathan Keith Francis Tait

Infrared and Raman Studies of Thin Polymer Films

Jonathan Keith Francis TAIT B.Sc.$_{(Hons)}$, M.Phil.$_{(Brad)}$

(Hatfield College)

Submitted in Partial Fulfilment of the Requirements for the Degree of Doctor of Philosophy, Department of Chemistry, University of Durham.

1994

Abstract.

'Raman and Infrared Studies of Thin Polymer Films.'

Jonathan Keith Francis Tait, B.Sc.$_{(Hons)}$, M.Phil.$_{(Brad)}$

[Keywords:- Waveguide; Raman; Attenuated Total Reflection; Infrared; Polymer Films; Barrier Films; Epoxy; Diffusion; Isocyanate; Crosslinking Agents; Cure Time; Kinetics; Urethane; Film Quality]

This thesis describes the experimental work carried out between October 1st, 1990 and 30th September, 1993, in the Chemistry Department of the University of Durham, in association with Courtaulds Coatings plc, in partial fulfilment of the requirements for the degree of Doctor of Philosophy.

The thesis is divided into three sections, namely Theoretical Considerations (three Chapters), Experimental Results (three Chapters) and Discussion of Results (one Chapter). There are also three appendices.

The theoretical section presents a working description of Paint Chemistry, Vibrational Spectroscopy, Waveguide Raman Spectroscopy, Attenuated Total Reflection Fourier Transform Infrared Spectroscopy and Diffusion Processes.

The experimental section is divided into three chapters. The first describes methods of film preparation and characterisation and includes methods of film thickness determination and the development of an off-line waveguiding rig at the University of Durham. Raman spectroscopic results are detailed in the second chapter, and include waveguide experiments on both single polymer films and laminate systems, some of which are reported for the first time, along with some FT-Raman results, also reported for the first time. The FT-IR ATR spectroscopic results are presented in the third chapter and include some barrier film studies on polymeric laminate systems, plus the study of certain diffusion processes, along with an estimation of the associated diffusion coefficients and some kinetic parameters, occurring in epoxy resins, which are reported for the first time.

The discussion section concentrates on a full elucidation of the results, and conclusions that may be drawn from them, and ends with suggestions for future work.

Refractive indices quoted, unless otherwise stated, refer to indices measured using 632.8 nm radiation, and have been estimated either using previous literature, or with the off-line rig. It is accepted that electric field calculations performed with these values will be slightly different to the actual fields observed in the Raman experiments, due to slightly different refractive indices at 514.5 nm. 'I' in tables, unless otherwise stated, refers to band intensities in absorbance units.

Finally, the attention of the reader is drawn to the fact that some of the materials used in the course of this project have no precise structure given. This is due to the fact that some of the substances used are of either a highly complicated and/or confidential nature.

Acknowledgements

I wish to express my sincere gratitude to Dr. Jack Yarwood for his invaluable advice, inexhaustible encouragement and first-class supervision during the course of this Ph.D. programme. His concern and general interest in this project has kept me, more or less, on the straight and narrow, through both the good and the not so good times.

Grateful thanks are also due to Courtaulds Coatings plc for financial support, and especially to Dr. Gerald Davies and Dr. Bob McIntyre for direction, supervision and provision of experimental facilities for much of the infrared work carried out. I also wish to record my sincere appreciation to numerous employees of Courtaulds Coatings, especially to Dr. Brian Johnson and Mrs. Elaine McCloud, of the Surface Spectroscopy Unit, for allowing me the use of their resources, for allocating me valuable instrument time and for their advice and help given in various aspects associated with this project.

Sincere thanks must also be expressed to Terry Harrison, for technical assistance in all aspects of my work; to Simon Nunn, for the development of the Macro packages for the spectrometer in Durham; to Dr. Neil Everall for his kind assistance in the set-up of the off-line waveguiding rig; to Dr. Ken Durose, for his advice on the use of the alpha-stepper; to Marcia Pierra, for her kind assistance regarding her diffusion calculation software; to Dr. Howell Edwards and Dennis Farwell, at Bradford University, for their help in using the FT-Raman spectrometer; to David Ruckwood, for proof-reading, and to all the technical and support staff in the Department of Chemistry at Durham, for their excellent work over the past three years.

Finally, I must thank my parents, for their love and support, which has been expressed in many ways throughout my time at Durham. I would also like to record my appreciation to my many friends in Durham, especially to Hatfield MCR, John's SCR, DULOG and DUSCR, for many laughs, pints and good times to treasure.

Original Objectives.

This project was originally set-up to utilise waveguide Raman and attenuated total reflection infrared spectroscopies to examine the liquid/solid interface between an anti-foul marine paint and sea water, with a view to enhance understanding of the protein absorption mechanism which can occur at this interface. Following such a study, it was further proposed to examine the effect of different paint additives on this absorption process, with a view to enhancing both paint effectiveness and environmental impact.

About a year into the project, a change in direction was implemented, due to changes at Courtaulds Coatings plc brought on by the physical failure of specific coatings in certain climatic conditions. Hence, it was decided to utilise the same two spectroscopic techniques to study inter-layer adhesion in such systems, with the obvious goal of improved adhesion in mind.

The work described in this thesis was carried out at The University of Durham and Courtaulds Coatings plc. between 1st October 1990 and 30th September 1993, and except where indicated is, to the best of my knowledge, believed to be the original work of the author.

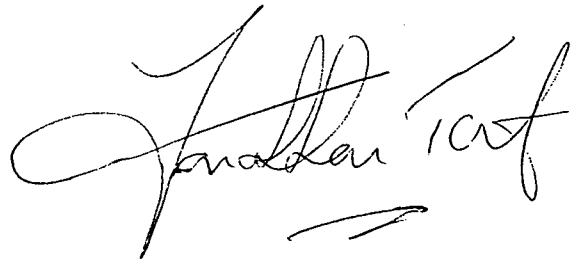

J.K.F.Tait - September 1994

List of Contents.

Chapter One - Paint Chemistry

Chapter One - Paint Chemistry

1.1 - Introduction to Paint Chemistry[1]

A paint may be described as a liquid material capable of being applied or spread over a solid surface, on which it subsequently dries, or hardens, to form a continuous, adherent, obliterating film. The performance limitations of the paints produced were basically attributable to the available raw materials, which were of a predominantly natural origin, e.g. oxides of iron for pigments and various blends of vegetable oils and natural resins for binders. Although these traditional coatings adequately fulfilled the demands of the time, more recently, the demand for long life, high-performance systems have brought about significant advances in paint technology. These progressions have involved the introduction and development of synthetic raw materials and intermediates, which have alleviated the traditional restrictions imposed on the paint chemist, as well as establishing a much more scientifically based industry, which can now supply reproducible products with an accurately predicted performance.

The modern surface coating industry now provides many different generic types of coatings, which can be utilised in a wide range of environments, and applied by numerous different methods; these range from conventional liquid paints, applied by brush and drying at ambient temperatures via oxidation, to powder coatings applied by means of an electrostatic spray, and cured ('set') by heating.

A 'paint' has basically three components, namely:-

1). A *'Binder'* (other terms include resin, film former and polymer). The binders are the film-forming components of the paint, and predominantly determine the principal physical and chemical characteristics, and the paint is generally named after their binder constituent, e.g. epoxy paints and alkyd paints etc. The major function of the binder is to give a permanent, continuous film, which is responsible for adhesion to the coated surface, and also contributes to the overall resistance of the system to the environment. Binders used in the manufacture of paints fall into two classes, namely convertible and non-convertible. This classification depends solely upon how they form a film. A convertible coating, when dry, will be chemically different from the paint in the can, whereas with a non-convertible coating, the dry film and wet paint differ only in the solvent content, and chemically remains essentially the same. In the course of this project, only convertible coatings have been used, which undergo a curing reaction on application.

2). A *'Pigment' and 'Extender'*. These are used in paints in the form of fine powders, and are dispersed into the binder to particle sizes of about 5-10 microns, for finishing paints and approximately 50 microns for primers (so-called undercoats). These materials are divided into the four following types:-

a). Anticorrosive pigments: Prevent the corrosion of metals by chemical and electrochemical means, e.g. red lead and zinc chromate.

b). Barrier pigments: Increase the impermeability of the paint film e.g. aluminium and micaceous iron oxide (M.I.O.).

c). Colouring pigments: Give permanent colour to the film and can be of organic or inorganic origin.

d). Extending pigments: These are more commonly referred to as 'extenders', and they adjust (or 'extend') the pigmentation of the paint until the required pigment volume concentration is achieved. They are all inorganic powders, with various particle sizes and shapes, and, although making little or no contribution to the colour or opacity of the paint, they do have a significant influence on the physical properties, including flow, degree of gloss, antisettling properties, sprayability, water and chemical resistance and mechanical strength. Common examples of extenders are china clay, barium sulphate and mica.

3). The *'solvent'*. These are used in paint systems principally to facilitate application, and dissolve the binder and consequently reduce the viscosity of the paint to a level which is suitable for the various methods of application, i.e. brush, roller etc. After application, the solvent evaporates and plays no further role in the final paint film, and is therefore a high-cost waste material. Liquids used for solvation purposes can be described in one of three ways:-

a). True solvent: A liquid which completely dissolves the binder and is completely compatible with it.

b). Latent solvent: A liquid which is not a true solvent, but when mixed with a true solvent has stronger dissolution properties than the true solvent alone.

c). Diluent solvent: Also a liquid which is not a true solvent, and is normally used as a blend with true solvent/latent solvent mixes to reduce costs. Binders, however, will only tolerate limited quantities of diluents.

There are numerous different solvents used in the paint industry, due to the number of different properties which have to be taken into account when selecting a solvent or solvent blend, in addition to commercial factors.

Other Additives. Modern paints along with the principal ingredients, i.e. those discussed above, require various other additives which aid manufacture, shelf life, application, film formation, curing and properties of the paint. Typical groups of paint additives are:-

a). Aids to Manufacture: e.g. dispersion agents and defoamers

b). Aids to Shelf Life: e.g. stabilisers, antisettling agents, anti-skinning agents (i.e. antioxidants), preservatives, thickening agents and moisture absorbers.

c). Aids to Application: e.g. flow-promoting agents, solvent retarders, conductivity controllers and antistatic agents.

d). Aids to Film Formation: e.g. antifloating agents, pattern additives and matting agents.

e). Aids to Film Curing: e.g. dryers and curing agents/catalysts.

f). Others: e.g. deodorants, flash-point controllers, heat stabilisers, fire retarders, optical brighteners, slip and antislip agents, antifouling agents, fungicides, bactericides, insecticides, UV absorbers, antiscuff agents and corrosion inhibitors.

1.2 Epoxy Coatings

1.2.1 - Chemical Considerations[2].

Epoxy resins are usually prepared from epichlorohydrin and a dihydroxy compound, usually a diphenol, and in particular bisphenol-A. Two successive reactions of the phenolic hydroxyl bring about the polymerisation:-

1). Condensation with chlorine to eliminate HCl:-

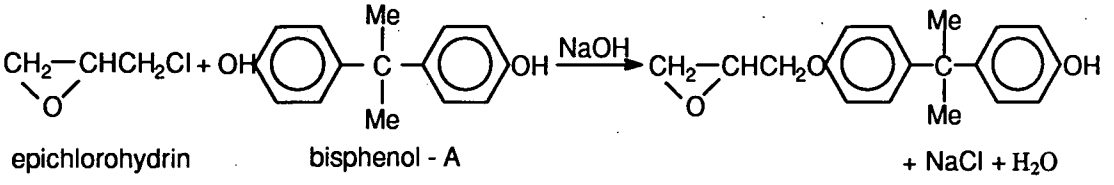

Reaction 1

2). Addition to epoxide group, opening the ring. It should be noted that this reaction produces one hydroxyl group per monomer unit added.

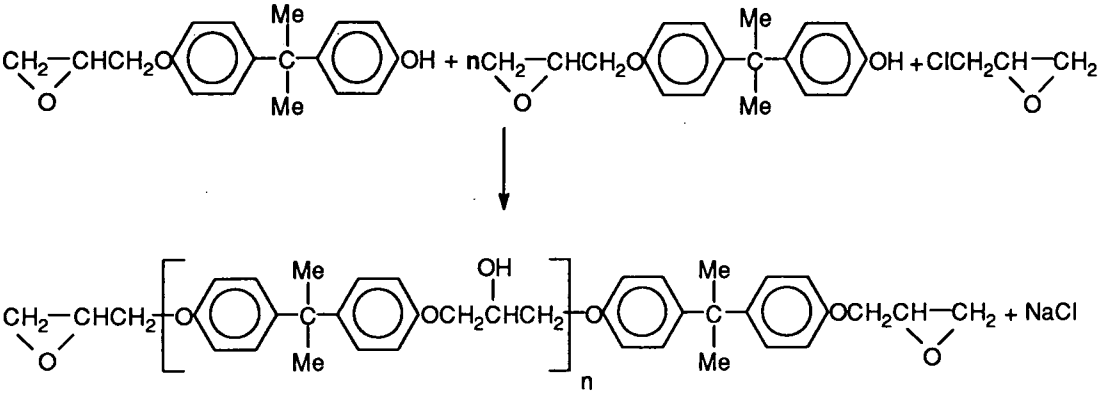

Reaction 2

Thus this type of epoxy resin contains the maximum number of two epoxide rings at the ends of the molecule and a number (which may be zero) of hydroxyl groups along the chain. These groups make the resin a polar one and ensure good adhesion to polar or metallic surfaces. The polymer chain also contains the chemically stable carbon-carbon and ether linkages, which bestow great chemical resistance to epoxy resins. Epoxy resins (above a critical molecular weight of 700, below which they are viscous liquids) are relatively brittle materials, and only form useful films when crosslinked

with other molecules, through the reactive epoxide rings and hydroxyl groups. These crosslinking sites are well separated by 3 carbon atoms, 2 oxygen atoms and 2 benzene rings, and the fact that the crosslinks cannot be closely spaced gives rise to the flexibility of the crosslinked films. However, aromatic epoxy resins absorb U.V. radiation, leading to degradation and chalking (becomes brittle), if used in topcoats out of doors.

1.2.2 Amine Crosslinking of Epoxy Resins[2,3].

There are many different ways by which epoxy resins may be crosslinked, or 'cured', and much of the current literature regarding epoxy resins has concentrated on areas closely associated with such curing processes, including curing kinetics[4,5,6,7,8], development of new curing agents[9,10,11], curing mechanism[12,13,14,15,16,17,18,19], and structure/mechanical behaviour of the final crosslinked species[20,21,22,23,24,25]. In this project, however, we are concerned only with amine crosslinking of epoxy resins, the chemistry of which is described here in detail.

The addition reaction between the epoxide ring and primary and secondary amino groups provides a means of curing the resins at room temperature. There is a wide variety of amine 'curing agents', which vary from simple amines to amine epoxy adducts, modified amines and polyamides. It is one of the objectives of the paint chemist to select or tailor-make the correct curing agent for the required end use of the composition. Simple polyamines such as ethylene diamine (functionality = 4) and diethylene triamine (functionality = 5) used, are supplied in the form of an activator solution, and are added to the resin before use. Such paints, however, are subject to surface exhudation (the so-called 'amine bloom', formed when unreacted amine leaches out of the film, and reacts with carbon dioxide and water at the polymer/air interface forming a crystalline solid), which can be avoided in one of two ways. The first is to allow the mixture to stand for 12-16 hours before use, but the alternative, more reliable method is to pre-react some epoxy resin with an excess of amine, producing an amine epoxy adduct, containing unreacted amino hydrogen atoms:-

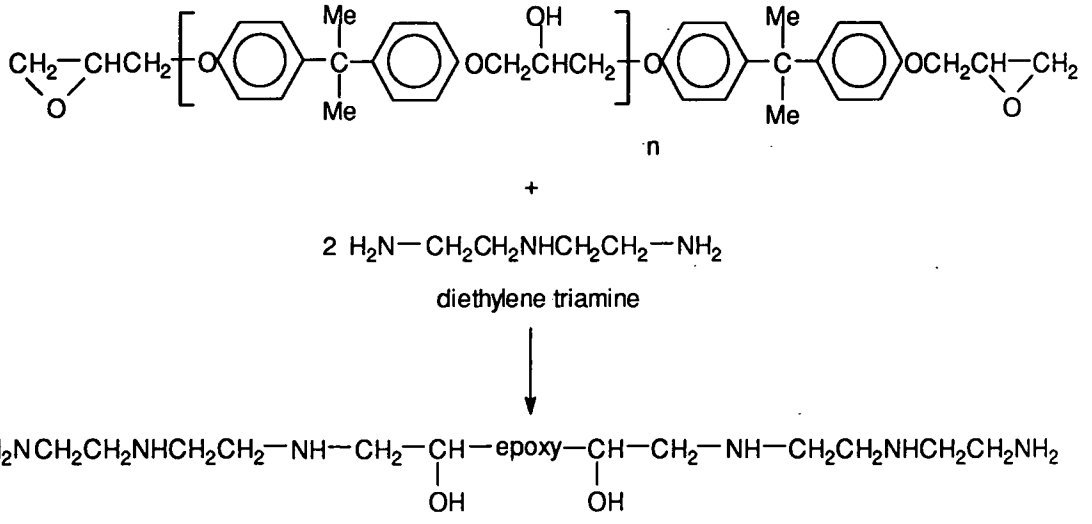

Reaction 3

The terminal amine groups of the adduct are able to react with the epoxide rings of the resin. Only relevant functional groups are shown in the following scheme, to avoid confusion, and the misleading cyclic looking structure is merely a function of this simplification:-

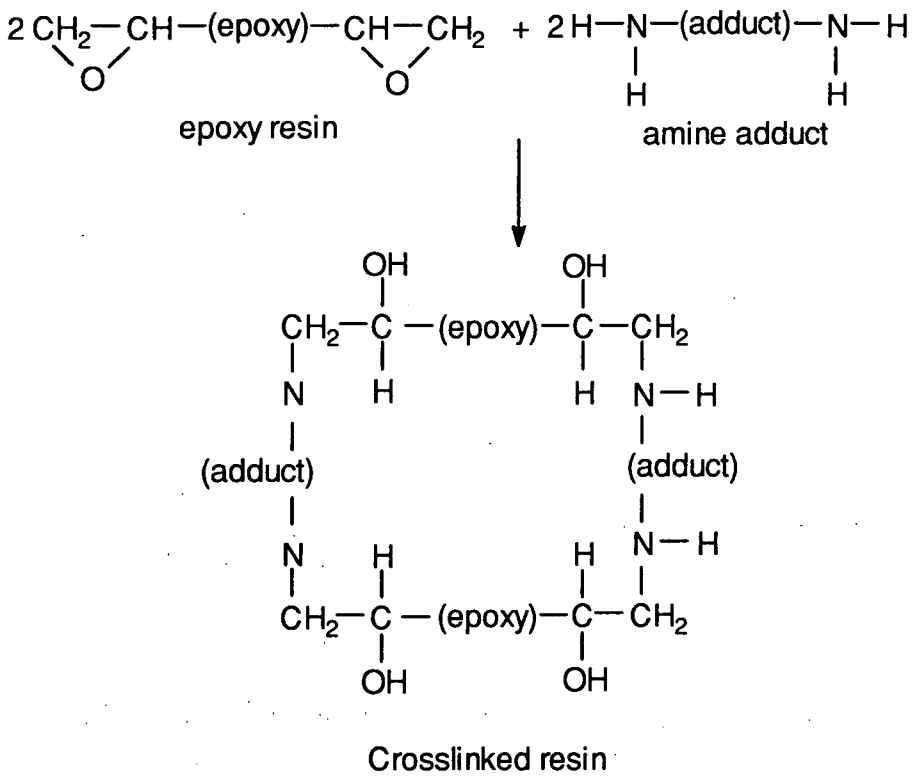

Reaction 4

1.2.3 Epoxy Coatings for Ships[3]

Because there are two types of epoxy resin, i.e. liquid, lower molecular weight and solid, higher molecular weight systems, there are two different types of coating, namely those which are solvent-free, and those which contain a solvent. The liquid resins constitute the solvent-free compositions, and rely on the chemical reaction of the crosslinking process ('curing') to set into hard films, whereas the solid resins are dissolved in a solvent, at which point crosslinking may be induced. This basic difference dictates the use of the different types of epoxies. For example, in cold conditions, i.e. below 10°C, it would be unwise to use an epoxy formulation based on a liquid epoxy, because the wet film could be susceptible to contamination and damage, and even if it eventually set, there is a distinct possibility of separation of components.

Epoxies of either type can be mixed with other resins to change properties to suit the area of the vessel in question. The most common modifier in this respect is coal tar, which is mixed with the epoxy resin to compositions varying in tar to epoxy ratio from 3:1 to about 1:1. There are two major benefits that arise from such addition, namely better water resistance and cheaper product. There are, however, major drawbacks in the loss of chemical resistance, in particular loss of solvent resistance, and of course

when refined cargoes are to be carried, they cannot be used as tank coatings, due to contamination. The other major constituent of epoxy resins is the crosslinking agent, detailed above.

Epoxy Resins therefore have a wide applicability, and some of their marine based uses are summarised below:-

Tanks.
a). Refined Cargo Tanks.

Solid, pure epoxy resins are used, which have been amine-cured for highest chemical resistance. Such coating systems generally consist of three coats, and have a dry film thickness of the order of 225-250μm.

b). Crude Oil and Ballast Tanks.

Coal tar epoxies are usually used, rather than pure epoxies, due to the increased water resistance and greater economy. The minimum dry film thickness here is 250μm. If the ventilation of such tanks is good, then solvent-containing formulations are used, but where ventilation is restricted, solvent-free systems must be used.

Underwater Area.

The demand here is for good water resistance and good abrasion resistance, and coal tar epoxies are outstanding in both respects. A dry film thickness of approximately 250μm is used. The main complication that arises, which is not present in tanks, is that an antifouling layer must be used over the coal tar epoxy, and it is a difficult technical problem to achieve satisfactory adhesion of the antifouling layer to the epoxy. It is thus necessary to enforce strict time limits on the interval between successive coats.

Boot-top and Topsides Area.

Similar demands regarding water and abrasion resistance apply, as for the underwater area, but additionally, the appearance must be acceptable, cosmetically. Thus, solid pure epoxies are used, and a cosmetic overlayer also added, with a total dry film thickness of about 250μm. One limit of a pure epoxy application in an exposed, above water position, is that over a period of time, of between six months and a year, chalking will inevitably occur, and thus, eventually, the coat will require re-application.

Decks.

The same conditions apply to the main deck as to the topsides, with the addition that the final coat be made non-slip, by incorporation of a suitable aggregate.

Superstructure.

In this area of high exposure, the problem of pure epoxy chalking is a major problem, so generally an epoxy primer is utilised, with a high-performance topcoat, such as a

polyurethane, which is not only long-lasting, but also minimises maintenance by the crew. The one disadvantage, however, is the high cost of such coatings.

Summary

The development of epoxy-based paints has been a significant step forward in the ability to protect vessels against corrosion, but at the same time allowing great adaptability to a particular environment. Such is the number of such climatic conditions that successful utilisation of these, and all other, coatings, depends on constant research and development, so that specific coatings can be formulated for all different environmental and climatic conditions.

1.2.4 Epoxy Resins and Crosslinking Agents Used in this Project.

In the course of the work described in this thesis, several different resins are used, which have different molecular weights. The resins discussed all have the prefix 'Epikote'[26] which is a brand-name referring to resins such as those described in Reactions 1-4 above, and a number, which refers to the degree of polymerisation (or 'n' in Reactions 1-4 above) and hence molecular weight...the higher the number, the greater the degree of polymerisation. The three resins examined in this project were Epikotes[26] 828, 1001 and 1004, which have degrees of polymerisation[27] before crosslinking of approximately 1, 2.64 and 4.67 respectively. For the convenience of the reader, these figures will be quoted whenever important. Epikotes[26] 1001 and 1004 are solids in the pure state, whereas Epikote[26] 828 is a viscous liquid. Epikotes[26] 1001 and 1004 are dissolved up in a number of different solvent systems, but the ones we have been concerned with are a mixture of xylene, n-butanol and 'shellsol' (which is an industrial solvent, consisting of low purity mesitylene) for Epikote[26] 1001, and methylisobutylketone (MIBK) for Epikote[26] 1004. The dissolution of the resins in these solvent systems was always carried out at Courtaulds. Samples were taken from bulk preparations, hence the purity of the solvents used was not ideal. Several attempts were made to prepare resins from high purity solvents, but because of the highly viscous nature of even moderately dilute solutions, and because of the lack of powerful mixing equipment at Durham, we were never able to succeed. This issue, and its consequences, will be discussed further in the experimental section.

Two crosslinking agents were utilised in the course of this project, namely KH0092 (referred to simply as KH92 throughout the rest of this thesis) and Cardanol. Both possessed amine functionality and thus crosslinked the resins in the method described in Reaction 4 above. KH92 is essentially diethylene triamine adducted to epikote 1001, which has a degree of polymerisation (n) of approximately 2.64. Cardanol was an altogether more complicated affair[28], and is essentially a di-Mannich base made from cashew nutshell fluid and ethylene diamine. Upon heating, 40% of the amine is lost and a molecule is formed whose structure is presumed to be that given in Figure 1.1:-

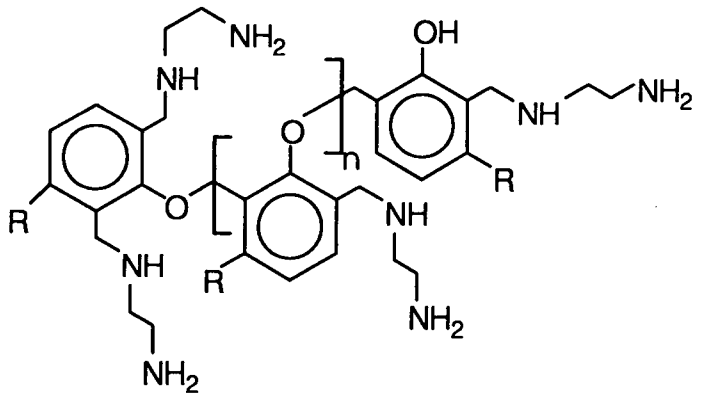

R = pentadec-8-enyl

Figure 1.1 - Cardanol

Thus this molecule is highly functional and reactive, but the long aliphatic side chains probably exercise some steric hindrance, which will restrict the reactivity of the molecule. The value of 'n' is not known to the best of my knowledge.

A fully detailed treatment of the preparation of the crosslinked resins will be given in the experimental section of this thesis.

1.3 Other Chemical Considerations.

Epoxy resins, as detailed above, often form the bottom layer (or layers) of a multilayer system, with an upper layer (or layers) above it. This upper system can be referred as 'finisher' or 'topcoat', the latter being used throughout this report. One of the major thrusts of this project involved the investigation of the interaction of this topcoat with the epoxy underlayer, which, in some cases constituted an actual diffusion of a species from the topcoat into the epoxy resin. Diffusion of species into epoxy resins has been studied before and the relevant literature will be considered later. In the course of this project one particular topcoat, its individual constituents and one associated substance were used. The topcoat was essentially a high performance urethane finish, which would probably be utilised as a Superstructure, Boot-top or Topside coating. The constituents, and the resulting topcoat formulation, are detailed below, but first, three basic chemical reactions need documentation:-

1.3.1 - The Reaction between an Isocyanate and an Alcohol[29].

Isocyanates react with alcohols, to form a urethane, or a carbamate:-

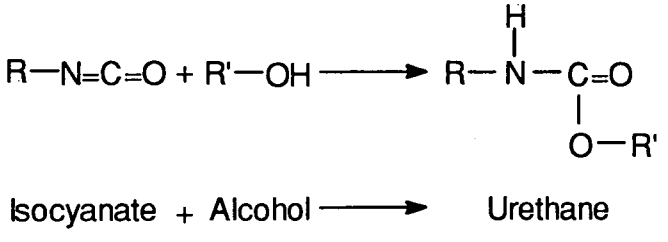

Reaction 5

where R and R' are aliphatic or aromatic species. In the infrared spectrum[30] of a urethane, the carbonyl absorption responsible for the amide I band is seen in the 1730-1720 cm^{-1} range for primary urethanes[33] in dilute solutions in chloroform, but at rather higher frequencies in carbon tetrachloride. A wide range of frequency distribution is observed on passing through secondary to tertiary systems[31-35], with a range from 1705-1739 cm^{-1}, depending on solvent and whether the resulting urethane is aryl or alkyl.

1.3.2 - The Reaction between an Isocyanate and an Amine[46].

Isocyanates and amines react in a similar way to that shown above, between an isocyanate and an alcohol:-

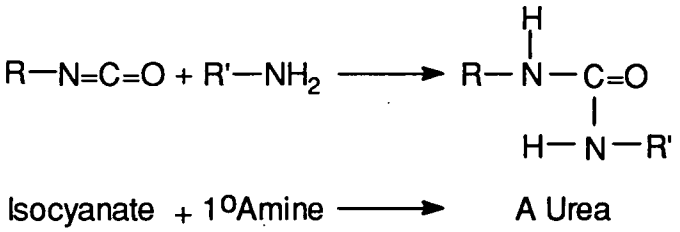

Reaction 6

Again R and R' can be either aliphatic or aromatic. The infrared spectrum[36-45] for ureas has three bands in the 1650-1500 cm^{-1} region for a monoalkyl system, which correspond to the carbonyl (amide I), and NH bending (amide II). The carbonyl frequency is markedly lower than that found in a 'normal' amide, being in the 1605 cm^{-1} region, and the NH amide II band at 1575-1550 cm^{-1}.

1.3.3 - Reaction between Isocyanates and Epoxy resins[47].

Isocyanates react with epoxy resins via the epoxy group to produce an ozalolidone structure, or with a hydroxyl group to yield a urethane linkage. It is actually possible to form a crosslinked system from a di- or polyfunctional isocyanate and a polyepoxide[48].

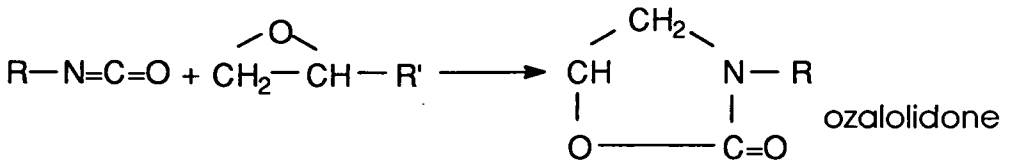

Reaction 7 - Polyepoxide Formation

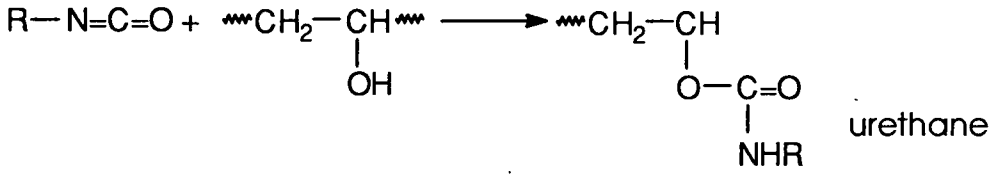

Reaction 8 - Urethane Formation

Reactions 7 and 8

1.4 - Topcoat Formulations.

The topcoat formulation used in this project, as indicated earlier, is a urethane-based finisher, and relies on the type of reaction shown in reaction 5, above. The two major constituents are a trimeric isocyanate, known as CCA315, and an acrylic polymer, the structure of which is not available but will be of a similar form to polymethylmethacrylate, shown in Appendix 3, which contains OH functionality to allow the formation of a urethane. It is worth reiterating, at this juncture, the point made in the abstract section of this thesis, that some of the materials used in the course of this project have structures which are not available, due to interests of confidentiality, or the fact that the precise formulation is simply unknown. The trimeric isocyanate (known as an isocyanurate), however, has a well-documented structure, being commercially available from three major chemical manufacturers. The structure is essentially a cyclic trimer and is based on three hexamethylene diisocyanate (H.M.D.I.) molecules, and has the following structure:-

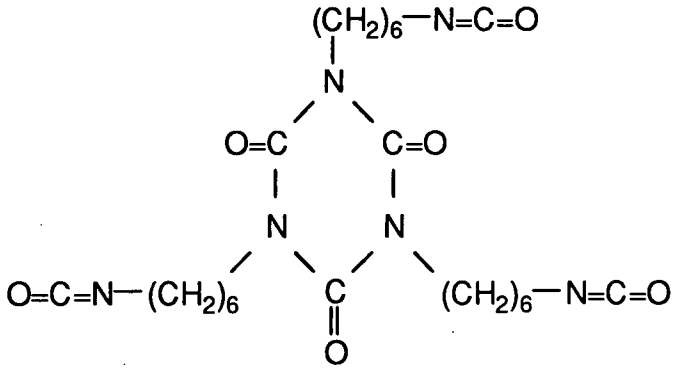

Figure 1.2 - CCA315

The carbonyl groups present in the actual ring, formed from the diisocyanate molecule, are infrared and Raman active, and are reported[48] to have an infrared carbonyl absorption in the range 1700-1680 cm^{-1}, with a weak shoulder at 1715-1710 cm^{-1}, with a separate isocyanate stretch at 2260 cm^{-1}. This trimer may be formed through a principal self addition reaction, which takes the form of :-

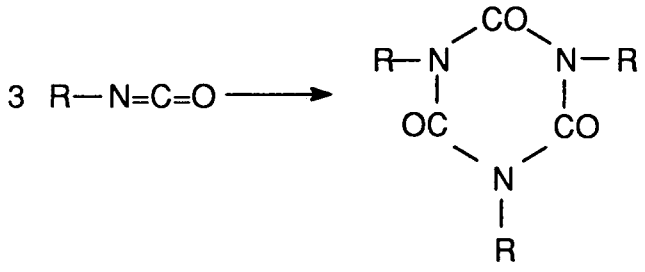

R = $OCN(CH_2)_6$ isocyanurate

Reaction 9

Reaction 9 is, however, hard to control, and thus there is considerable interest in other methods of production. The two methods cited in the literature are high pressure synthesis[49] and the use of catalysts, such as triethylenediamine[50-52].

When this isocyanurate (trimer) is mixed with the hydroxyl functional acrylic, and a small amount of a tin-based catalyst, it quickly reacts, as shown in Reaction 5, to form a solid urethane, which forms the basic component of the finisher.

For reference purposes, the structure of H.M.D.I. is as follows:-

$$O=C=N-(CH_2)_6-N=C=O$$

Figure 1.3 - Hexamethylenediisocyanate (H.M.D.I.)

The isocyanate groups have been found to have an infrared frequency for the stretching mode $\upsilon_{(N=C=O\ antisym.)}$ at 2266 cm^{-1} in the course of our experimentation using horizontal ATR, but are reported[53] in the course of a transmission experiment to have a frequency of 2249 cm^{-1}. The reason for this anomoly is not clear, but as we consistantly found the former frequency in ATR experiments, we will assume it is correct.

H.M.D.I. is a liquid which is a respiratory irritant, as well as having powerful effects on the skin and eyes. It is worth noting here that considerable caution was exercised when handling both isocyanates described in this thesis. Precautions included the use of gloves and safety spectacles, and the materials were handled in a fume hood.

1.5 Summary

In this chapter the important principles involved in paint chemistry have been outlined, with an especial emphasis placed on the systems used in marine paints, and hence in connection with this project. It is worthy of note that the number of different systems used in the modern paint industry is vastly varied and the details presented above represents a mere 'scratch on the surface'.

References

1/. 'General Resume of Paint and Ingredients', International Marine Technical Course, 1991, Section 1.
2/. 'Introduction to Paint Chemistry and Principles of Paint Technology', G.P.A.Turner, Chapman and Hall Publishers, 3rd Edition, 1988, Chapter 14, Pages 183-197.
3/. 'Epoxy Coatings for ships', International Marine Technical Course, 1991, Section 5.
4/. J.H.Wei, M.C.Hawley & M.Demeuse, Abstracts of Papers of the American Chemical Society; 203, Apr, (1992), 243.
5/. W.X.Zukas, N.S.Schreider & W.J.MacKnight, Abstracts of Papers of the American Chemical Society; 186, (1983), 129.
6/. V.Spacek, J.Pouchly & J.Biras, Eur.Polym.J., 23, 5, (1987), 377-382.
7/. V.P.Privalko, V.Y.Kramarento & A.M.Feinleib, Makromolekulare Chemie - Macromolecular Symposia; 44, May, (1991), 247.
8/. C.J.Debakker, N.A.StJohn & G.A.George, Abstracts of Papers of the American Chemical Society, 203, Apr, (1992), 175.
9/. C.C.Riccardi, H.E.Adabbo & R.J.J.Williams, J.Appl.Polym.Sci., 29, 8 (1984),2481.
10/. L.Matejka, S.Podzimek, W.J.Simonsick, P,Spacek & K.Dusek, J.Polym.Sci, PartA-Polymer Chemistry, 30, 10, (1992),2109.
11/. Y.V.Rao, R.A.Tewari & S.Maiti, J.Ind.Chem.Soc., 69, 2, (1992), 90.
12/. K.Dusek, Advances in Chemistry Series, 208, (1984), 3.
13/. E.W.Crandall & W.C.Mih, Abstracts of Papers of the American Chemical Society, 184, Sept, (1982), 141.
14/. K.Dusek, Advances in Polymer Science, 78, (1986), 1-59.
15/. A.Gross, H.Brockmann & H.Koller, Int.J.Adhesion & Adhesives, 7, 1, (1987), 33.
16/. W.X.Zukas, D.A.Dunn & M.D.Gilbert, Abstracts of Papers of the American Chemical Society, 193, (1987), 83.
17/. A.Gross, H.Koller, A.Schormann & H.Brockmann, Int.J.Adhesion & Adhesives, 8, 3, (1988),147.
18/. D.J.Plazek & Z.N.Fund, J.Poly,.Sci, Part B - Polymer Physics, 28, 4, (1990), 431.
19/. S.Matsuoka, X.Quan, H.E.Bair & D.J.Boyle, Macromolecules, 22, 10, (1989), 4093.
20/. A.Fischer, K.Schlothauer, A.Pfitzmann & J.Spevacek, Polymer, 33, 7, (1992), 1370.
21/. R.Lovell & A.H.Windle, Polymer, 32, 12, (1991), 2272.
22/. F.M.Thuillier, H.Jullien & M.F.Grenierlavstalot, Polym.Commun., 27, 7, (1986), 206.
23/. J.L.Han; S.M.Tseng, J.H.Mai & K.H.Hsieh, Angewandte Makromolekulare Chemie, 182, Nov, (1990), 193.
24/. M.Ogata, N.Kinjo, S.Eguchi, T.Kawata & T.Urano, Kobunshi Ronbunshu, 47, 8, (1990), 639.
25/. J.Kaiser, Kuntstoffe-German Plastics, 79, 10, (1989), 1064.
26/. Shell brand-name
27/. V.M.Vakil & G.C.Martin, J.Appl.Pol.Sci, 46, (1992), 2089
28/. Internal Courtaulds Coatings Communication, ARM/01C/31/89/GS/2758, page 2.
29/. 'Organic Chemistry', R.J.Fessenden and J.S.Fessenden, 3rd Edition, Brooks/Cole Publishers, (1986), p. 663.
30/. L.J.Bellamy, "The Infra-red Spectra of Complex Molecules", Volume 1 (3rd Edition), Chapman and Hall, London, (1975), Chapter 12, pp. 248 & 249.
31/. J.Renema, Ph.D. Thesis, University of Utrecht, 1972.
32/. R.A.Nyquist, Spectrochim. Acta., 19, (1963), 509.
33/. S.Pinchas & D.Ben-Ishai, J.Am.Chem.Soc., 79, (1957), 4099.

34/. A.R.Katritzky & R.A.Jones, J.Chem.Soc., (1960), 676.
35/. M.Sato, J.Org.Chem, 26, (1961), 770.
36/. L.J.Bellamy, "The Infra-red Spectra of Complex Molecules", Volume 1 (3rd Edition), Chapman and Hall, London, (1975), Chapter 12, p. 250.
37/. H.M.Randall, R.G.Fowler, N.Fuson & J.R.Dangl, "Infra-red Determination of Organic Structures", Van Nostrand, 1949.
38/. H.W.Thompson, D.L.Nicholson & L.N.Short, Discuss.Faraday Soc., 9, (1950), 222.
39/. H.J.Becher & J.Griffel, Naturweiss, 43, (1956), 467.
40/. H.J.Becher, Chem.Ber., 89, (1956), 1593.
41/. J.L.Boivan & P.A.Boivan, Can.J.Chem., 32, (1954), 561.
42/. P.A.Boivan, W.Bridgeo & J.L.Boivan, Can.J.Chem., 32, (1954), 242.
43/. C.I.Jose, Spectrochim. Acta, 25A, (1969), 111.
44/. Y.Mido, Spectrochim.Acta, 28A, (1972), 1508.
45/. D.F.Kutepov & S.S.Dubov, J.Gen.Chem.(Moscow), 30, 92, (1960), 3448.
46/. 'Organic Chemistry', R.J.Fessenden and J.S.Fessenden, 3rd Edition, Brooks/Cole Publishers, (1986), p.663.
47/. Gerald Davies (Courtaulds Coatings); Private Communication.
48/. Gerald Davies (Courtaulds Coatings); Private Communication.
49/. Y.Taguchi, I.Shibuya, M.Yasumoto, T.Tsuchiya & K.Yoremoto, Bull.Chem.Soc.Jap., 63, 12, (1990), 3486.
50/. J.I.Jones & N.G.Savill, J.Chem.Soc., (1957), 4392.
51/. B.D.Beitchman, Ind.Eng.Chem.Prod.Res.Dev., 5, (1966), 35.
52/. T.Nawata, J.E.Kresta & K.C.Frisch, J.Cell.Plas., (1975), 267.
53/. Aldrich FT-IR Database, 1, (1), 871A.

Chapter Two - Vibrational Spectroscopic Theory

Chapter Two - Vibrational Spectroscopic Theory.

2.1 Introduction

The main tool used in the course of this project to study thin polymer films, interfaces and diffusion processes, is vibrational spectroscopy. In particular Fourier Transform-Infrared Attenuated Total Reflection (FT-IR ATR) and Waveguide Raman (WGR) spectroscopies are the vibrational spectroscopic surface techniques utilised. In this chapter, a general consideration of the basic principles involved with infrared and Raman spectroscopies is presented, followed by a full theoretical description of both of the specific techniques used. Finally, a citation of previous work involving the two techniques and their application to thin polymer films is given.

2.2 - Molecular Vibrations.[1,2]

2.2.1 - The Harmonic Oscillator and Diatomic Molecules.

If we consider the 'ball and spring' model, which approximately describes the vibrations of a diatomic molecule, then for small displacements, the stretching and compression of the 'bond' obeys Hooke's Law:-

$$\text{'Restoring Force'} = -\frac{dV_{(x)}}{dx} = -kx \qquad (1)$$

where V is the potential energy, k is the force constant, whose magnitude reflects the strength of the bond, and x is the displacement from the equilibrium bond length, r_e, ($x = r - r_e$). If we integrate this equation, we get:-

$$V(x) = \tfrac{1}{2} kx^2 \qquad (2)$$

Now, the quantum mechanical Hamiltonian (sum of potential and kinetic energies) for a one-dimensional harmonic oscillator is given by:-

$$H = -\frac{\hbar^2}{2\mu}.\frac{d^2}{dx^2} + \tfrac{1}{2} kx^2 \qquad (3)$$

where μ is the reduced mass of the nuclei, and $\hbar = h/2\pi$, where h is Plank's constant. Thus the Schrödinger equation becomes:-

$$\frac{d^2\Psi_\upsilon}{dx^2} + \frac{2\mu E v}{\hbar^2} - \frac{\mu k x^2}{\hbar^2}.\Psi_\upsilon = 0 \qquad (4)$$

from this expression, it may be deduced that:-

$$E_\upsilon = h\nu\,(\upsilon + \tfrac{1}{2}) \qquad (5)$$

where ν is the *classical vibration frequency*, given by :-

$$\nu = \frac{1}{2\pi}\left(\frac{k}{\mu}\right)^{\frac{1}{2}} \qquad (6)$$

Obviously, ν will increase with k (which can be envisaged as the bond 'stiffness'), and will decrease with μ. It is more usual, however, to use the vibrational wavenumber, $\bar{\nu}$, rather than the frequency, where:-

$$E_\upsilon = hc\bar{\nu}(\upsilon + \tfrac{1}{2}) \qquad (7)$$

where h is Plank's constant, c is the speed of light in a vacuum and the *vibrational* quantum number, υ, can take the values 0, 1, 2... Thus we are able to show that the vibrational levels are evenly spaced by $hc\omega$, and that the $\upsilon = 0$ level has an energy of $\frac{1}{2}hc\bar{\nu}$, known as the zero point energy. This is the minimum energy a molecule may possess, even at absolute zero.

2.3 Infrared Spectra[1,2].

The transition moment for a transition between lower and upper states, with vibrational wavefunctions Ψ''_υ and Ψ'_υ respectively is given by:-

$$R_\upsilon = \int \Psi'^{*}_\upsilon \mu \Psi''_\upsilon . dx \qquad (8)$$

where x is $(r - r_e)$, the displacement of the intermolecular distance from equilibrium. The dipole moment, μ, is zero for a homonuclear diatomic molecule, e.g. N_2 or O_2, which results in $\mathbf{R}_\upsilon = 0$, and all vibrational transitions being forbidden. However, for a heteronuclear diatomic molecule, μ is non-zero and varies with x. This variation may be expressed in a Taylor series expansion:-

$$\mu = \mu_e + \left(\frac{d\mu}{dx}\right)_e x + \frac{1}{2!}\left(\frac{d^2\mu}{dx^2}\right)_e x^2 + \ldots \qquad (9)$$

where subscript 'e' refers to the equilibrium configuration. The transition moment of Equation 8 now becomes:-

$$R_\upsilon = \mu_e \int \Psi'^{*}_\upsilon \Psi''_\upsilon . dx + \left(\frac{d\mu}{dx}\right) \int \Psi'^{*}_\upsilon x \Psi''_\upsilon . dx + \ldots \qquad (10)$$

Since Ψ'_υ and Ψ''_υ are eigenfunctions of the same hamiltonian, namely that in Equation 3, they are orthogonal, which means that, when $\upsilon' \neq \upsilon''$,

$$\int \Psi'^{*}_\upsilon \Psi''_\upsilon . dx = 0 \qquad (11)$$

Equation 10 now becomes:-

$$R_\upsilon = \left(\frac{d\mu}{dx}\right)_e \int \Psi'_\upsilon {}^* \Psi''_\upsilon . dx + \ldots \qquad (12)$$

The first term in this series is non-zero only if:-

$$\Delta\upsilon = \pm 1 \qquad (13)$$

This constitutes the *vibrational selection rule.* Since $\Delta\upsilon$ refers to $\upsilon_{upper} - \upsilon_{lower}$, the selection rule is effectively $\Delta\upsilon = +1$. In the harmonic oscillator, where all level spacings are equal, all transitions obeying this selection rule are coincident at a wavenumber, $\bar{\nu}$.

When the spectrum is observed in absorption, as it usually is, and at normal temperatures, intensities of the transitions decrease rapidly as υ" increases, since the population , $N\upsilon$, of the υth vibrational level is related to N_0 by the Boltzmann factor:-

$$\frac{N_\upsilon}{N_0} = \exp\left(-\frac{E_\upsilon}{kT}\right) \qquad (14)$$

Each vibrational transition observed in the gaseous phase gives rise to a 'band' in the spectrum, with the term 'line' reserved for the fine structure arising from the transition between rotational levels associated with the two vibrational levels. In solid or liquid phase, this fine structure is not present, and 'line' is often and safely used.

Transition intensities are proportional to $|\mathbf{R}_\upsilon|^2$ and therefore, according to equation 12, to $(d\mu/dx)^2_e$. Figure 2.1 shows how the magnitude, μ, of the dipole moment varies with internuclear distance in a typical heteronuclear diatomic molecule.

Obviously, $\mu \rightarrow 0$, when $r \rightarrow 0$, and the nuclei coalesce, and for neutral diatomics, $\mu \rightarrow 0$ when $r \rightarrow \infty$, because the molecule dissociates into neutral atoms. Therefore, between $r = 0$ & ∞, there must be a maximum value of μ. An important general point is that the spectroscopic selection rules merely tell us whether a transition *may* occur, but tell us nothing about the intensities, which may be accidentally zero or very low.

2.4 Raman Scattering[1,2]

Electronic, vibrational and rotational transitions may be involved in Raman scattering, but here, we are only concerned with vibrational transitions. The property of a molecule that determines the degree of scattering is the *polarisability,* α. When the incident radiation is in either the visible or near-ultraviolet region (as it usually is in Raman spectroscopy), the polarisability is a measure of the degree to which the electrons in the molecule can be displaced, relative to the nuclei. In general the polarisability of a molecule is an anisotropic property, which means that, at equal distances from the centre of the molecule, α, may have different magnitudes, when measured in different directions.

A surface drawn so that the distance from the origin to a point on the surface has a length $1/\alpha^{1/2}$ (see Figure 2.2), where α is the polarisability *in that direction,* and forms an ellipsoid.

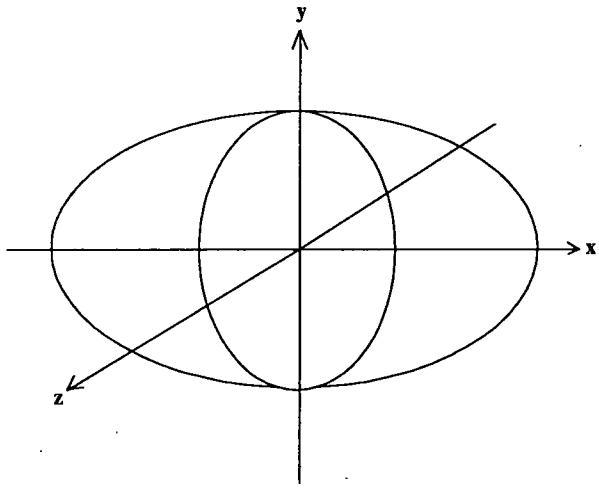

Figure 2.2 - A Polarisability Ellipsoid

Like other anisotropic properties, polarisability is a tensor property, and can be expressed in matrix form:-

$$\alpha = \begin{pmatrix} \alpha_{xx} & \alpha_{xy} & \alpha_{xz} \\ \alpha_{yx} & \alpha_{yy} & \alpha_{yz} \\ \alpha_{zx} & \alpha_{zy} & \alpha_{zz} \end{pmatrix} \qquad (15)$$

where the diagonal elements, α_{xx}, α_{yy} and α_{zz} are the values of α along the principal Cartesian axes of the molecule. As the matrix is essentially symmetrical, there are six different components of α, namely α_{xx}, α_{yy}, α_{zz}, α_{xy}, α_{xz} and α_{yz}. Each of these can be assigned to one of the symmetry species of the point group to which the molecule belongs.

When *monochromatic* radiation falls on a molecular sample in the gas phase, and is not absorbed, the oscillating electric field, E (the electric component of electromagnetic radiation) of the radiation induces in the molecule an electric dipole, μ, which is related to E by the polarisability, such that:-

$$\mu = \alpha . E \qquad (16)$$

where μ and E are vector properties. The magnitude E of the vector may be written:

$$E = A . \sin 2\pi . c \bar{\nu} t \qquad (17)$$

where A is the amplitude, and $\bar{\nu}$ is the wavenumber of the monochromatic radiation. The magnitude of the polarisability varies during vibration, leading to the vibrational Raman effect. This can be envisaged as being due to the polarizability ellipsoid (Figure 2.2) expanding and contracting as the bond length increases and decreases with

vibration. A classical treatment leads to a variation with time of the dipole moment, μ, induced by irradiation of the sample with intense monochromatic radiation of wavenumber, $\bar{\nu}_0$, given by:-

$$\mu = \alpha_{0,\upsilon} A \sin 2\pi c\bar{\nu}_0 t - \tfrac{1}{2}\alpha_{1,\upsilon} A \cos 2\pi c(\bar{\nu}_0 + \bar{\nu}_{vib})t + \tfrac{1}{2}\alpha_{1,\upsilon} A \cos 2\pi c(\bar{\nu}_0 - \bar{\nu}_{vib})t \quad (18)$$

where $\alpha_{0,\upsilon}$ is the average polarisability during the vibration, $\alpha_{1,\upsilon}$ is the amplitude of the change of polarisability due to vibration, A is the amplitude of the oscillating electric field of the incident radiation (Equation 17) and $\bar{\nu}_{(vib)}$ is the vibration wavenumber. The first term in Equation 18 corresponds to Rayleigh scattering of unchanged wavenumber, $\bar{\nu}_0$, and the second and third terms correspond to the anti-Stokes and Stokes Raman scattering, with wavenumbers of $(\bar{\nu}_0+\bar{\nu}_{(vib)})$ and $(\bar{\nu}_0-\bar{\nu}_{(vib)})$ respectively. As shown in Figure 2.3, monochromatic radiation may induce transitions of the molecule from the υ=0 state to a virtual state V. It may then return to υ=0, via a Rayleigh scattering process, or to υ=1 in a Stokes Raman transition. Alternatively, however, it may go from the υ=1 state to the virtual state V, and return to υ=1 (Rayleigh) or to υ=0 (Raman anti-Stokes). However, in many molecules at normal temperature, the initial population of the υ=1 state is so low, that the anti-Stokes scattering is often too weak to observe.

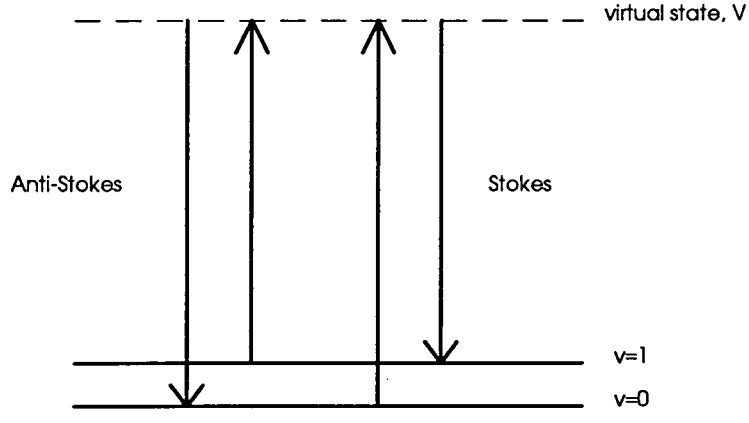

Figure 2.3 - Stokes and anti-Stokes Vibrational Raman Scattering

The dipole moment, change of polarisability with vibrational displacement, x, can be again expressed as a Taylor expansion series:-

$$\alpha = \alpha_e + \left(\frac{d\alpha}{dx}\right)_e x + \frac{1}{2!}\left(\frac{d^2\alpha}{dx^2}\right)_e x^2 \ldots \quad (19)$$

Also, by analogy with Equation 10, the vibrational Raman transition moment $\mathbf{R}_\upsilon$, is given by:-

$$R_\upsilon = \left(\frac{d\alpha}{dx}\right)_e A \int \Psi_\upsilon'^{*} x \Psi_\upsilon'' . dx + \ldots \quad (20)$$

The first term is only non-zero if $\Delta\upsilon = \pm 1$, and constitutes the Raman selection rule. This is the same for infrared vibrational transitions, but vibrational Raman spectroscopy has the advantage that transitions are allowed in homonuclear as well as heteronuclear diatomic molecules.

Intensities of Raman transitions are proportional to $|\mathbf{R}_\upsilon|^2$ and therefore from equation 20, to $(d\alpha/dx)_e^2$. Since α is a tensor property, we cannot illustrate its variation with x easily; thus we use the mean polarisability, α, where:-

$$\alpha = \tfrac{1}{3}\left(\alpha_{xx} + \alpha_{yy} + \alpha_{zz}\right) \qquad (21)$$

Figure 2.4 shows how α varies with r; $d\alpha/dr$ is usually positive but, unlike $d\mu/dr$ in Figure 2.1, varies little with r.

2.5 Anharmonicity[1,2].

A molecule may exhibit anharmonicity, and one effect of this is to modify the $\Delta\upsilon = \pm 1$ infrared and Raman selection rule to $\Delta\upsilon = \pm 1, \pm 2$ etc. However, these so-called overtone transitions with $\Delta\upsilon = \pm 2$ etc., are usually weak compared with those with $\Delta\upsilon = \pm 1$.

Vibrational term values (energy levels), $G_{(\upsilon)}$, invariably have dimensions of wavenumber, and for a harmonic oscillator, we have, from equation 7:-

$$\frac{E_\upsilon}{hc} = G_{(\upsilon)} = \bar{\nu}\left(\upsilon + \tfrac{1}{2}\right) \qquad (22)$$

However, anharmonicity modifies such vibrational term values to a power series in $(\upsilon + \tfrac{1}{2})$, giving:-

$$G_{(\upsilon)} = \bar{\nu}_e(\upsilon + \tfrac{1}{2}) - \bar{\nu}_e x_e(\upsilon + \tfrac{1}{2})^2 + \bar{\nu}_e y_e(\upsilon + \tfrac{1}{2})^3 \ldots \qquad (23)$$

where $\bar{\nu}_e$ is the vibrational wavenumber, and $x_e, y_e \ldots$ are anharmonicity constants.

2.6 Attenuated Total Reflection Fourier Transform-Infrared Spectroscopy.

2.6.1 Introduction and History[3].

The observation by Newton[4] nearly 200 years ago of a so called 'Evanescent Field' in a lower index of refraction medium in contact with a medium of higher index of refraction in which a propagating wave of radiation undergoes Total Internal Reflection (TIR) marks the beginning of interest in ATR spectroscopy. The exploitation of this phenomenon, however, did not commence until Harrick[5,6] and Fahrenfort[7] conducted pioneering work for the production of absorption spectra. The resulting frenzy of research, indicating new and wide-ranging applications for the technique, justified a monograph by Harrick[8] and a comprehensive review by Wilks

and Hirschfield[9]. Despite the promise illustrated by the ATR technique to tackle problems which were difficult with other techniques, such as transmission IR, there were general doubts about its reproducibility and quantitative capabilities, and thus the ATR technique was relegated to qualitative or semi-quantitative uses. A resurgence of interest in ATR occurred in the mid-1970s, mainly due to the order of magnitude improvements made in the practice of infrared spectroscopy by the advent of commercially available Fourier Transform Infrared (FT-IR) instrumentation[10] which offered high quantitative accuracy and large data-handling capability, due to its high signal to noise ratio and the data-processing flexibility of a built in minicomputer. The use of such instruments, along with computer-controlled dispersive spectrometers, has resulted in a wealth of research, which has renewed vitality in the ATR technique.

2.6.2 - Theoretical Considerations[3].

The basic theoretical principles of ATR were considered initially by Harrick[5,6] and Fahrenfort[7], and subsequently described in detail and compared with experimental data, by Harrick[11] and Harrick and duPre[12]. Treatments of the theory of ATR centre on the properties of the evanescent field, since by virtue of its existence the phenomenon of ATR spectroscopy is possible.

Figure 2.5 illustrates the basic ATR experiment and the properties of the evanescent field.

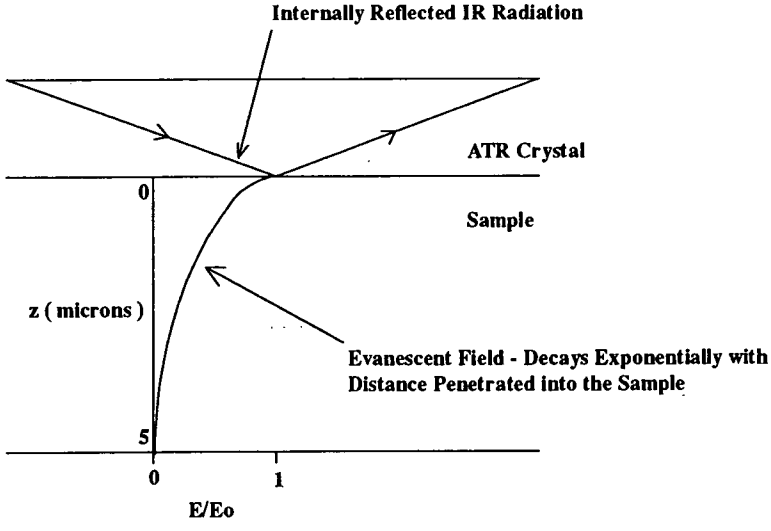

Figure 2.5 - The ATR Experiment

The radiation propagating in the optically more dense medium 1, (with index of refraction n_1), undergoes total internal reflection at the interface with the optically rarer medium 2, (with index of refraction n_2), when the angle of incidence, θ (measured from the normal), exceeds the critical angle, θ_c. This critical angle is defined by:-

$$\theta_c = \sin^{-1} n_{21} \qquad (24)$$

where $n_{21} = n_2/n_1$. This phenomenon of total internal reflection is most easily described for an infinite plane wave at an interface between semi-infinite non-absorbing

media. The properties of the evanescent field in the rarer medium 2 under these conditions can be enumerated as follows[13]:-

a). The field intensity in medium two is not zero, but there is an instantaneous normal component of energy flow into medium 2, whose time average is zero. Thus, there is no loss of energy, and the propagating radiation in medium 1 is totally internally reflected.

b). The evanescent field in medium 2 is a non-transverse wave and has components in all spatial directions.

c). The evanescent field is confined to the vicinity of the surface of medium 2 and decreases in intensity with distance into medium 2, normal to the surface.

d). There is a non-zero energy flow parallel to the surface, resulting in a displacement of the incident and reflected waves. This is the so-called Goos-Hanchen shift[14,15,16].

The amplitude of the evanescent field in medium 2 under these conditions can be conveniently expressed as an exponential function of distance into medium two, perpendicular to the surface. The decay of the electric field amplitude at the surface of medium 2, E_0, to some value E at a distance z from the surface, can be written as:-

$$E = E_0 \exp(-\gamma z) \qquad (25)$$

where

$$\gamma = \frac{2\pi \sqrt{\sin^2\theta - \left(\frac{n_2}{n_1}\right)^2}}{\lambda_1} \qquad (26)$$

where $\lambda_1 = \lambda/n_1$, and is the wavelength of the radiation in medium 1, λ is the wavelength in free space, and Z is the distance from the surface[17]. One important feature of the evanescent wave is that it is *not* a transverse wave, and thus has vector components in all spatial directions, which in turn can interact with dipoles in all directions.

This idealised picture of ATR gives a convenient description of the evanescent field and its associated properties, but is clearly unrealistic, due to the condition that medium 2 must be non-absorbing, as absorption must occur for a measurement to be taken. A more realistic set of conditions for the ATR experiment includes an absorbing rarer medium and a finite diameter irradiating beam. Furthermore, an absorbing medium will also require consideration of the dispersion of refractive index across the absorption band. Harrick[11] noted that the inclusion of these conditions causes the theoretical treatment to become unmanageable, and thus a few improvements in the theory have been proposed, so as to replace Equation 25. However, the refractive index of the rarer medium is known to undergo dispersion through an absorption band[8], which will clearly compromise the validity of Equation 25. Also, the TIR of a beam of finite diameter has been treated by Picht[18], who showed that the time average flow of energy into the rarer medium is not strictly zero in this case. In actual fact,

Equation 25 is quite adequate for experimental interpretation, considering that it represents an idealised case, based on apparently unrealistic conditions.

Harrick[12] defined a parameter, d_p, called the depth of penetration, when E decays to a value of E_0 exp [-1]. This occurs at a value of $Z = d_p = 1/\gamma$. This parameter is often a source of confusion, due to the name of this arbitrarily defined entity, and is often taken to be the actual depth sampled in the ATR experiment. The arbitrary nature of the parameter is emphasised by noting that the definition of 'depth of penetration' was the depth at which the electric field amplitude falls to one half of its value at the surface ($Z = 0.693 / \gamma$) in an early publication by Harrick[11]. However, since the electric field amplitude at d_p is 37% of its value at the surface, it is clear that the actual depth sampled is greater than d_p. This was tested[19] for polypropylene and polystyrene on KRS-5, and it was found that the actual depth sampled (d_s) was about three times d_p. This is a more realistic sampling depth and appears to indicate the validity of Equation 25, but it should be stressed that the major fraction of information is gathered from substantially shallower depths in an ATR experiment. This serves to confirm the extent of the evanescent wave in the rarer medium, as predicted by Equation 25, for the zero absorption case. The effect of absorption, however, turns out to be relatively small, and especially so for polymers.

The case of an absorbing rarer medium can be treated in terms of the intensity loss per reflection. If I_0 is the incident intensity and I is the reflected intensity, then the reflectivity, R, can be expressed as:-

$$R = I/I_0 \qquad (27)$$

For total reflection, $I = I_0$, and $R = 1$. This is analogous to the transmission case, for which :-

$$T = \exp(-\alpha d) \qquad (28)$$

where T is the transmittance, α is the absorption coefficient and d is the sample thickness.

The ATR case yield, for weak absorbers is:-

$$R = \exp(-\alpha d_e) \approx (1 - a) \qquad (29)$$

for a single reflection. The absorption coefficient, α, is identical for transmission and ATR. The effective thickness, d_e, is defined as the thickness of the film of the sample material which would give the same absorbance for transmission at normal incidence as that obtained in the ATR experiment[11]. The absorption parameter, a, is equal to αd_e for a single reflection. Equation 29 is only valid for weak absorbers and the ATR absorption follows a more complex law for strong absorbers.

2.6.3 - Application of FT-IR ATR Spectroscopy to Thin Polymer Films

Mirabella[3] quotes a number of research reports regarding ATR studies of synthetic polymeric systems. These include studies of poly(ethylene-vinyl acetate)[20,21], polyethylene and polypropylene[20,22,23], paint vehicles[24], silicone rubbers and elastomers[25,26], polyamides[27], epoxies[28] and polyurethanes[29,30]. Other applications of ATR to polymers and related systems include determination of organic compounds using a polymer-coated ATR crystal (also referred to as an Internal Reflection Element)[31], studies on the functional layers of adhesive tape[32], and a technique for the identification of stamp adhesives[33]!

The important issue of the application of FTIR-ATR to the study of diffusion processes in polymeric materials will be discussed in the next chapter, and the relevant literature reviewed there.

2.6.4 Depth Profiling Using FT-IR ATR Spectroscopy[3].

Concentration depth profiling using ATR is not a straightforward process, due to the fact that, even in the absence of an absorption, the evanescent wave decays exponentially in the sample surface and is thus not characterised by one constant field intensity throughout the depth observed. It can thus be appreciated that defining an unknown concentration depth profile with an exponentially decaying probing field is somewhat formidable. The simplification used in most depth profile studies is to assume that the depth sampled is d_p[34-37]. This approach gives a semi-quantitative description of the concentration depth profile, but d_p is not the actual depth sampled (discussed in section 2.4.2 of this chapter). Also, no simple relationship between the depth profile, based on d_p, and the true depth profile can be expected, which was pointed out by Carlsson and Wiles[35]. Other studies have utilised the effective thickness, d_e, as the definition of the depth sampled[38-40]. This is not, however, a legitimate use of d_e, as it is the total interaction parameter, with d_p being only one of five factors that control d_e, the other four being electric field amplitude decay constant, electric field intensity at the surface, the sampling area and the refractive index matching. The combination of these factors produces a measure of the strength of the coupling between the evanescent wave and the probed medium.

Such studies, employing d_p or d_e as the depth parameter, were conducted by recording ATR spectra at several different angles of incidence on one or more ATR crystals, thus varying the depth sampled at each condition.

Several attempts have been made to treat the depth profiling problem in a more rigorous way. Tompkins[41] argued that it was possible to demonstrate that some profiles could not be distinguished from each other, but if a distribution was assumed, information about depth and concentration could be obtained by taking measurements at several angles of incidence, and a method proposed and demonstrated to obtain the concentration-depth profile of an assumed step profile.

An experimental approach to the problem of depth profiling is the use of 'barrier' layers applied to the surface of the ATR crystal. If the thickness of the barrier layer can be determined, the penetration of a fraction of the evanescent field beyond the barrier

layer can be estimated. Typically, the thickness of the barrier layers is determined from surface coverage considerations, or by monitoring a 'thickness' band in the transmission IR spectrum, or, in Durham, the use of an alpha-stepper, described later. The measured variable can then be plotted against depth beyond the barrier layer penetrated by the evanescent wave. This yields an approximation to a depth-concentration profile. The variable used most frequently to determine the depth samples is d_p, and, obviously, the barrier layer must be transparent in the spectral region of interest. The use of this 'barrier' method for ATR measurements is well documented[19,29,30,42,43].

A completely new approach was proposed by Hirschfield[44], who examined the quantitative nature of the distribution of silicon oil at the surface of polystyrene and water coated on glass. The equations presented therein have been found to be in error by Fina and Chen[45], but Hirschfield nevertheless presents the basis for the use of Laplace transformations to convert from angular space to distant space, thus presenting a solution to the concentration gradient problem for the first time. An equivalent expression to find depth-dependent absorption coefficients from relevant spectra, based on perturbation, is presented by Rozanov and Zolotarev[46]. Finally, Hong et al.[47], have examined flame-treated poly(vinyl fluoride) layers, using depth profiling.

2.6.5 Theoretical Considerations of FT-IR ATR Depth Profiling[45].

Maxwell's equations and the Fresnel coefficients[48] can be used to exactly model the reflected intensities in the ATR experiment, but the Fresnel coefficients are usually written in a general form, which assumes that plane parallel layers are isotropic (i.e. independent of orientation). Thus the coefficients cannot be used as a model for the depth profiling experiment, where interest is in the determination of inhomogeneous distributions, which occur as a result of surface activity, surface reactions, diffusion etc. A simplified expression may be written to describe the reflection properties from an anisotropic layer, based on the equivalence of electric field intensities in the transmission and attenuated total reflection modes:-

$$\langle E_T^2 \rangle . d_e = \frac{1}{\cos\theta} \int_0^\infty \langle E_2^2 \rangle . dz \qquad (30)$$

The left side of Equation 30 represents the transmission case where d_e is the effective thickness, which is the thickness in transmission that is equivalent to the amount of material probed in the ATR experiment. The right hand side represents the ATR case, where the electric field is integrated over distance z, perpendicular to the interface. The $1/\cos\theta$ is a sample area factor and must be modified if the infrared beam displays significant divergence. The decay of the evanescent field with distance into the rarer medium may be represented as:-

$$\langle E_2^2 \rangle = \langle E_{02}^2 \rangle \exp\left(\frac{-z}{d_p}\right) dz \qquad (31)$$

d_p (depth of penetration) is here represented as the point where the electric field intensity decays to exp(-1) of the value at the surface, $\langle E^2_{02} \rangle$. The electric fields in two media are related through their refractive indices, hence:-

$$n_1\langle E_1^2\rangle = n_2\langle E_2^2\rangle \qquad (32)$$

Thus, combining this with Equations 30 and 31, we arrive at the standard definition for the effective thickness:-

$$d_e = \frac{\langle E_{02}^2\rangle n_{21}}{\cos\theta}\int_0^\infty \exp\left(\frac{-z}{d_p}\right)dz \qquad (33)$$

The relationship between Beer's Law and total internal reflection is based on the equivalence of d_e, and the transmission sample thickness. Beer's law may be written as:-

$$T = I/I_0 = \exp(-\alpha d) \qquad (34)$$

which, in the case of small α (absorption coefficient) values, may be written as T= 1 - αd. By analogy, ATR intensities are written:-

$$R = 1 - \alpha d_e \qquad (35)$$

If this is substituted into Equation 33, we obtain the Beer's law analog for ATR:-

$$1 - R_{(\theta)} = \frac{\langle E_{02}^2\rangle n_{21}}{\cos\theta}\int_0^\infty \alpha(z)\exp\left(\frac{-z}{d_p}\right)dz \qquad (36)$$

Hirschfield[44] points out that this is the Laplace transform of the absorption coefficient, $\alpha(z)$, which transforms angular space into distance space. Equation 36 shows that the reflected intensities depend on the electric field intensity and the depth of penetration, which are both in turn dependent on the value of the absorption coefficient, A. Equation 36 may be solved using real variables rather than complex ones, as long as conditions of low absorption hold, but despite this the solution is not necessarily unique, given the finite signal to noise ratio of the data and the small dependence of $R(\theta)$ on absorption processes which occur at large distances from the interface.

The application of ATR to the study of diffusion processes in polymeric materials will be considered in the next chapter.

2.7 Waveguide Raman Spectroscopy

2.7.1 Introduction and History[49].

The introduction of Waveguide Raman Spectroscopy (WGRS) as a tool for examining thin films has represented an important turning-point in non-destructive characterisation of thin films. The combination of Raman Scattering and the Integrated Optics technique has produced a versatile technique, capable of lowering significantly the limits for Raman detectability. In this section, a brief introduction to the history of Waveguide Raman spectroscopy is presented, followed by a detailed examination of the theoretical principles behind the technique.

Integrated optical devices have been the subject of many investigations[50,51], motivated primarily by the desire to achieve a compact efficient optical system for the transferral of information. During the development process, much has been learned about the fabrication of thin-film waveguides, prisms and grating couplers, along with other miniature optical components. It was thus only a matter of time before interest blossomed in other scientific areas, where applications, such as Raman scattering, awaited. Early methods for obtaining Raman spectra from thin films relied on single or multiple reflection of the laser beam by a metallic surface, in order to maximise sampling volume. These methods, however, produced weak signals, which required large slit widths for detection, and thus the resolution achieved was very poor. In addition, these techniques also had the disadvantage that, owing to the standing wave nature of the optical field, a node in the optical field exists at the surface where good sensitivity is required[52,53]. A total reflection technique described by Cipriani et al.[54] was used to obtain reasonable Raman spectra of the strong CH vibrations in a barium stearate layer, and internal reflection measurements had also been obtained for molecules on surfaces of water (water/CCl_4, water/air and water/quartz)[55-57].

The first waveguide Raman experiments, however, were carried out by Levy et al.[58,59] on polymeric films about 1μm thick. However, broad features, attributable to the substrate (glass), resulted in a spectrum with a rather poor signal to noise ratio. However, a wealth of subsequent experiments examining very thin polymer films[60-84], laminate systems[85-87], Langmuir-Blodgett films[88-91], polymer films with liquid superstrates[92-98], Protein absorption[95,99,100], and the use of Fourier Transform Raman techniques[101-104], has finally firmly established the field of WGRS.

2.7.2 Theoretical Consideration[49].

The theory behind waveguiding is exceptionally complicated, and has been dealt with adequately in other texts[e.g. 49]. Hence, a detailed derivation of the difficult mathematics is not presented here, but rather an overview of the important concepts.

The detection, identification and observation of Raman scattering from thin films on a substrate, with sufficient signal-to-noise ratios, requires both a reasonable optical field at the surface and a long path length, to increase scattering volume. Thus optical waveguides appear an ideal solution. In an asymmetric slab waveguide, the optical field is condensed into a narrow region near the surface, and is thus of high intensity and has one of two unique polarisations (TE or TM). With the long path length, many

scattering sites are encountered as the beam passes through the guide, and the resulting streak is usually long enough to fill the entrance slit of the monochromator.

The analysis of optical waveguide transmission follows from Maxwell's equations, and the matching of **E** and **H** electric fields at each interface. The two common approaches used are the Fresnel coefficients[48,105], or a solution of an eigenvalue equation[60,106-111]. Each method has limitations. If the Fresnel coefficient method is used, a small imaginary term (absorption) has to included with the refractive index of the film, in order to extract some energy, to result in a calculated minimum. If this is not included, the Fresnel coefficients will sum all reflections to the value of the incident intensity. In the actual experiment, energy is extracted by the wave propagation along the film, which is not returned to the reflected beam. With the eigenvalue equation option, the only determined positions for waveguide modes are with the results for waveguides with no losses, i.e. only propagating waves. Perturbation methods have been used to include small losses[112], and this is usually more than adequate because significant losses from a waveguide would prevent effective propagation, and would thus rapidly attenuate the beam.

The Fresnel coefficient derivation is not needed here, but a full discussion of the eigenvalue solution is given, as this solution forms the basis of the software used for calculations of waveguiding parameters, described and utilised in Chapter 5.

2.7.3 - Eigenvalue Solution.

The waveguiding modes, their angles and the optical fields may all be calculated using an eigenvalue equation. If the optical field is written in each region, namely superstrate, film and substrate, and the **E** and **H** fields matched at each interface, the TE mode can be obtained, with real k_z, i.e. no optical absorption in any layer:-

$$E_{y1} = A_1 \exp^{k_{(z1)}z} \qquad (37)$$

$z = 0$

$$E_{y2} = A_2 \cos(k_{(z2)}z + \phi) \qquad (38)$$

$z = d$

$$E_{y3} = A_3 \exp^{-k_{(z3)}(z-d)} \qquad (39)$$

where ϕ is the phase shift in the film.

The choice of axes is such that the positive z direction is downwards. The E_y field can then be matched at z = 0 and z = d (d= film thickness), and H_x can also be matched at both interfaces[48,105]. This results in two equations for ϕ, the phaseshift in the film, which, when equated give:-

$$\tan^{-1}\beta^s_{12} + \tan^{-1}\beta^s_{32} + m\pi = k_{z2}d_2 \qquad (40)$$

The β's are half the negative phase shifts in reflection at the two interfaces, and the term on the right is the phase shift in transversing the film in the z direction. When these sum to a multiple of π, reinforcement of the light rays occurs, and a mode propagates in the film. For the TM mode, the eigenvalue is the same but, as with reflectivity, the expression for β is modified[48,105].

The optical field in the waveguide is a propagating wave, and those outside the guide, evanescent waves. This means that k_{z1} and k_{z3} must be imaginary for the propagating wave $e^{i(\omega t - k(z)z - k(x)x)}$ to become evanescent. As a consequence $\beta \rightarrow i|\beta|$ and the reflectivity becomes:-

$$\frac{1+i|\beta|}{1-i|\beta|} = \rho.\exp^{i\delta} \text{ and } \tan\delta = \frac{2\beta}{1-\beta^2} \text{ or } \tan\frac{\delta}{2} = \beta \qquad (41)$$

Hence the phase shifts, δ, at each interface, plus the phase shift in the round trip transversing the film must equal 2π for a mode to exist. The eigenvalue Equation 40 has been divided by 2 and the integer, m, labels the mode and gives the number of antinodes in the field distribution.

In order to determine the solution for the eigenvalue equation 40, one of several approaches may be adopted[113-116]. By rearrangement of terms in equation 41, it can be cast in the following form[113]:-

$$d_2 = f(n_2, m) \qquad (42)$$

that is, the thickness is a function of the refractive index of the guiding layer and the mode number. Since the calculated thickness for all the modes must be the same, the equations can be solved for the 'best value' or least squares value of n_2, which then can be used to determine d_2. An alternative method[114] combines the TE and TM modes to give equations for the same film thickness for all modes and both polarisations, but assumes the film to be isotropic.

For four-layered systems, i.e. a laminate system, the expression for one of the β is modified, depending on whether the layer is an overcoat or an undercoat[74,116]. For a guiding layer, this expression becomes:-

$$\beta_{32} \rightarrow \beta_{32}\left(\frac{\beta_{43} - \tan k_{(z3)}d_3}{1+\beta_{43}\tan k_{(z3)}d_3}\right) \qquad (43)$$

and for a non-guiding layer, i.e. only an evanescent field in the layer, the expression becomes:-

$$\beta_{32} \rightarrow \beta_{32}\left(\frac{\beta_{43} + \tanh k_{(z3)}d_3}{1+\beta_{43}\tanh k_{(z3)}d_3}\right) \qquad (44)$$

Solutions to the eigenvalue for a four-layered system can be difficult to evaluate, as the parameters can diverge. Usually the lower film is first measured as a single layer, and then these parameters, thickness and refractive index, are used in the total calculation. Unfortunately, the coupling must be at the same point as in the single layer, and a further complication can arise because the application of the second layer can cause a change in the thickness of the first film. It has been suggested[74] that the set of parameters for the lower film should be varied consecutively in a set of calculations to arrive at the 'best fit', i.e. the one having the lowest error.

Thus, films from ~0.3 μm to 4-5 μm can give accurate results for both the thickness along with in-plane and out-plane refractive indices. As such, this is a powerful method which gives much information about a thin film. Thicknesses greater than 2 μm are desirable, as more than two modes are available to obtain a solution to the eigenvalue equation. For four-layered laminates, either the over- or undercoat needs to be in the region of 0.1 μm, in order to obtain sufficient angular shifts in mode-coupling angles, for solutions to the eigenvalue equation.

The intricacies, conditions and difficulties associated with conducting waveguide Raman experiments will be considered in the experimental section of this thesis.

References.

1/. 'Modern Spectroscopy' (2nd Edition); J.Michael Hollas; John Wiley & Sons publishers. Chapter 1.
2/. 'Modern Spectroscopy' (2nd Edition); J.Michael Hollas; John Wiley & Sons publishers. Chapter 6.
3/. F.M.Mirabella Jr.,'Internal Reflection Spectrosopy', Appl.Spectr.Rev., 21, 1 & 2, (1985), 45.
4/. I.Newton, Optiks II, Book 8, 1817, p.97.
5/. N.J.Harrick, Phys.Rev.Lett., 4, 5, (1960), 224.
6/. N.J.Harrick, J.Phys.Chem., 64, (1960), 1110.
7/. J.Fahrenfort, Spectrochim. Acta, 698, (1962)
8/. N.J.Harrick, "Internal Reflection Spectroscopy", Harrick Scientific Corp., New York, 1967.
9/. P.A.Wilks Jr. & T.Hirschfield, Appl.Spectrosc. Rev., 1, 1, (1967), 99.
10/. T.Hirschfield, Appl.Optics, 17, 9, (1978), 1400.
11/. N.J.Harrick, J.Opt.Soc.Am., 55, (1965), 851.
12/. N.J.Harrick & F.K.du Pre, Appl.Optics, 5, (1966), 1739.
13/. J.A.Stratton, "Electromagnetic Theory", McGraw-Hill, New York, 1941, pp. 497-500.
14/. F.Goos & H.Hanchen, Ann.Phys., 1, (1947), 333.
15/. R.H.Renard, J.Opt.Soc.Am., 54, 10, (1964), 1190.
16/. S.S.Gupta & D.P.Tweari, Opt.Acta., 30, (1983), 1397.
17/. P.Drude, "The Theory of Optics", Longmans Green, London, 1902, pp. 299-301.
18/. J.Picht, Ann.Phys., 3, (1929), 433
19/. F.M.Mirabella, J.Polym.Sci., Polym.Phys.Ed., 21, (1983), 2403.
20/. F.M.Mirabella, J.Polym.Sci., Polym.Phys.Ed.,20, (1982), 2309.
21/. A.R.French, J.V.Benham & J.Pullukat, Appl.Spectrosc., 28, (1974), 477.
22/. H.A.Willis & V.J.I.Zichy, in "Polymer Surfaces" (Eds D.T.Clark & W.J.Feast), Wiley, New York, 1978.
23/. A.Garton, S.W.Kim & D.M.Wiles, J.Polym.Sci., Polym.Lett.Ed., 20, (1982), 273.
24/. R.J.McGowan, Anal. Chem., 35, (1963), 1665.
25/. G.Gidaly & R.Kellner, Microchim.Acta.(Wein), 1, (1981), 131.
26/. W.W.Hart, P.C.Painter, J.L.Koenig & M.M.Coleman, Appl.Spectrosc., 31, (1977), 220.
27/. R.E.Baier & W.A.Zisman, Macromolecules, 3, (1970), 461.
28/. J.F.Sprouse & B.N.Halpin Jnr., Army materials and mechanics res. cent., Watertown, Massachusetts, U7917, Rep. No. AMMRC-TR-78-45, Nov. 1978.
29/. C.S.P.Sung & C.B.Hu, Adv.Chem.Ser. (Multiphase Polym.), 176, (1979), 69.

30/. C.S.P.Sung, C.B.Hu & E.W.Merrill, A.C.S.Div.Polym.Chem., Polym.Prepr.,19, 1, (1978), 20.
31/. P.Heinrich & B.Schrader, Appl.Spectrosc., 44, 10 (1990), 1641.
32/. S.F.Simpson & J.M.Harris, J.Phys.Chem.,94,(1990),4649.
33/. A.J.Barnes, Barnes Instrum. News, 21, (1970), 1.
34/. C.S.Blackwell, P.J.Degen & F.D.Osterholtz, Appl. Spectrosc., 32, 5, (1978), 480.
35/. D.J.Carlsson & D.M.Wiles, Macromolecules, 4, (1971), 173.
36/. D.J.Carlsson & D.M.Wiles, Macromolecules, 4, (1971), 179.
37/. J.R.Webb, J.Polym.Sci.,Polym.Chem.Ed.,10, (1972), 2335.
38/. D.J.Carlsson & D.M.Wiles, Can.J.Chem., 48, (1970), 2397.
39/. D.J.Carlsson & D.M.Wiles, Macromolecules, 4, (1971), 173.
40/. J.P.Hobbs, C.S.P.Sung, K.Krishnan & S.Hill, Macromolecules, 16, (1983),193.
41/. H.G.Tompkins, Appl. Spectrosc., 28, (1974), 335.
42/. C.S.P.Sung, C.B.Hu, E.W.Merrill & E.W.Saltzman, J.Biomed.Mater.Res., 12, (1978), 791.
43/. C.B.Hu & C.S.P.Sung, A.C.S. Div. Polym. Chem., Polym. Prepr., 21, 1 (1980), 156.
44/. T. Hirschfield, Appl.Spectrosc., 31, (1977), 289.
45/. L.J.Fina & G.Chen, Vib.Spectrosc., 1, (1991), 353.
46/. N.N.Rozanov & V.M.Zolotarev, Opt. Spectrosc. Engl. Transl., (1980), 506.
47/. J.W.Hong, J.B.Lando & J.L.Koenig, Appl. Spectrosc., 45, 8, (1991), 1296.
48/. M.Born & E.Wolf, "Principles of Optics", Pergamon Press, Oxford, 4th Edition, 1970, Chapter 1.
49/. J.F.Rabolt & J.D.Swalen, "Spectroscopy of Surfaces", Eds. R.J.H.Clark and R.E.Hester, J.Wiley and Sons, London, 1988, Chapter 1.
50/. P.K.Tien, "Light Waves in Thin Films and Integrated Optics", Appl.Opt., 10, (1971), 2395
51/. D.Marcuse, "Theory of Dielectric Optical Waveguides", Academic Press, Inc., New York, 1974, Chapters 1-2.
52/. R.G.Greenler & T.L.Slager, Spectrochim. Acata. A, 29, (1973), 193.
53/. M.L.Howe, K.L.Walters & R.G.Greenler, J.Phys.Chem., 80, (1976), 582.
54/. J.Cipriani, S.Racine, R.Dupeyrat, H.Hasmonay, M.Dupeyrat, Y.Levy & C.Imbert, Opt.Commun., 11, (1974), 70.
55/. T.Takenaka & T.Nakanaga, J.Phys.Chem., 80, (1976), 582.
56/. T.Takenaka & H.Fukuzaki, J.Raman.Spectrosc., 8, (1979), 151.
57/. T.Takenaka & K.Yamasaki, J.Colloid Interface Sci., 78, (1980), 37.
58/. Y.Levy, C.Imbert, J.Cipriani, S.Racine & R.Dupeyrat, Opt.Commun., 11, (1974), 66.
59/. Y.Levy & R.Dupeyrat, J.Physique.Coll.C5, 38, (1975), 253.
60/. J.D.Swalen, J.Phys.Chem., 83, (1979),1438.
61/. J.F.Rabolt, R.Santo & J.D.Swalen, Appl.Spectrosc., 33, (1979), 549.
62/. J.F.Rabolt, R.Santo & J.D.Swalen, Appl.Spectrosc., 34, (1980), 517.
63/. R.Dupeyrat, Ber.Bunsenges.Phys.Chem., 85, (1981), 490.
64/. N.E.Schlotter, J.F.Rabolt & J.D.Swalen, Bull.Am.Phys.Soc., 26, 3, (1981), 328.
65/. J.F.Rabolt, R.Santo, N.E.Schlotter & J.D.Swalen, IBM Res.Div., 26, (1982), 209.
66/. J.D.Swalen & J.F.Rabolt, "Vibrations at Surfaces", Eds. R.Caudano, J.M.Giles and A.A.Lucas, Plenum Press, New York, 1982, p.413-20.
67/. J.D.Swalen, J.F.Rabolt, N.E.Schlotter, W.Knoll, A.Girlando & M.R.Philpott, Proceedings of the Society of Photo-Optical Instrumentation Engineers, 362, (1982), 31.
68/. W.Knoll, M.R.Philpott, J.D.Swalen & A.Girlando, J.Chem.Phys., 77, 5, (1982), 2254.
69/. J.D.Swalen & J.F.Rabolt, J.de.Phys.Coll. C10, 12, 44, (1983), 501
70/. N.E.Schlotter & J.F.Rabolt, J.Phys.Chem.,88, 10, (1984), 2062.
71/. N.E.Schlotter & J.F.Rabolt, Appl.Spectrosc.,38, 2, (1984), 208.
72/. J.D.Swalen, IBM Research Report, RJ 4352 (47430), (1984).
73/. J.F.Rabolt & J.D.Swalen, IBM Research Report, Surface Science, (1986).
74/. D.R.Miller, O.H.Han & P.W.Bohn, Appl.Spectrosc., 41, 2, (1987), 245.
75/. D.R.Miller, O.H.Han & P.W.Bohn, Appl.Spectrosc., 41, 2, (1987), 249.
76/. D.R.Miller & P.W.Bohn, Anal.Chem., 60, (1988), 407.
77/. D.R.Tallant, K.L.Higgins & A.F.Stewart, Appl.Spectrosc, 42, 2, (1988), 326.
78/. D.R.Miller & P.W.Bohn, Appl.Opt., 27, 12, (1988), 2561.
79/. J.T.Ives & W.M.Reichert, J.App.Polym.Sci., 36, (1988), 429.
80/. I.Savatinova, S.Tonchev, R.Todorov, E.Venkova, E.Lairokapir & E.Anastassakir, J.App.Phys., 67, 4, (1990), 2051.
81/. S.F.Simpson & J.M.Harris, J.Phys.Chem., 94, (1990), 4649.

82/. R.H.Page, M.C.Jurich, B.Reck, A.Sen, R.J.Twieg, J.D.Swalen, G.C.Bjorklund & C.G.Willson, J.Opt.Soc.Am., B-Optical Physics, 7, 7, (1990), 1239.
83/. A.Skumanich, M.C.Jurich & J.D.Swalen, App.Phys.Lett., 62, 5, (1993), 446.
84/. C.J.Wung, W.M.K.P.Wijekoon & P.N.Prasad, Polymer, 34, 6, (1993), 1174.
85/. J.F.Rabolt, N.E.Schlotter & J.D.Swalen, J.Phys.Chem.,85, 26, (1981), 4141.
86/. J.D.Swalen, N.E.Schlotter, R.Santo & J.F.Rabolt, J.Adhesion, 13, 2, (1981), 189.
87/. N.M.Dixon, N.Everall & J.Yarwood, Unpublished Work.
88/. C.W.Pitt & L.M.Walpita, Thin Solid Films, 68, (1980), 101
89/. J.P.Rabe, J.D.Swalen & J.F.Rabolt, J.Chem.Phys., 86, 3, (1987), 1601.
90/. J.D.Swalen, Thin Solid Films, 160, 1-2, (1988), 197.
91/. W.Hickel, G.Duda, M.C.Jurich, T.Krohl, K.Rochford, G.I.Stegeman, J.D.Swalen, G.Wegner & W.Knoll, Langmuir, 6, 8, (1990), 1403.
92/. G.L.Mitchell, IEE J.Quant.Electr., QE-13, (1977), 173.
93/. W.Lukosz & K.Tiefenthaler, Opt.Lett., 8, (1983), 537.
94/. W.M.Reichert, J.T.Ives, P.A.Suci & V.Hlady, Appl.Spectrosc., 41, (1987), 636.
95/. J.T.Ives & W.M.Reichert, App.Spectrosc., 42, (1988), 68.
96/. S.S.Saavadra & W.M.Reichert, Appl.Spectrosc., 44, 7, (1990), 1210.
97/. S.S.Saavadra & W.M.Reichert, Appl.Spectrosc., 44, 8, (1990), 1420.
98/. S.S.Saavadra & W.M.Reichert, Anal.Chem., 62, 20, (1990), 2251.
99/. S.S.Saavadra & W.M.Reichert, Langmuir, 7, (1991), 995.
100/. D.S.Walker, M.D.Garrison & W.M.Reichert, J.Coll.Interf.Sci., 157, 1, (1993), 41.
101/. C.G.Zimba, V.M.Hallmark & J.F.Rabolt, Abs.Paps.Am.Chem.Soc., 196, Sept, (1988), 49.
102/. C.G.Zimba, V.Hallmark, S.Turrell, J.D.Swalen & J.F.Rabolt, J.Phys.Chem., 94, (1990), 939.
103/. J.F.Rabolt, IBM Research Report RJ8476 (76697), (1991).
104/. C.G.Zimba & J.F.Rabolt, Thin Solid Films, 206, 1-2, (1991), 388.
105/. O.S.Heavens, "Optical Properties of Thin Solid Films", Dover Publishers, New York, (1965).
106/. P.K.Tien, R.Ulrich & R.J.Martin, App.Phys.Lett., 14, (1969), 291.
107/. P.K.Tien & R.Ulrich, J.Opt.Soc.Am., 60, (1970), 1325.
108/. R.Ulrich, J.Opt.Soc.Am., 60, (1970), 1337.
109/. R.Ulrich & R.Torge, App.Opt., 12, (1973), 2901.
110/.D.Marcuse, "Integrated Optics", IEEE Press, New York (1973).
111/. J.D.Swalen, M.Tacke, R.Santo, K.E.Rieckhoff & J.Fischer, Helv.Chim.Acta., 61, (1978), 960.
112/. M.Tacke & J.D.Swalen, IBM Research Report RJ2368, (1978).
113/. R. Th. Kersten, Opt.Commun., 9, (1973), 427.
114/. D.J.Walter, Thin Solid Films, 23, (1974), 153.
115/. J.D.Swalen, M.Tacke, R.Santo & J.Fischer, Opt.Commun., 18, (1976), 387.
116/. J.D.Swalen, R.Santo, M.Tacke & J.Fischer, IBM J.Res.Dev., 21, (1977), 168.

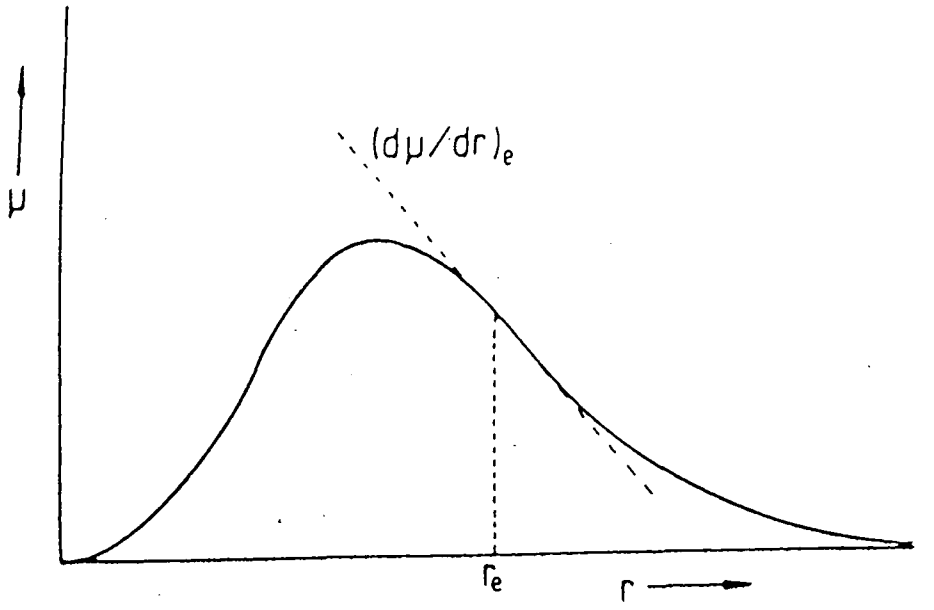

Figure 2.1 - Variation of dipole moment with internuclear distance in a heteronuclear diatomic molecule.

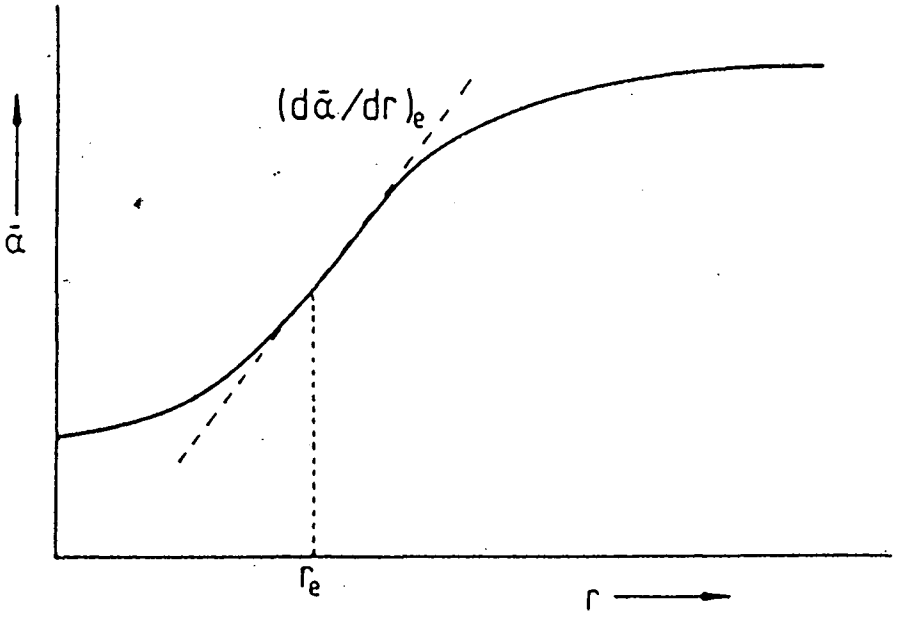

Figure 2.4 - Variation of the mean polarizability with internuclear distance in a diatomic molecule.

Chapter Three - Diffusion Processes in Polymeric Materials

Chapter Three - Diffusion Processes in Polymeric Materials

3.1 Introduction[1]

The transport of small molecules and polymers in polymeric materials is a subject of great technical and commercial importance. It is technically important, because factors, such as morphology and molecular interactions, which control diffusion, are not well understood. Also, the existing theory of diffusion, based on macroscopic parameters, is difficult to interpret in terms of interactions occurring between the polymer matrix and the diffusants. The commercial importance arises from the use of polymeric materials in a wide range of industrial applications, such as wire coatings and barrier layers (such as paints). A good understanding of diffusion processes in such systems can lead to a better understanding of important issues, such as adhesion and loss of stabilisers, which can lead to system failure. This improved understanding can hence lead to a product with enhanced properties and lifetime. The commercial advantages of such refinements are obvious.

When a polymer is placed in contact with a compatible penetrant, the penetrant enters the polymer, forming a swollen gel phase in the wetted region. In uncrosslinked polymers, dissolution will follow. If the polymer is crosslinked, however, the resulting gel will only swell to some equilibrium state at which the retractive force of the network balances the swelling force, similar to an osmotic pressure. The formation of the gel phase is accompanied by sharply reduced mechanical properties, and increased permeability in the swollen region.

In semi-crystalline polymers, diffusion is thought to be confined to the amorphous regions, and the diffusion is primarily classical Fickian in a rubbery matrix[4]. The degree of crystallinity and the morphological organisation (i.e. internal structure of the polymer) will have a large impact on the overall diffusion behaviour. This contrasts with glassy type polymers, where observations of a sharp boundary to the penetrant front are well documented[5-9]. Such a diffusion front, that also moves with a constant velocity, is termed a Case II diffusion process[6,7,9-11]. In both of these cases, however, the solvent's ability to diffuse in a polymer can be drastically modified by both defects and the presence of even trace amounts of other molecules[5, 11-13]. Additionally, evidence is presented that surface concentrations are not simple continuations of adjacent bulk concentrations[9, 14-17]. Various forms of anomalous diffusion have been noted[9, 14, 16, 18, 19]. This 'anomalous diffusion' often refers to deviations from a simple diffusion model, in which the Fickian solution shows a linear mass sorption increase relative to $t^{1/2}$, and the existence of pores and cracks has been suggested[11, 14, 20-23]. In glassy polymers, relaxation phenomena also occur, which modify diffusion, and are in turn modified by the penetrant concentration[11, 15, 17, 24]. In some cases, this is incorporated in models, by introducing a concentration dependent diffusion coefficient[2, 25]. Another response has been to incorporate the polymer's mechanical response to the osmotic pressure due to the solvent at the diffusion front[26-29]. However, despite all this, there is no model yet developed which has been fully successful in predicting all observations of diffusion[30].

In Case II diffusion, the stress between the glassy core and the solvent swollen surface can control the dimensional behaviour of the swelling[6,7]. In extreme cases, the

pressure differences established by the diffusing material are enough to cause a fracture[10,11], and/or stress-induced orientation[31,32]. A related phenomenon occurs under conditions of applied stress, in that crack behaviour and failure times are influenced by solvent concentration[13,14]. However, in the melt and above Tg, diffusion is usually 'well-behaved', compared with the glassy state[33-48].

Techniques reported to follow diffusion, include optical detection of chemical labels[5-7,16,49], Rutherford backscattering (R.B.S.)[9,17,24,50,51], radioactive labels[52-56], Raman microprobe on Sections[8], rotating-polariser ellipsometry[57], laser interferometry[58], capillary column inverse gas chromatography[47], simple weighing[2,12,16,18,20,21,23,33,34,36,37,44,46,48,59-62], mechanical measurement of thickness resulting from swelling[6,7,32,63,64], birefringence[2,32], nuclear magnetic resonance (N.M.R.)[2,65-74], U.V. adsorption[2], optical density of thin layers[45], forward recoil spectroscopy (F.R.E.S.)[38,40,75-85], electron spin resonance (E.S.R.)[86-90], microscopy (optical and electron)[91-95], transmission Fourier transform infrared (FT-IR) spectroscopy[62, 96], external reflection infrared spectroscopy[97], FT-IR attenuated total reflection (ATR) spectroscopy[98-104], FT-IR photo-acoustic (P.A.S.) spectroscopy[105,106], and waveguide Raman spectroscopy (W.G.R.S.), plus other optical waveguide techniques[20,107-112]. In the course of this project, vibrational spectroscopy (especially ATR) is utilised for determining diffusion processes in polymeric systems.

3.2 Diffusion Processes[1,2,3]

Fick's first law is the fundamental law of diffusion. It states that the flux (amount of substance (diffusant) moving across unit area in unit time) in the x-direction ($F_{(x)}$) is proportional to the gradient ($\partial c/\partial x$).

$$F_{(x)} = -D\left(\frac{\partial c}{\partial x}\right) \qquad (1)$$

where D is the diffusion coefficient. The first law can only be applied to diffusion in the steady state, i.e. where there is no change in concentration with time.

Fick's second law describes the non-steady state, and the flux gradients are obtained by differentiating equation 1, so that:-

$$\left(\frac{\partial c}{\partial t}\right) = D\left(\frac{\partial^2 c}{\partial x^2} + \frac{\partial^2 c}{\partial y^2} + \frac{\partial^2 c}{\partial z^2}\right) \qquad (2)$$

Under circumstances where diffusion is limited to the x-direction, it simplifies to:-

$$\left(\frac{\partial c}{\partial t}\right) = D\left(\frac{\partial^2 c}{\partial x^2}\right) \qquad (3)$$

Equation 3 is generally the starting-point for most models of diffusion, and it can be modified to incorporate diffusion constants that depend on concentration,

inhomogeneous media, and a host of boundary conditions, which can assume many forms.

It is helpful, and common, to express the experimental diffusion observations according to the three following categories.

3.2.1 - Case I Diffusion.

This is essentially Fickian diffusion, which occurs when the rate of diffusion is much less than the relaxation rate of the polymer. For diffusion into a semi-infinite medium from an infinite solvent source, mass sorption is proportional to $t^{1/2}$ (initial medium concentration is zero, and surface concentration is constant). If, however, there is a semi-infinite sheet, in an infinite solvent source, the $t^{1/2}$ relationship only holds at short times, at best[113].

3.2.2 - Case II Diffusion.

Here, diffusion is very rapid, compared with the polymer relaxation process. Frequently a sharp solvent front which propagates into the polymer at a constant velocity is associated with a Case II diffusion. The resulting mass sorption is thus directly proportional to time[10]. For this situation, it is assumed that the solvent front demarcates a rubbery shell from a glassy core. If the mechanical properties of the two states are sufficiently different, fracture can occur in the glassy core.

The theoretical basis for Case II diffusion was first described by Kormeyer et al.[2,30]. The diffusion of a solvent (penetrant) into a semi-infinite polymer is described by Fick's first law, which may be written[111]:-

$$\left(\frac{\partial C_1}{\partial \tau}\right)=\left(\frac{\partial}{\partial \xi}\right)D_1\left(\frac{\partial C_1}{\partial \xi}\right) \qquad (4)$$

where

$$C_1 = {}^{C_{(w)}}\!/_{C_{(w,e)}} \qquad (5)$$

and C_1 is the normalised solvent concentration, D_1 is the solvent diffusion coefficient, τ is the normalised time, ξ is the normalised position in the direction of diffusion, C_w is the solvent concentration in the film at any given time, and $C_{w,e}$, is the equilibrium solvent concentration in the polymer. Time, t, is normalised to the swollen film, solvent diffusion coefficient and the initial thickness, L_o, and the position is also normalised to the thickness.

$$\tau = {}^{D_{(1,s)}t}\!/_{L_0^2} \qquad (6)$$

$$\xi = {}^{x}\!/_{L_0} \qquad (7)$$

Equation 4 can be solved analytically for the situation where there is no swelling, and the diffusion coefficient is not dependent on the solvent concentration. The film is modified as a stack of extremely thin elements for the numerical integration, each with a thickness $\Delta\xi_0$. This solution is:-

$$C_{1(\tau)} = 1 + (2/\pi).\sum_{n=1}^{\infty} (\cos(n\pi) - 1) / n \sin(n\pi\xi) \exp(-n^2\pi^2 r) \qquad (8)$$

When polymer swelling is included, the individual thickness elements, $\Delta\xi_0$, are replaced by:-

$$\Delta\xi_i = \Delta\xi_0 / (1 - \upsilon_{(1,e)} C_{(1,i)} \qquad (9)$$

where $\upsilon_{1,e}$ is the equilibrium volume fraction of the solvent in the film, and $C_{1,i}$ is the solvent concentration in the element. Initially, the swelling is anisotropic, being constrained by the glassy core to swell only in the ξ direction. The total thickness can be calculated by summing the element thicknesses. The $C_{1,i}$ term in the denominator will account for the front penetration from one element to the next. When the front has reached the substrate, the anisotropic swelling constraints are relaxed and the film swells isotropically, the element thickness becoming:-

$$\Delta\xi_i = \left[(\Delta\xi_0)^3 / (1 - \upsilon_{1,e} C_{1,i}) \right]^{1/3} \qquad (10)$$

A further added refinement is the effect of a concentration-dependent solvent diffusion coefficient,

$$D_1 = D_{1,s} . \exp(-\beta_1 (1 - C_1)) \qquad (11)$$

Here, $D_{1,S}$ is the rubbery polymer diffusion coefficient, β_1 is a constant and C_1 is the solvent concentration in the film. These calculations have been proved effective in predicting experimental behaviour in thick films very well[30], and accurately predict the sharp concentration profile indicative of Case II diffusion.

3.2.3 - Case III Diffusion.

This is also referred to as non-Fickian, or anomalous, diffusion, and occurs when diffusion and relaxation rates are similar. Basically, all cases that cannot be satisfactorily modelled using either Cases I or II are collected as Case III. It is suggested that anomalous diffusion can be described by mass sorption being related to time raised to a power between 0.5 and 1.

Fickian diffusion and Case II diffusion represent the extremes of diffusion behaviour. Fickian diffusion is based on a random 'walk' without interactions with the substrate,

while Case II has very strong interactions and a moving interface, and is generally accepted to describe most accurately the diffusion processes in polymeric materials[1].

3.3 - Diffusion into a Film[3,104].

If a polymeric film is placed in an infinite bath of diffusant, the concentrations of the two surfaces of the film (z=L and z =-L) are instantaneously established at a concentration, C_1. If the initial concentration of diffusant is zero, then the concentration, C, at points within the film, z, at time, t, is given by[3]:-

$$\frac{C}{C_1} = 1 - \frac{4}{\pi}\sum_{n=0}^{\infty}\frac{(-1)^n}{2n+1}.\exp\left[\frac{-D(2n+1)^2\pi^2 t}{4L^2}\right]x\cos\left[\frac{(2n+1)\pi z}{2L}\right] \quad (12)$$

The effects of diffusion at the edges of the film are not considered. Equation 12 may be integrated to give the following expression which describes the mass uptake (sorbed) by the film, M_t:-

$$\frac{M_t}{M_\infty} = 1 - \sum_{n=0}^{\infty}\frac{8}{(2n+1)^2\pi^2}\exp\left[\frac{-D(2n+1)^2\pi^2 t}{4L^2}\right] \quad (13)$$

Here, M_∞ is the mass uptake at equilibrium, and L is film thickness. At short times, this will reduce to:-

$$\frac{M_t}{M_\infty} = \frac{2}{L}\left(\frac{D}{\pi}\right)^{1/2} t^{1/2} \quad (14)$$

If M_t/M_∞ is plotted as a function of $t^{1/2}$, then the linear portion of the produced curve is used to determine the diffusion coefficient using Equation 14. At $M_t/M_\infty \leq 0.5$, the error in using Equation 12, rather than Equation 13, is in the order of 0.1%[114].

Depending on film thickness and the diffusion coefficient, there may be limited data at $M_t/M_\infty \leq 0.5$. Here the long time solution is:-

$$\frac{M_t}{M_\infty} = 1 - \frac{8}{\pi^2}.\exp\left(\frac{-D\pi^2 t}{4L^2}\right) \quad (15)$$

which can be used, usually in the form:-

$$\ln\left(1 - \frac{M_t}{M_\infty}\right) = \ln\left(\frac{8}{\pi^2}\right) - \frac{D\pi^2 t}{4L^2} \quad (16)$$

If a mass uptake plot of ln $(1-M_t/M_\infty)$ as a function of t is constructed, at $M_t/M_\infty \geq 0.5$, the error incurred using Equation 16 rather than Equation 13 is of the order of 0.1%[114]. Fickian diffusion with a concentration-dependent diffusion coefficient can also result in curves similar to those described above, with D being determined through

Equation 14 or Equation 16, depending on the values of M_t/M_∞, and is an average value over the applicable concentration range.

3.4 The Application of FT-IR ATR Spectroscopy to Diffusion Process Elucidation[103,104].

Fourier Transform Infrared Attenuated Total Reflection (FT-IR ATR or simply ATR) spectroscopy can be applied to the diffusion of spectroscopically active penetrants (liquid, gas or vapour) into thin polymer film systems, and the sorption kinetics measured in situ. This section will consider the theory of the application of ATR to the diffusion of a small molecule into a polymer film, as reported by G.T. Fieldson and T.A. Barbari in their recent publication[104]. Some of the expressions have already been mentioned previously, but are repeated here for the convenience of the reader.

The basis of this sort of applied spectroscopy is the basic relationship between the absorption of electromagnetic radiation and the quantity of absorbing material. In FT-IR transmission spectroscopy, this basic relationship is expressed by the Beer-Lambert law:-

$$\frac{dI}{I} = \alpha.dz = -\varepsilon CI.dz \qquad (17)$$

where I is the radiation intensity at z, α is the absorption coefficient, ε is the molar extinction coefficient and C is the concentration of the absorbing species. If we integrate this expression, we obtain:-

$$A = -\ln\left\{\frac{I}{I_0}\right\} = \int_{-L}^{L} \varepsilon CI.dz \qquad (18)$$

where A is the absorbance, I_0 is the intensity of the incident radiation, I is the intensity of the transmitted light and 2L is the thickness over which the absorbing group is present.

The absorbance (A), given in Equation 18 is analogous to the mass uptake in Equation 17, as it involves an integration of the concentration profile over the film thickness. Using transmission spectroscopy to measure the sorption kinetics with Equation 18 will suffer from a similar disadvantage to that encountered with the so-called 'Pat and Weigh' technique, which is a widely used method for determining diffusion kinetics. Both require the polymer film to be immersed in a penetrant bath, with the measurements being taken after removal from the bath and blotting to remove excess penetrant. Obviously, if the film is rather thin, or the diffusion coefficient too high, significant amounts of penetrant will desorb during the time it is not immersed. Although this can be remedied by using a thicker sample, the increased experimental time, plus the repeated handling of the sample means the technique is far from desirable, and can, by no means, be described as in situ.

The very nature of the ATR experiment, however, allows the determination of the diffusion kinetics while the film is in direct contact with the penetrant. As described in

Chapter Two, Section 2.6.2, the ATR experiment is possible by virtue of the so-called evanescent wave, which decays exponentially with distance into the film, away from the film/ATR crystal interface, the decay being given by[115,116]:-

$$E = E_0.\exp(-\gamma z) \qquad (19)$$

where E_0 is the electric field strength at the interface, and γ is defined as the reciprocal of the penetration depth, and is the distance to which the evanescent field decays to 1/e of its value at the interface. In terms of refractive indices, wavelength (λ) and the angle of incidence (θ), γ is given by:-

$$\gamma = \frac{2n_2\pi\sqrt{\sin^2\theta - \left(\frac{n_1}{n_2}\right)^2}}{\lambda} \qquad (20)$$

where n_1 is the refractive index of the rarer medium and n_2 is the refractive index of the ATR crystal (propagating medium). To combine the evanescent field strength equation with the Beer-Lambert law, it is necessary to assume that only weak absorption occurs. Thus, we can write:-

$$\frac{I}{I_0} = e^{-A} \approx (1-A) \qquad (21)$$

or:-

$$dI = -I_0 dA \qquad (22)$$

If we thus substitute Equation 22 into the differential form of the Beer-Lambert law, Equation 16, and integrate, we obtain:-

$$A = \int_0^L \frac{\varepsilon.CI}{I_0}.dz \qquad (23)$$

In the ATR configuration, the penetrant enters the film only from one side, hence the integration from 0 to L. Since $I = E^2$, we can substitute the field strength of the evanescent wave (Equation 19) and rewrite the expression for multiple reflections, N, as:-

$$A = \int_0^L N_\varepsilon.CE_0^2.\exp(-2\gamma z).dz \qquad (24)$$

where $\varepsilon^* = \varepsilon / I_0$. Substituting Equation 12, the Fickian concentration profile, into Equation 24, and integrating, gives Equation 25.

$$\frac{A_t}{A_\infty} = 1 - \frac{8\gamma}{\pi[1-\exp(-2\gamma L)]} x \sum_{n=0}^{\infty}\left[\frac{\exp(g)[f\exp(-2\gamma L)+(-1)^n(2\gamma)]}{(2n+1)(4\gamma^2+f^2)}\right] \qquad (25)$$

where:-

$$g = \frac{-D(2n+1)^2 \pi^2 t}{4L^2} \qquad (26)$$

and:-

$$f = \frac{(2n+1)\pi}{2L} \qquad (27)$$

Equation 25 is analogous to the mass uptake expression, used in gravimetric sorption experiments (Equation 13), the notable difference being that the Fickian concentration profile is convoluted with the FT-IR ATR absorption equation before it is integrated. Furthermore, A_∞ represents the absorbance at equilibrium, and is analogous to M_∞.

Furthermore, Equation 25 represents an exact solution for FT-IR ATR absorption of a penetrant in a thin film. At Durham, computer software has been developed[117] which utilises these expressions to calculate diffusion coefficients, and this is utilised in Chapter 6.

References.

1/. N.E.Schlotter & P.Y.Furlan, Polymer, 33, 16, (1992), 3323.
2/. R.W.Korsmeyer, S.R.Lustig & Nikolaus A.Peppas, J.Polym.Sci., Polymer Physics Edition, 24, (1986), 395.
3/. "Polymer Permeability", Ed. J.Comyn, Chapter 1, Elsevier Applied Science Publishers, London and New York.
4/. J.S.Chiou, Y.Maeda & D.T.Paul, J.Appl.Polym.Sci., 30, (1985), 4019.
5/. G.S.Hartley, Trans.Faraday Soc., 45, (1949), 820.
6/. N.L.Thomas & A.H.Windle, Polymer, 18, (1977), 1195.
7/. N.L.Thomas & A.H.Windle, Polymer, 19, (1978), 255.
8/. J.Klier & N.A.Peppas, Polym.Bull., 16, (1986), 359.
9/. P.J.Mills & E.J.Kramer, J.Mater.Sci., 21, (1986), 4151.
10/. T.Alfrey, Chem.Eng.News, 43, 41, (1965), 64.
11/. T.Alfrey Jr., E.F.Gurnee & W.G.Lloyd, J.Polym.Sci.;Part C, 12, (1966), 249.
12/. A.G.Thomas & K.Muniandy, Polymer, 28, (1987), 408.
13/. K.Tonyali, C.E.Rogers & H.R.Brown, Polymer, 28, (1987), 1472.
14/. G.S. Park, Trans. Faraday Soc., 48, (1951), 11.
15/. J.Crank, J.Polym.Sci., 11, (1953), 151.
16/. F.A.Long & D.Richman, J.Am.Chem.Soc., 82, (1960), 513.
17/. C.Y.Hui, K.C.Wu, R.C.Lasky & E.J.Kramer, J.App.Phys., 61, (1987), 5129.
18/. L.Mandelkern & F.A.Long, J.Polym.Sci., 6, (1951), 457.
19/. A.Peterlin, Polym.Lett., 3, (1965), 1083.
20/. A.S.Michaels, H.J.Bixler & H.B.Hopfenberg, J.App.Polym.Sci., 12, (1968), 991.
21/. J.L.Garcia-Fierro & J.V.Aleman, Eur.Polym.J., 21, (1985), 753.
22/. J.R.Scherer, G.F.Bailey, S.Kint, R.Young, D.P.Malladi & B.Bolton, J.Phys.Chem., 89, (1985), 312.
23/. D.T.Turner, Polymer, 28, (1987), 293.
24/. C.Y.Hui, K.C.Wu, R..C.Lasky & E.J.Kramer, J.App.Phys., 61, (1987), 5137.
25/. R.W.Korsmeyer, E.Von Meerwell & N.A.Peppas, J.Polm.Sci., Polm.Phys.Edition, 24, (1986), 409.
26/. J.H.Petropoelos & P.P.Roussis, J.Membr.Sci., 3, (1978), 343.

27/. N.Thomas & A.H.Windle, Polymer, 21, (1980), 613.
28/. C.Gostoli & G.C.Sarti, Polym.Eng.Sci., 22, (1982), 1018.
29/. N.L.Thomas & A.H.Windle, Polymer, 23, (1982), 529.
30/. R.W.Korsmeyer & N.A.Peppas, Polym. News., 9, (1984), 359.
31/. H.B.Hopfenberg & H.L.Frisch, Polym.Lett., 7, (1969), 405.
32/. N.L.Thomas & A.H.Windle, Polymer, 22, (1981), 627.
33/. S.Prager & F.A.Long, J.Am.Chem.Soc., 73, (1951), 4072.
34/. R.J.Koles & F.A.Long, J.Am.Chem.Soc., 75, (1953), 6142.
35/. A.Aitken & R.M.Barrar, Trans.Faraday Soc., 51, (1955), 116.
36/. M.J.Hayes & G.S.Park, Trans.Faraday Soc., 51, (1955), 1134.
37/. H.Fujita, A.Kishimoto & K.Matsumoto, Trans.Faraday Soc., 56, (1960), 424.
38/. P.F.Green, P.J.Mills, C.J.Palmstrom, J.W.Mayer & E.J.Kramer, Phys.Rev.Lett., 53, (1984), 2145.
39/. E.J.Kramer, P.Green & C.J.Palmstrom, Polymer, 25, (1984), 473.
40/. P.J.Mills, P.F.Green, C.J.Palmstrom, J.W.Mayer & E.J.Kramer, App.Phys.Lett., 45, (1984), 957.
41/. P.F.Green, C.J.Palmstrom, J.W.Mayer & E.J.Kramer, Macromolecules, 18, (1985), 501.
42/. J.Koszinowki, J.App.Polym.Sci., 32, (1986), 4765.
43/. E.Sada & H.Kumazawa, J.App.Polym.Sci., 32, (1986), 5567.
44/. Y.Iwai, M.Kohno, T.Akiyama & Y.Arai, Polym.Eng.Sci., 27, (1987), 837.
45/. T.Ito, J.Seta & H.Urakawa, Coll.Polym.Sci., 265, (1987), 557.
46/. S.Kalachandra & D.T.Turner, Polymer, 28, (1987), 1749.
47/. C.A.Pawlisch, A.Macris & R.L.Laurence, Macromolecules, 20, (1987), 1564.
48/. D.T.Turner & A.K.Abell, Polymer, 28, (1987), 297.
49/. T.G.Ryan & P.D.Calvert, Polymer, 23, (1982), 877.
50/. P.J.Mills, C.J.Palmstrom & E.J.Kramer, J.Mat.Sci., 21, 5, (1986), 1479.
51/. J.F.Romanelli, J.W.Mayer, E.J.Kramer & T.P.Russell, J.Polym.Sci., Part B-Polymer Physics, 24, 2, (1986), 263.
52/. M.Johnson & J.F.Westlake, J.App.Polym.Sci., 19, (1975), 1745.
53/. J.F.Westlake & M.Johnson, J.App.Polym.Sci., 19, (1975), 319.
54/. C.K.Rhee & J.D.Ferry, J.App.Polym.Sci., 21, (1977), 773.
55/. G.S.Park & T.V.Hoang, Eur.Polym.J., 15, (1979), 817.
56/. R.S.Payne, A.S.Clough, P.Murphy & P.J.Mills, Nuclear Instruments & Methods in Physics Research, Section B-Beam Interactions with Materials and Atoms, 42, 1, (1989), 130.
57/. J.Manijkow, J.S.Papanu, D.S.Soong, D.W.Hess & A.T.Bell, J.App.Phys., 62, (1987), 682.
58/. H.M.Tong, K.L.Saenger & C.J.Durning, J.Polm.Sci., Part B-Polym.Phys., 27, (1989), 689.
59/. O.T.Aboul-Nasr & R.Y.M.Huang, J.App.Polym.Sci., 23, (1979), 1819.
60/. M.T.Aronhime, S.Neumann & G.Marom, J.Mater.Sci., 22, (1987), 2435.
61/. A.W.Czanderna & T.M.Thomas, J.Vac.Sci.Technol., 5, (1987), 2412.
62/. D.Vesely & S.J.Zhang, Procs. of 3rd Int. Conf. on Diffusion in Polymers, York, (1991), PRI publishers, page 2.
63/. M.J.Smith & N.A.Peppas, Polymer, 26, April, (1985), 569.
64/. L.Y.Shieh & N.A.Peppas, J.App.Polym.Sci., 42, 6, (1991), 1579.
65/. J.L.Koenig, Appl.Spectrosc., 43, (1989), 1117.
66/. L.A.Weisenberger & J.L.Koenig, Macromolecules, 23, (1990), 2445.
67/. L.A.Weisenberger & J.L.Koenig, Macromolecules, 23, (1990), 2454.
68/. S.R.Smith & J.L.Koenig, Macromolecules, 24, (1991), 3496.
69/. R.A.Grinsted & J.L.Koenig, Macromolecules, 25, (1992), 1229.
70/. R.A.Grinsted, L.Clark & J.L.Koenig, Macromolecules, 25, (1992), 1235.
71/. W.P.Rothwell & P.P.Gentempo, Bruker Rep., 1, (1985), 46.
72/. C.Chang & R.A.Komoroski, Macromolecules, 22, (1989), 600.
73/. B.Blumich, P.Blumler, E.Gunther & G.Schauss, Bruker Rep., 2, (1990), 22.
74/. P.Maffei, L.Kiéné & D.Canet, Macromolecules, 25, (1992), 7114.
75/. P.J.Mills, P.F.Green, C.J.Palmstrom, E.J.Kramer & J.W.Meyer, App.Phys.Lett., 45, 9, (1984), 957.
76/. P.F.Green, Ph.D. Thesis, Cornell University, 1985.
77/. P.F.Green, P.J.Mills, E.J.Kramer, Polymer, 27, (1986), 1063.
78/. P.F.Green & E.J.Kramer, Macromolecules, 19, (1986), 1108.
79/. P.J.Mills, P.F.Green, C.J.Palmstrom, J.W.Mayer & E.J.Kramer, J.Polm.Phys., Part B - Polymer Physics, 24, 1, (1986), 1-9.

80/. P.F.Green, Macromolecules, 24, (1991), 3373.
81/. P.F.Green, D.B.Adolf & L.R.Gilliom, Macromolecules, 24, (1991), 3373.
82/. R.J.Composto, J.W.Mayer, E.J.Kramer & D.M.White, Phys.Rev.Lett., 57, (1986), 1312.
83/. R.J.Composto, Ph.D. Thesis, Cornell University, 1987.
84/. R.J.Composto, E.J.Kramer & D.M.White, Macromolecules, 21, (1988), 2580.
85/. P.F.Nealey, R.E.Cohn & A.S.Argon, Macromolecules, 26, (1993), 1287.
86/. H.Nishide, H.Kawakami, T.Suzuki, Y.Azechi, Y.Soejima & E.Tsuchida, Macromolecules, 24, (1991), 6306.
87/. Y.Kaptan & O.Pekcan, J.App.Polym.Sci., 37, (1989), 2577.
88/. Y.Kaptan, O.Pekcan & O.Guven, J.App.Polym.Sci., 44, (1992), 1595.
89/. W.H.Yang, V.F.Smolen & N.A.Peppas, J.Memb.Sci., 9, (1981), 53.
90/. D.Li, S.Zhu & A.E.Hamielec, Polymer, 34, 7, (1993), 1383.
91/. F.P.Price, P.T.Gilmore, E.L.Thomas & R.L.Laurence, J.Polym.Sci., Polym. Symp., 63, (1978), 33.
92/. P.T.Gilmore, R.Falabella & R.L.Laurence, Macromolecules, 13, (1980), 880.
93/. A.Parker & D.Vesely, Inst.Phys.Conf.Ser., 68, (1984), 11.
94/. D.Vesely, Ultramicroscopy, 14, (1984), 279.
95/. M.A.Parker & D.Vesely, J.Polym.Sci., Part B - Poly.Phys., 24, (1986), 1869.
96/. M.S.High, P.C.Painter & M.M.Coleman, Macromolecules, 25, 2, (1992), 797.
97/. G.Boven, R.H.G.Brinkhuis, E.J.Vorenkamp & A.Schouten, Macromolecules, 24, (1991), 967.
98/. E.J.Vorenkamp, J.van Ruiten, F.A.Kroesen, J.G.Meyer, J.G.Hoekstra & G.Challa, Polym.Commun., 24, (1990), 325.
99/. N.Schlotter, Abs.Paps.Am.Chem.Soc., 202, Aug, (1991), 332.
100/. N.E.Schlotter & P.Y.Furlan, Vib.Spectrosc., 3, (1992), 147.
101/. J.G.Van Alsten & S.R.Lustig, Macromolecules, 25, 19, (1992), 5069.
102/. P.Y.Furlan, Macromolecules, 25, (1992), 6516.
103/. E.Jabbari & N.A.Peppas, Macromolecules, 26, 9, (1993), 2175.
104/. G.T.Fieldson & T.A.Barbari, Polymer, 34, 6, (1993), 1146.
105/. M.W.O'Han & J.L.Koenig, Appl.Spectrosc., 40, (1986), 994.
106/. J.C.Donini & K.H.Michaelian, Infrared Phys., 24, (1984), 157.
107/. D.R.Miller, O.H.Han & P.W.Bohn, Appl.Spectrosc., 41, (1987), 245.
108/. D.R.Miller, O.H.Han & P.W.Bohn, Appl.Spectrosc., 41, (1987), 249.
109/. P.W.Bohn & N.F.Fell, Chemical, Biochemical & Environmental Applications of Fibres, S.P.I.E., 990, Society of Photo-Optical Instrumentation Engineers, Bellingham, Washington, (1988), 130.
110/. D.R.Miller & P.W.Bohn, Anal.Chem., 60, (1988), 407.
111/. N.F.Fell, Jr & P.W.Bohn, Appl.Spectrosc., 45, 7, (1991), 1085.
112/. N.E.Schlotter, J.Phys.Chem., 94, (1990), 1692.
113/. J.Crank, "The Mathematics of Diffusion", 2nd Edition, Oxford University Press, London, 1975.
114/. J.M.Vergnaud, "Liquid Transport Processes in Polymeric Materials: Modelling and Industrial Applications", Prentice-Hall, Englewood Cliffs, 1991.
115/. N.J.Harrick, J.Opt.Soc.Am., 55, (1965), 851.
116/. H.G.Tompkins, Appl.Spectrosc., 28, (1974), 335.
117/. M.R.Pereira, University of Durham, 1992.

Chapter Four - Film Preparation

Chapter Four - Film Preparation.

4.1 Introduction.

The need to produce films of known, and controlled, thickness and of a certain quality was of paramount importance to this project. Films of good optical quality and fairly uniform thickness are required for successful waveguide Raman experiments, and factors such as solvent quality, solvent blends and drying conditions can greatly affect the final film quality. On the other hand, film optical quality is not of such importance for actual practical performance of FT-IR ATR experiments (although obviously it is if fully quantitative measurements are required). However, it was found that film quality dictated the nature of the diffusion process which was subsequently studied in this project. Again solvent quality and blend were the key issues affecting this. In this short chapter, the mechanics of film preparation and parameter determination (film thickness etc.) are considered first, followed by two sections focusing on the intricacies of film preparation required for successful manipulation of the two spectroscopic techniques used.

4.2 The Mechanics of Film Preparation.

There are many different techniques which can be used for the preparation of thin polymer film, which vary in complexity depending on the accuracy of film thickness and uniformity required. The four readily accessible methods are horizontal flow, doctor blading, spin coating and dipping.

Horizontal Flow:- This involves placing a small amount of polymer solution at one end of the required substrate and then, by placing the substrate at an angle, allowing it to run down, under the influence of gravity. It is a good method for purely qualitative work, as it is quick and requires no apparatus, and provides a method of coating for just one side of the substrate. Its major disadvantage, however, is the lack of control of film thickness. Thus this method is not suitable for quantitative analysis.

Doctor Blading:- This method is similar to the horizontal flow technique, but rather than allowing the solution to run down, it is spread, using a knife or sharp, flat edge, along the substrate. Again this is a suitable method for qualitative studies, but again it lacks the control parameters necessary for quantitative work. It also introduces the added complication of ridges, which are formed when the blade is not drawn smoothly across the surface, which, depending on the extent of the irregularities, could pose serious problems to successful waveguiding in the film.

Spin Coating:- This technique involves dropping small amounts of a polymer solution on to a quickly revolving substrate, thus spreading the solution out into a film by the centrifugal force. Although this method is regularly used for producing good quality, smooth and uniform films for waveguiding work, it can tend to produce films which are of excellent quality in the centre, but which are not of such good quality away from this central region. Several attempts were tried using this method during a previous project at Durham[1], but the films produced were never deemed satisfactory, and were found to be incapable of producing a waveguide. However, since this technique was never employed during the course of this project, due to difficulties obtaining access to

relevant equipment, and considering certain complications arising from the dipping procedure, described below, further investigations into its possible utilisation could be useful.

Dipping:- The simple technique found to be most satisfactory for the production of thin films, for surface experiments, was a simple dipping device. Figure 4.1 shows a diagram of this piece of apparatus, which is essentially a sample holder, in the form of a simple clip, attached to a Teflon block which is driven by a screw and thread attached to a simple variable speed motor.

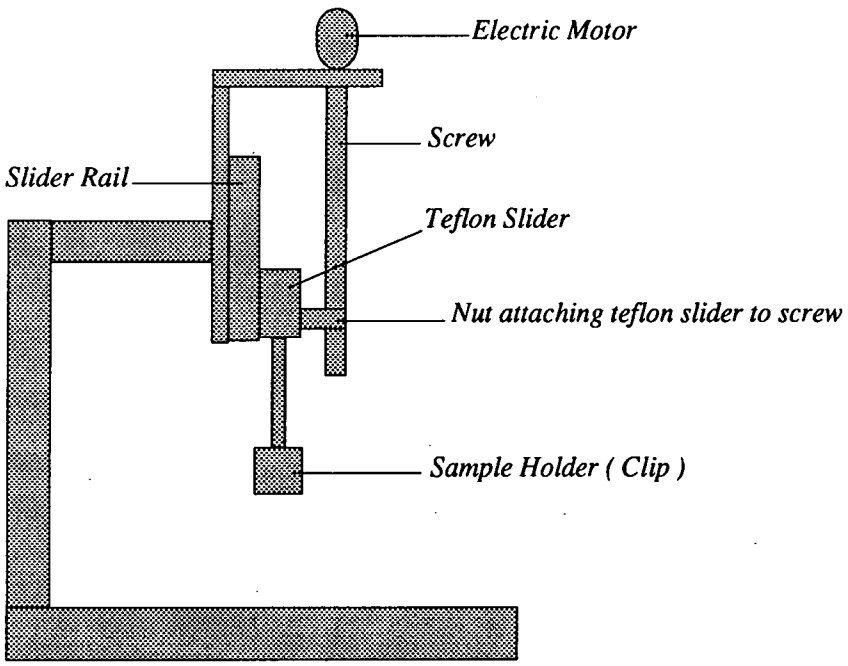

Figure 4.1

The control of the electric motor is achieved by use of a small adjustable switch. Unfortunately, the settings are in no way related to the speed of the motor, hence a graph, shown in Figure 4.2, was constructed to relate control setting to dipping speed, measured in millimetres per second. Most dipping experiments described in the course of this project were conducted at control setting 5.5 (referred to as Dipping Speed in this report), which corresponded to an actual speed of 4.8 mm sec^{-1}. Obviously, the dipping method produces a film on both sides of the substrate, whereas the three other methods described above will produce a film only on one side of the substrate.

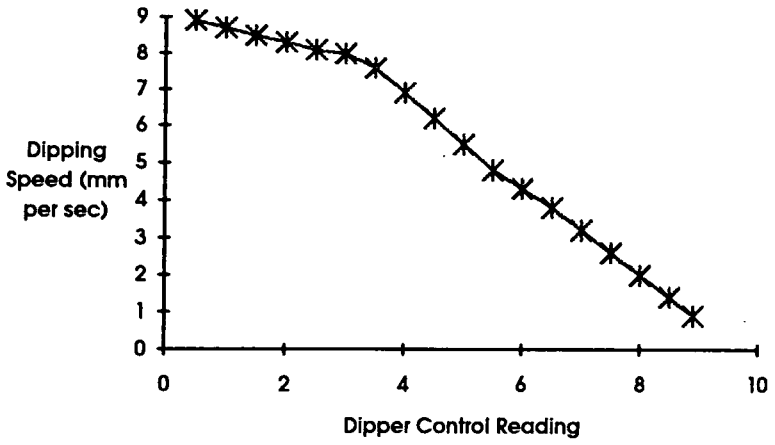

Figure 4.2 - Dipper Control Setting vs Dipping Speed

Two such dipping systems have been built in Durham, being first developed in the Department of Physics, but modified by us to include a greater range of dipping speeds and smoother travel of the Teflon block, which is attached to the substrate holder. The latter modification is very important to the production of satisfactory films, as variations in dipping speed can introduce irregularities into the film, similar to those observed from a poor doctor blading process, mentioned above. The key to the smooth travel of Teflon block, lies in the actual screw, which must be straight and as free from kinks as reasonably and economically as possible. Without a specially constructed precision thread, however, a small amount of irregularity will be inevitably present, but minimum movement will cause only negligible ridging in the film, which, we have found, does not significantly impede the waveguiding capability, which has been reported[2] as being sensitive to such fluctuations.

One notable drawback encountered with the dipping technique was that films produced usually had a gradient extending away from the bare, uncoated substrate towards the coated end. This is almost certainly due to the actual dipping geometry, which will allow the still mobile polymer solution to run down the substrate, under the influence of gravity. Various attempts were made to minimise this effect by removing the substrate at the earliest possible moment, and suspending the substrate horizontally (being careful not to disturb the deposited film !). However, the effect of this was found to be negligible, when such films were compared to films dried vertically, by simply propping them up. Hence, it has to be concluded that this is a flaw in the dipping process which must be accepted, and certainly paves the way for a further examination of the use of spin coating for film preparation. Figure 4.6 below shows an alpha-step where this sloping phenomena is clearly demonstrated.

Samples for waveguiding purposes were always deposited on glass or quartz substrates of similar dimensions to those of microscope slides. It was thus necessary to prepare polymer solutions in vessels, large enough to accommodate such dimensions. Such vessels were generally quite large diameter jars, which thus necessitated preparation of considerable volumes, usually up to 100 mls, of polymer solution to obtain a film of reasonable length. This situation is clearly inadequate, requiring relatively large quantities of the polymer, which in many cases is simply not available.

Hence, a Teflon boat was designed and built, which consisted simply of a block of Teflon, which had a slit drilled in it to accommodate the slide. Thus, much smaller quantities, usually of the order of about 5 mls, of polymer solution could be used to produce films suitable for waveguiding purposes. Figure 4.3 shows a diagram of this boat.

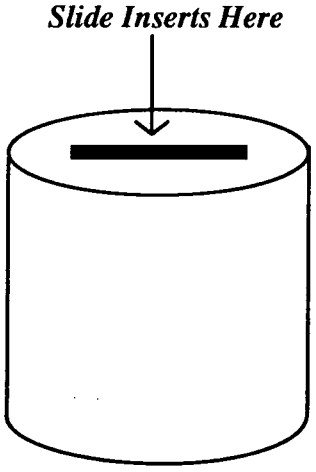

Figure 4.3 - The Teflon Boat

An important film parameter in this project was film thickness. In the case of films dipped using the above apparatus, this can be achieved in one of two ways, either by varying dipping speed or by changing the concentration of the polymer solution. We have actually found that differing solution concentration, and hence viscosity, is a far more effective method of varying the film thickness. This effect was also noted by Schlotter[3]. Figure 4.4 shows a graph of film thickness versus solution concentration, measured at a constant dipping speed of 5.5 (4.8 mm sec^{-1}), and Figure 4.5 shows a similar graph for film thickness versus dipping speed for a constant solution concentration of 44%, by weight. Both sets of data were obtained using solutions of Epikote[4] 1001 plus crosslinking agent in a solvent blend of 1:1, xylene:butan-1-ol, with film thicknesses determined using an alpha-stepper, detailed later.

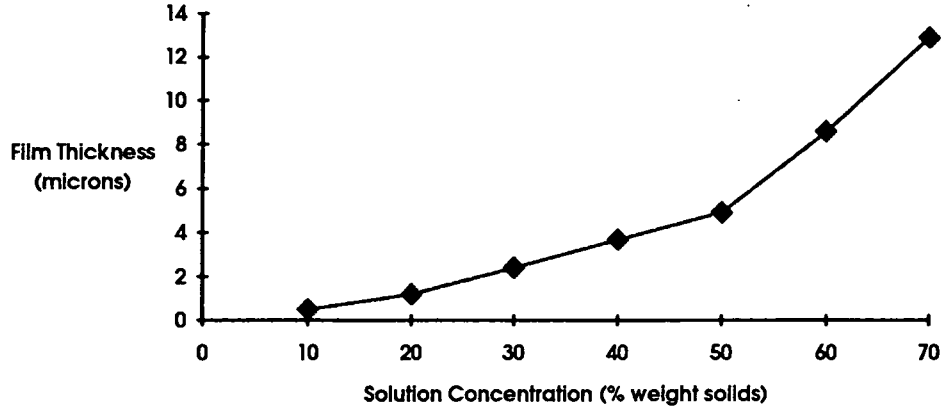

Figure 4.4 - Solution Concentration vs Film Thickness

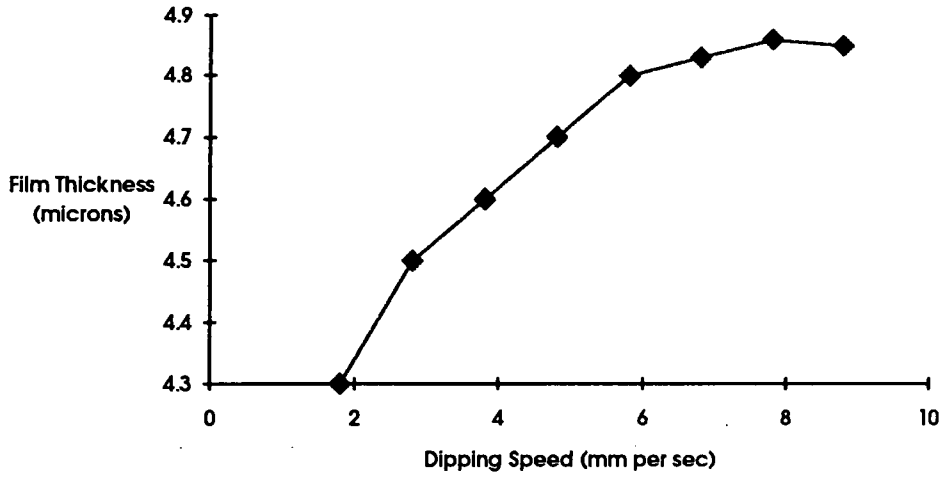

Figure 4.5 - Dipping Speed vs Film Thickness

4.3 - Film Thickness Determination.

This also can be achieved in a number of different ways, but the two methods investigated during the course of this project were alpha-stepping and off-line waveguiding, the latter method being detailed in the section on waveguiding. The alpha-stepper, however, relies on the mechanical process of dragging a stylus over the edge of, or a break in, the film. The instrument used during the course of this project was a Tencor Instrument, alpha-step 200, which has a dynamic range (sensitivity of film thickness) from 5 Å to 3,200 Å. The machine has a built in computer, which analyses the trace to form an output, such as that shown in Figure 4.6.

The software allows the thickness of the film to be determined, relative to the substrate, at any point along the measured portion of the film. There are various different scanning parameters, such as length of scan (up to a maximum of 1000 μm), stylus weight and direction of scan. Scans taken during the course of this project were always obtained using a stylus weight of 13 mg, and a 1000 μm scan, which commenced on the bare substrate and proceeded into the film. The alternative to using a length of scan parameter was physically to remove some sections of the film using a scalpel and scan over a region of film incorporating this break. This, however, was found to introduce two serious sources of inaccuracy to the measurements.

The first of these inaccuracies arose from the fact that most of the ATR work was carried out using epoxy resins on a zinc-selenide crystal. These resins firmly adhere to their substrate, and thus, even exercising the greatest of care, when removed, damage was sustained to the rather fragile crystal. This was obviously undesirable, because not only did quite significant damage to the expensive crystal occur, but an inaccurate value for film thickness was obtained, because of 'gouging' of the crystal. The second inaccuracy arises from the sheer area of film examined. When a measurement obtained using a shorter scan distance is compared with one obtained at the maximum distance (1000 μm), the seemingly flat and even film seen in the shorter scan is revealed as being undulating, and far from flat, as shown in Figure 4.6. Hence, by using several longer scan distances, it was possible to obtain a good idea of the errors associated

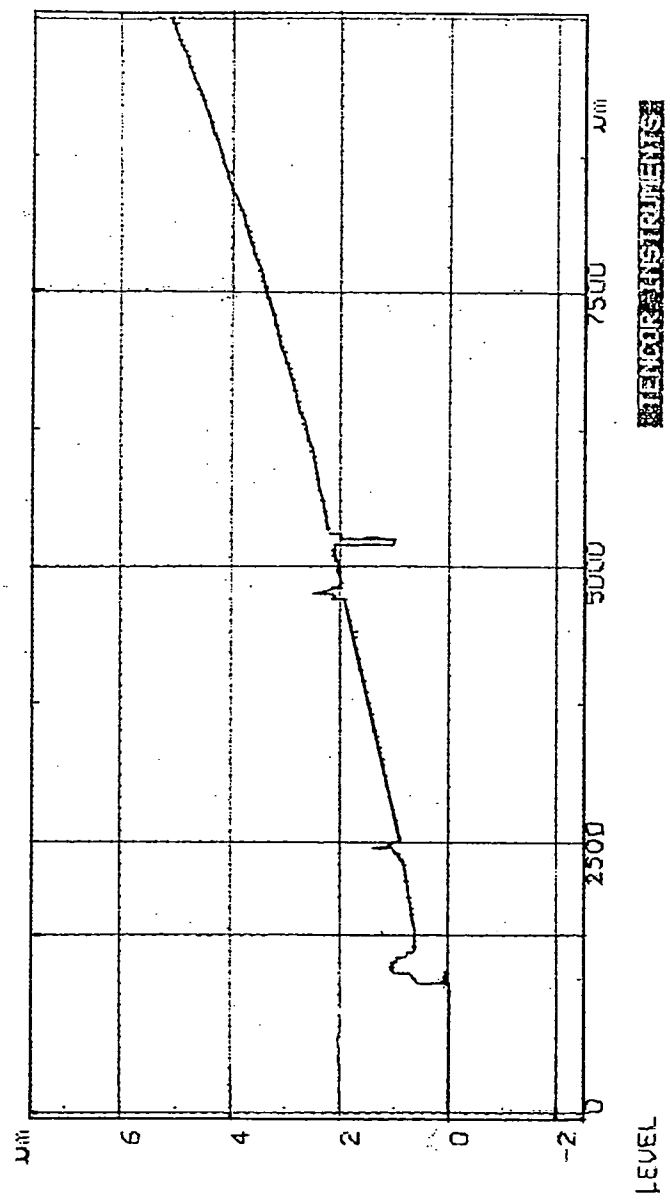

Figure 4.6 - A Typical Alpha-Step

with the film thickness, and these errors are incorporated into film thicknesses given in this thesis.

The alpha-stepping method was the only method employed for film thickness determination in the course of this project, as it is felt by the author that the waveguiding method introduces an error, not discussed in previous work, which will be discussed further at the relevant section of this Chapter.

4.4 Films for Spectroscopic Experiments.

4.4.1 - Waveguiding Experiments[1,2].

In waveguiding experiments, the propagating wave actually travels within the polymeric film, so it can be appreciated that film quality is of optimum importance. It has been reported[1,2] that one of the major restrictions on the waveguiding technique is the film quality. Rabolt and Swalen[2] mention that films containing dust, cracks and/or domains with dimensions of the order of the wavelength of visible light will scatter rather than guide, and that problems also arise when using films which absorb in the visible region of the spectrum. During the course of this project, we have found that the complications associated with obtaining a film of sufficient quality for waveguiding experiments to be successfully conducted are considerable, and often unique to particular polymers and solvents. In the remainder of this section, we will consider the general difficulties encountered, and, where applicable, the remedy. Specific problems associated with individual systems will be considered at the relevant point of Chapter 5.

4.4.1.1 - Solvent Effects.

It has been found that choice of solvent and solvent quality is one of the most important limiting factors for good film quality production. Generally, it has been found that the use of solvents of too high or too low volatility produce problems with the resulting films. A solvent of high volatility at room temperature, such as acetone or methanol, tends to produce a cloudy film, which is believed to be caused by the rapid evaporation of the solvent from the polymer film, with a resulting formation of microcrystallites. The use of a solvent with a lower volatility appears to eradicate this problem. Although Rabolt and Swalen[2] hint that it may be possible to waveguide in such cloudy systems, no evidence to support this has been found in this project.

On the other hand, if a solvent of very low volatility, for example water, is used at room temperature, then the films produced tend to contain a marked raised ridge along the so-called long axis of the film, which is defined in Figure 4.7.

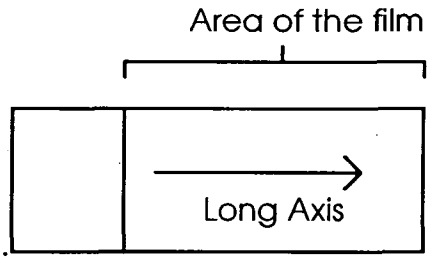

Figure 4.7 - The Long Axis of a Film.

Such ridging makes waveguiding difficult, mainly because the presence of the ridge prevents good production of a coupling spot for the laser (see later), but also because of the gross lack of uniformity in the film, which is reported as having a serious detrimental effect on waveguiding[1,2]. It has been discovered that careful elevation of drying temperature alleviates this problem, but that too enthusiastic heating produces cloudy films, due to reasons similar to those discussed earlier.

In the preparation of laminate systems (in this project, the term laminate refers to a bilayer system) by solution deposition, the problems associated with solvents is doubled, and further complicated by the need for a solvent for the upper layer which does not disturb (especially dissolve) the lower layer. Different problems were encountered for the various systems examined, and they will thus be discussed at the relevant point in Chapter 5.

4.4.1.2 - Other Factors Affecting Film Quality.

As mentioned by Rabolt and Swalen[2], the inclusion of foreign particles within films for waveguiding purposes presents further serious problems to the successful execution of such experiments. It has been observed that the presence of foreign material, such as atmospheric dust, will provide a scattering centre, which, if in direct line with the waveguide streak (usually a thin bright line of light, traversing the long axis of the film (Figure 4.7)), will cause this streak to 'fan out', which causes a severe loss of scattering volume, hence reducing the signal to noise (S/N) ratio. Such scattering centres can render a film useless for waveguide Raman experiments.

The actual inclusion of such foreign particles can arise from any of the stages associated with film production. They are present in the solvents used, especially if the solvent is of industrial origin, they are present in the atmosphere, and, of course and probably most importantly, they are present in the polymer solid. To combat their inclusion, the use of filtration devices such as a micropore is encouraged. It was found that the use of a 10 μm pore size was sufficient, as this appeared to remove particles from solvents successfully, but also allowed filtration of more dilute polymer solutions. However, more concentrated polymer solutions, required for thicker films, generally would not pass through the filter, and thus particle-free solvents and, if possible, high purity-polymers were used. When the polymers were dried, it was found to be advantageous to store the samples in a sealed desiccator, to prevent airborne dust settling on the 'wet' films.

Such precautions were in the main fairly successful, but even with them, the inclusion of foreign matter in polymer films proved to be a major bane of the waveguide spectroscopist's life!

4.4.2 - ATR Experiments.

Film quality, as mentioned earlier, is not as important to the actual practical performance of FT-IR ATR experiments, although, of course, it is of paramount importance if accurate quantitative measurements are required. The actual propagating wave travels within the high refractive index ATR prism, rather than the film itself, and sampling occurs via the penetration of the evanescent field into the film. However, in the course of this project, it was found that the diffusion processes studied were radically affected by film quality.

4.5 - Differences in Epoxy Resin Film Quality.

In the course of the project, diffusion processes occurring in epoxy resin systems (see Chapter 1, Reactions 2-4 for chemical structure) were monitored by ATR spectroscopy. The diffusion experiments are described in detail in Chapter 6, but here the different film qualities referred to are discussed in detail. Again, the dominant factor which determined the film quality produced was the solvent blend and quality. The details of this solvent dependence is discussed later, but first a description of the structural differences between the two types is presented.

A poor-quality film is one which is dull in appearance and has a rough surface. Figure 4.8 shows an alpha-step profile of such a film, and it can be easily seen that large peaks and troughs exist on a macroscopic scale. Figure 4.9 shows a scanning electron micrograph (S.E.M.) of such a film, taken using the S.E.M. facility at Courtaulds Coatings plc. This micrograph shows the microscopic structure of the embedded 'particles' which account for the irregularities. Both micrographs can be seen at the end of this Chapter.

On the other hand, a good-quality film is generally of shiny appearance and has a smooth surface. Figure 4.10 shows the alpha-step profile of such a good film, and although there are undulations, they are generally not as localised. Any small defects probably arise from the inclusion of foreign particles in the film, such as atmospheric dust, and impurities present in both raw polymer and solvent.

The slope of the deposited film (discussed above) can be clearly seen in this alpha-step. Error values quoted throughout this work, when dealing with waveguiding experiments and good-quality films in the ATR work, arise, in the main, from this effect, which was discussed earlier. Figure 4.11 shows an SEM picture of a good-quality film. The fine details, which appear to be small pores, are in fact due to the film beginning to degrade under the harsh conditions required for high magnification, using an electron beam.

It is important to note that the type of film produced may be predicted with reasonable accuracy from the type of polymer solution used to deposit the film. A poor-quality film is usually produced from a cloudy solution, whereas a good-quality film is

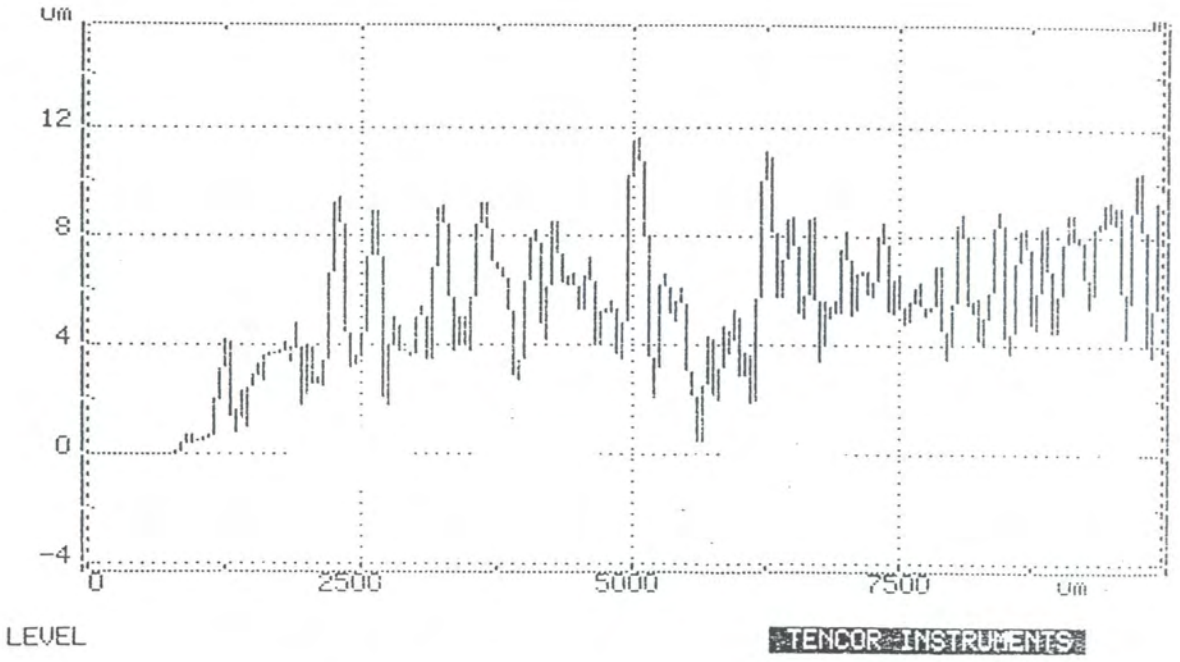

Figure 4.8 - An Alpha-Step of a Poor Quality Film

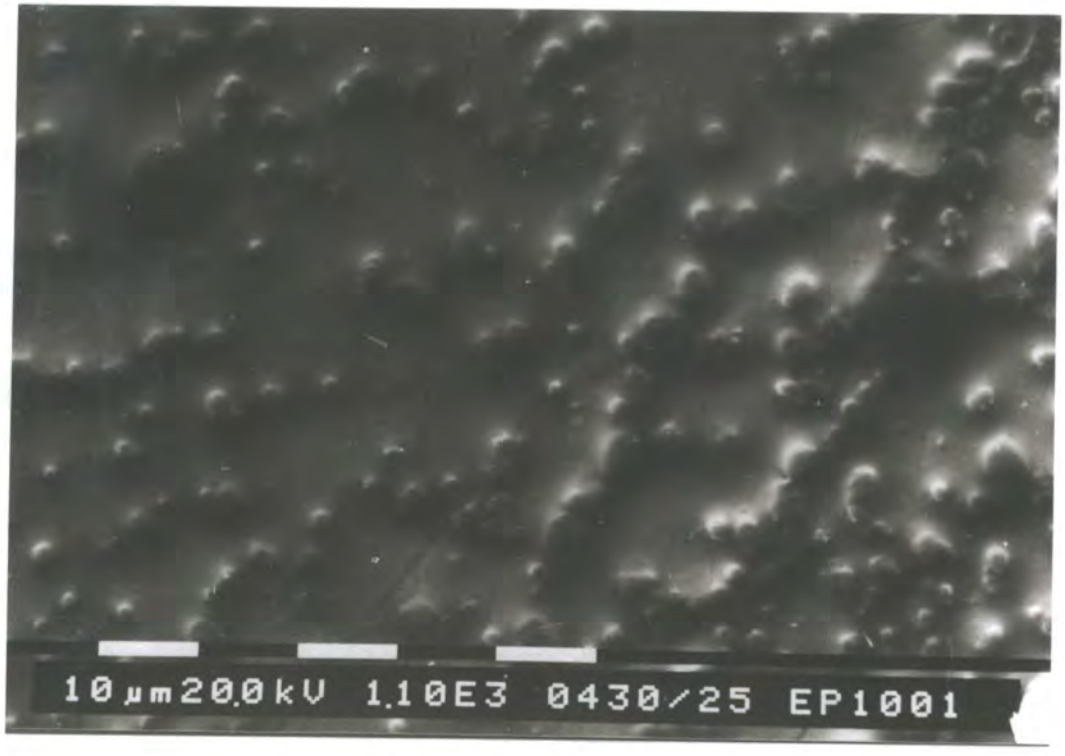

Figure 4.9 - An SEM Micrograph of a Poor Quality Film

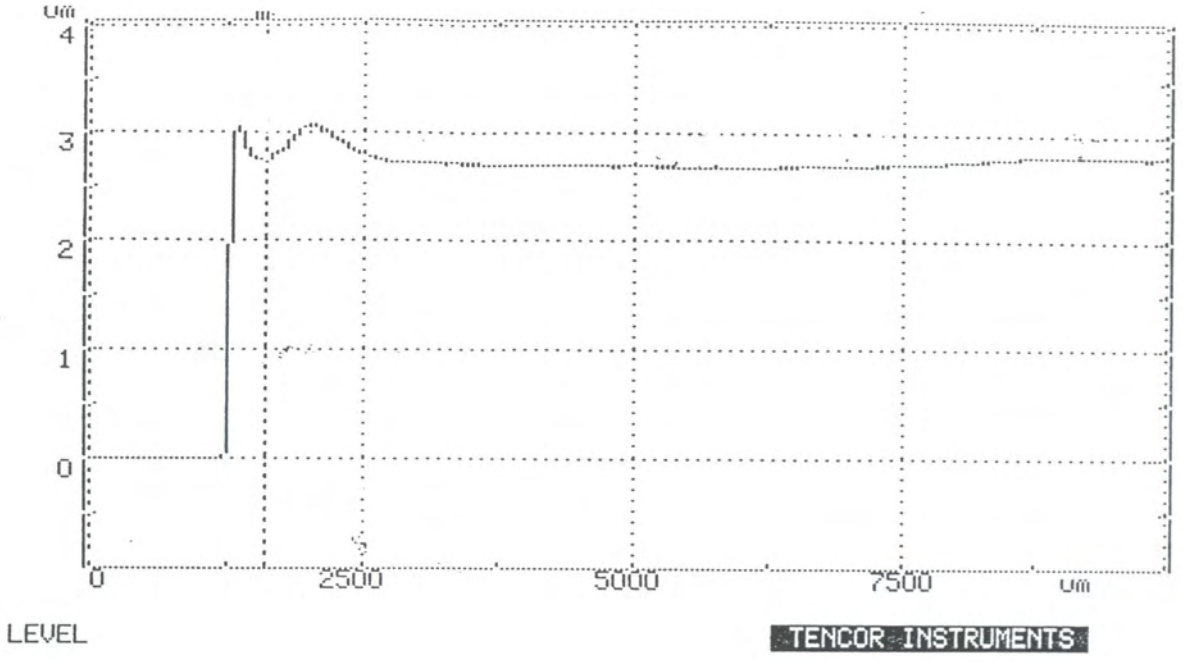

Figure 4.10 - An Alpha-Step of a Good Quality Film

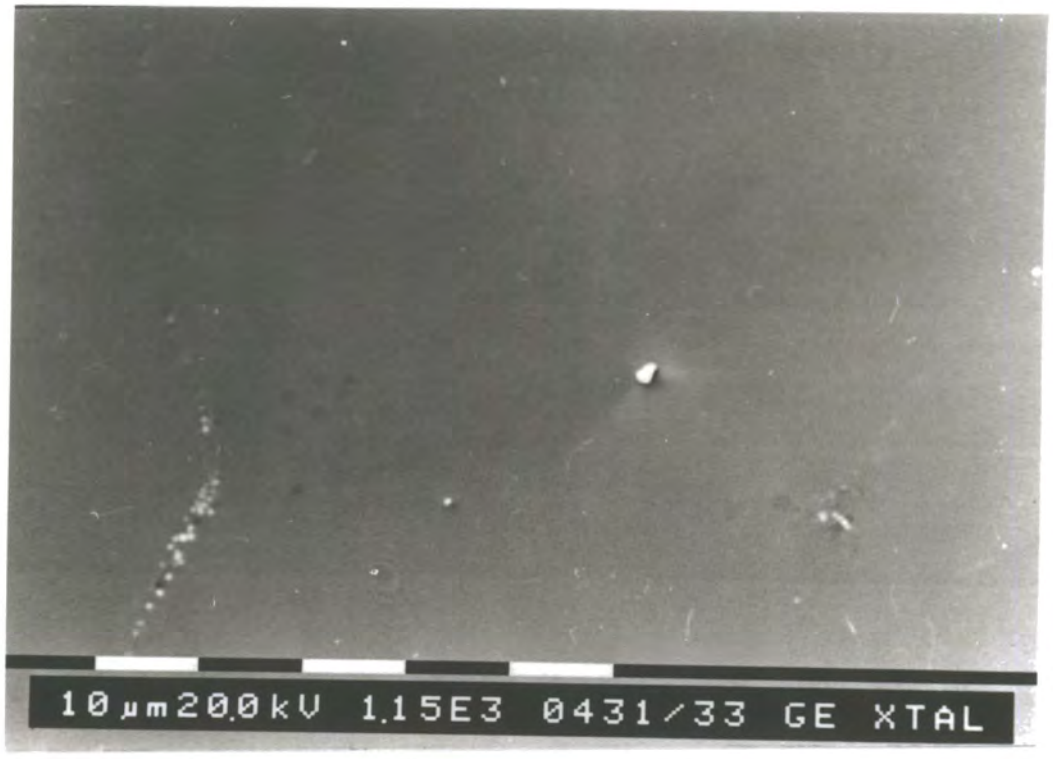

Figure 4.11 - An SEM Micrograph of a Good Quality Film

produced from a clear solution. The factor determining the quality was found to be the dissolution of the crosslinking agent, KH92 (described in Chapter 1, reaction 3) which is essentially an epoxy resin, tipped with diethylene triamine at each end of the molecule. This was found to be only sparingly soluble in both butan-1-ol and xylene, but satisfactory dissolution was achieved in all cases upon the addition of approximately 20% by volume aliquots of methanol. This also suggests that poor-quality films would be crosslinked to a lower extent than good-quality films, and would thus possess quite different properties. This important consideration is discussed further in Chapters 6 and 7, where it can be properly evaluated in relation to experimental observations.

Solution appearance was thus found to be directly related to the solvent blend and quality. Initial experiments were conducted using industrial grade solvents, and the original blend used for the production of films for ATR experiments was a mixture of 1 part xylene and 1 part butan-1-ol. These films were hence of poor quality, containing a high proportion of undissolved KH92. The decision to attempt to study similar systems using waveguiding brought the need for a change in solvent blend, as films produced using the original system were cloudy, and hence would not support a waveguide. It was consequently discovered that the use of a blend of 2 parts xylene, 2 parts butan-1-ol and 1 part methanol (all industrial solvents), produced films of a good enough quality to support a waveguide, and were thus clear.

It was consequently decided that pure solvents should be used, in order to introduce a further element of control into the process. Subsequent work discovered that poor-quality films were produced only from xylene, after the mixture was stirred to encourage homogenisation. If stirring was not carried out, the KH92 and solvent simply would not mix, but once stirred, separation, and hence a reversion to the two separate phases, did not occur. The presence of butan-1-ol and/or methanol, in moderate excess (approximately 1 part xylene to 2.5 parts alcohol), however, was always found to produce a clear solution, and hence good-quality films. A blend of 2 parts xylene, 2 parts butan-1-ol and 1 part methanol also produced good-quality films, as in the low grade systems, but if a higher proportion of methanol was used, cloudy films were produced, probably due to high rate of solvent evaporation, similar to that described in the waveguiding section above.

The above factors affecting film quality can be thus summarised:-

1/. A poor-quality film is rough and dull, whereas a good-quality film is smooth and shiny.

2/. A poor-quality film has 'particles' of undissolved crosslinking agent present, whereas a good-quality film has no 'particles', as satisfactory dissolution of the crosslinker occurs.

3/. A poor-quality film is formed from a cloudy solution, in which the crosslinking agent, KH92, dissolves only sparingly, the undissolved proportion forming a suspension, whereas a good-quality film results from a clear solution, where satisfactory dissolution of the crosslinking agent is achieved.

4/. For *pure solvent systems*, a cloudy solution, and hence a poor-quality film, is formed from a solvent blend of low polarity, i.e. pure xylene, containing no methanol or butan-1-ol, the addition of which encourages satisfactory dissolution of the cross-linker, and hence a good-quality film. For an *industrial solvent system*, that is using the solvents provided by Courtaulds Coatings plc, a cloudy solution is formed from solvent blends containing only xylene and butan-1-ol, with the important controlling factor being the presence of methanol, which encourages satisfactory crosslinker dissolution, and hence clear solutions. The blend of xylene, butan-1-ol and mesitylene, similar to a system used on site at Courtaulds Coatings plc, produces a poor-quality film.

One final important point is that the solvent blend of xylene, butan-1-ol and Shellsol (a low-grade mesitylene) used at Courtaulds Coatings for several formulations of epoxy resins always produced, in the course of this project, films of poor quality, when used in conjunction with KH92. Hence, such systems used by Courtaulds will be of poor quality.

Thus, it has been proved that solvent composition and quality radically affect the final quality of the film. Many of the experiments described in this project, as discussed above, were conducted in an industrial environment, and were performed using the industrial, low-grade solvents used on site. Many of the solvents used by Courtaulds Coatings are of a startlingly low quality, examples being the acetone which is only partly immiscible with water. Hence, during a high proportion of the experiments described in this thesis, high-purity solvents were used wherever possible, but in the case of the epoxy resins used, in particular the solvents used to make up the resin, were of industrial origin. Attempts were made to make up a mixture using high-quality solvents, but the absence of high-powered mixing equipment at Durham prevented the preparation of these highly viscous materials.

References.

1/. N.M.Dixon, N.Everall & J.Yarwood, Unpublished work, 1989.
2/. J.F.Rabolt & J.D.Swalen, "Spectroscopy of Surfaces", Eds. R.J.H.Clark and R.E.Hester, J.Wiley and Sons, London, 1988, Chapter 1.
3/. N.E.Schlotter, J.Phys.Chem., 94, (1990), 1692.
4/. Shell brand-name.

Chapter Five - Experimental Waveguide Raman Spectroscopy

Chapter Five - Experimental Waveguide Raman Spectroscopy.

5.1 Introduction.

This chapter concentrates on all aspects of the waveguide Raman spectroscopic experiments conducted during the course of this Ph.D. project. The first section describes the actual practical considerations that must be met for successful performance of waveguide Raman experiments, and includes a description of the waveguiding accessory used in conjunction with the CARY 82 spectrometer in Durham. The second section is a brief schematic explanation of the CARY 82 Raman spectrometer, along with the SCADAS instrument computer control system. The third section focuses on the off-line waveguiding apparatus constructed and used during the course of this project for elucidation of parameters such as film refractive index and waveguiding mode angles. The apparatus involved is fully described first, followed by examples of the measurements made using it, including a critique of the experimental procedures. Finally, a brief overview of the software developed for use in conjunction with this off-line apparatus is given. The fourth, and final, section details the actual thin polymer film systems from which waveguiding measurements were obtained, and is divided into three sections, namely single films, laminates, and other experiments, which includes details of attempts to study diffusion processes, along with other interesting observations made during the experimental stages of this project. It is worth reiterating at this juncture that refractive indices cited here, unless otherwise stated, refer to those measured at 632.8 nm. Structures of the polymeric materials used are given in Appendix 1.

5.2 - Practical Considerations.

Figure 5.1 shows a diagram of the arrangement required to effect prism coupling of light into an optical waveguide:-

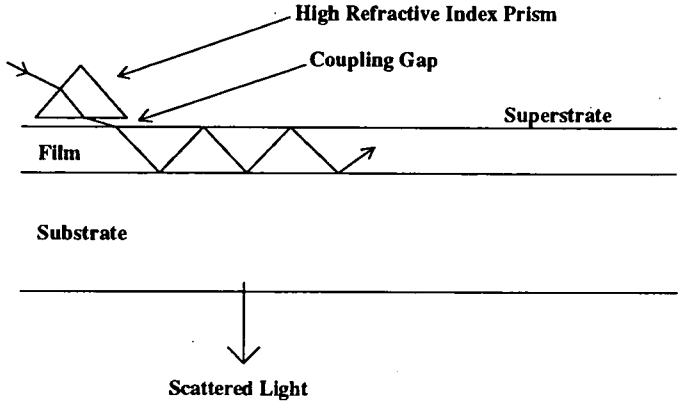

Figure 5.1 - Schematic Representation of Prism Coupled Optical Waveguiding.

For successful waveguiding to occur in a single thin film, three practical parameters must be satisfied, namely:-

1/. The polymer film of interest must have a refractive index which is numerically greater than both the substrate (usually glass (n = ~ 1.5) or fused quartz

(n = 1.457)), and the superstrate (usually, but not always, air). Furthermore the prism used should be of higher refractive index. The refractive index relationship between the film, prism and the substrate/superstrate can be summarised:-

$$\left(n_{superstrate} \langle n_{film} \rangle n_{substrate}\right) \langle n_{prism}$$

2/. The polymer film thickness must be greater than about 1/3 of the wavelength of the incident radiation, which implies a practical lower limit of about 0.2 μm for a single film at visible wavelengths.

3/. As discussed in Chapter 4, the polymer film must be free from foreign particles, such as dust and impurities which will restrict the propagation of light. Cloudiness and coloured materials will also prevent satisfactory experimentation.

Spectral enhancement resulting from waveguide experiments, compared to what may be expected from conventional Raman measurements, have been calculated by Rabolt and Swalen[1] to be in the region of 100,000 times. Two orders of magnitude enhancement arises from the increase in scattering volume, brought on by the creation of the waveguide 'streak', which has been found to be, in favourable instances, up to 50 mm in length. A further two orders of magnitude arise because the optical electrical field of a laser beam of diameter 100 μm is compressed into an approximately 1 μm thin film, which results in a large increase in effective electric field in the scattering volume.

To obtain different modes of waveguide propagation through the film, and hence Raman scattering from different areas of the film, it is necessary to vary the angle at which the incident beam strikes the film. This has been achieved by the use of a simple optical set-up, shown diagramatically in Figure 5.2, on the next page.

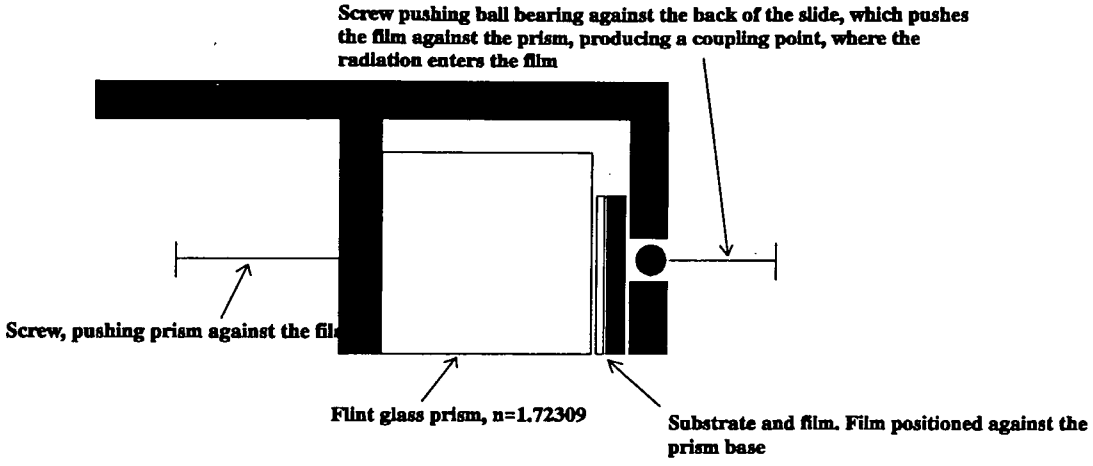

Figure 5.2 - The Waveguiding Apparatus

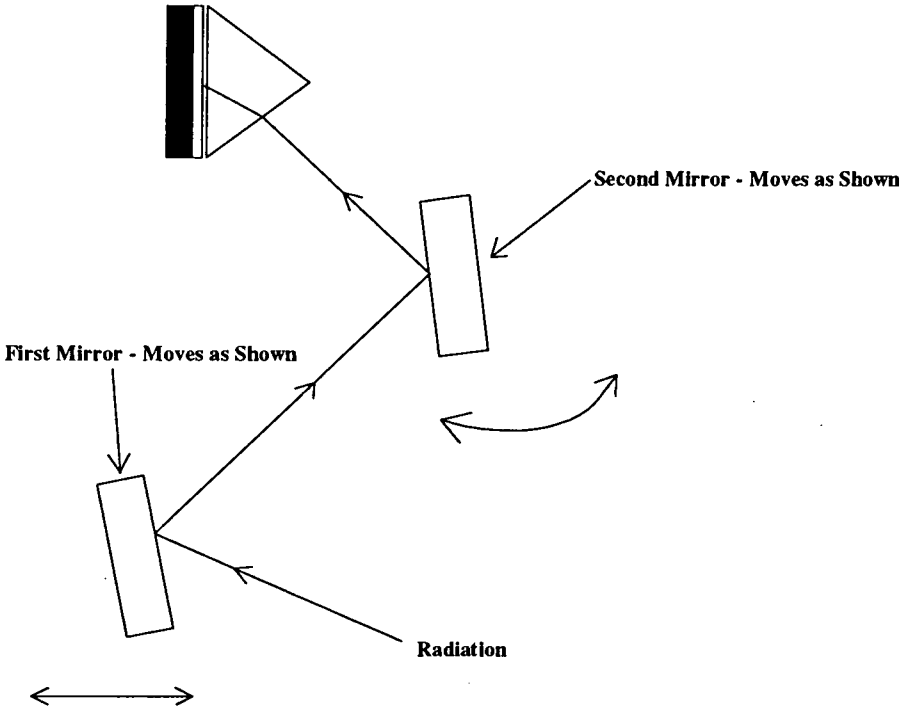

The apparatus shown in Figure 5.2 allows the incoming laser beam to be rotated relative to the high refractive index prism, thus changing the angle of the incident radiation and hence allowing different waveguiding modes to propagate through the film. The beam enters the film via the coupling spot, created by the pressure of a ball-bearing, pressed against the substrate by the simple action of a thumb-screw. The beam is then focused on to the coupling spot by manipulating the x and y translation stages, which are incorporated into the Raman sample holder (shown later). Then, by careful manipulation of the 2nd mirror, the different waveguiding modes are induced and the scattered light focused on to the slits of the monochromator. At this stage, it is now possible to make Raman spectroscopic measurements.

5.3 The Raman Spectrometer.

The Raman spectra were collected in Durham using a CARY 82 spectrometer linked to a Glen Spectra IBM-SCADAS (Spectrometer Control and Data Acquisition System). Excitation was provided by the 514.5 nm line from a Cambridge Lasers CL-4 argon ion laser. The incident light passes through a premonochromator, where it is dispersed by prisms set to allow only the 514.5 nm line to reach the sample. The scattered light is focused on to the entrance slit of the monochromator. Detection is provided by a cooled photomultiplier, linked to the photon-counting electronics of the SCADAS computer system.

5.4 The Off-Line Waveguiding Rig.

The use of such a piece of apparatus to measure the angles at which waveguiding modes propagate through a film is documented in the literature[2,3]. Figure 5.3 shows a diagrammatic plan of the whole set-up, and Figure 5.4 shows the optical stage (sample holder) in detail.

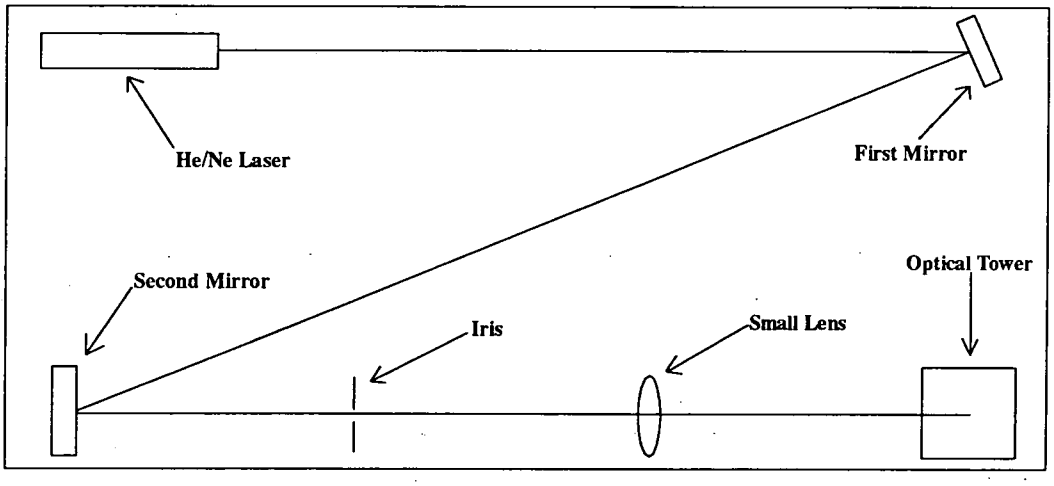

Figure 5.3 - Off-Line Rig Layout

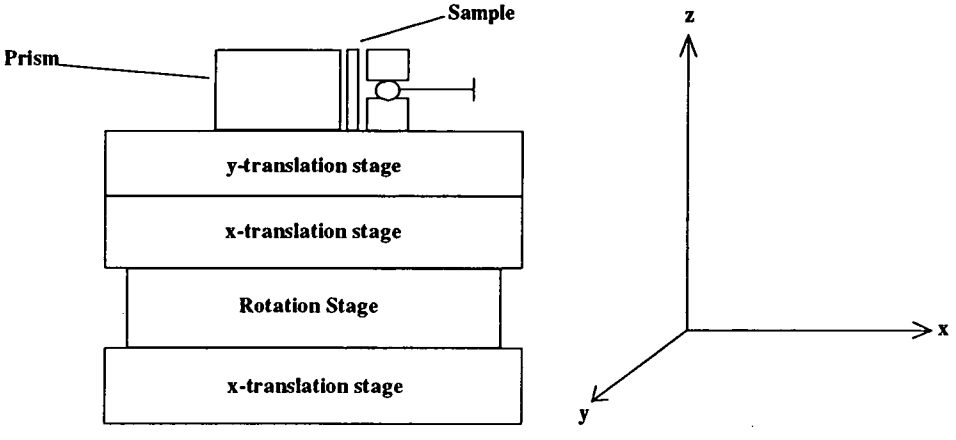

Figure 5.4 - The Optical Tower

In order for accurate measurements to be made using this apparatus, it is imperative that all the optics are aligned properly. In the course of setting up the apparatus in Durham, numerous problems were encountered, many of which were undoubtedly due to the nature of the optical table. This preferably should be a precision breadboard, which facilitates easy movement of the components, ensures the components are mounted precisely upright and provides some protection from vibrations arising from other usage of the laboratory. However, such breadboards are extremely expensive, and thus it was decided to use a slab of aluminium, with holes carefully drilled in it at relevant positions. This slab, although offering a compromise for the first two qualities of a breadboard, offered no resistance to vibration, and the equipment was thrown out of alignment by even the shutting of the door. Several methods of damping the vibrations were considered, and finally it was decided the best option was to move the rig as far as possible from the door, which was found to have a desirable, although not remedying, effect. The possibility of using some sort of soft bed for the table was obviously considered, but it was decided that this would not only render the whole table unstable, but also introduce a large inaccuracy in the table's plane, which needs to be as level as possible for accurate measurements, which will be discussed later.

5.4.1 - Rig Construction and Optimisation[2,3].

Before a description of the optimisation of the rig is discussed, a brief description of the roles the individual components play in the overall function of the apparatus is given.

The laser is usually a red, He/Ne laser, which produces a low milliwatt power beam, of wavelength 632.8 nm. This particular laser type is used for convenience of size and low power (safety), although other lasers may be used equally well.

The mirrors, which should be mounted on 3 inch high posts (shorter ones make accurate adjustment virtually impossible), are simple ones contained in adjustable holders. Good control of mirror adjustment is vital to ensure the beam travels parallel to the substrate, which is required for accurate determination of the mode angles.

The following three components stand on the optical rail, which simply facilitates lateral movement of the components with respect to the substrate.

The half-wave plate is required for measurements requiring plane polarised light, which has not been required during this project.

The iris ensures the beam is centralised and facilitates the adjustment of the beam position, with respect to the substrate. It should be protected from atmospheric dust at all times, when not in use, as such particles will foul the delicate machinery of the component.

The lens is a simple, cheap one, which merely helps to focus the beam on to the coupling spot. It should be situated at its optical focal length on the optical rail, preferably behind the iris.

The optical stage consists of two x translation stages, one y translation stage, a precision rotary stage and the actual prism holder. The prism holder is identical to the one used in the Raman accessory, complete with ball-bearing and screw to raise the coupling point. This is mounted on one x and one y translation stage, which ensure good alignment of the prism, with respect to the beam. These, in turn, are mounted on the rotation stage, which allows precise determination of the waveguiding mode angles. The final stage, mounted on to the optical rail, is the other x translation stage, which is used for offset alignment (see later).

Once the equipment is set up, as shown in Figures 5.3 and 5.4 and described above, the following steps are required before it can be used for determination of waveguide parameters:-

1/. The iris should be adjusted so that the beam strikes the *back* of the screw, used to raise the coupling point in the film. This is achieved by adjusting the height of the iris so that the beam hits the screw.

2/. Ensure that the beam hits the screw parallel to the plane of the bench, which should be as level as possible to ensure good accuracy. This is achieved by moving the iris close to the screw and adjusting the secondary mirror so that the beam once again hits the screw, then moving the iris as far as possible from the screw and adjusting the beam using the primary mirror. This procedure is repeated until the beam hits the screw, irrespective of the position of the iris, and when this has been achieved the lens is positioned, ideally behind the iris on the rail, at its optical focal length from the screw.

3/. The offset should now be set. The offset is the distance the base x translation stage must be moved from its central position, which ensures the beam remains motionless on the coupling point as the rotation stage is turned. This is a vital stage, because if the beam wanders from the coupling point during rotation, inaccurate values are obtained. The coupling point is calculated for each different type of prism used, and is determined from the relationship[2,3]:-

$$x = \frac{l_p}{n_p}$$

where, l_p is the distance the beam travels within the prism, and n_p is the refractive index of the prism. In the case of the prism used in Durham, the offset was found to be 5.9 mm.

A further parameter, α, is the angle between the incident beam axis and the axis perpendicular (normal) to the prism face, adjacent to the polymer film. If α is greater than 0, when waveguiding modes propagate, the mode angles are positive. If, however, α is less than 0, for waveguiding modes, then the mode angles are negative.

The apparatus, when correctly aligned, was tested using a polystyrene film, which was prepared from 2.94 grams of polystyrene in 13.57 grams of toluene, thus producing a

polystyrene solution of 21.66% solids. A film dipped at dipping speed 5.5 was determined to be of thickness 3.82 μm using the alpha-step. The film was observed to give rise to 5 waveguiding modes, the angles of which are given in Table 5.1

Table 5.1

Mode Number	Measured Angle	Angle from Normal
4	337°20'	5°20'
3	340°30'	8°30'
2	341°10'	9°10'
1	343°0'	11°0'
0	343°30'	11°30'

It should be noted that m=0 mode is always that furthest from the normal, and is often the most intense streak. When this was analysed using one of the items of software called Optwg[4], which allows calculation of film thickness and refractive index, from input of mode angles for a 3-layer case (see later), a value of 1.582 was obtained for the refractive index, which compares favourably to the reported value of 1.583, representing an error of a mere 0.06%. The value obtained for the film thickness, however, was not so good, being 1.67 μm, which represents an error of some 56%, compared to the value obtained from the alpha-stepper (3.82 μm). Ulrich and Torge[3], however, actually mention that film thicknesses, using this method, refer to the thickness at the coupling point, which is under pressure from the screw and is thus compressed. Hence, this method of mode angle determination is not appropriate for accurate determination of film thicknesses, but appears to provide an excellent method of refractive index determination.

This method was also used for determination of the refractive indices of the crosslinked epoxy resins, used extensively in FT-IR ATR experiments, described fully in Chapter 6. These are listed in Table 5.2

Table 5.2

Epoxy Resin System	Calculated Refractive Index
Epikote[13] 828 (n=1)	1.552
Epikote[13] 1001 (n ≈ 2.64)	1.579
Epikote[13] 1004 (n ≈ 4.67)	1.581

n refers to the degree of polymerisation present in the uncrosslinked epoxy resin (see Chapter 1, reaction 2)

The trend observed here is reasonably consistent with the molecular structure, with an increase in refractive index with increase in chain length, which introduces a higher proportion of phenyl rings, which in turn will cause an increase in refractive index. It is perhaps surprising that the refractive index for Epikote[13] 1004 is not larger. However, to the best of my knowledge, there is no report of the refractive index of these materials, so it is impossible to comment further.

Most of the waveguide experiments reported in this thesis were conducted before this piece of apparatus was commissioned. All reported angles etc. presented in the remainder of this thesis were determined, unless otherwise stated, using the film thicknesses obtained using the alpha-step, and subsequent calculations using the software developed in an earlier project[4] and by IBM, and which is discussed next. The potential use of this piece of apparatus is considerable, and future workers should be able to utilise its potential fully.

5.4.2 - Software.

This apparatus is used in conjunction with several pieces of software, some of which was developed by Dr. N.M. Dixon, during postdoctoral work conducted in collaboration between Durham and ICI[4], with the other ones originating from work carried out at IBM, by Rabolt and Swalen[5]. Here the use of this software is considered fully.

5.4.2.1 - 'Angle'[4,5]

This allows calculation of mode angles from the thickness and refractive index of a single film. Below are three examples of the use of this program, which clearly show how different film thicknesses and refractive indices affect the waveguiding characteristics of polymeric films:-

Example 1: A 1 μm film of polystyrene, refractive index = 1.583 on quartz.

Table 5.3

Mode Number	Mode Angle (From Normal)
0	9°58'
1	3°91'
2	-3°61'

Example 2: A 3 μm film of polystyrene, refractive index = 1.583 on quartz.

Table 5.4

Mode Number	Mode Angle (From Normal)
0	11°36'
1	10°48'
2	9°04'
3	7°09'

Example 3: A 1 μm film of poly(vinylacetate), refractive index = 1.466 on quartz.

Table 5.5

Mode Number	Mode Angle (From Normal)
0	-3°73'

5.4.2.2 - 'Optwg'.

This program has already been demonstrated for the epoxy resin system, described above in Table 5.2, and calculates the film refractive index and thickness from the mode angles obtained from the waveguiding rig. However, to demonstrate this program further, the angles obtained from Example 1 for program 'Angle' above were used. This example refers to a conjectural system, consisting of a 1 μm film of polystyrene (R.I. = 1.583) deposited on quartz. However, the values for the refractive index and film thickness from the calculated angles are:-

Average Thickness = 1.23 μm
Refractive Index = 1.551

It can thus be appreciated that mode angles calculated using the 'Angle' program are not particularly accurate, compared with those obtained from the off-line rig. This is possible as the off-line rig deals with actual, practical waveguiding, with all the experimental quirks discussed already, whereas the calculations performed in these programs deal with theoretical waveguiding. However, the error involved is rather high, and thus it is more likely that there is a defect in the software. This was not resolved during the course of this project, and is something future workers should investigate.

5.4.2.3 - 'Thick1' [4].

This allows the calculation of the film thickness and optical field density in a single film system, and requires both the film refractive index and the actual mode angle of interest to be known. Here, we examine an example of polystyrene (refractive index = 1.583), on a quartz substrate (refractive index = 1.457), which has mode number = 0, with an angle of 9°58' (which is that calculated in Example 1 from the 'Angle' program):-

Film Thickness = 1.23 μm

with

98.27% of the optical field in the film,
1.60% of the field in the substrate,
0.13% of the field in the air.

Here, again, the film thickness is different from the value entered into the original program, and this is again believed to be associated with software errors.

5.4.2.4 - 'Index4'.

This program calculates optical electric fields for a laminate system from the input of refractive indices and thicknesses of the individual films, plus the relevant observed mode angle. The example given involves a laminate consisting of an upper layer of 0.6 μm polystyrene (refractive index = 1.583) and a lower layer of 6.3 μm poly(vinylpyrrolidine) (refractive index = 1.517)[4]. Figure 5.5 shows the spectra obtained between the regions 900-1100 cm^{-1}, which contains the 1002 cm^{-1} band which arises from the polystyrene molecule, along with the 934 cm^{-1} band from the poly(vinylpyrrolidine). It can clearly be seen that different spectra arise from different modes of propagation. This arises from the change in optical electric field density with different angle of incidence, and hence mode number. Figure 5.6 shows the electric field distribution obtained for the 4 modes, and the distribution clearly reflects the observed spectra. Figure 5.7 shows the spectra obtained from the pure polymers, for reference purposes.

5.5 Experimental Results.

This section is divided into three sections, single films, laminate systems and miscellaneous experiments, which include attempts to study diffusion using waveguide Raman methods and Total Internal Reflection (TIR) experiments. Polymer structures are given in Appendix 1.

5.5.1 Single Film Systems - Common Polymeric Materials.

1/. Polystyrene (PS).

This was an ideal polymer (refractive index = 1.583) to start waveguide Raman experiments with, as it forms excellent quality films, using toluene as solvent, and has a high Raman scattering cross-section, which arises from vibrations of the phenyl rings[6]. Figure 5.8 shows the spectrum obtained from a 2.78 ± 0.01 μm film of polystyrene, which was prepared by dipping on to quartz, at dipping speed of 4.8 mm sec^{-1}, from a solution of 3 grams polystyrene in 12 grams toluene.

The strong band at 1002 cm^{-1} is assigned[6] to the ring breathing modes of the phenyl groups, along with the band at 1032 cm^{-1} band, and the bands at 1584 cm^{-1} and 1604 cm^{-1} are also assigned to aromatic ring vibrations. The band at 1450 cm^{-1} band is the deformation mode of the CH_2 group, $\delta(CH_2)$, with the strong bands at 3054 cm^{-1}, 2905 cm^{-1} and 2857 cm^{-1}, assigned to the aromatic CH stretching, anti-symmetric aliphatic CH stretching and symmetric CH stretching modes, respectively.

2/. Poly(vinylacetate) (PVAc).

This polymer has a low refractive index of 1.466, which necessitated the use of a quartz substrate for successful waveguiding experiments. Good films were produced from solutions of toluene, this one being produced from a solution of 1.68 grams of polymer in 7.96 grams of toluene, and having a thickness of approximately 3 μm. This

Figure 5.5 - 900 - 1100 cm^{-1} Region of a PS/PVP Laminate
(Reproduced Courtesy of J.Wiley Publishers)

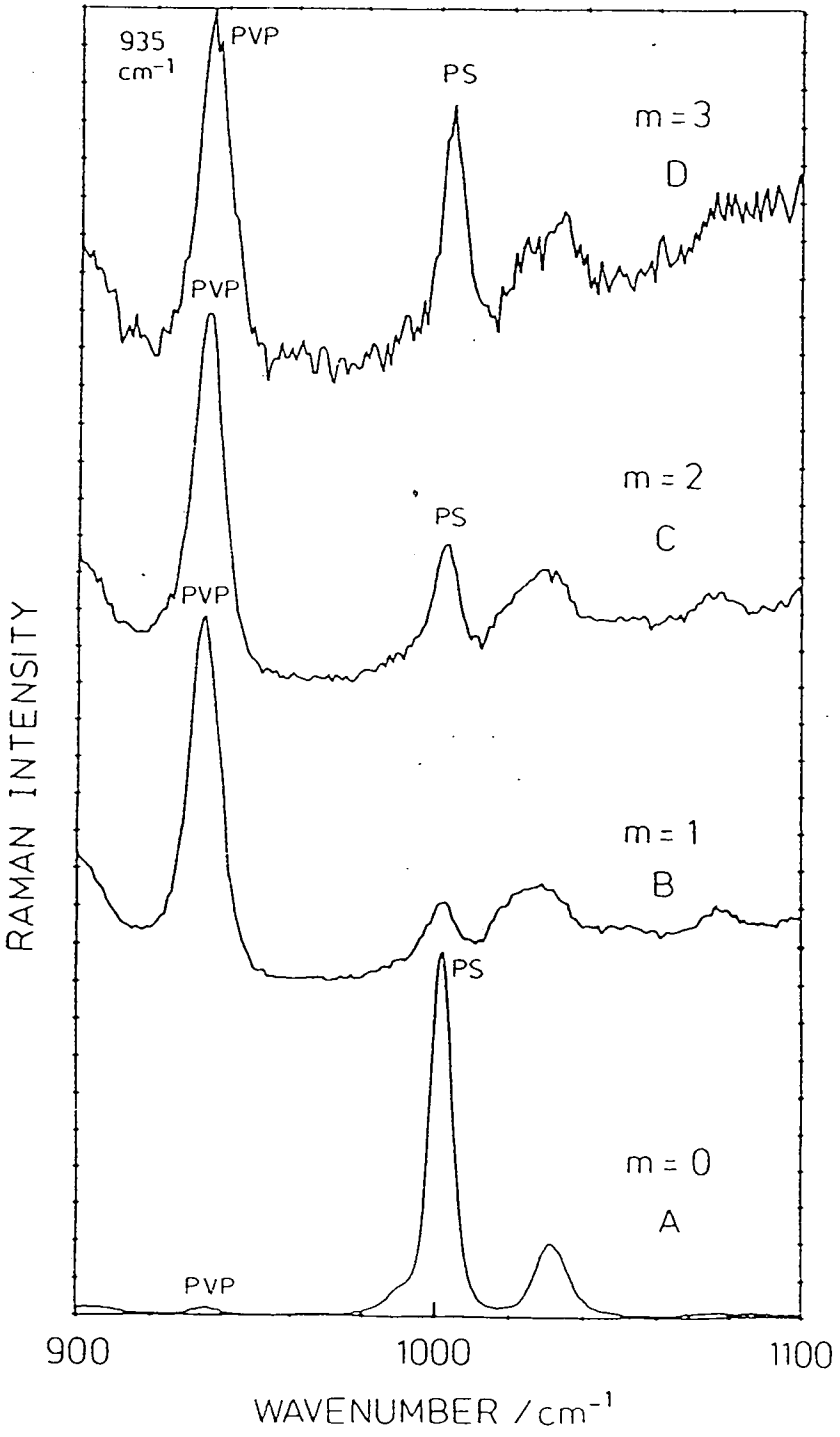

Figure 5.6 - Electric Field Distribution for the PS/PVP Laminate, Shown in Figure 5.5 (Reproduced Courtesy of J.Wiley Publishers)

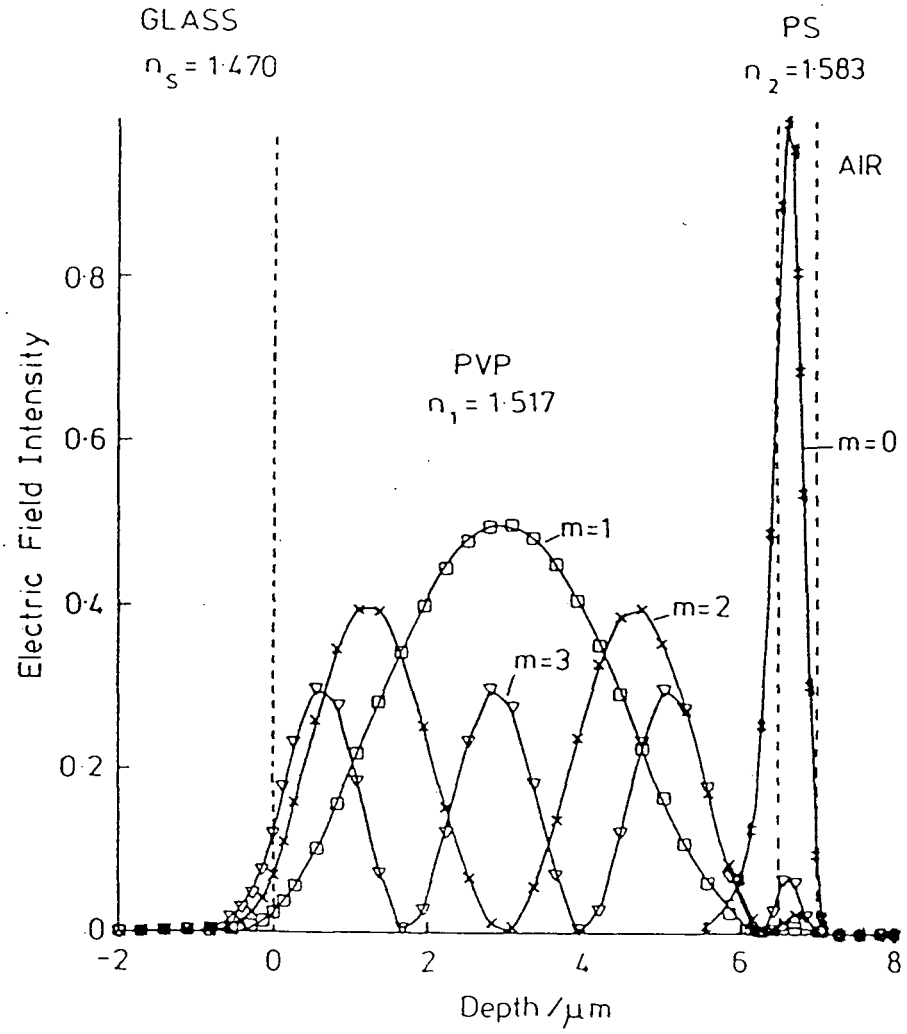

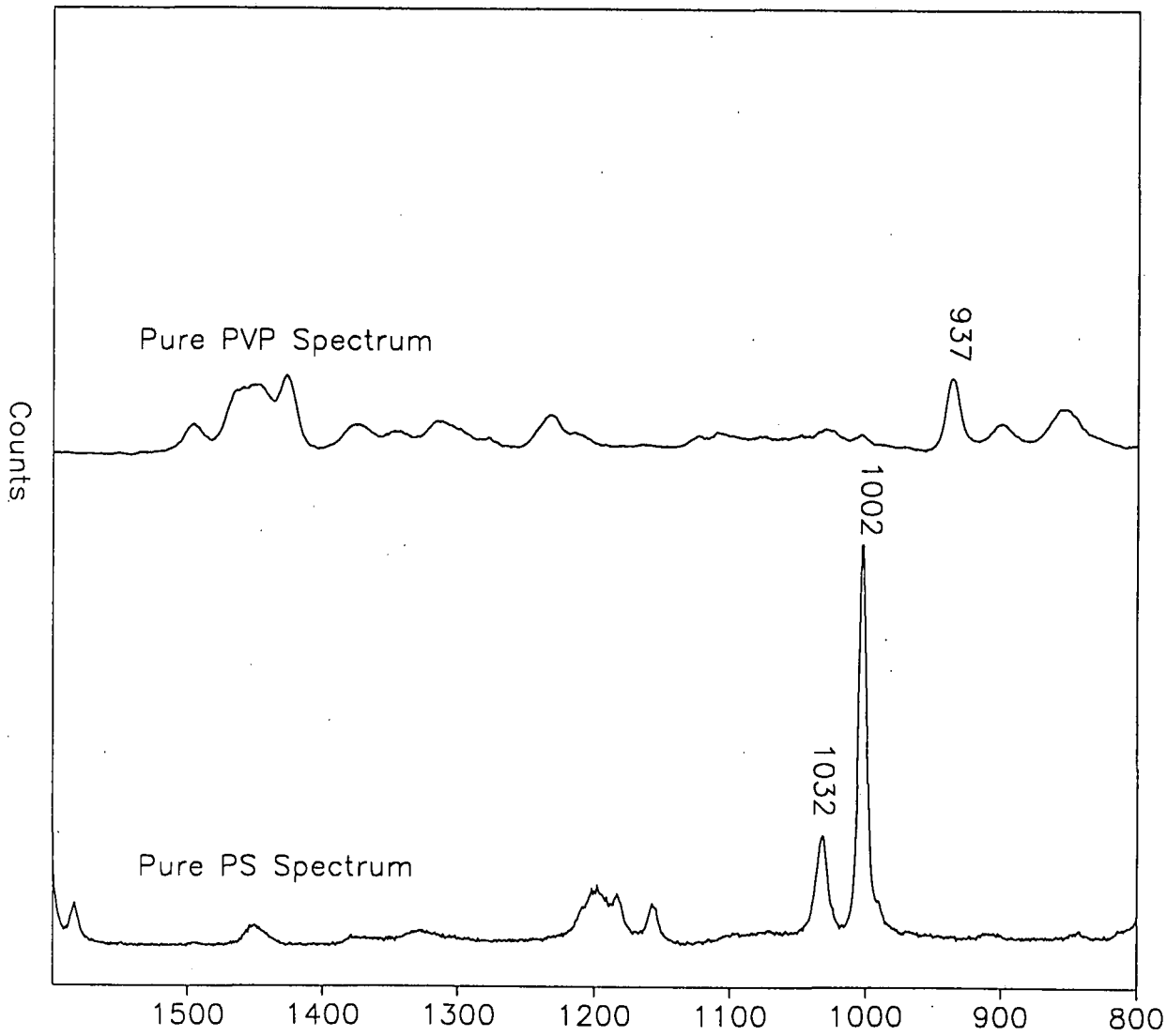

Figure 5.7 – Pure PVP and Pure PS Spectra

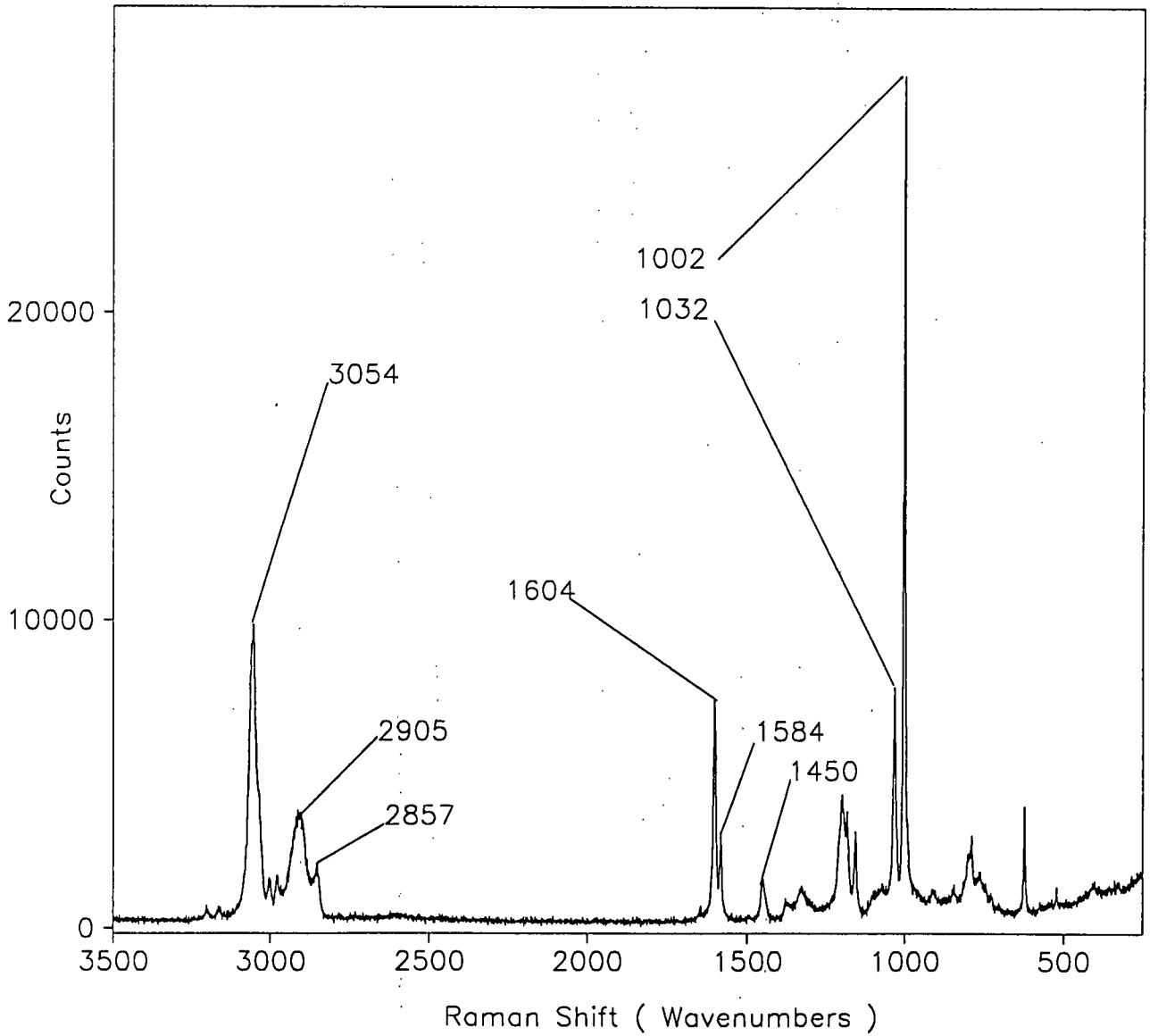

Figure 5.8 – Pure Polystyrene Spectrum

film was not produced by dipping, but by use of the horizontal flow technique. Figure 5.9 shows the spectrum obtained.

The carbonyl group vibration can be clearly seen at 1733 cm^{-1}. The CH_2 anti-symmetric and symmetric stretching modes are assigned to the bands seen at 2938 cm^{-1} and 2863 cm^{-1} respectively. The band at 1438 cm^{-1} is assigned to the CH_2 deformation mode, and the band at 633 cm^{-1} to the CH_2 wagging mode. Also visible is the C-O stretching mode at 1030 cm^{-1}, and the C-CH_3 stretching mode at 1358 cm^{-1}.

3/. Poly(vinylchloride) (PVC).

This polymer has a reported refractive index of 1.545, and is also reported to form good films from solutions of stabilised tetrahydrofuran (THF). However, great difficulty in obtaining a good film from the stabilised THF available in Durham was encountered, with films produced being cloudy, and thus opaque for waveguiding purposes. On closer examination, however, it was found that the departmental THF was not actually stabilised, despite belief to the contrary. Once pure, stabilised THF was procured, good films were indeed produced, as they were from dimethyl formamide (DMF). It is thus believed that the presence of THF radicals (formed by fissure of one carbon-oxygen linkage), causes degradation of the polymer, which in turn, leads to the cloudy nature of the film. This raises a very important issue regarding general safety when using bulk solvents, such as THF, which when unstabilised is a very reactive entity (due to homolytic cleavage of one of the two O-C bonds present in the THF molecule, which forms a highly reactive free radical species). If the batch of THF used in the production of the PVC film had been used as a solvent for a synthesis reaction of some kind, a very serious accident could have resulted. This should serve as a warning to those who use THF as a solvent.

Figure 5.10 shows the spectrum produced from a solution of 2.27 grams PVC in 11.56 grams of DMF. Again, this film was produced using the horizontal flow, and this has a thickness of approximately 3.5 μm.

The two bands at 639 cm^{-1} and 694 cm^{-1} are probably due to the CH_2 wagging and C-Cl stretching modes respectively, with the band at 1434 cm^{-1}, being the CH_2 deformation mode. The CH_2 anti-symmetric and symmetric stretching modes are assigned to the bands seen at 2917 cm^{-1} and 2852 cm^{-1} respectively. This is believed to be the first time a waveguide Raman spectrum of this material has been reported.

4/. Poly(vinylalcohol) (PVA).

Obtaining a good film of PVA (refractive index = 1.52) proved to be more difficult than first anticipated. Previous work at Durham[4] had used water as the solvent, followed by drying in an oven at 110°C, but when this was attempted, a prominent ridge was observed along the central long axis (see Chapter 4, Figure 4.7), which is thought to have been due to the solvent leaving the film too slowly (see Chapter 4, Section 4.4). The presence of this ridge makes raising a suitable coupling point difficult. Dimethyl formamide (DMF) was tried as an alternative solvent, being listed as such in the polymer handbook[7]. Despite this, however, it was found the PVA was

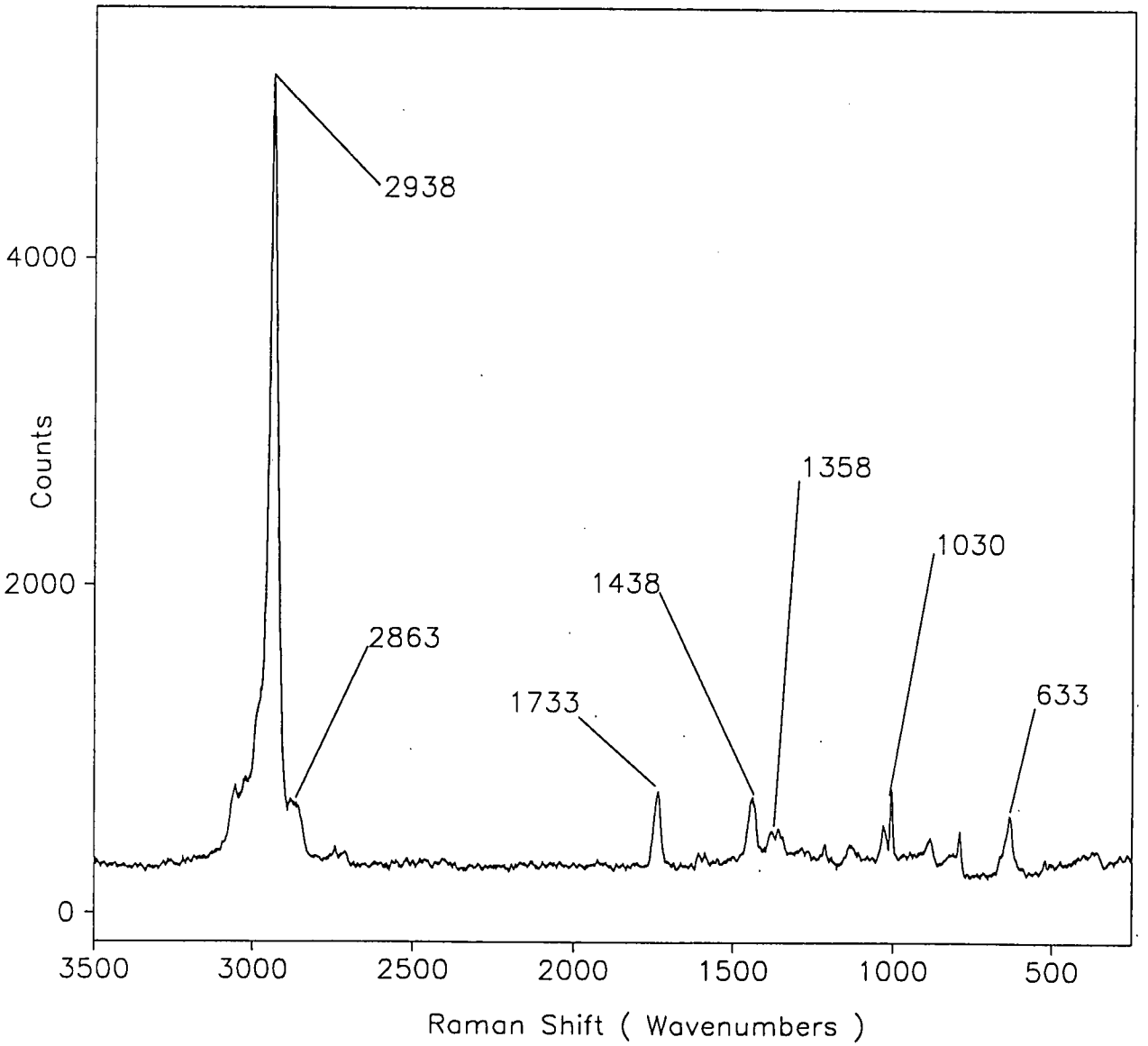

Figure 5.9 – Pure Poly(vinylacetate) Spectrum

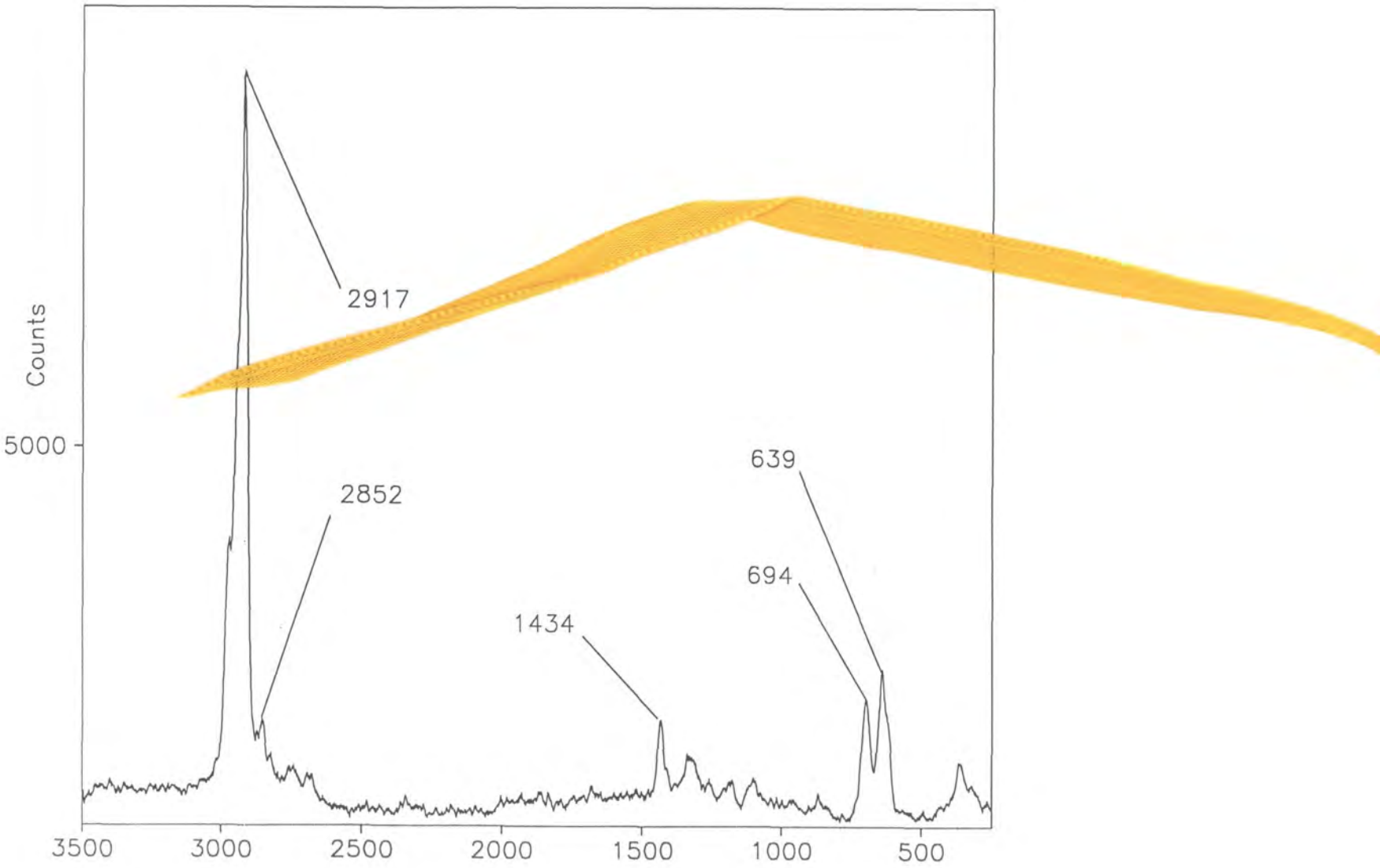

Figure 5.10 – Pure Poly(vinylchloride) Spectrum

most reluctant to dissolve in DMF, even at elevated temperatures (heating taking place carefully in a fume cupboard, using a heating mantle and reflux apparatus). This raises the point, which was encountered several times during this project, that this particular list is not always strictly accurate, as materials are either described as soluble or insoluble, with nothing in between. In fact, PVA was found to be *sparingly* soluble in DMF, because a very thin film, of presumably PVA, was deposited on to a slide from the residual DMF after heating. Films were then deposited from hot water, and then dried in the oven, reasonable films being eventually produced from aqueous solutions at 60°C and an oven temperature of 80°C. Hotter solutions and/or oven temperature produce cloudy films, thought to be due to too rapid evaporation of solvent (see Chapter 4, Section 4.3). Figure 5.11 shows the spectrum of a PVA film produced from a solution of 3.04 grams PVA in 12.24 grams water. The film was dipped at a speed of 4.8 mm sec^{-1}, from the solution heated to 70°C (to allow for cooling to 60°C), and then dried in an oven at 80°C for 3 hours. The dried film thickness was measured using the alpha-step, and a thickness of 1.9 ± 0.5 μm recorded.

This spectrum, although rather simple, is nevertheless of interest. The CH_2 anti-symmetric and symmetric bands, are, as usual, clearly visible at 2909 cm^{-1} and the shoulder at 2829 cm^{-1}, with the CH_2 deformation band also visible at 1437 cm^{-1}. The two broad features at 3311 cm^{-1} and 1360 cm^{-1} are due to the OH stretching, and possibly the OH bending modes, respectively, although the latter is usually at a somewhat higher frequency, around 1650 cm^{-1}. The two bands of most interest are the major broad features at 1020 cm^{-1} and 806 cm^{-1}, which provided a puzzle when they were observed in this and numerous other spectra, although by no means all. They were found to be attributable to the quartz substrate, a fact that has been proved by a Total Internal Reflection experiment within the quartz substrate itself, which is shown in Figure 5.12.

The two broad features are thought to arise from the Si-O linkages, with the further complicated spectral structure at the lower end of the spectrum attributable to crystal lattice vibrations (ie. intermolecular vibrations). Substrate bands have been seen before[8,9], but were present only as one broad band, centred at approximately 500 cm^{-1} [9], with nothing noted, as above at approximately 800 cm^{-1} and 1025 cm^{-1}. The experiments described by Levy and Dupeyrat[9], were conducted on two films of PMMA, 1 μm and 6 μm thick respectively on glass. These interesting features are discussed in Chapter 7.

5/. Polymethylmethacrylate (PMMA).

Good films of this material (refractive index = 1.489), were prepared from toluene and gave good spectra, such as that shown in Figure 5.13, which was dipped at dipping speed of 4.8 mm sec^{-1}, from a solution of 1.5 grams PMMA in 13.5 grams of toluene. The film thickness, determined using the alpha-step, was found to be 1.6 ± 0.2 μm.

This spectrum reflects the fairly complicated nature of the molecule (see Appendix 1), with the carbon-hydrogen stretching region (shown in detail in Figure 5.15) containing not only bands arising from the chain CH_2 and CH_3 stretching modes, but also bands due to the ester methyl (CH_3) group vibrations, which will obviously be in a

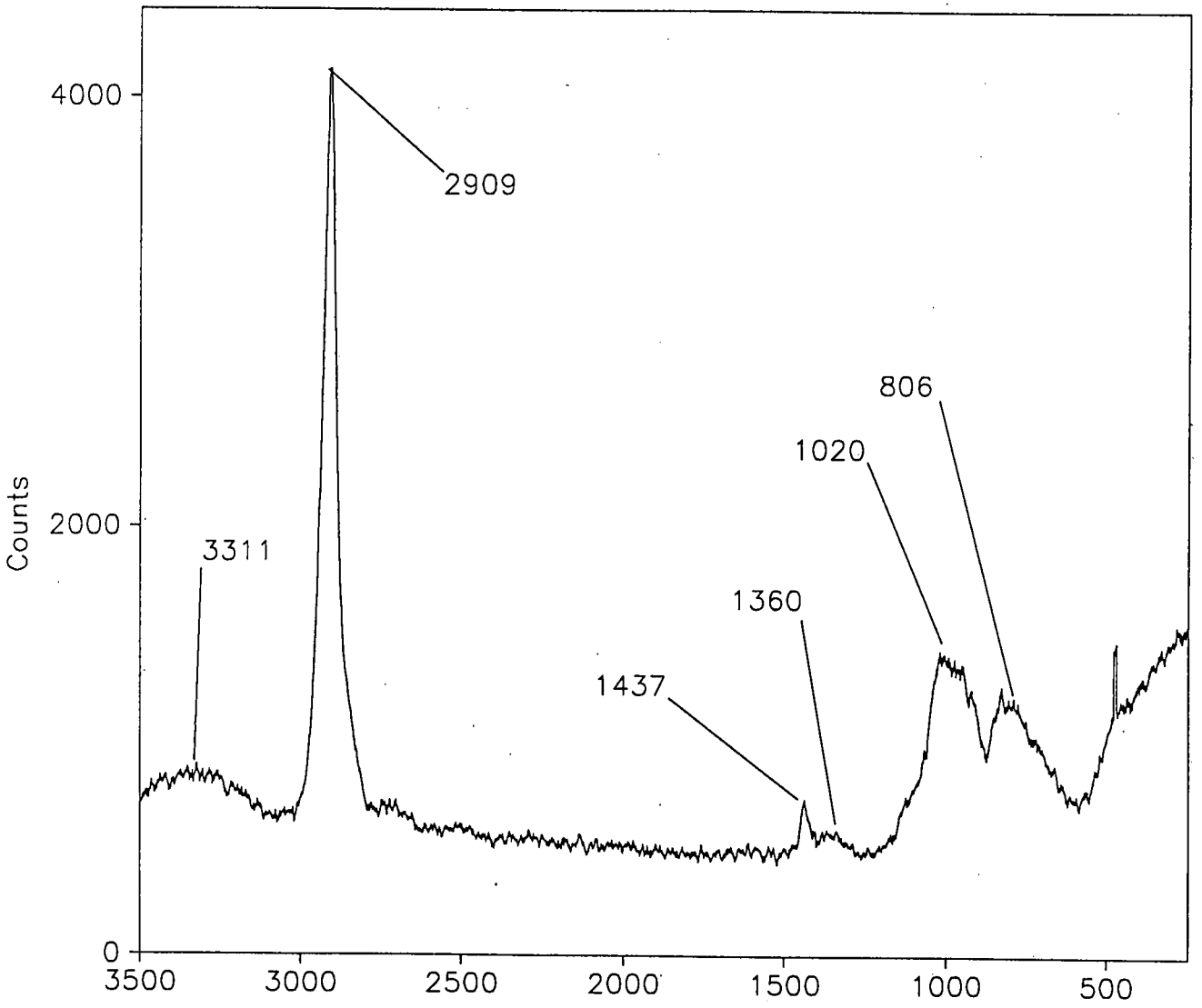

Figure 5.11 – Pure Poly(vinylalcohol) Spectrum

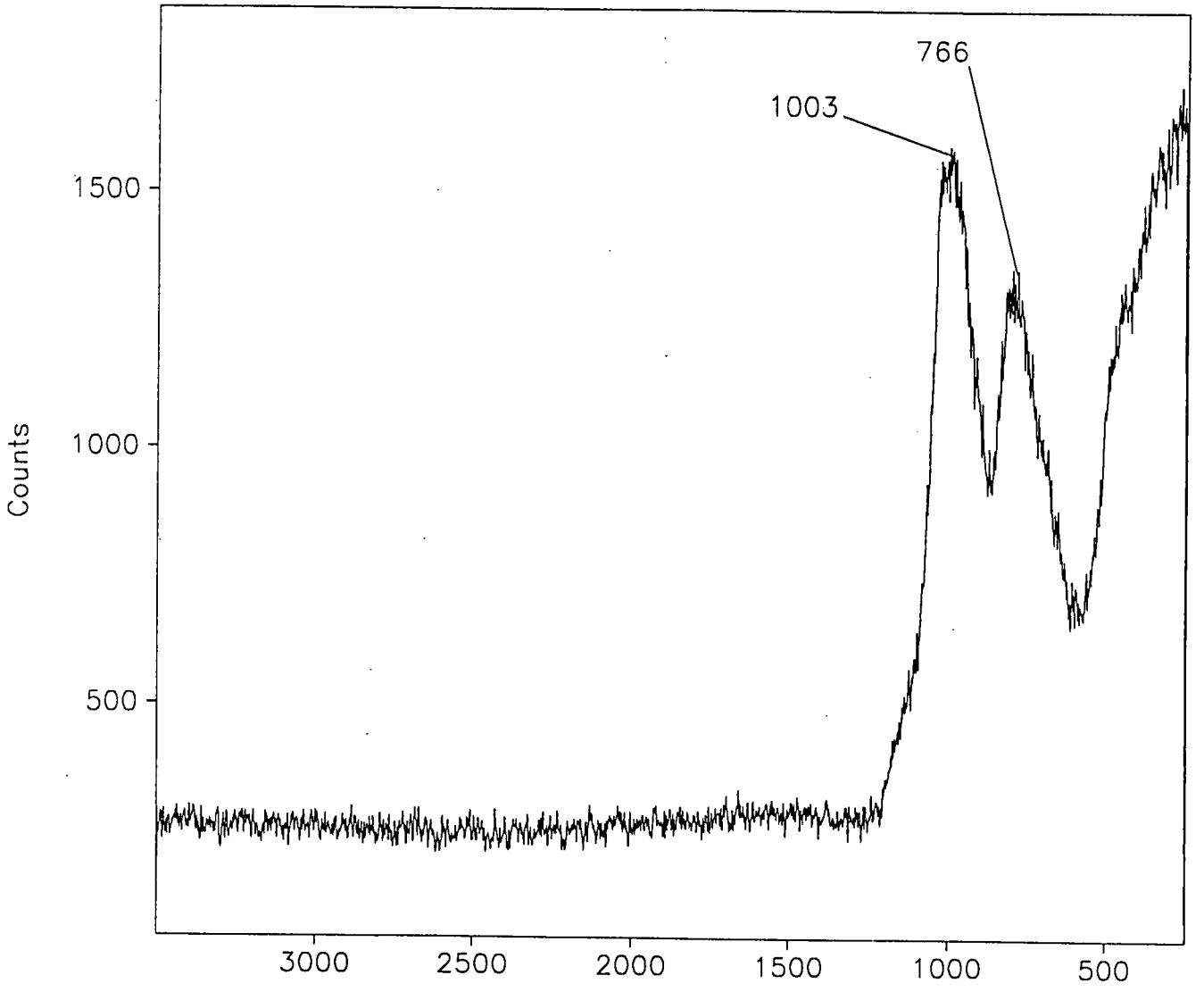

Figure 5.12 – TIR Raman Spectrum of Quartz

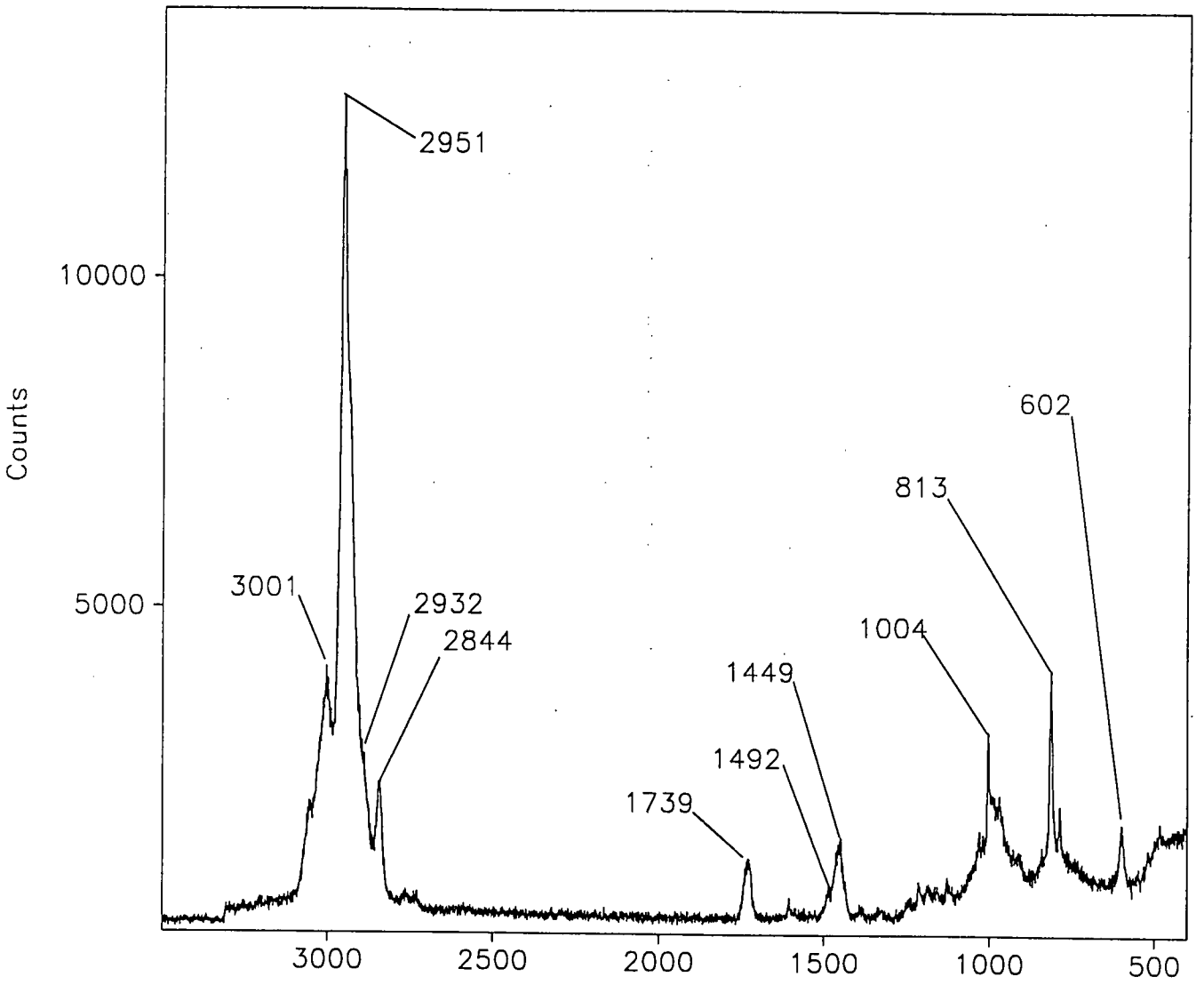

Figure 5.13 – Pure Poly(methylmethacrylate) Spectrum

different chemical environment and will thus vibrate at a different frequency. Hence, the 3001 cm^{-1} and 2932 cm^{-1} bands are respectively assigned to the anti-symmetric and symmetric stretching modes of the methyl group adjacent to the carbonyl, whereas the 2951 cm^{-1} and 2844 cm^{-1} bands are respectively assigned to the anti-symmetric and symmetric stretching of the chain CH_2 and CH_3 groups. The 1739 cm^{-1} band is attributable to the carbonyl group, and out of the several bands between 1250 cm^{-1} and 1100 cm^{-1}, the one at 1210 cm^{-1} is thought to be due to the C-O stretching mode. The band at 1449 cm^{-1} arises from the chain CH_2 and CH_3 deformation modes, whereas the shoulder at 1492 cm^{-1} is expected to arise from the deformation mode of the methyl group adjacent to the carbonyl group. The band at 602 cm^{-1} is thought to be the CH_2 wagging mode, and the two bands around 813 cm^{-1} are probably due to the carbon chain skeletal vibrations.

Again, the substrate bands, arising from the Si-O groups, are clearly visible, and if we examine Figure 5.14, lower spectrum, which is an expansion of this area, we can see something of interest.

In the lower spectrum, two weak bands are seen, situated at 1003 cm^{-1} and 1029 cm^{-1}. These band frequencies correspond to frequencies associated with the ring breathing modes of a phenyl group. These bands are believed to arise from residual toluene (the solvent for this PMMA sample). The middle spectrum in Figure 5.14 shows the spectrum of pure toluene in this spectral area, and it can be clearly seen that the two sets of bands do indeed correlate. Added to this, the upper spectrum of Figure 5.14 is the waveguide Raman spectrum of a PMMA film, cast using xylene as the solvent. Not only are the solvent peaks absent, but also the substrate peaks are no longer visible. The absence of solvent peaks is expected, as xylenic phenyl rings do not show the strong ring breathing modes which are seen in toluene[10]. The absence of the substrate bands cannot be explained so readily. These substrate features are discussed in Chapter 7.

Further evidence of the presence of toluene in the film can be seen in Figure 5.15, in which a small band appears at 3055 cm^{-1}. This is thought to arise from the aromatic CH stretching mode, which must be associated with toluene, as PMMA does not contain any aromatic functionality.

6/. Poly(vinylpyrrolidine) (PVP).

This polymer has a refractive index of 1.517, and is reported[4] as producing good films from water, although it was found that methanol produced better films, as 'ridging' similar to that reported for PVA films occurred when water was used. Figure 5.16 shows the spectrum obtained from 3.37 grams PVP in 9.48 grams methanol, which was found to give a film of thickness of approximately 5.6 μm, using horizontal flow. It is interesting to note that when a film of PVP, deposited from methanol, was dried at room temperature, the back of the substrate cooled to such an extent that atmospheric water was observed condensing on it.

The complicated set of peaks centred at 2929 cm^{-1} obviously correspond to the different anti-symmetric and symmetric stretching modes arising from the different types of C-H species which exist in this molecule. The band at 1655 cm^{-1} is

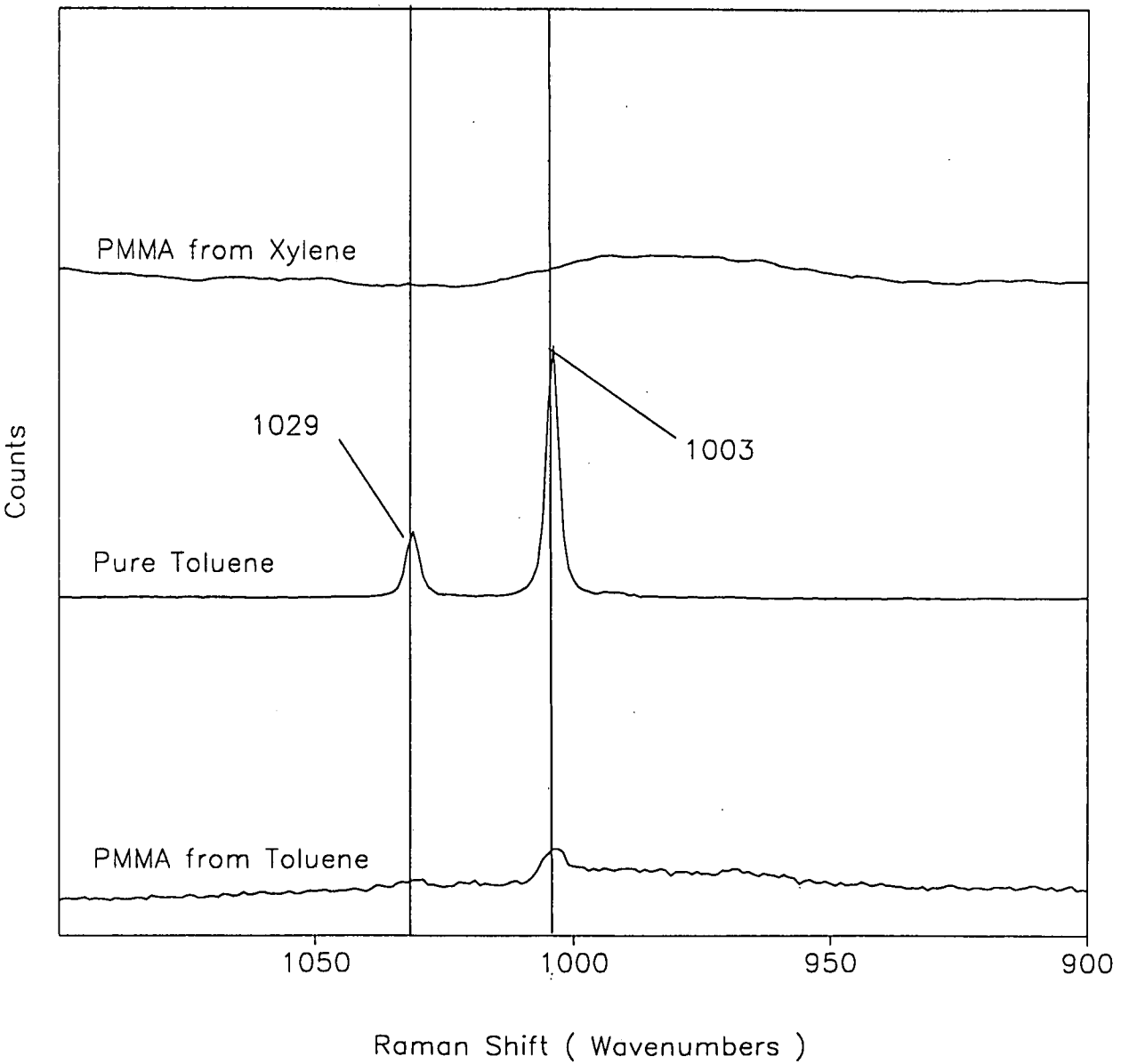

Figure 5.14 - Comparison of Pure Toluene with that seen in a PMMA Film

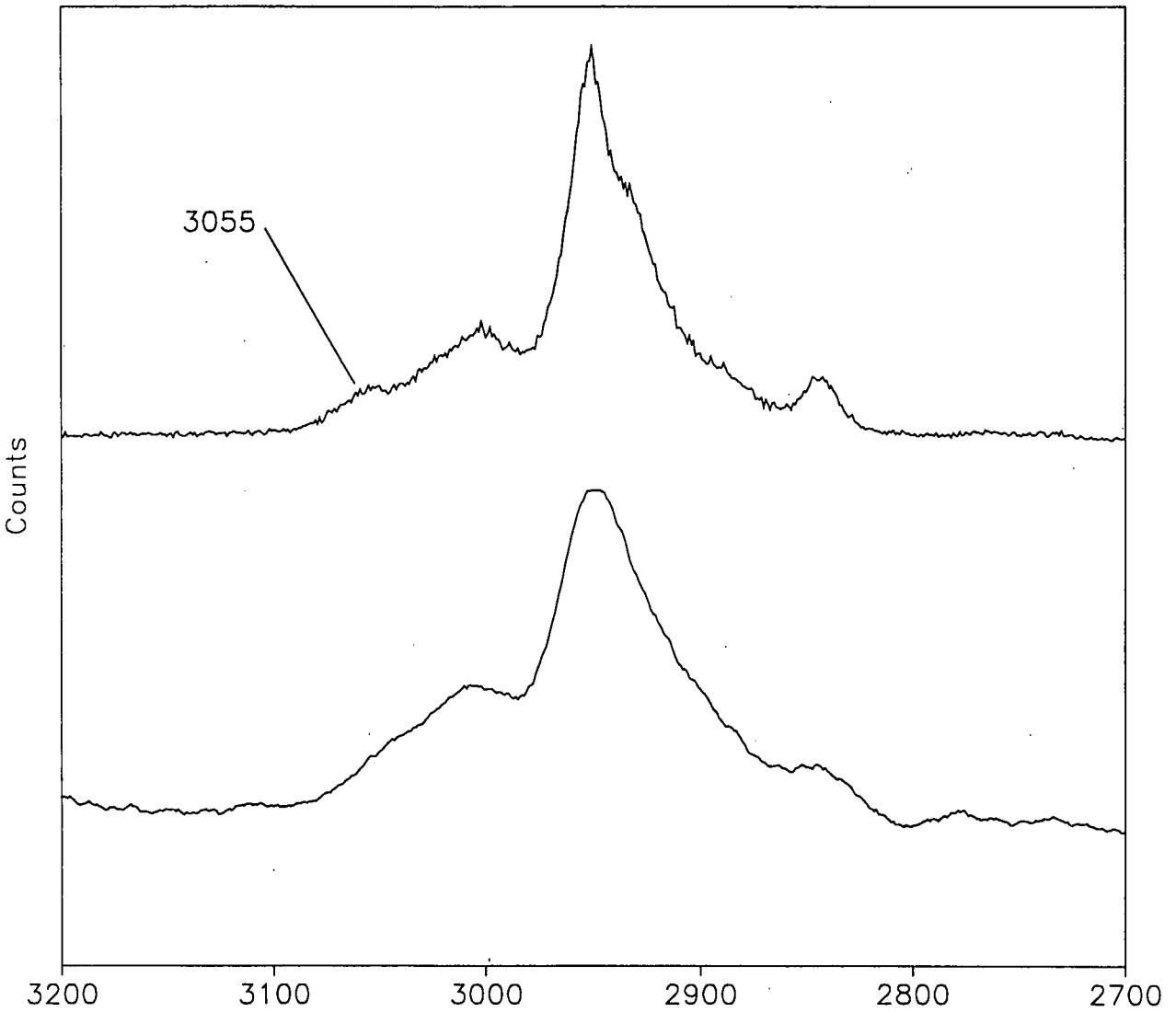

Figure 5.15 - Comparison of the CH Stretching region from two PMMA Films, Showing the Toluene Peak

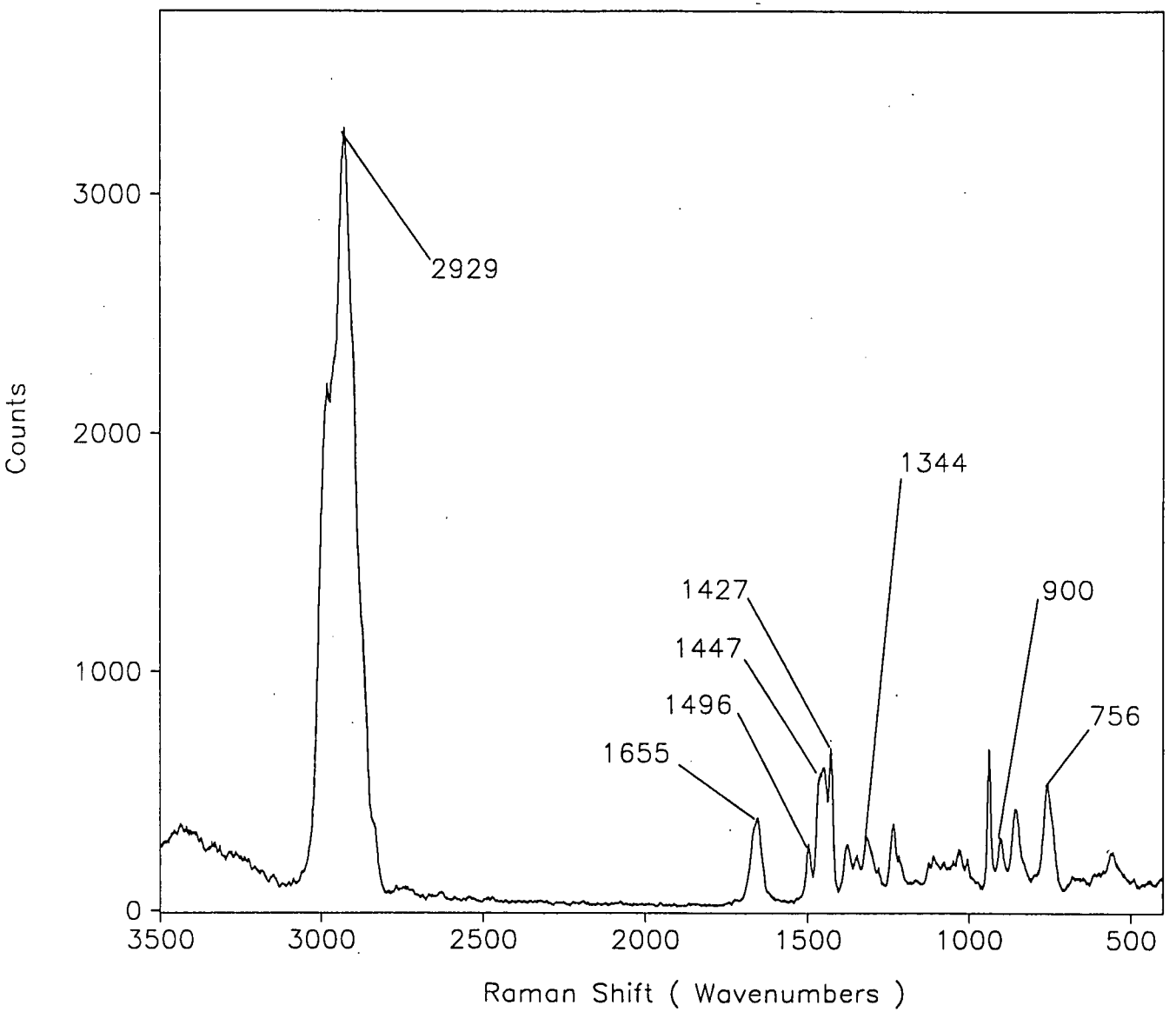

Figure 5.16 – Pure Poly(vinylpyrollidine) Spectrum

undoubtedly due to the carbonyl stretching mode, and the three bands at 1496 cm^{-1}, 1447 cm^{-1} and 1427 cm^{-1} probably arise from the carbon-hydrogen deformation modes. The three bands centred on 1344 cm^{-1} probably arise from the C-N-CO linkage, and the band at 756 cm^{-1} is assigned to the CH_2 wagging mode. Finally, the bands centred at 900 cm^{-1} are probably carbon chain skeletal vibrations.

7/. Polyethylene (PE).

Numerous attempts were made to try to obtain a spectrum from this substance, but on each occasion a cloudy, crystalline film was obtained, which would not support a waveguide. The use of lower-density polymers were tried and several different solvents, including boiling xylene, carbon tetrachloride and tetrachloroethane, were all tried to no avail. Rabolt and Swalen[1] report being able to obtain the waveguide Raman spectrum of this material, but mention 'careful processing conditions', which are not specified and were thus obviously not reproduced in Durham!

5.5.2 - Single Film Systems: Industrial Polymeric Systems.

1/. Crosslinked Polydimethylsiloxane (PDMS).

PDMS is a viscous liquid, which reacts with tetraethyloxysilane (TEOS) in the presence of dibutyl tin dilaurate (DBTDL), via the following reaction:-

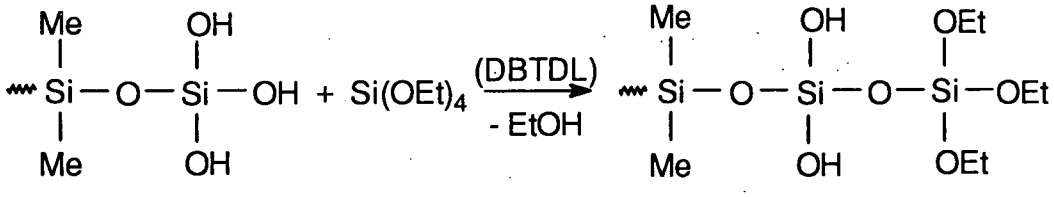

(Reaction 1)

The crosslinking proceeds via this reaction, as the OEt groups can react with any of the hydroxyl groups, thus forming a crosslinked mesh, which produces a polymer belonging to the generic group of a silicone rubber. The crosslinking reaction takes several hours at room temperature. It was reported[11] that it is possible to make the mixture up, then cast films from the solution. It was found, however, that the solution tended not to wet the substrate particularly well, and hence rather poor films resulted. As it happens, this did not particularly matter, because after several unsuccessful attempts to produce a waveguiding streak, it was discovered that the refractive index of this material was reported[11] as being 1.41. Hence one of the fundamental requirements for successful waveguiding was not adhered to, i.e. that of the substrate being of a lower refractive index than the sample film, which explained the lack of waveguiding.

This problem was solved by the use of a modified PDMS, which contained a proportion of phenyl rings, the proportion being 14 phenyl rings to 86 methyl groups. The refractive index was hence higher, due to the presence of the phenyl groups, and

was reported[11] as being 1.478. A film was thus prepared from a solution of 1.360 grams phenylated PDMS, 0.015 grams TEOS and approximately 0.01 grams of DBTDL, which produced a film of 4.2 μm ± 0.6 μm. This produced only one waveguiding mode, which occurred at an incident angle very close to the point where Total Internal Reflectance (TIR) in the substrate occurs. This was evident by the amount of light which travelled beyond the film boundary in the substrate, ending in a bright spot at the tip of the slide. This is similar to that observed in the TIR experiment described above, and such observations were not seen in other waveguiding experiments performed. An optical electric field calculation performed on this system predicted four waveguiding modes, with the m=3 mode closest to the film/substrate interface. However, the proportion of field within the substrate is calculated at only 11%, which is not as excessive as that suggested from the experimental observations above. It is thought that the rubbery nature of the polymer accounts for this discrepancy, as the considerable pressure exerted on the film by both prism and coupling screw would drastically decrease the effective polymer film thickness. This will cause deviation from the theoretical predictions. The spectrum produced is shown in Figure 5.17, and shows a considerable contribution from the substrate.

The two substrate bands are clearly visible, but there is also a good spectrum of the phenylated PDMS. In the C-H stretching region, the band at 3054 cm^{-1} is assigned to the aromatic CH stretching mode, the band centred at 2966 cm^{-1} to the aliphatic CH_2 and CH_3 (arising from the methyl and ethyl groups) anti-symmetric stretching mode and the feature centred at 2906 cm^{-1} to the aliphatic CH_2 and CH_3 symmetric stretching modes. The two bands seen at 1594 cm^{-1} and 1572 cm^{-1} are thought to be aromatic ring modes, as are the two features on the top of one of the substrate peaks, at 1030 cm^{-1} and 1001 cm^{-1}, which arise from phenyl ring breathing modes. The weak feature at 1412 cm^{-1} is assigned to the aliphatic carbon-hydrogen deformation mode, and the band at 620 cm^{-1} to the CH_2 wagging mode. The feature at 715 cm^{-1} is thought to arise from the Si-C vibrations, with the weak bands at 1120 cm^{-1} and 1158 cm^{-1} due to the Si-O vibrations. This is believed to be the first time a waveguide Raman spectrum of this material has been reported.

A further attempt was made to obtain a waveguide Raman spectrum from the original, non-phenylated PDMS, using a substrate of silver, which was deposited by evaporation techniques on to a glass microscope slide. This was unsuccessful, but deserves further efforts, as a silver substrate is reported to have a refractive index index of 0.2[12], which would allow waveguiding experiments to be conducted using polymers which have refractive indices lower than that of quartz. Attempts have been made to perform such experiments by Dr.Y.P.Song in Durham, but none have been particularly successful. More work is, however, planned in this potentially very useful area.

2/. AF137.

This is an industrial polymer, which consists of 24% polymethylmethacrylate (PMMA), 56% polyethylmethacrylate (PEMA) and 20% methyl acrylic acid (MAA). This produces good films from isopropyl alcohol (IPA), and Figure 5.18 shows the spectrum obtained from an approximately 2.5 μm film deposited via horizontal flow from 1.96 grams AF137 in 9.79 grams IPA.

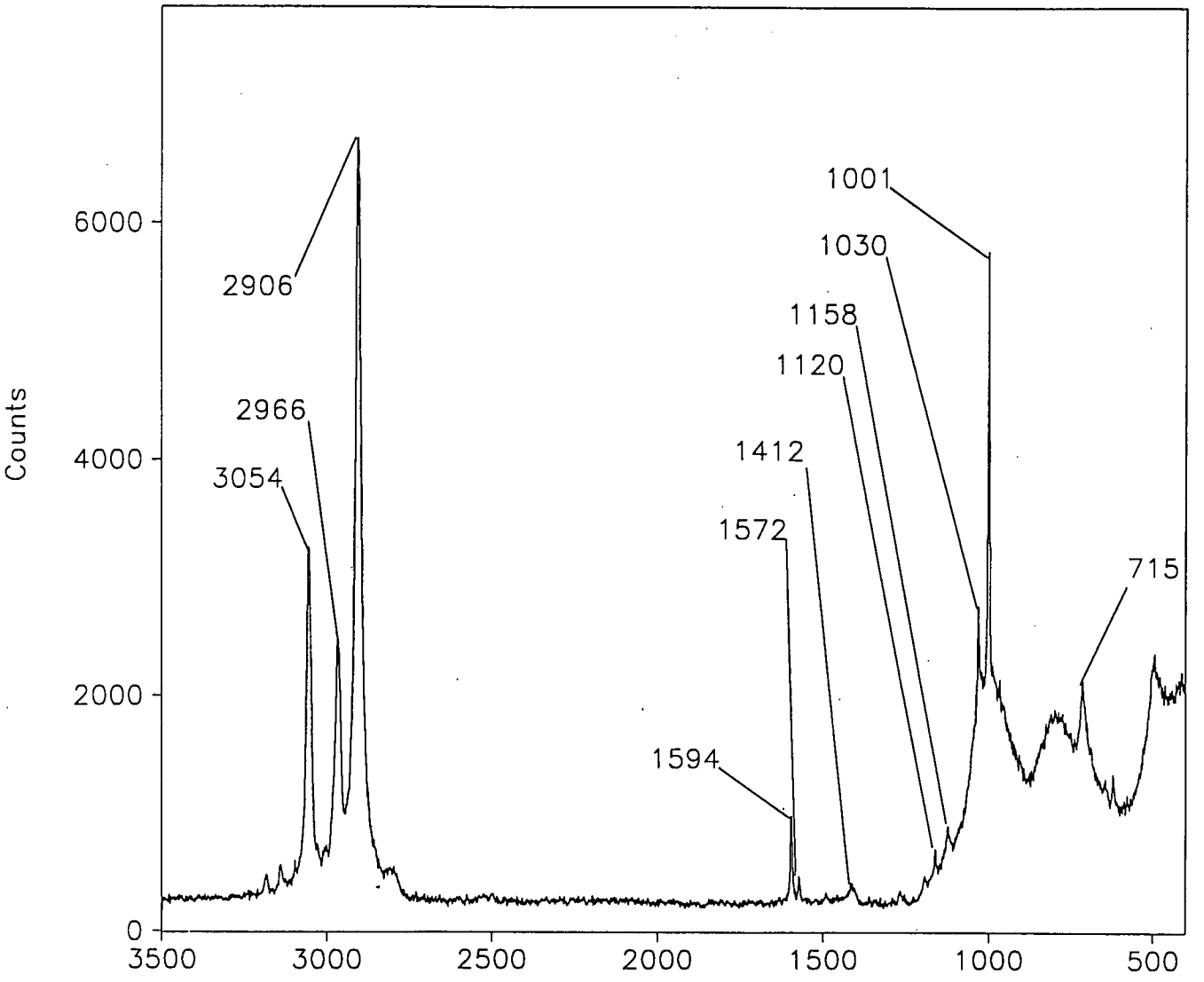

Figure 5.17 – Pure Phenylated Polydimethylsiloxane Spectrum

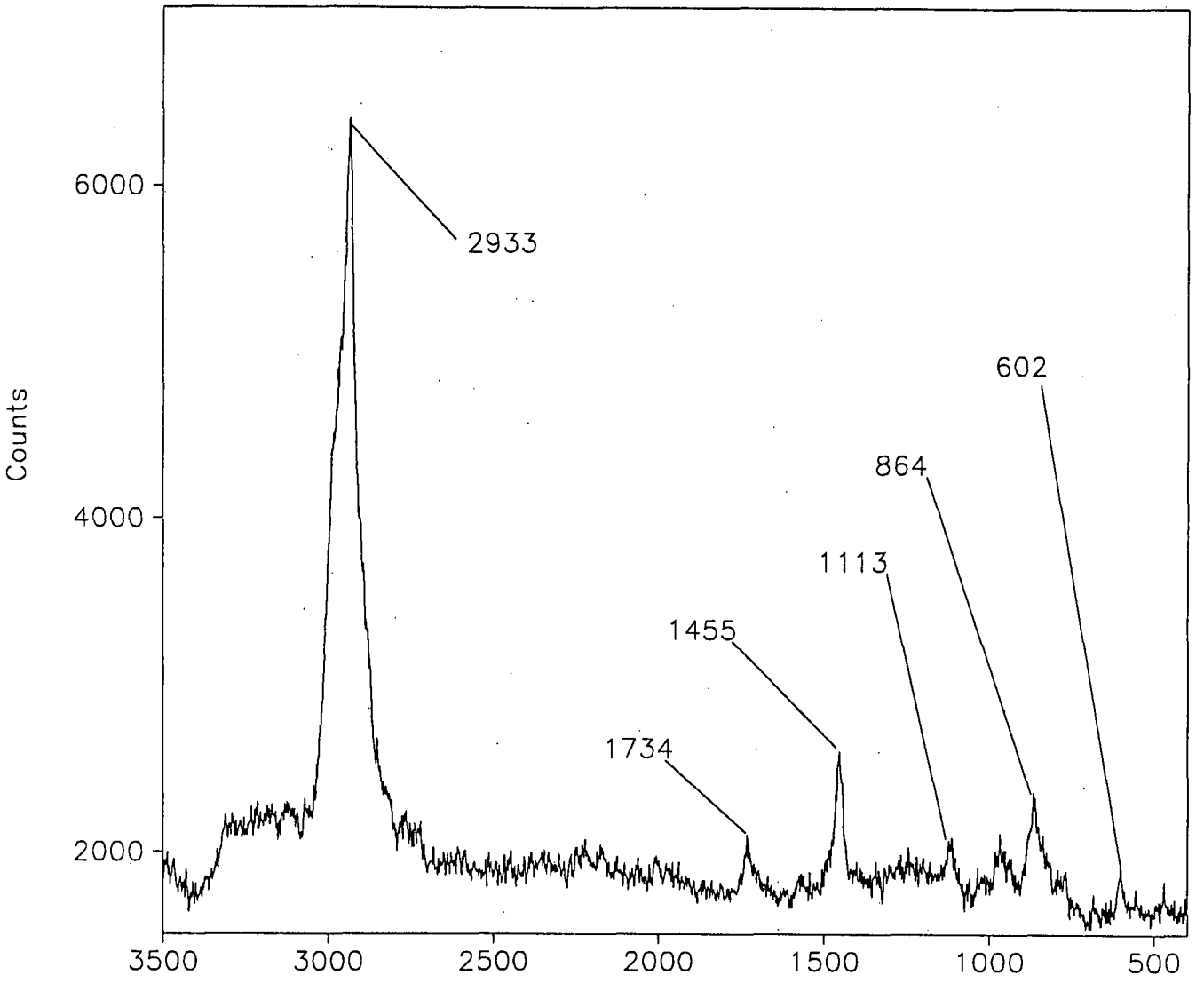

Figure 5.18 – Pure AF137 Spectrum

This spectrum has a somewhat disappointing signal to noise (S/N) ratio, but the main features expected are visible. The bands centred at 2933 cm^{-1} are assigned to the CH_2 and CH_3 stretching modes, with the band at 1455 cm^{-1} assigned to the CH_2 deformation mode and the band at 602 cm^{-1} assigned to the CH_2 wagging mode. The band centred at 1734 cm^{-1} is assigned to the carbonyl group vibrational mode, which is probably a composite of the three different type of carbonyls present in this species. The band at 1113 cm^{-1} probably arises from the C-O vibrational mode, and the band visible at 864 cm^{-1} probably arises from carbon chain skeletal vibrations. This is believed to be the first time that this material has been examined using waveguide Raman spectroscopy.

3/. XK91.

This polymer is another material of industrial relevance, which is essentially AF137 plus an aromatic amine, known as Rosin amine D, the structure of which is shown in Figure 5.46 later in this chapter. This amine, when mixed with the AF137, reacts with the methyl acrylic acid to form an amide salt. The whole mixture was dissolved in IPA, and produced films of reasonable quality. Despite this, however, it was found to be impossible to obtain a waveguide spectrum, because any waveguide produced soon faded, before any measurements could be obtained. This was due to the yellow colour of the amine, which resulted in the incident green laser beam being absorbed, which in turn led to localised heating of the sample, around the coupling point. Such heating leads to degradation (melting or burning) of the polymer film at this point, which causes the waveguide to fade as the polymer is removed from this spot. Upon examination of such films after the waveguiding experiment, the path where the waveguiding streak had been was clearly visible, as a path of clear material through the yellow XK91. This problem can be addressed with the use of different laser lines, dye lasers or, recently, the use of near-infrared excitation, used in FT-Raman instruments. In Section 5.5.3.3, the FT-Raman spectrum is presented of Rosin amine D, the source of the colour, but conventional waveguide Raman experiments on XK91, however, had to be abandoned.

4/. Epoxy Resins.

Waveguide Raman experiments were performed using these materials as part of a bid to re-create the diffusion experiments, described in the next chapter, which were studied using FT-IR ATR spectroscopy. The actual attempts to study diffusion processes in these systems will be discussed in a later section of this chapter, but the spectra obtained, and problems encountered in obtaining waveguide spectra of the pure materials, will be discussed here.

The first system examined was crosslinked Epikote[13] 1001, which consisted of 2.67 grams of Epikote[13] 1001 plus 1.33 grams KH92 (crosslinking agent), in 2.40 grams each xylene and n-butanol, plus 1.20 grams methanol. A film from this on quartz substrate, dipped at dipping speed 4.8 mm sec^{-1}, produced a film thickness of 16 $\mu m \pm 1$ μm, measured using the alpha-step. Thinner films of this material produced waveguides that faded within ten minutes or so, due to absorption of the laser line by the yellow colour imparted to the film by the crosslinking agent, KH92, which is an amine-based compound (see Chapter 1, section 1.2.2). An FT-Raman spectrum of the

crosslinking agent, KH92, is presented in Section 5.5.3.3. When a thicker film was used, the waveguide, although it slowly faded, remained at a reasonable intensity long enough for the spectrum to be obtained. Figure 5.19 shows the spectrum produced.

The band centred at 3076 cm^{-1} is attributed to the aromatic CH stretching mode, with the band centred at 2938 cm^{-1} assigned to aliphatic CH_2 and CH_3 anti-symmetric and symmetric stretching modes. A further aromatic ring band is seen at 1611 cm^{-1}, with the C-H deformation mode seen in the band at 1459 cm^{-1}, and the CH_2 wagging mode seen in the band at 685 cm^{-1}. The band at 1295 cm^{-1} is thought to arise from the C-Me stretching mode, with the feature at 1227 cm^{-1} probably arising from the C-O-C stretching mode. The remaining bands at 1186 cm^{-1}, 1114 cm^{-1} and 820 cm^{-1}, are thought to be due to the C-N-C bending mode, which arises from the crosslinks (see Chapter 1, section 1.2.2), the C-OH stretching mode and the epoxy C-O-C stretching mode respectively.

The use of too thick a film is undesirable for waveguiding experiments, as the individual waveguiding modes tend to merge together, sometimes to the extent of becoming one continuous mode, which is obviously undesirable for quantitative experimentation. This was indeed the case, with Figure 5.19 being obtained from such a continuous waveguiding mode. It has the further disadvantage that the software processes large numbers of calculations, which leads to extremely long processing times on standard PCs.

Thus, a further epoxy system was sought, which contained a lower proportion of the coloured crosslinking reagent, KH92, from which the problem arose. It was finally decided to use Epikote[13] 1004, which has a larger degree of polymerisation (n), being 4.67, compared with 2.64 for Epikote[13] 1001. This also required a substantially lower amount of KH92 for sufficient crosslinking to occur, requiring 1 part KH92 to 6.6 parts Epikote[13] 1004, compared with 1 part KH92 to 2 parts Epikote[13] 1001. Figure 5.20 shows the waveguide Raman spectrum of a film of 3.8 $\mu m \pm 0.6$ μm of this material.

The bands are assigned in the same way as those in the Epikote[13] 1001 spectrum. One interesting feature, however, is the almost total lack of substrate bands in the Epikote[13] 1004 spectrum. This allows some weaker features, probably due to the skeletal vibrations of the carbon backbone, to be observed. It is believed that this is the first time that epoxy resins have been examined using waveguide Raman spectroscopy. A detailed discussion of the substrate peaks is given in Chapter 7.

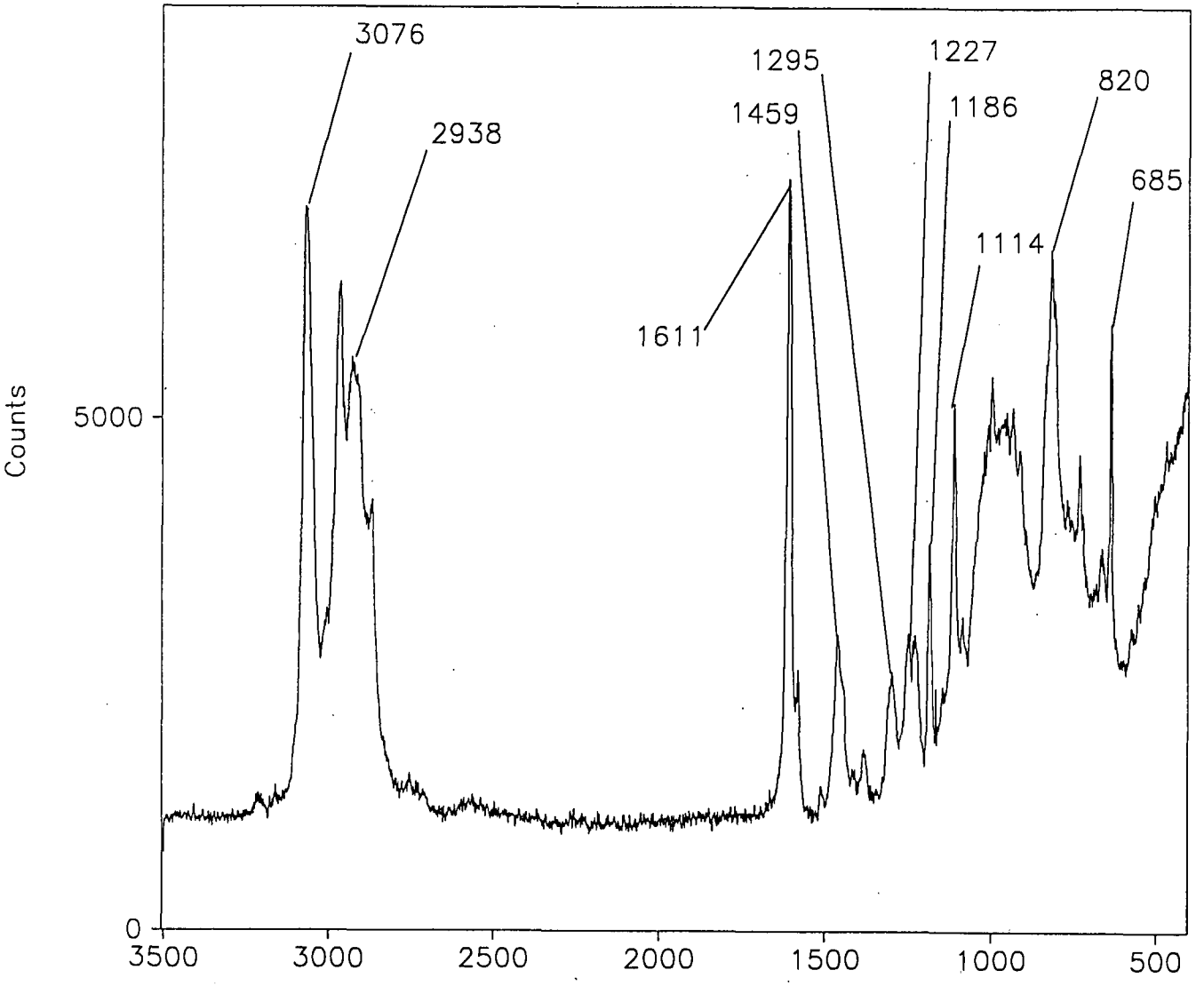

Figure 5.19 – Pure Epikote 1001 Spectrum

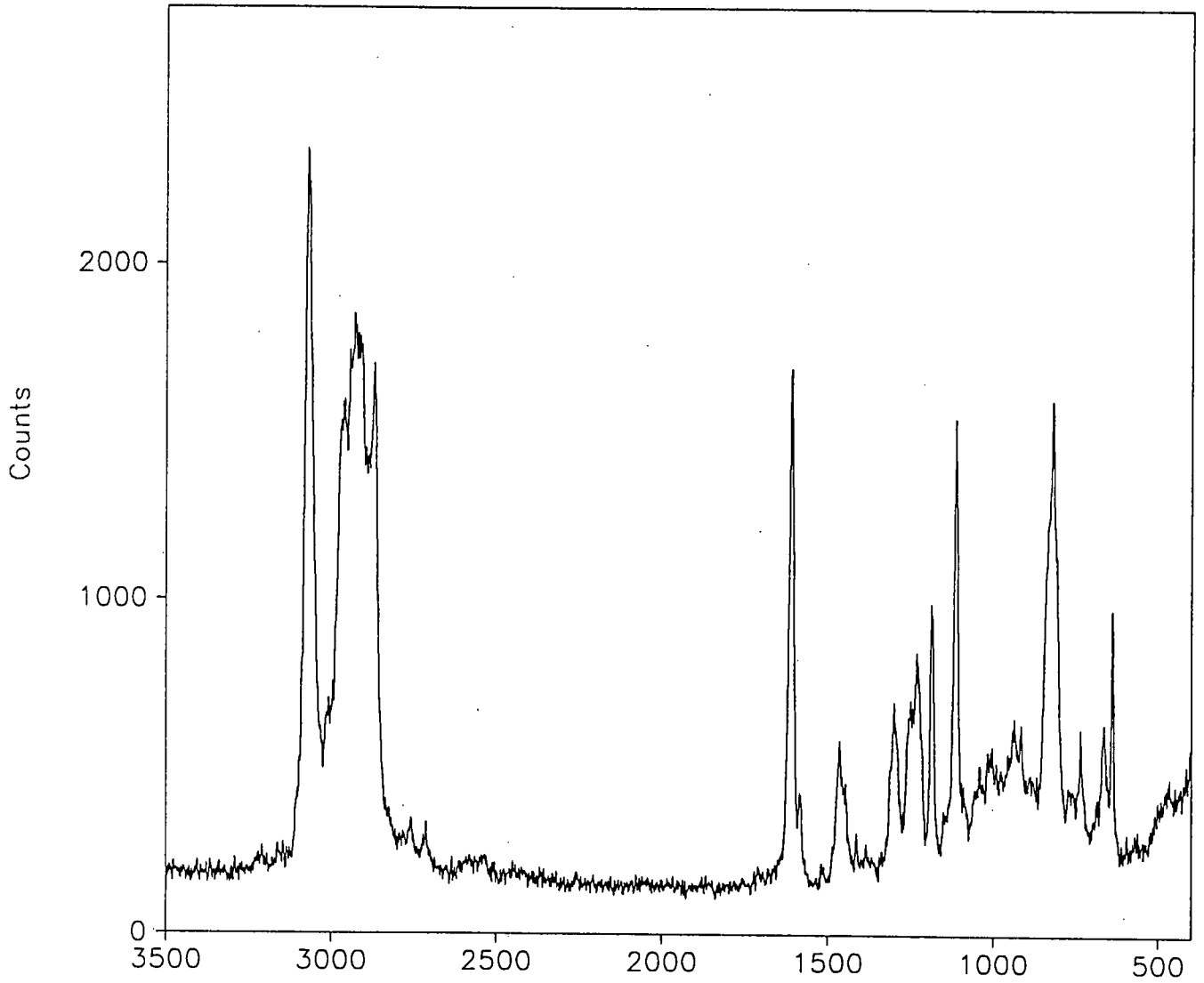

Figure 5.20 – Pure Epikote 1004 Spectrum

5.5.3 - Laminate Systems.

One of the important theoretical applications of waveguide Raman spectroscopy is as a probe for possible examination of interfacial regions which exist between different layers in laminated systems. This is made theoretically possible by the significant enhancement resulting from the increased scattering volume arising from the waveguiding streak and the compression of the laser beam into micron-thick films. Rabolt and Swalen[1] claim to have seen interfacial interactions, arising from a laminated system of PVA and PMMA, and produce spectra to verify their claim. In this project, the intention was to examine numerous laminate systems, but for various practical reasons, only three were examined successfully. In this section, the experimental results are divided into two areas, the first part dealing with unsuccessful systems, and a brief discussion of these negative results. The second subsection deals with the three successful experimental systems, and presents practical considerations, spectra and electric field calculations.

To conclude this introduction, a brief description of practical considerations associated with laminate production is presented. In the experiments described here, the film of lower refractive index was deposited first, although strictly speaking, it does not really matter which substance is deposited first, as the waveguide propogates through both films[1].Once the first layer is deposited, it is always advisable to confirm that it is capable of supporting a waveguide, before proceeding. Following measurement of the lower film thickness, the deposition of the top film is the next stage, and it is here that careful choice of solvent becomes necessary. Consultation of literature such as the Polymer Handbook[7] is required, to choose a solvent for the top film, which is a non-solvent for the lower film. This is the cause of considerable frustration, as it has been found that potentially very interesting laminates simply cannot be produced using solution deposition methods. The actual deposition of the top film requires care, as it is possible for the solution to strip off the lower film, irrespective of solubility. This has been found especially true for aqueous solutions.

5.5.3.1 - Unsuccessful Systems.

The problems associated with the preparation of polymer laminates, discussed above, are essentially doubled in comparison with the successful preparation of single films, simply due to the presence of an additional film. It is therefore not surprising that the production of a polymer laminate, which meets the rigid quality requirements for good waveguiding, is a difficult process. In this subsection, individual laminates, which, for one reason or another, did not produce satisfactory waveguides, are discussed, in order that future investigators are aware of the difficulties associated with these systems. Most problems encountered are solvent-based, hence the use of other deposition methods, such as film production from the melt, is a possible solution, worth consideration.

Polystyrene (PS, n=1.583)/Poly(vinylacetate) (PVAc, n=1.466).

From a solvent point of view, this system should have been ideal, as PS is reported[7] as being soluble in carbon disulphide, which is listed as a non-solvent for PVAc. Several attempts were made to prepare this laminate, with a film of PVAc being deposited first from toluene, but the PS always produced a cloudy film, thought to be due to the high volatility of carbon disulphide, an effect often seen, and discussed before. Attempts to cool the system, and hence restrict the rate of evaporation, by using a cooled PVAc film and allowing the PS film to solidify in a fridge (in a sealed desiccator, due to the toxic nature of carbon disulphide), were unsuccessful, and thus, in the absence of any other suitable solvent system, this system had to be reluctantly abandoned.

2/. Poly(vinylpyrrolidine) (PVP, n=1.517)/Polymethylmethacrylate (PMMA, n=1.489).

Several attempts to produce a laminate of this system were made, with the PMMA film being deposited from xylene solutions and the PVP from methanol. On each occasion, however, despite films of reasonable appearance being produced, the waveguiding properties were poor, and thus the spectra produced were useless.

3/. Polystyrene (PS, n=1.583)/Polymethylmethacrylate (PMMA, 1.489).

Attempts to prepare this system were thwarted by the problem of cloudy films of polystyrene being produced from cyclohexane solutions, again due to rapid evaporation. Attempts to restrict the evaporation rate again failed, as did attempts to drive out the residual solvent by gentle heating.

5.5.3.2 - Successful Systems.

Three systems were examined successfully during the course of this project, and these will now be considered in depth. For each system, the practical preparation will be considered first, followed by a detailed analysis of spectra produced, along with the results of electric field calculations carried out on the systems.

1/. Polymethylmethacrylate (PMMA, n=1.489)/Poly(vinylalcohol) (PVA, n=1.52).

This system was of particular interest to us, as Rabolt and Swalen[1] report discovering new spectral features, attributable to interfacial interaction, and support these claims with spectral evidence. In the course of this project, three individual PVA/PMMA systems were examined, with varying thickness of the two components. Following the preparation details, each system will be considered individually, with general comments on the three experiments concluding this section.

All three laminates discussed here were prepared in a similar fashion, with PMMA, deposited from toluene, forming the lower layer, and the PVA layer, deposited from purified water, forming the upper. Considerable difficulties were encountered in the course of the deposition of the PVA, as it was found that the PMMA layer lifted if it was exposed to the aqueous medium for too long. The critical time was of the order of a few seconds, so merely using a very quick dipping speed did not alleviate the problem. Eventually, a solution was found that required the PMMA film to be heated gently (so as to avoid annealing) for several hours, which appeared firmly to fix the film to the substrate. After this, it was found that a film of PVA could be deposited successfully on top, using a hot aqueous solution.

(A). System One.

The first system produced that yielded a satisfactory waveguide consisted of a 0.6 μm ± 0.2 μm layer of PMMA, with a 2.2 μm ± 0.6 μm layer of PVA on the top. This arrangement gave rise to three waveguiding modes, of which two (m=0 and m=2) had waveguiding streaks from which Raman spectra could be accumulated. The other mode (m=1) was exceptionally weak and yielded no spectra, even when high laser powers, wide slits and low scan speeds were used. Figure 5.21 shows the full spectrum obtained from both waveguiding modes, plus the spectra of the two pure materials, where the spectra labelled m=0 and m=2 refer to those obtained from the waveguiding modes of the laminate. Figure 5.22 shows the same four spectra, but with the area around the carbon-hydrogen stretching mode region expanded.

If Figure 5.22 is examined closely, a small frequency shift can be seen, with the m=0 band appearing at 2912 cm^{-1}, the m=2 band seen at 2916 cm^{-1}, the pure PVA band centred at 2912 cm^{-1} and the pure PMMA band seen at 2951 cm^{-1}. This is thought not to be due to any interfacial interaction, but simply to the different optical electric field distributions in the two systems. This will cause the relative intensities of the bands associated with the two polymers to change as the optical electric field distribution changes. Hence, the bands will appear to shift, due to these changes in band relative intensities. In other words, the band occurring in the m=2 waveguiding mode has a greater contribution from PMMA, as the optical field density is greater in the PMMA

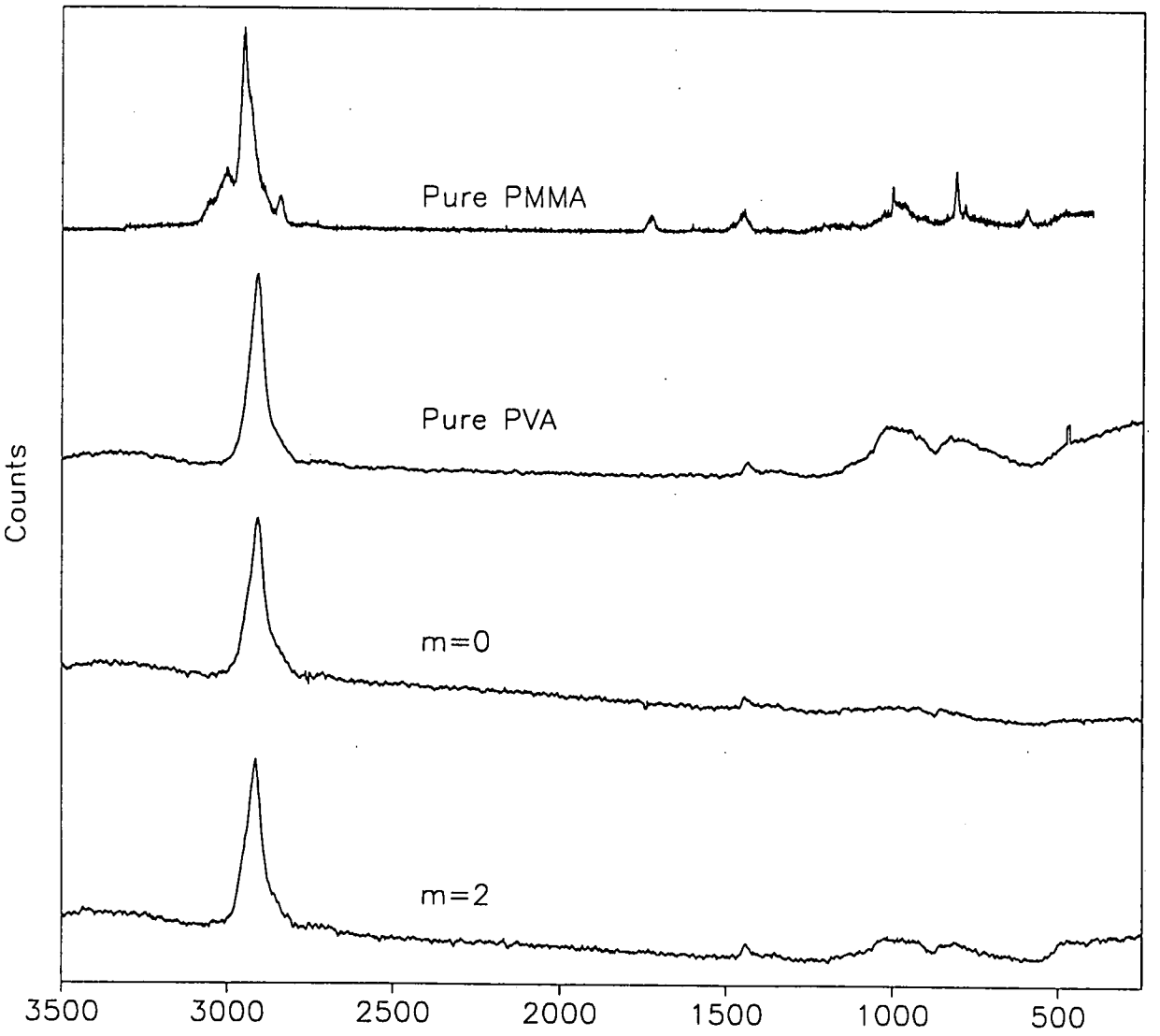

Figure 5.21 - PMMA/PVA Laminate; System One

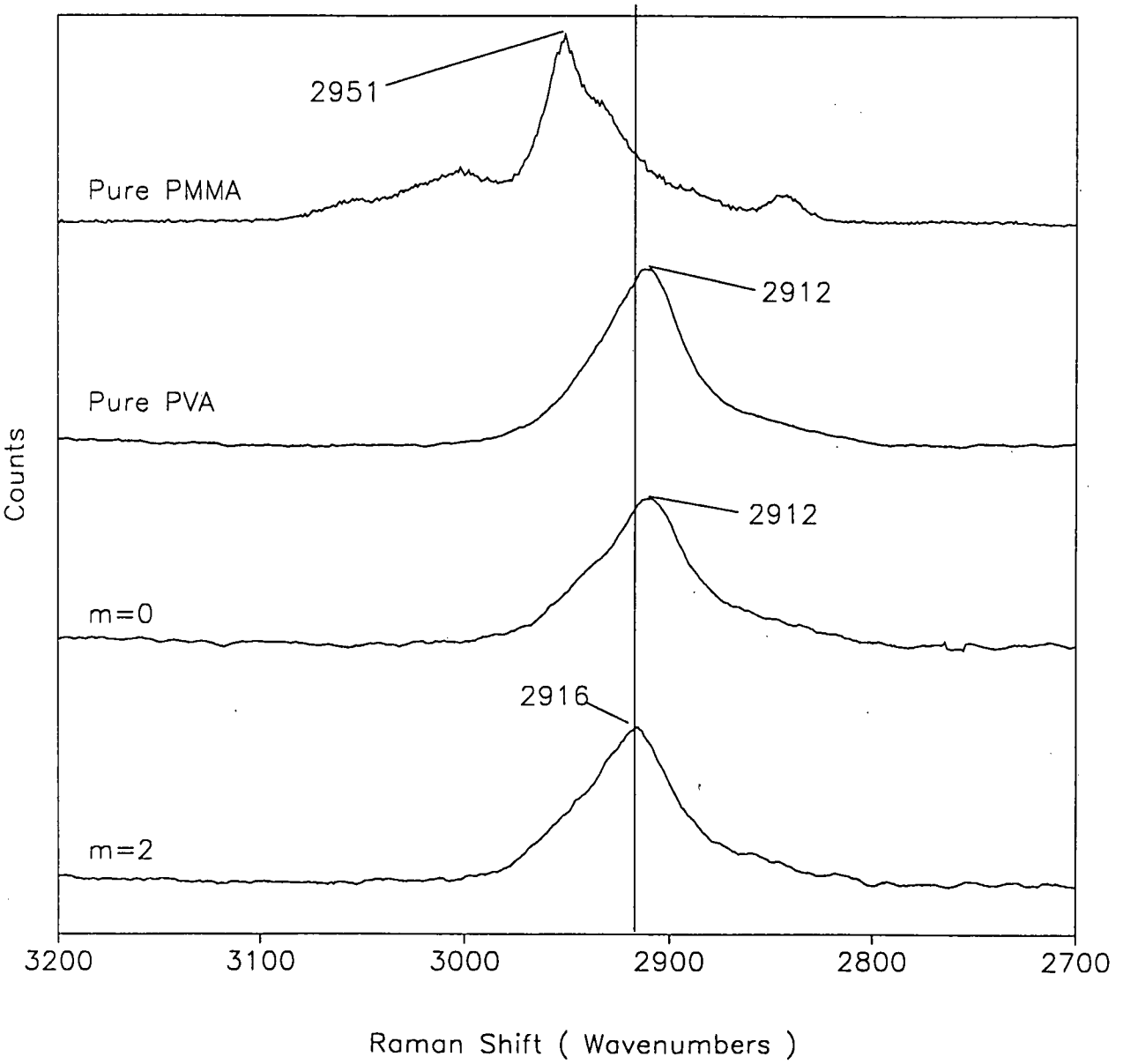

Figure 5.22 - PMMA/PVA Laminate; System One

compared with the m=0 mode. This is clearly shown by the figures in Table 5.6 below. The waveguiding mode angles were determined using the off-line waveguiding rig, and the resulting angles analysed using the program 'Index4' [4], described above.

Table 5.6

Mode Number	Mode Angle (From Normal)	Electric Field Distribution	
		PMMA	PVA
0	2°86'	1.4%	98.6%
2	-0°24'	27.2%	72.7%

As explained above, it was not possible to scan m=1, due to the very poor nature of the waveguide. Figure 5.23 shows a diagram of the electric field distribution in this laminate.

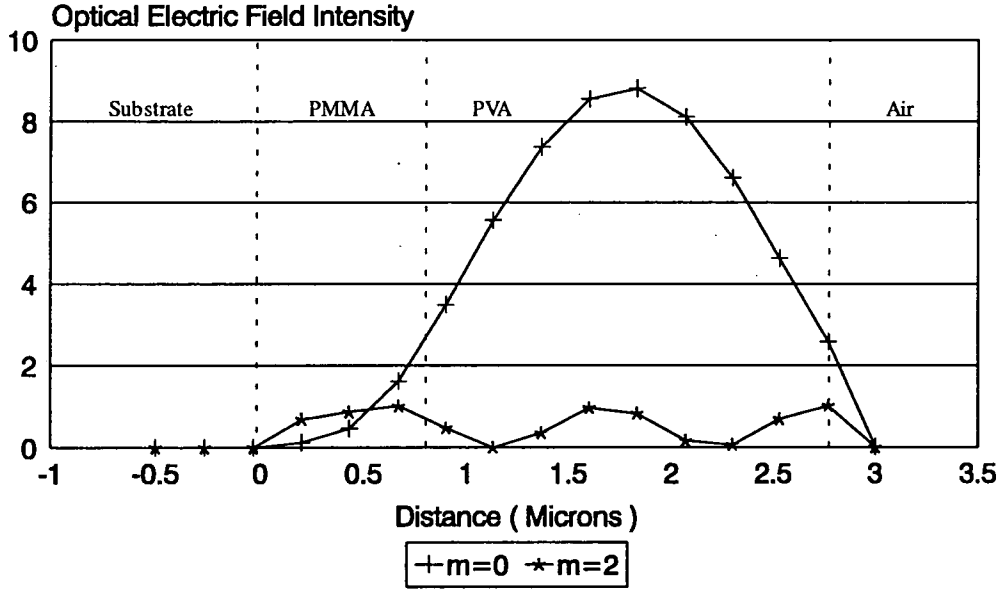

Figure 5.23 - Optical Electric Field Distribution

From this data, we can predict that the mode which may show some evidence of interfacial interactions is m=0, where the sampling electric optical field is stronger at the PMMA/PVA interface. A probable place for any interfacial interaction to be evident is in the area around the carbonyl stretching mode associated with the PMMA layer. The carbonyl group has a significant dipole associated with it, which could interact, via hydrogen bonding, with other charged groups, such as the hydroxyl group associated with the PVA. This area is shown in detail in Figure 5.24.

It can be clearly seen that little or no signal is in evidence from the carbonyl stretching mode in the two laminate spectra, but this is reasonable, as the sampling optical field at the interface is not very strong.

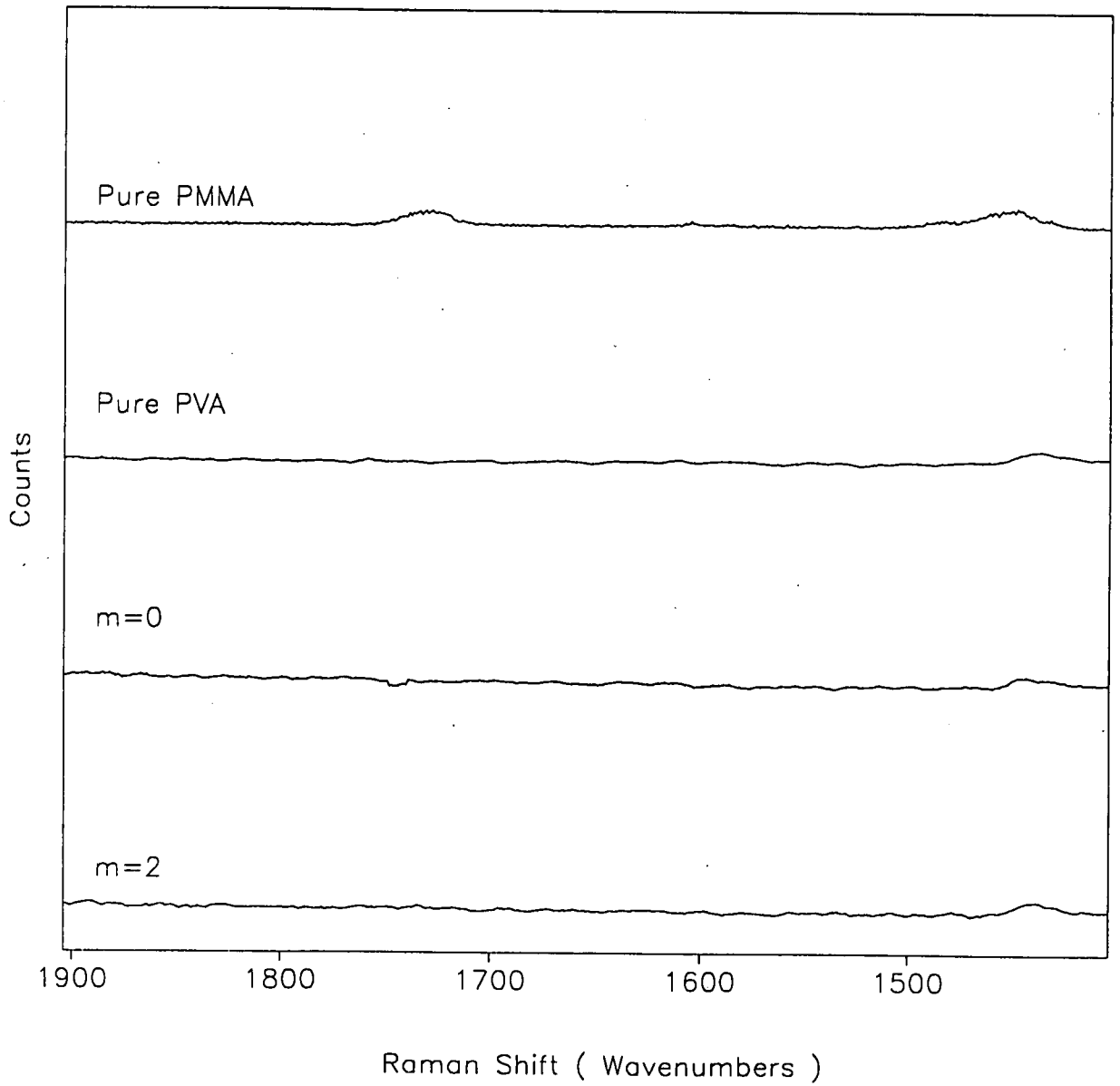

Figure 5.24 - PMMA/PVA Laminate; System One

(B). System 2.

Here, the thicknesses of the two films were reversed, with a thick film of 2.7 μm ± 0.2 μm PMMA under a thinner film of approximately 1 μm PVA. This gave rise to a system which yielded 5 waveguiding modes, of which only two were intense enough to examine, namely the m=1 and m=2 modes, the others, including the m=0 mode, being too weak to produce any sensible results. The spectra of these two modes are shown in Figure 5.25, along with the spectra of the individual components:-

The electric field distribution of these two modes are given below in Table 5.7

Table 5.7

Mode Number	Mode Angle (From Normal)	Electric Field Distribution PMMA	PVA
1	-0.56	86.6%	12.4%
2	-1.13	72.4%	24.7%

This is rather interesting. The spectra appear to indicate that the sampling optical field is present more or less wholly in the PMMA layer, whereas the theoretical calculation predicts that both modes should show some PVA presence. Figure 5.26 shows the results of three spectral subtractions, which appear to rule out data-handling errors. The lower spectrum, involving the subtraction of the m=1 mode from the m=2 mode, has a subtraction factor of 1, at which no features would have been seen if the two had been identical, and the two upper spectra present each individual mode, with pure PMMA subtracted to the same degree of subtraction. The two spectra appear dissimilar.

The peaks remaining after the subtraction of the pure PMMA are thought to be wholly due to the residual toluene in the PMMA film. These toluene bands appear more intense in this laminate case than in the single film system described earlier. This is probably due to the fact that the PMMA film is approximately 1 μm thicker in the laminate system than it was in the single film, hence the concentration of toluene is effectively greater.

Figure 5.27 shows a comparison of pure PMMA, mode m=1, and the same mode m=1, but with pure PMMA subtracted out.

The positions of the carbon-hydrogen deformation bands are clearly very similar, with the band shapes from the laminate and pure PMMA seemingly very similar. The pure PMMA spectrum is a little noisy, so it isn't possible completely to rule out the possibility that the small shoulder, on the low frequency side of the laminate band, could be partly due to PVA.

Figure 5.28 shows a diagram of the electric field distribution in this case.

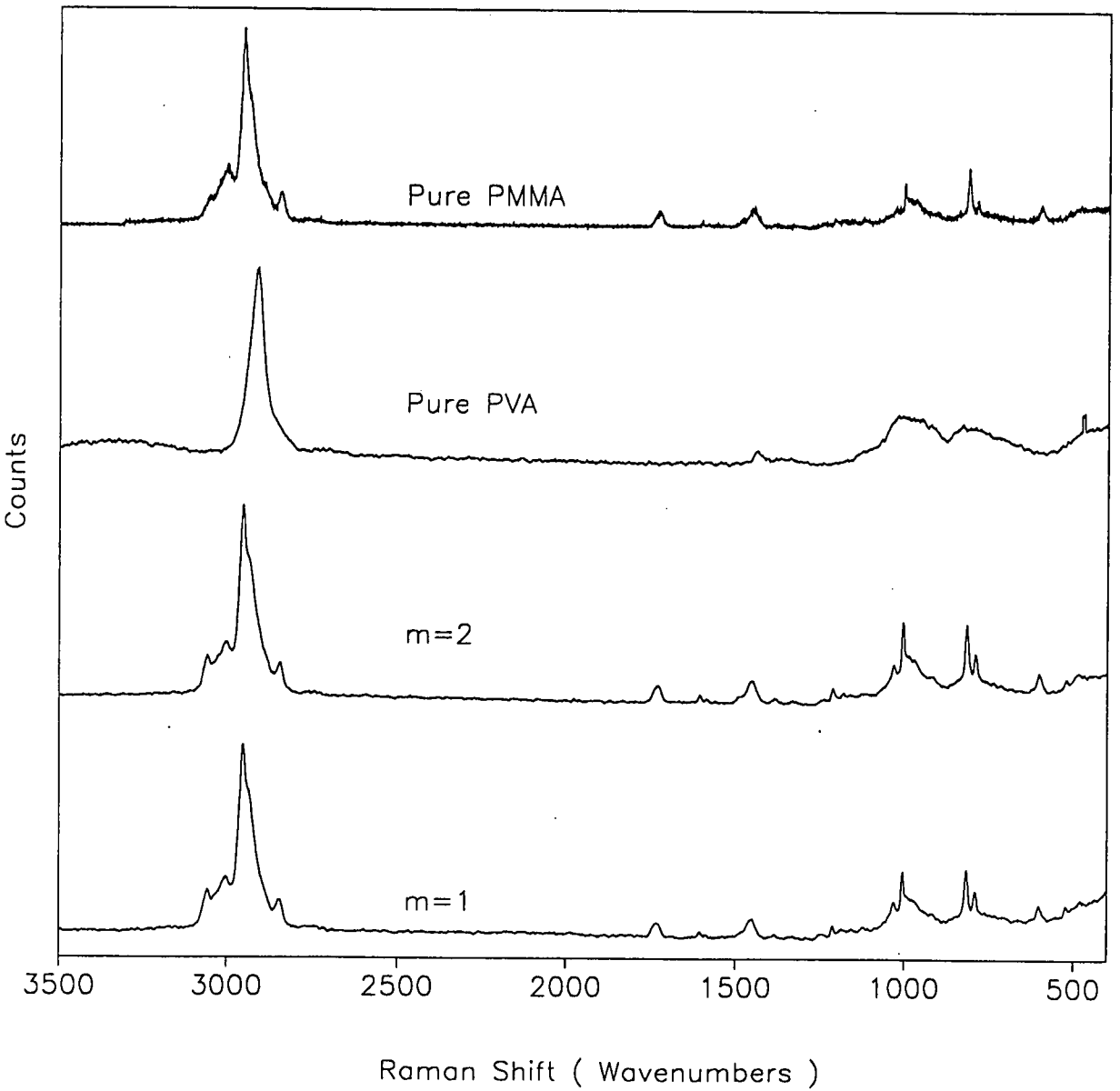

Figure 5.25 - PMMA/PVA Laminate; System Two

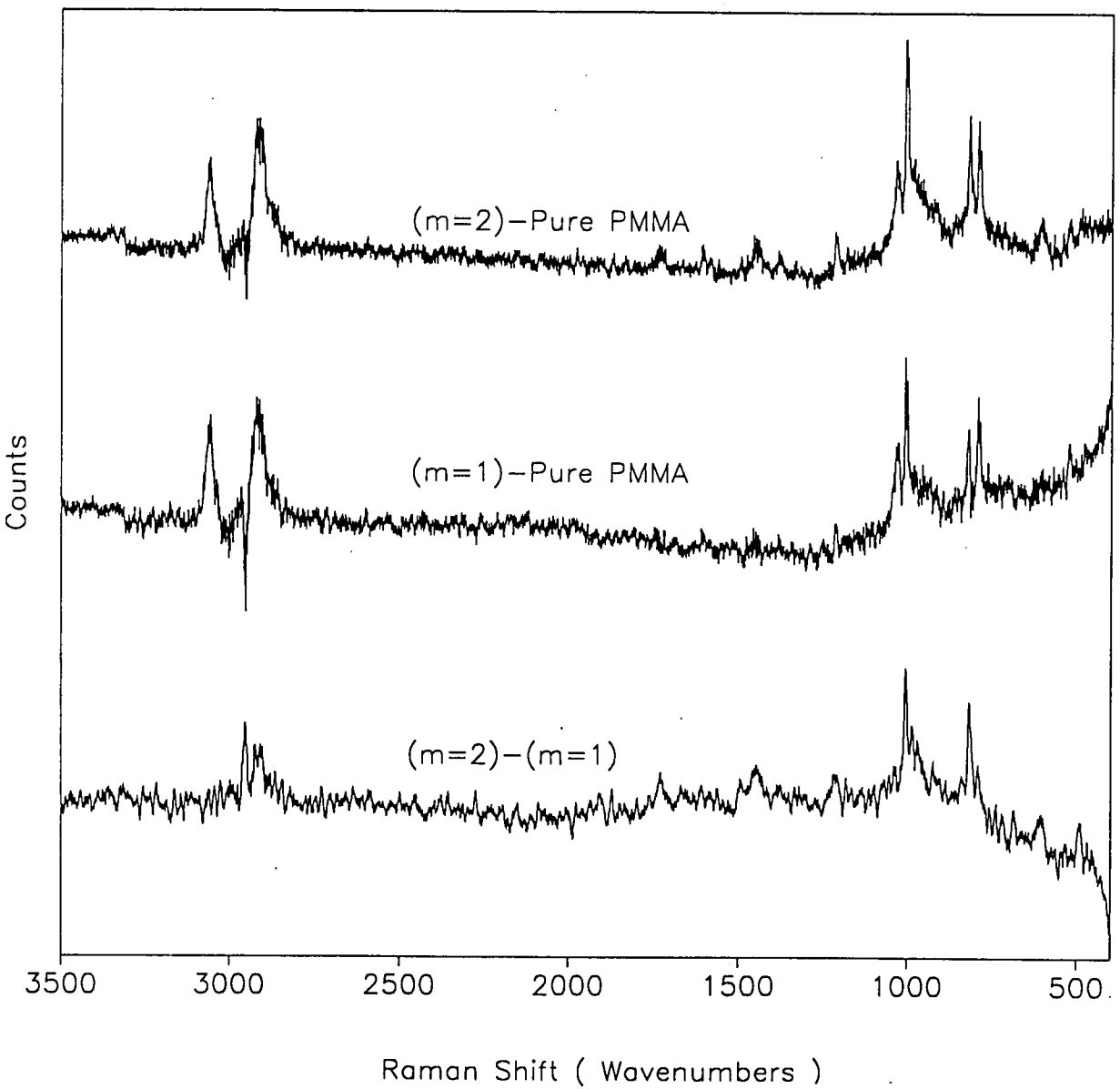

Figure 5.26 - PMMA/PVA Laminate; System Two

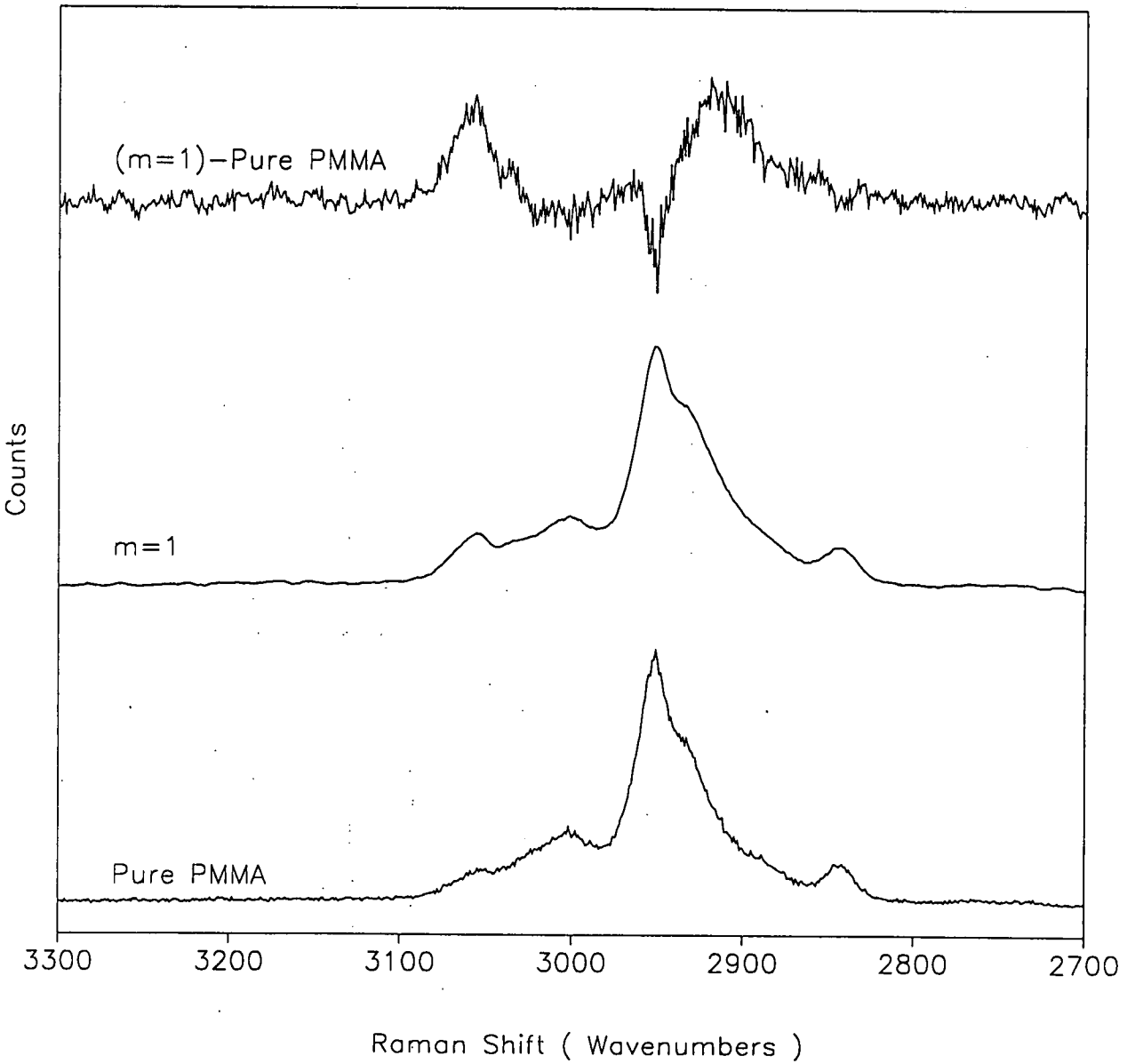

Figure 5.27 - PMMA/PVA Laminate; System Two

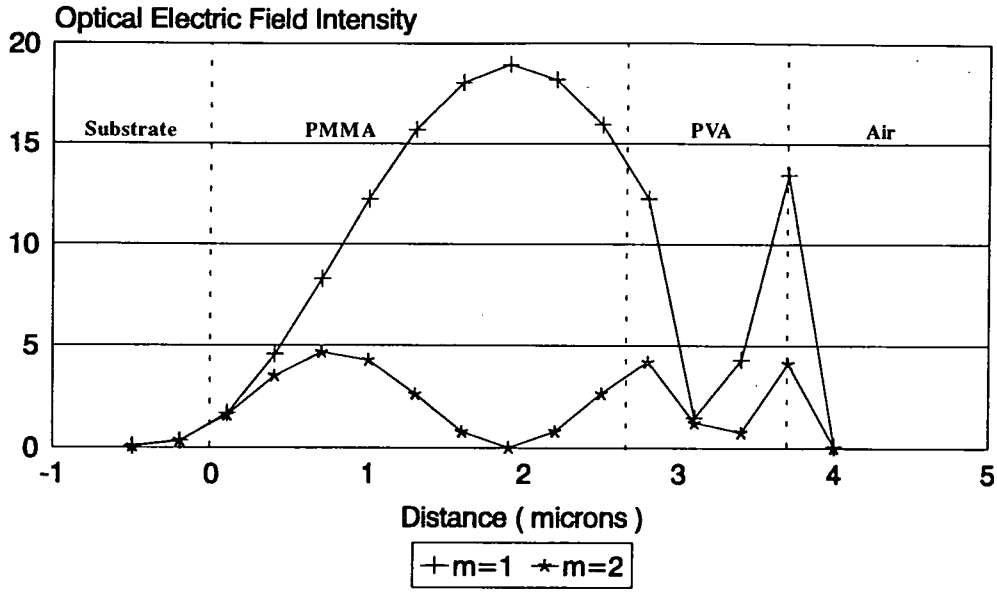

Figure 5.28 - Optical Electric Field Distributions

Figure 5.29 shows the substrate peaks arising from three different systems, namely the waveguiding mode, m=2, from this system, a pure PMMA film and the m=2 waveguiding mode obtained from system 1, above, where the sampling optical electric field was concentrated in the upper (PVA) layer.

This is rather interesting, and acts as proof of the model of waveguiding propogation, proposed by Swalen and Rabolt[1]. They state that in a laminate, the beam totally internally reflects through all layers of the laminate, the reflection occuring at the laminate/substrate and laminate/superstrate interfaces. However, the sampling optical field is concentrated in certain regions of the laminate, dependent mostly on the angle of incidence of the beam, but also on the film thicknesses and refratcive indices. In System 2, the sampling optical field is concentrated in the lower film (See Figure 5.28), and thus the presence of substrate peaks is easily understood, but if Figure 5.23 is examined, the converse is true, with the sampling optical field concentrated in the upper layer. However, substrate peaks are also in evidence in this system. Thus, substrate features must be due to evanescent wave penetration into the substrate at the point of reflection at the substrate/laminate interface, a hypothesis vaguely suggested by Levy *et al.*[8]. The issue of substrate peaks is discussed more fully in Chapter 7.

(C). System 3.

This system comprised a 0.5μm ± 0.1μm PMMA and 1.5μm ± 0.1μm PVA, which were dipped, at dipping speed 4.8 mm sec^{-1}, from solutions of toluene and water respectively. Two waveguide modes were seen, and using the software 'Angle4' and 'Index4', described above, the electric field distributions in Table 5.8 were produced.

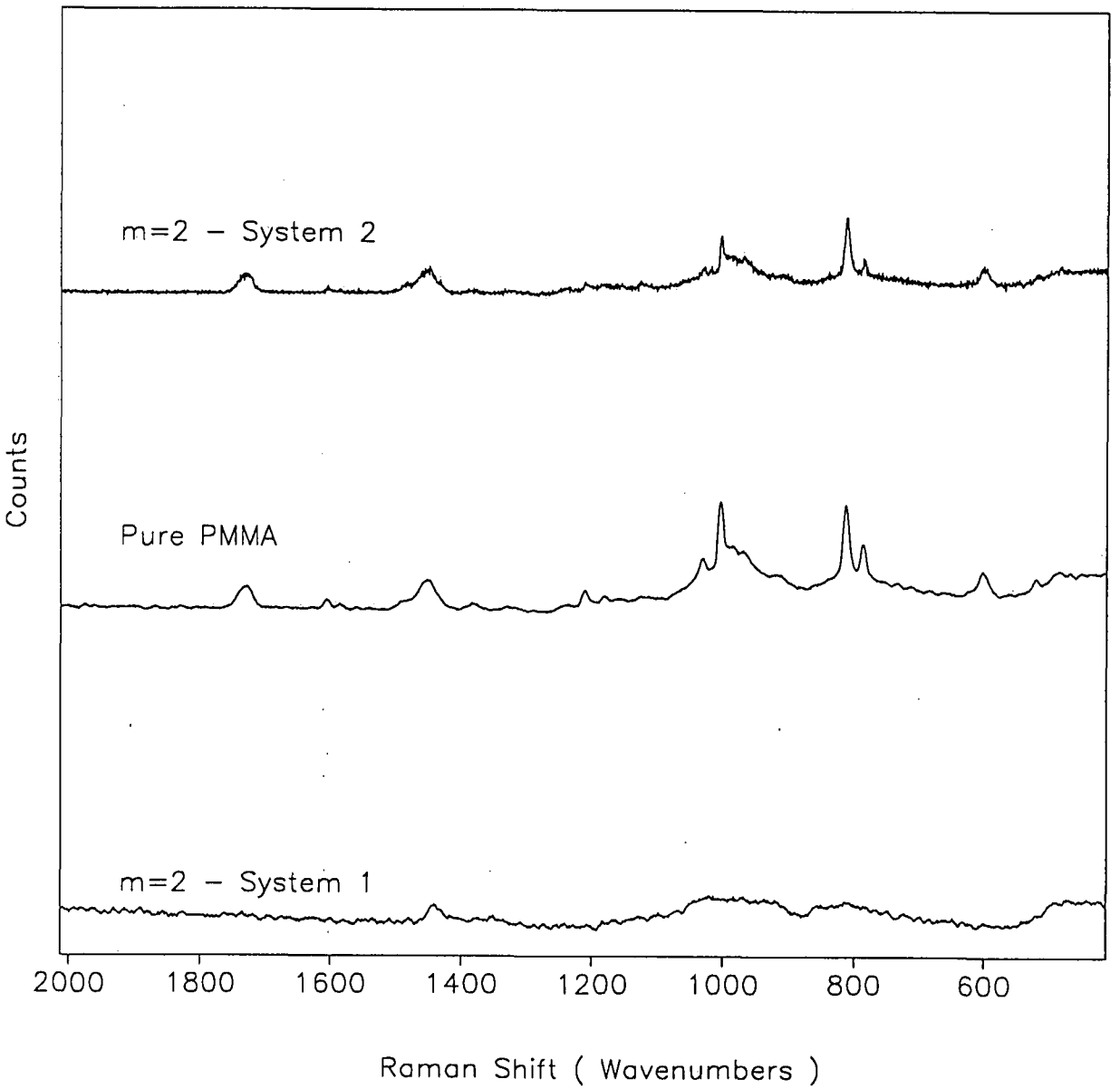

Figure 5.29 - PMMA/PVA Laminate; System Two

Table 5.8

Mode Number	Mode Angle (From Normal)	Electric Field Distribution PMMA	PVA
0	$1^{o}56'$	12.8%	87.0%
1	$-1^{o}95'$	68.6%	23.5%

A further mode is predicted by the calculations, but no evidence for this mode was found when examining the system, so the details have been excluded. Figure 5.30 shows the carbon-hydrogen stretching region, which clearly shows this distribution. The waveguiding mode, m=0, when compared with the pure polymer spectra, is clearly dominated by the PVA spectrum, but the shoulders on the high frequency side of the band shows a small influence of the PMMA spectrum. The waveguiding mode, m=1, however, shows a larger degree of the sampling electric field being in the PMMA layer, with a composite band of the two polymers, exhibiting a shift in relative frequencies, thus moving the band to a frequency higher than the m=0 band and between the positions of the bands in the pure polymer spectra.

The actual electric field distributions are shown in Figure 5.31.

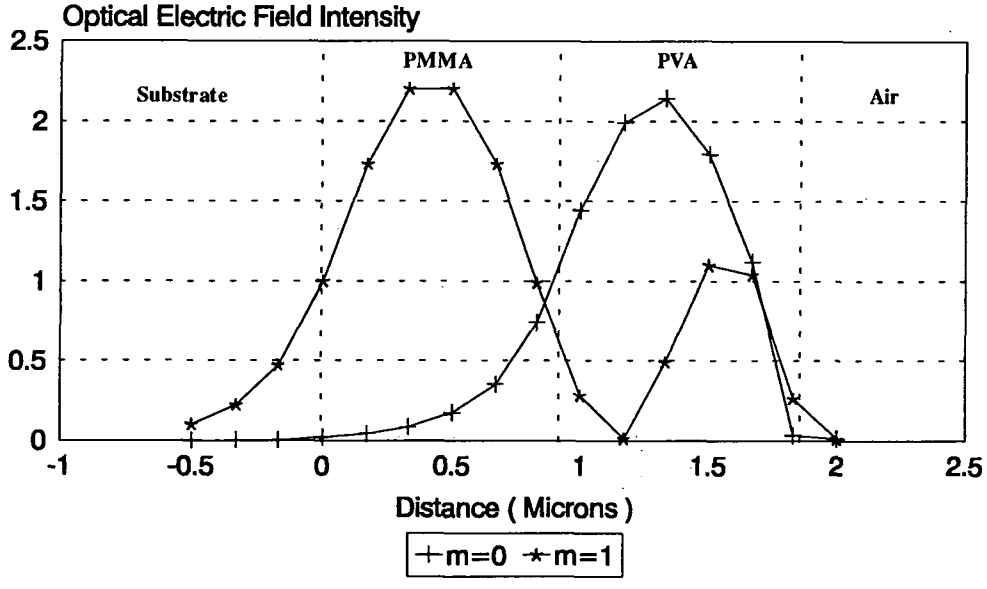

Figure 5.31 - Optical Electric Field Distribution

If the possibility of examining interfacial regions is to be realised, then a maximum electric field intensity is required at that position. However, it can be seen that in neither case is the electric field intensity sufficient at the PMMA/PVA interface for successful observation of interfacial effects.

2/. Polystyrene (PS, n=1.583)/Poly(vinylalcohol) (PVA, n=1.52).

This system presented considerable difficulties, in that although seemingly good-quality films were produced, the waveguide properties of such films were often very poor, with waveguiding streaks of insufficient intensity to give rise to a Raman spectrum. The system has been examined before by Rabolt and Swalen[1], who reported a system

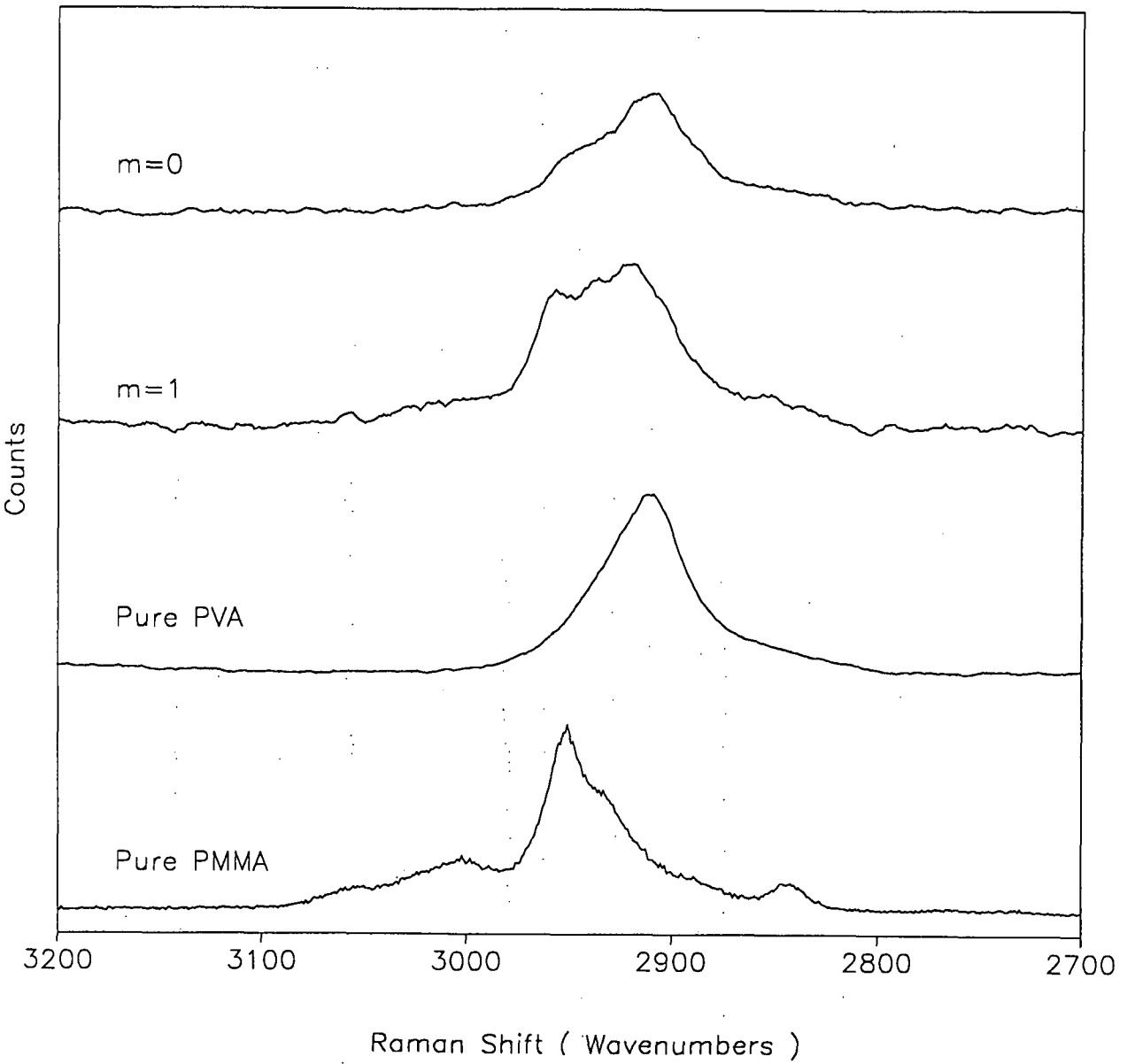

Figure 5.30 - PMMA/PVA Laminate; System Three

which gave rise to four waveguiding modes, but did not exhibit any interfacial interactions, which is not surprising if the chemistry of the two polymers are considered (see Appendix 1). However, it was decided that it would be of merit to repeat the work, and hence systems were prepared from aqueous solutions of PVA, which were dried in the oven at 65°C for several hours. The PS layer was then dipped on top from a solution of toluene. After many unsuccessful attempts, including one laminate that gave rise to a spectacular curved waveguiding streak, one system was finally produced which gave rise to reasonable Raman spectra. This was produced from a hot solution of 2.65 grams PVA and 9.37 grams water, dried at 65°C for three and a half hours in an oven, with a PS film, dipped from a solution of 11.25 grams PS in 60 grams toluene. The dimensions of the two films were PS, 1.1μm ± 0.2μm and PVA, approximately 0.6μm. As the off-line rig was not in operation when this experiment was performed, the mode angles were calculated using the program 'Angle4'[5], which is a version of the 'Angle'[5] program described above, but which calculates angles for a four layered case, from input of refractive indices and film thicknesses. These calculated angles were then entered into the 'Index4 [4]' program, which produced the electric optical field distributions listed in Table 5.9.

Table 5.9

Mode Number	Mode Angle (From Normal)	Electric Field Distribution	
		PVA	PS
0	9°96'	2.3%	96.9%
1	5°43'	18.7%	80.9%
2	0°75'	56.7%	35.9%
3	-2°52'	42.5%	39.7%

Figure 5.32 shows the spectra produced from this particular laminate, in the carbon-hydrogen stretching region:-

The band marked at 3056 cm^{-1} is attributed to the aromatic CH stretching mode, arising from the polystyrene, with the band centred at 2906 cm^{-1} arising from a combination of the aliphatic CH stretching modes of both polystyrene and poly(vinylalcohol). As the field changes from being concentrated mainly in the PS, the aromatic band decreases relative to the aliphatic band, which confirms the optical electric field distribution calculated for this system. Figure 5.33 shows a diagram of the optical electric field produced by this system.

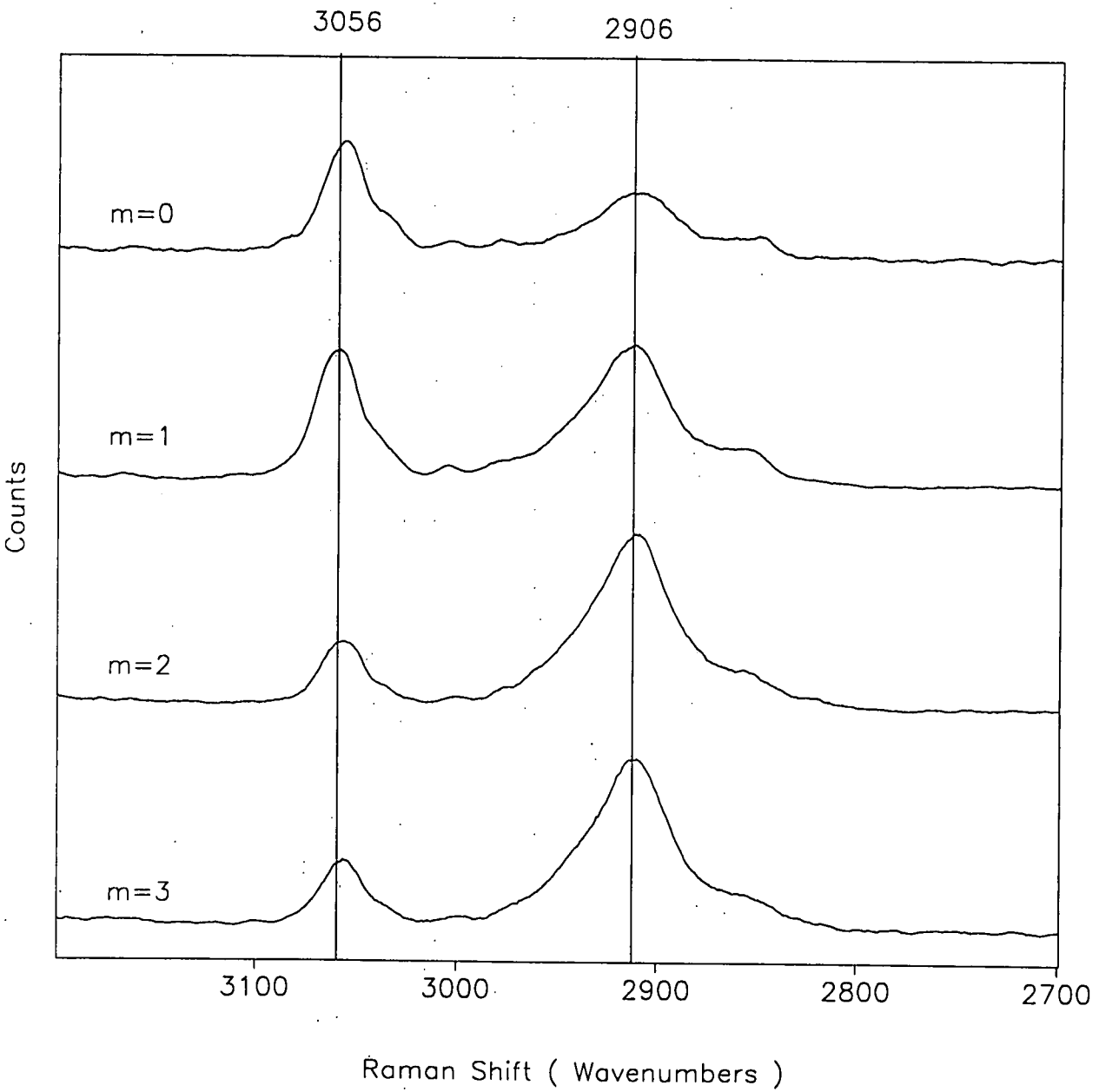

Figure 5.32 - PS/PVA Laminate

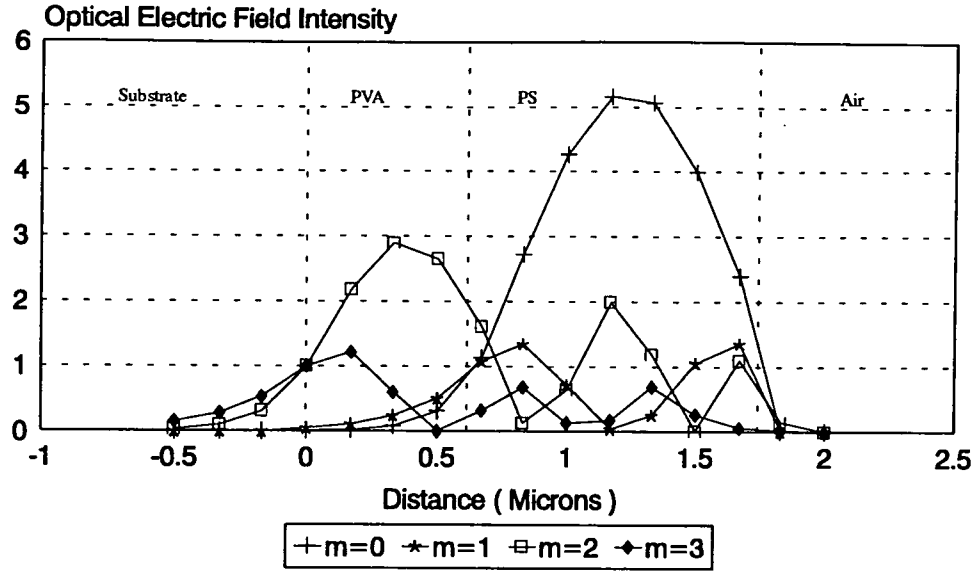

Figure 5.33 - Optical Electric Field Distribution

The functionality of these two polymers would appear to suggest that little interaction would occur between the two films. Hence it is believed that evidence of interfacial interactions would not be available.

3/. Polystyrene (PS, n=1.583)/Poly(vinylpyrrolidine) (PVP, n=1.517).

This system has been examined before, by Dixon[4], and was used in the course of this project as an introductory system. Several systems were examined, but only two gave good waveguide Raman spectra, and are the two described here. The first system is rather unusual due to the rather high number of observable modes which are produced from it, whereas the other is worthy of note simply because little variation in the sampling optical electric field occurs with variation in the mode number. Both systems were constructed with the PVP layer being deposited first, from solutions of methanol, with the PS layer placed on top from solutions in toluene.

System 1.

This system consisted of a 0.8μm ± 0.1μm layer of PVP, on to which a 3.5μm ± 0.5μm film of PS was deposited. The system was prepared using horizontal flow from solutions of 3.25 grams PS in 10.48 grams toluene and 1.01 grams PVP in 6.47 grams methanol. This system gave rise to nine observed waveguiding modes, of which seven gave rise to Raman spectra, six of which were of excellent quality signal-to-noise. The other two modes could just be distinguished, but were far too weak to permit collection of Raman data. Using both the 'Angle4' and 'Index4' programs, the data presented in Table 5.10 was produced.

Table 5.10

Mode Number	Mode Angle (From Normal)	Electric Field Distribution PVP	PS
0	11°44'	0.3%	99.7%
1	10°78'	0.6%	99.4%
2	9°71'	1.5%	98.5%
3	8°25'	2.9%	96.9%
4	6°45'	5.3%	94.6%
5	4°38'	10.1%	89.7%
6	2°18'	19.2%	78.8%
7	0°45'	39.7%	56.3%
8	-1°22'	36.5%	55.6%
9	-3°54'	17.2%	75.3%

The calculations predict the presence of a tenth mode, which we did not observe. This is likely to be due to the fact that the mode is far too weak to be seen, as the observed modes 6, 7 and 8 were also weak. The modes that, although present, did not give rise to spectra were numbers 6 and 8. This is rather unusual. Waveguide streak intensity does tend to decrease with increasing mode number, but the decrease is generally linear, so the fact that mode m=7 is more intense than mode m=8 is a rather interesting result. Also, a large number of distinctly separate waveguiding modes is rather extraordinary, as systems supporting such a high number are usually quite thick, as this one is, and thus the waveguiding modes tend to get so close together that they are indistinguishable. Figures 5.34 and 5.35 show the seven Raman spectra produced from this system in the 900-1100 cm^{-1} region.

The spectrum arising from m=7 was so noisy that a 7-point boxcar smoothing procedure was used to remove spurious noise, thus leaving only the salient features. The spectra shown in both Figures do not seem to show very much, but if we examine the ratios of the 934 cm^{-1} PVP band to the 1002 cm^{-1} PS band presented in Table 5.11, we can indeed see a difference.

Table 5.11

Mode Number	Ratio (PS : PVP) (Band Intensities)
0	1 : 0.06
1	1 : 0.08
2	1 : 0.10
3	1 : 0.11
4	1 : 0.13
5	1 : 0.19
7	1 : 0.15

The surprising result in mode number m=7 is thought to be due to the poor signal-to-noise ration of the spectrum and the influence of the smoothing procedure. It can clearly be seen that the electric field does indeed shift gradually from the polystyrene layer into the PVP. The relatively low changes in the observed band intensity ratios are

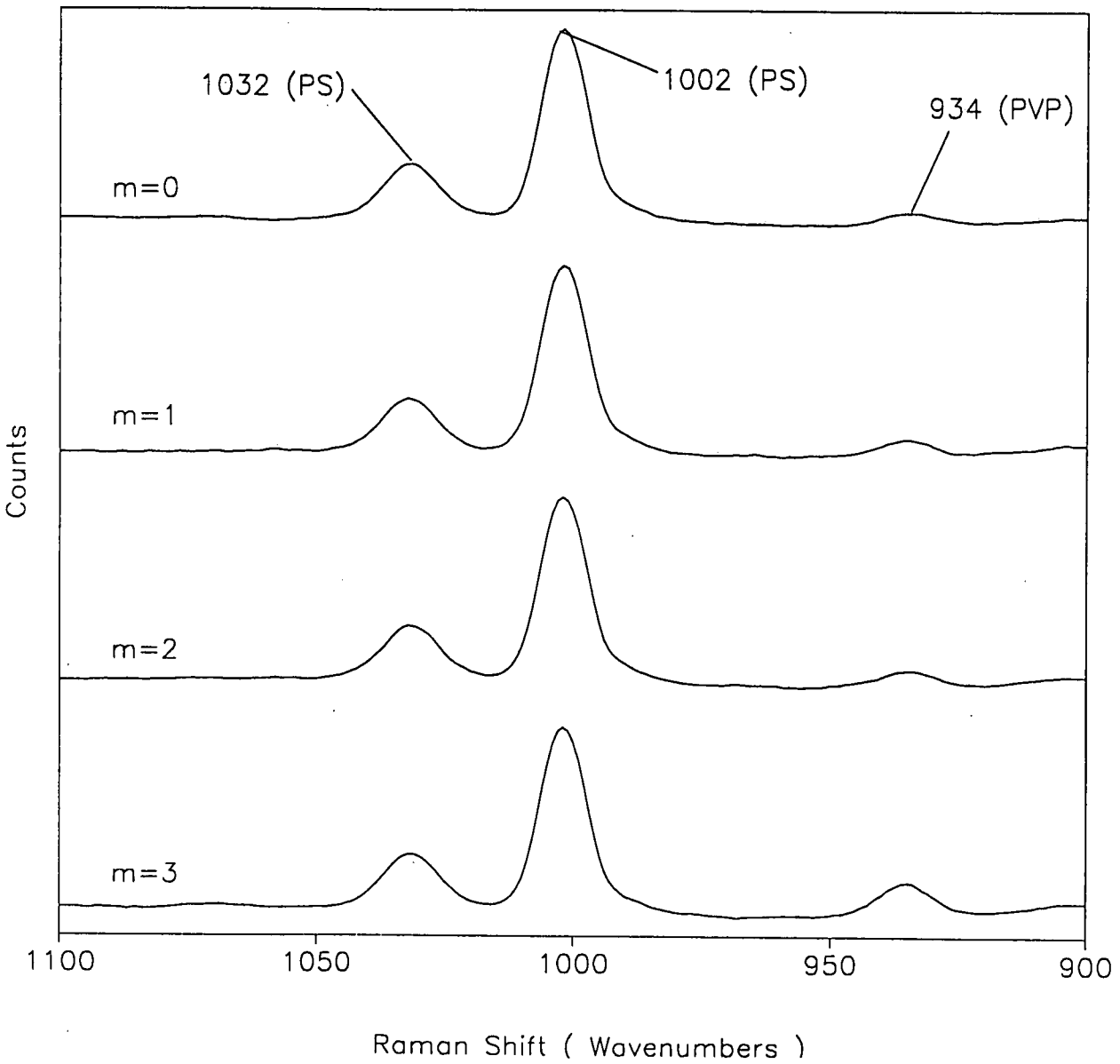

Figure 5.34 - PS/PVP Laminate; System One

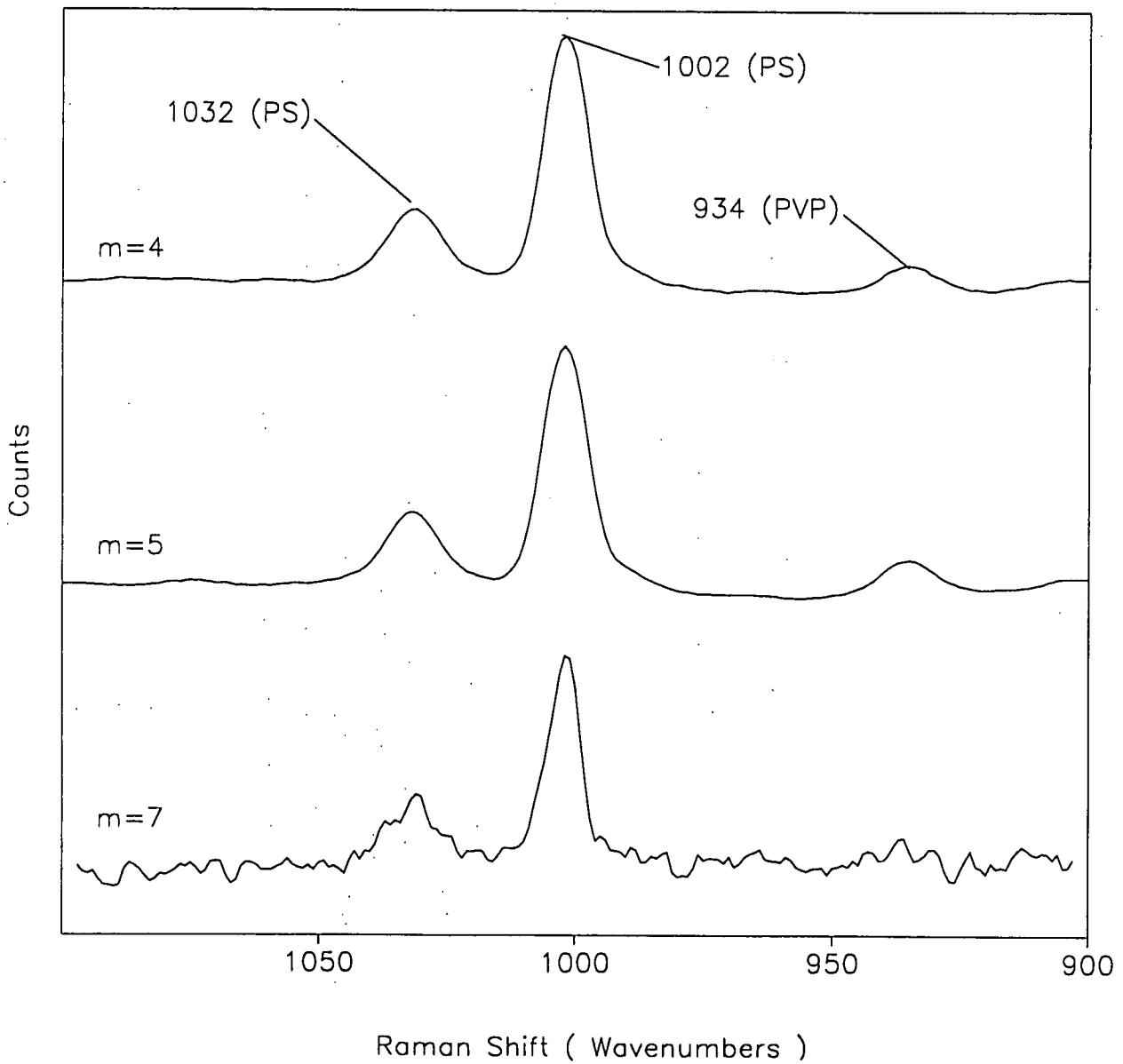

Figure 5.35 - PS/PVP Laminate; System One

probably due to the high Raman scattering cross-section of the polystyrene compared with that of poly(vinylpyrrolidine). The small shift in the 934 cm^{-1} is thought to be too slight to be significant, being a mere 1 cm^{-1}, and probably arises from spectral distortions. Figure 5.36 shows the electric field distribution for the modes examined for this system, except for the m=0 mode, which was so intense it obscured the other six modes.

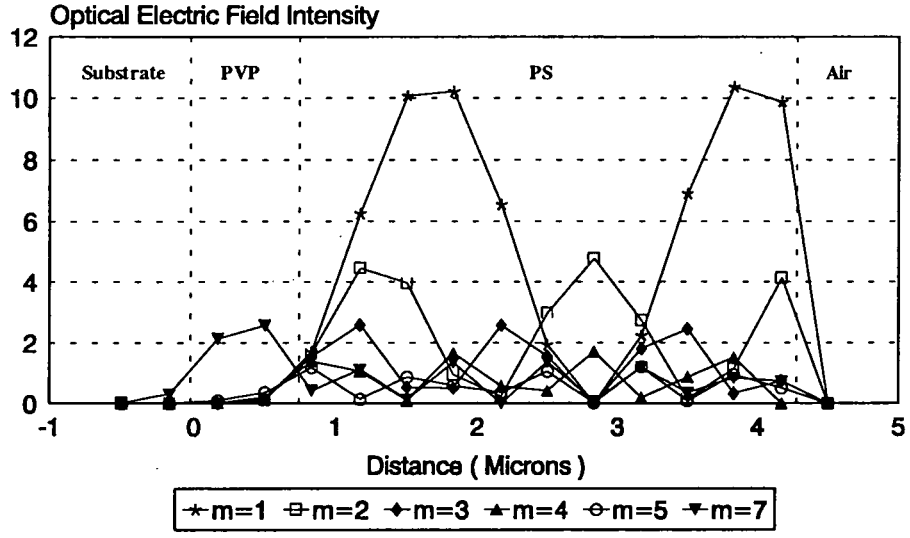

Figure 5.36 - Optical Electric Field Distribution

System 2.

This particular system is rather similar to that shown in System 1, and is included as a further demonstration of the effect on sampling region of the change in mode angle. The system was prepared from 2.43 grams PS in 9.89 grams toluene, and 0.46 grams PVP in 5.89 grams methanol, and the two layers were deposited at dipping speed 4.8 mm sec^{-1}, and produced film thicknesses, measured by the alpha stepper, of PS, 2.5μm ± 0.2μm and PVP, 0.3μm ± 0.1μm. The waveguiding modes and electric field distributions were calculated using the 'Angle4' and 'Index4' programs, which produced the data presented in Table 5.12.

Table 5.12

Mode Number	Mode Angle (From Normal)	Electric Field Distribution	
		PVP	PS
0	11°25'	0.3%	99.7%
1	10°04'	1.2%	98.8%
2	8°10'	3.2%	96.6%
3	5°54'	7.2%	92.5%
4	2°50'	9.8%	88.7%
5	-0°78'	15.8%	79.1%
6	-3°68'	19.1%	62.3%

Of these seven predicted modes, only five were observed, namely, numbers zero to four. The signal-to-noise ratio was rather poor in all these spectra, so a 3-point boxcar

smoothing procedure was used to cut down the noise level. The resulting spectra obtained are shown in Figure 5.37.

Again, the spectra produced do not clearly show the changing optical electric field distribution, which becomes more apparent when the PS, 1002 cm^{-1} is ratio'd against the 934 cm^{-1} PVP band, shown in Table 5.13 below.

Table 5.13

Mode Number	Ratio (PS : PVP) (Band Intensities)
0	1 : 0.05
1	1 : 0.06
2	1 : 0.09
3	1 : 0.10
4	1 : 0.14

This demonstrates quite nicely the increase in optical electric field intensity in the PVP layer, and the corresponding intensity decrease in the PS layer, as the mode angle decreases. A diagram of the electric field distribution is shown in Figure 5.38.

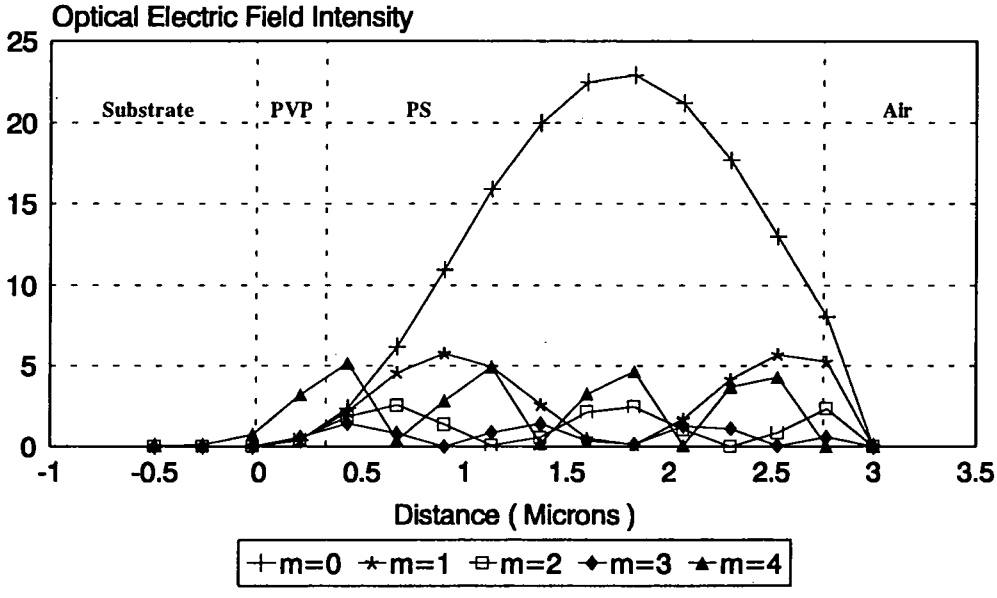

Figure 5.38 - Optical Electric Field Distribution

The seemingly quite significant shift of the PVP band, from 934 cm^{-1} to 939 cm^{-1}, is found to be, on closer inspection, merely the product of remaining noise in mode m=0, which produces a small spike (generally small, sharp spurious peaks) at 939 cm^{-1}, which is the highest intensity in the area of the peak. Thus it is selected as the peak centre by the software annotator. All other modes, when investigated closely, do not exhibit any significant shift, being situated, as in System 1, at 934 ± 1 cm^{-1}.

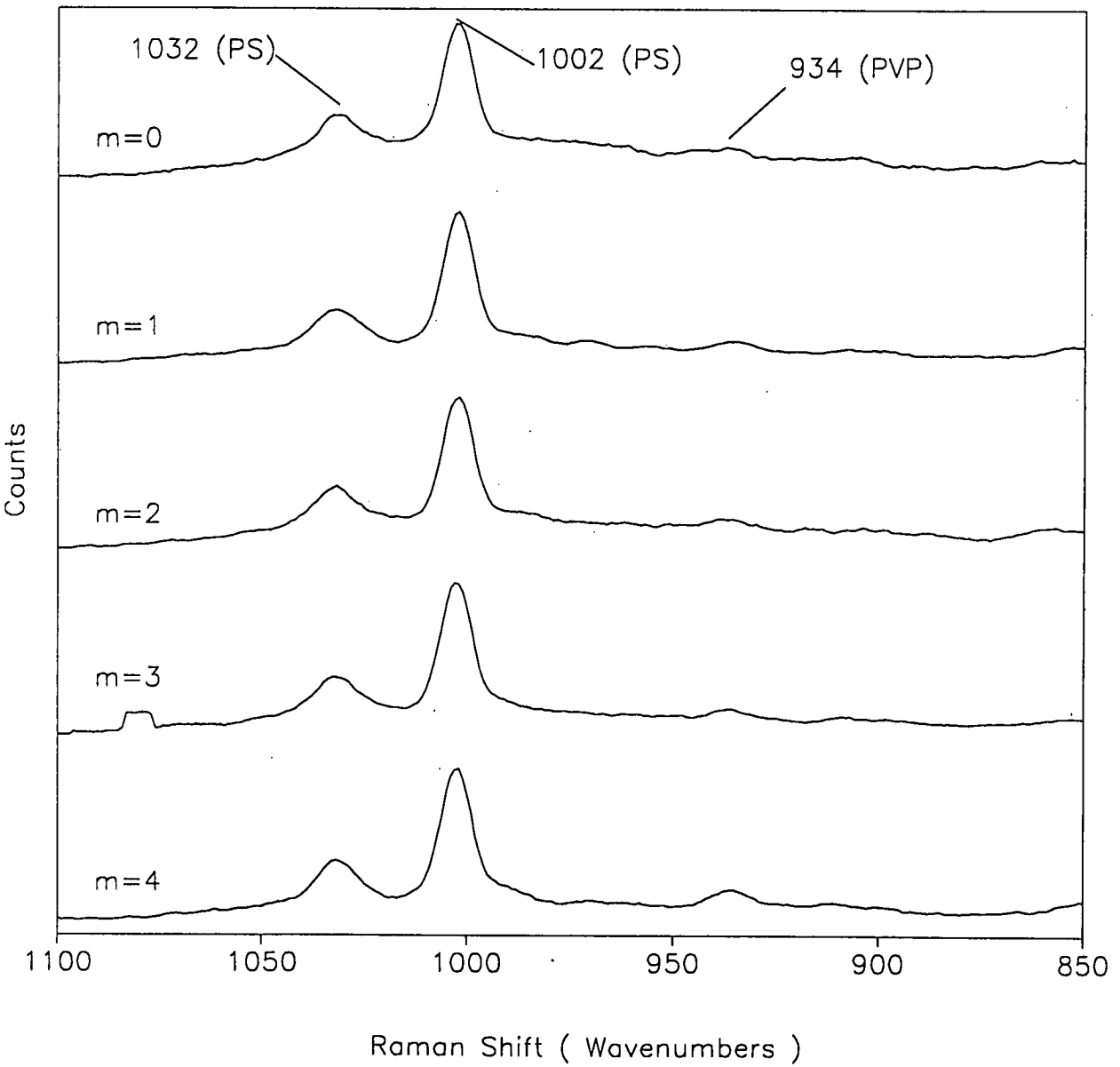

Figure 5.37 - PS/PVP Laminate; System Two

5.5.4 Miscellaneous Experiments.

In the course of this project, several exploratory experiments were undertaken, either out of curiosity or to attempt to recreate experiments performed using other techniques. Such studies were generally unsuccessful in attaining their projected aims, but are described here for sake of completion and interest.

5.5.4.1 Diffusion Processes.

Waveguide Raman spectroscopy (WGRS), along with other integrated optical techniques, have been reported as being a useful tool for examining diffusion processes in polymeric materials[14-20]. Schlotter[19]describes a method which uses WGRS as a tool to monitor, in situ, by use of a liquid flow cell, the diffusion of a binary mixture of ethanol and perdeuterotoluene into polystyrene waveguides of thickness between 1-2 μm. Spectra are produced to verify the claim and shows the diffusion of this mixture to be an unidentifiable non-Fickian process. Fell and Bohn[20] use a method by which analysis of film thickness and refractive index is used, followed by optical modelling to determine the time dependence diffusion processes. This is reported as indicating that n-hexane diffuses into polystyrene films of thicknesses 1-7 μm via a Case II mechanism, but with a leading Fickian edge.

Several attempts were made in the course of this project to study diffusion processes, all of which were unsuccessful. The factor that prevented successful experimentation was the simple fact that all waveguide streaks faded completely when the diffusant was applied. This effect will be evaluated fully later. However, one particular system is described here, which was examined as a follow-up to the infrared work described in Chapter 6. It is thus relevant for future discussions, but also contains a Raman spectrum of a material which, it is believed, has not been reported before.

1/. Isocyanate Diffusion into Epoxy Resins.

In the course of section 5.5.1(B), on the waveguide Raman spectra of single films of industrial polymeric materials, the difficulties in obtaining a reasonable spectrum from films of epoxy resins were discussed. Once this was achieved, waveguide Raman experiments were conducted in an attempt to observe the diffusion of the trimeric isocyanate material (described in Chapter 1, Section 1.4, Figure 1.2) into films of Epikote[13] 1004, which has the lowest proportion of coloured crosslinking agent present, as described above, and hence supports a waveguide for a length of time theoretically sufficient for a waveguide Raman spectrum to be obtained. In experiments described subsequently in Chapter Six, a diffusion process of a trimeric isocyanate into epoxy resins had been seen using FT-IR ATR spectroscopy, and thus attempts were made to also study this process using waveguide Raman spectroscopy. The chemical structure is given in Figure 5.39, and the spectrum of the pure isocyanate substance is shown in Figure 5.40.

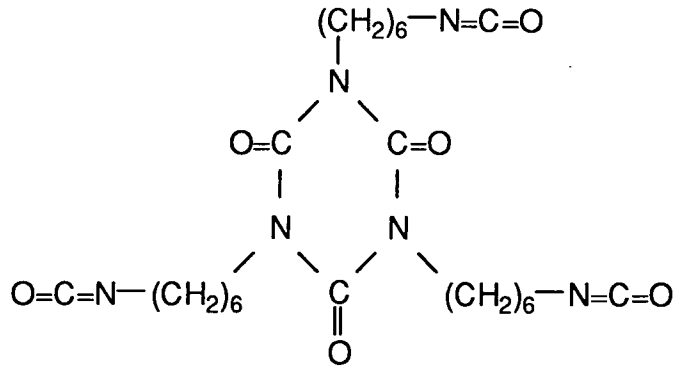

Figure 5.39 - Trimeric Isocyanate

The important features in the spectrum are annotated. The asymmetric and symmetric CH stretching modes are seen at 2936 cm^{-1} and 2879 cm^{-1} respectively, with the CH_2 deformation mode seen as the shoulder at 1458 cm^{-1}. The band at 1436 cm^{-1} is assigned to the symmetric stretching mode of the isocyanate group, which has been reported by other workers[21] as being so. The band at 1305 cm^{-1} is assigned to the C-N vibration, and the bands at 700 cm^{-1} and 644 cm^{-1} are probably due to a skeletal carbon chain mode and carbon-hydrogen wagging mode, respectively. The band centred at 1760 cm^{-1} is undoubtedly due to a carbonyl group. This area is shown in detail in Figure 5.41.

The dominant peak at 1760 cm^{-1} is undoubtedly due to the solvent heptyl acetate, but the smaller band at 1737 cm^{-1} is probably due to the carbonyl groups on the actual ring of the molecule. This is an important feature, as it is a further verification of the molecular structure. It is believed this is the first time that a Raman spectrum of this material has been reported.

Attempts to observe this material diffusing into Epikote[13] 1004 failed, the reason for which is explained further in Chapter 6. However, further experiments were carried out using Epikote[13] 1004 and Hexamethylene diisocyanate (the monomer from which the trimer is synthesised), but in this case, the waveguide was observed to die.

This observation was common to all diffusion experiments attempted, using waveguide Raman spectroscopy, during the course of this project. Such systems included the diffusion of acetone and MethylIsoButyl-Ketone (M.I.B.K.) into both polystyrene and Epikote[13] 1004, all of which were observed to occur using FT-IR ATR spectroscopy, plus a solution of potassium nitrate into polystyrene. All systems examined produced negative results due to the waveguide fading. These experiments will be discussed fully in Chapter 7.

5.5.4.2 Total Internal Reflection (TIR) Experiments.

There are several reports in the literature regarding the use of a TIR technique for the examination of thin films by Raman spectroscopy[22-29]. Most of these refer to experiments, similar to that described by Iwamoto et al[26], where a sample film, of refractive index n_2, is sandwiched between an Internal Reflection Element (IRE) of refractive index n_1, and a medium of lower refractive index, which can be a liquid, air

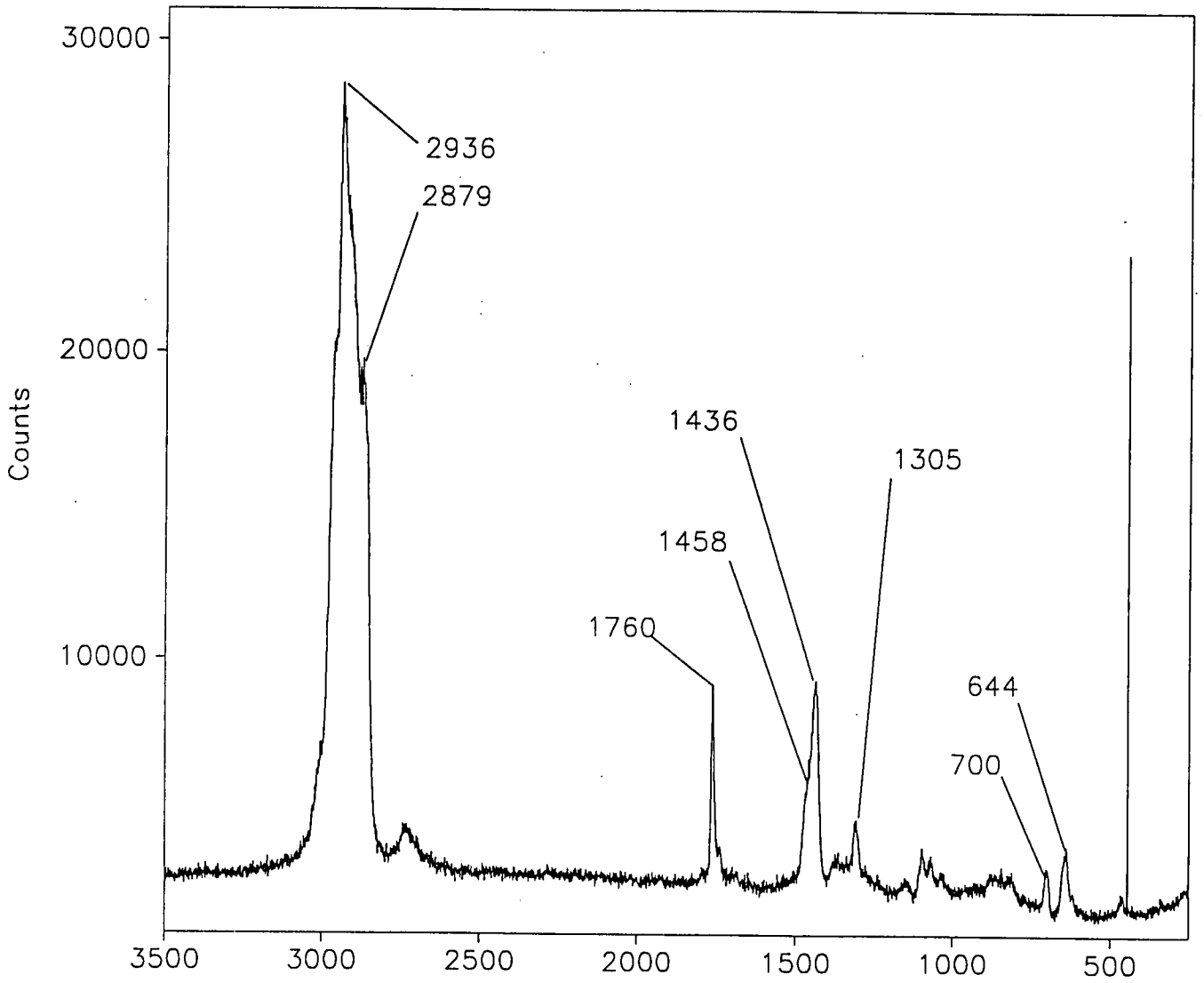

Figure 5.40 – Pure Trimeric Isocyanate (CCA315) Spectrum

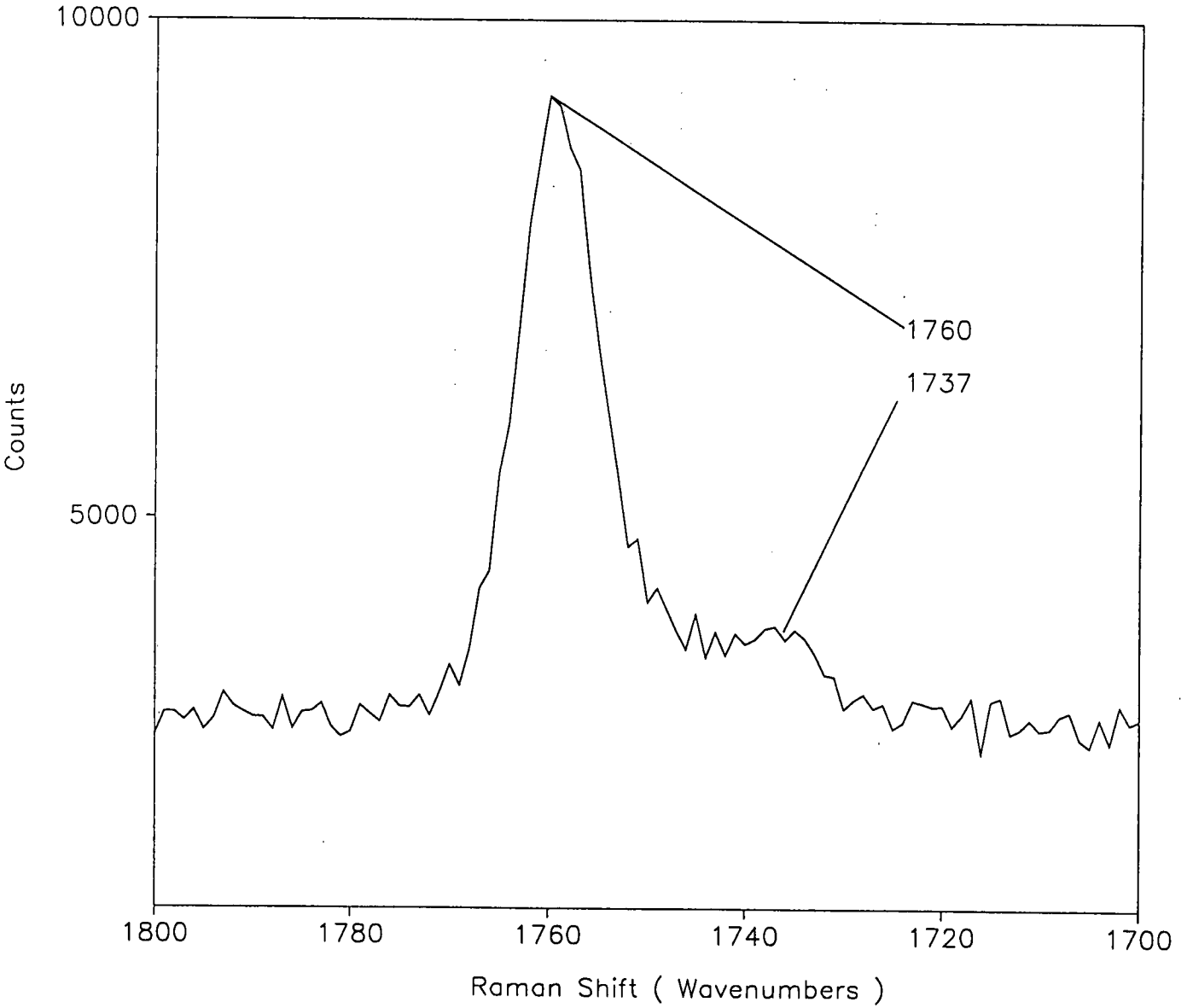

Figure 5.41 – Pure Trimeric Isocyanate; Spectral Region 1700–1800

or another polymer film, of refractive index n_3. The refractive index relationship between the layers is:-

$$n_3 < n_2 < n_1$$

The incident laser beam enters the sample film via the IRE, rather than via a prism coupler. To quote Iwamoto et al[26]:

"When a laser beam falls on the IRE-sample interface, near or below the critical angle, the refracted beam enters the sample with a small angle with respect to the interface and then comes upon the other interface between the sample and the other medium (of lower refractive index) . . . since the incident angle on to this interface is usually sufficiently larger than the critical angle (defined as $\theta_c = n_2/n_1$), the refracted beam in the sample is totally internally reflected thereon without refraction. When the reflected beam reaches the interface between the sample and IRE again, some fraction of the beam is refracted into the IRE, and the other fraction repeats reflection in the sample."

This ingenious method has been reported as giving good Raman spectra of excellent signal-to-noise ratio, and also as being a sensitive approach to the study of the interfacial region.

Another method described[25,28] involves a more conventional approach to ATR spectroscopy, with the totally internally reflected beam contained within the IRE, with sampling into the film, via evanescent wave penetration. Iwamoto et al[25], use a sapphire IRE, which, unlike flint glasses, has a spectrum containing mainly sharp, well-defined peaks, compared with the broad peaks arising from flint glasses, seen in several spectra presented above. Thus peaks in the lower frequency area of the spectrum can be observed with relative ease. Nickolov et al.[28], however, used a hemispherical IRE, to examine thin films of polystyrene, and despite only using a single reflection, obtained spectra with reasonable signal-to-noise ratios.

It was thus decided to use the second method in an attempt to study the original polydimethylsiloxane (PDMS), which could not be studied using waveguiding, due to the refractive index of the polymer (n = 1.41) being lower than that of any substrate easily available. A film was thus dipped on to glass (refractive index approximately 1.5) from a solution of 9.65 grams PDMS, 0.3 grams tetraethyloxysilane (TEOS) and 0.05 grams of dibutyltindilaurate (DBTDL) in 10 grams xylene. This produced a film, on both sides of the substrate, which was measured by the alpha-step to be approximately 4.5 μm thick. The experiment was then conducted using the waveguide rig (see Figure 5.2), but using an angle of incidence which caused the beam to travel within the glass substrate. Several attempts were made to obtain a Raman spectrum of the material, but all attempts failed, with a spectrum similar to that shown in Figure 5.12, being produced, showing only substrate peaks.

5.5.4.3 Fourier Transform Raman Work[30].

Certain compounds used in this study have presented difficulties associated with the use of conventional Raman, due to the materials' colour, causing severe fluorescence, which obscures the entire spectrum. A particular example cited here has been the problems associated with the waveguide Raman study of epoxy resin systems, which are slightly coloured, due to the presence of a coloured crosslinking agent.

This problem can be overcome using FT-Raman technique, which uses a near-infrared laser for excitation. This wavelength is invisible in the visible spectrum, and thus overcomes most fluorescence problems. This technique is well known for such applications, and there are some reports of FT-waveguide Raman experiments[31-34]. In this section the FT-Raman spectra of the two crosslinking agents used in this project is presented, along with the spectrum of Rosin Amine-D, which is part of the XK91 anti-fouling system, discussed in Section 5.5.1 (B) above.

The spectra presented here were obtained using the Bruker IFS66 instrument, fitted with an FRA106 FT-Raman accessory, operating with a Nd-YAG laser at 1064 nm, which has a maximum power of 1 watt. Spectra were collected using 500 scans at 4.0 cm^{-1} resolution, and a laser power of 0.6 watts. The spectrometer is located in the Chemistry and Chemical Technology Department at the University of Bradford, UK, and this work was conducted outside the bounds of the experimental part of this project, but is included here as the materials were used in the experimental work, and are of interest to Courtaulds.

1/. KH92.

The structure of this material is presented in Chapter 1 (Reaction 3, page 4), but is essentially the basic epoxy resin unit, with diethylene triamine, adducted on to each end via a condensation reaction. The spectrum obtained is shown in Figure 5.42.

As this is such a complex spectrum, an assignment is given of only the main spectral features. The weak band at 3297 cm^{-1} is believed to be due to the NH_2 stretching mode. The aromatic CH stretching mode is visible in the band at 3055 cm^{-1}, with the complicated feature centred approximately at 2900 cm^{-1} corresponding to the different aliphatic CH stretching modes, which will be present in this molecule. The asymmetric CH deformation mode is seen in the band at 1448 cm^{-1}, and the symmetric deformation modes are seen in the bands at 1380, 1298 and 1249 cm^{-1}. The bands arising from the aromatic ring breathing modes, can be seen at 1032 and 1001 cm^{-1}, and the two bands at 1609 and 1582 cm^{-1} are probably due to the aromatic ring buckling modes.

This is believed to be the first time that a Raman spectrum of this material has been reported.

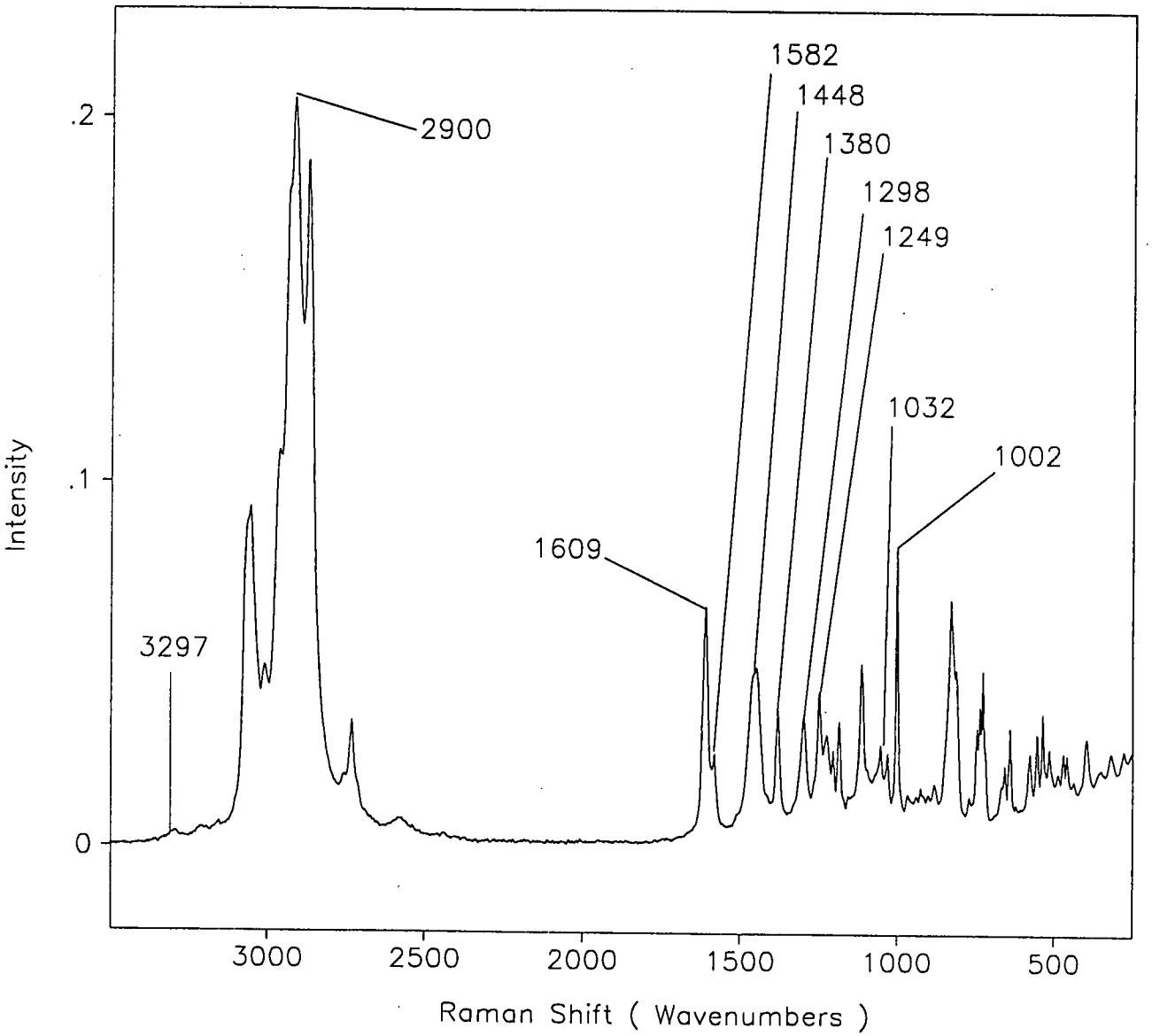

Figure 5.42 – FT–Raman Spectrum of Crosslinker, KH92

2/. Cardanol.

This epoxy-resin crosslinking agent is a highly-coloured di-Mannich base, prepared via the condensation (Mannich) reaction of an extract of cashew-nut shell oil and ethylene diamine. The structure is discussed in Chapter 1, but is reproduced in Figure 5.43 for convenience.

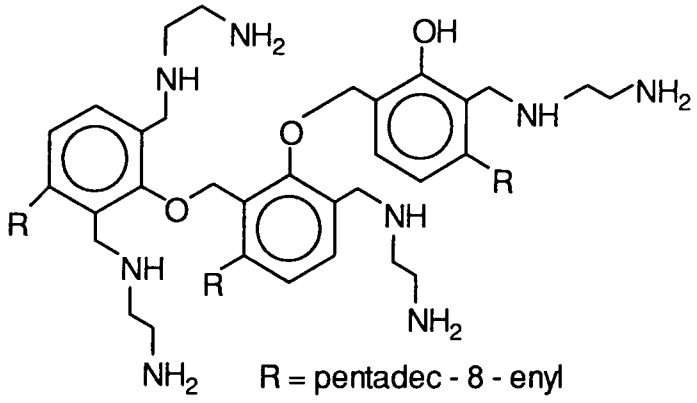

Figure 5.43 - Cardanol

The FT-Raman spectrum of Cardanol is shown in Figure 5.44.

Only the major spectral features are assigned here. The very weak feature seen at 3306 cm^{-1} probably arises from the NH_2 asymmetric stretching mode. The aromatic CH stretching mode is visible at 3010 cm^{-1}, with the various aliphatic CH stretching modes seen in the complex area centred at approximately 2900 cm^{-1}. The band seen at 1656 cm^{-1} is discussed below. The two aromatic buckling modes can be seen at 1625 and 1583 cm^{-1}, and the CH deformation mode is seen at 1444 cm^{-1}. The 1297 cm^{-1} band is thought to arise from a CH twisting mode, with the feature at 1262 cm^{-1} arising from the CN stretching mode. Below this wavenumber, the spectrum becomes too complex to make definitive assignments.

Figure 5.45 shows the result of a curvefitting procedure on the area around the band observed at 1656 cm^{-1}, which is assigned[35] to a combination of the cis- and trans-forms of the pentadec-8-enyl groups. Table 5.14 shows the numerical data produced.

Table 5.14

Wavenumber	Peak Intensity	Peak Area
1656	0.056	0.84
1642	0.014	0.21

This suggests that the ratio of cis:trans isomeric forms of the pentadec - 8 - enyl is approximately 1:4, as the 1656 cm^{-1} feature arises from the trans form of the double bond, whereas the 1642 cm^{-1} arises from the cis isomeric form. Thus this group exists mainly in the trans isomeric form. This is believed to be the first time that a Raman spectrum of this material has been reported.

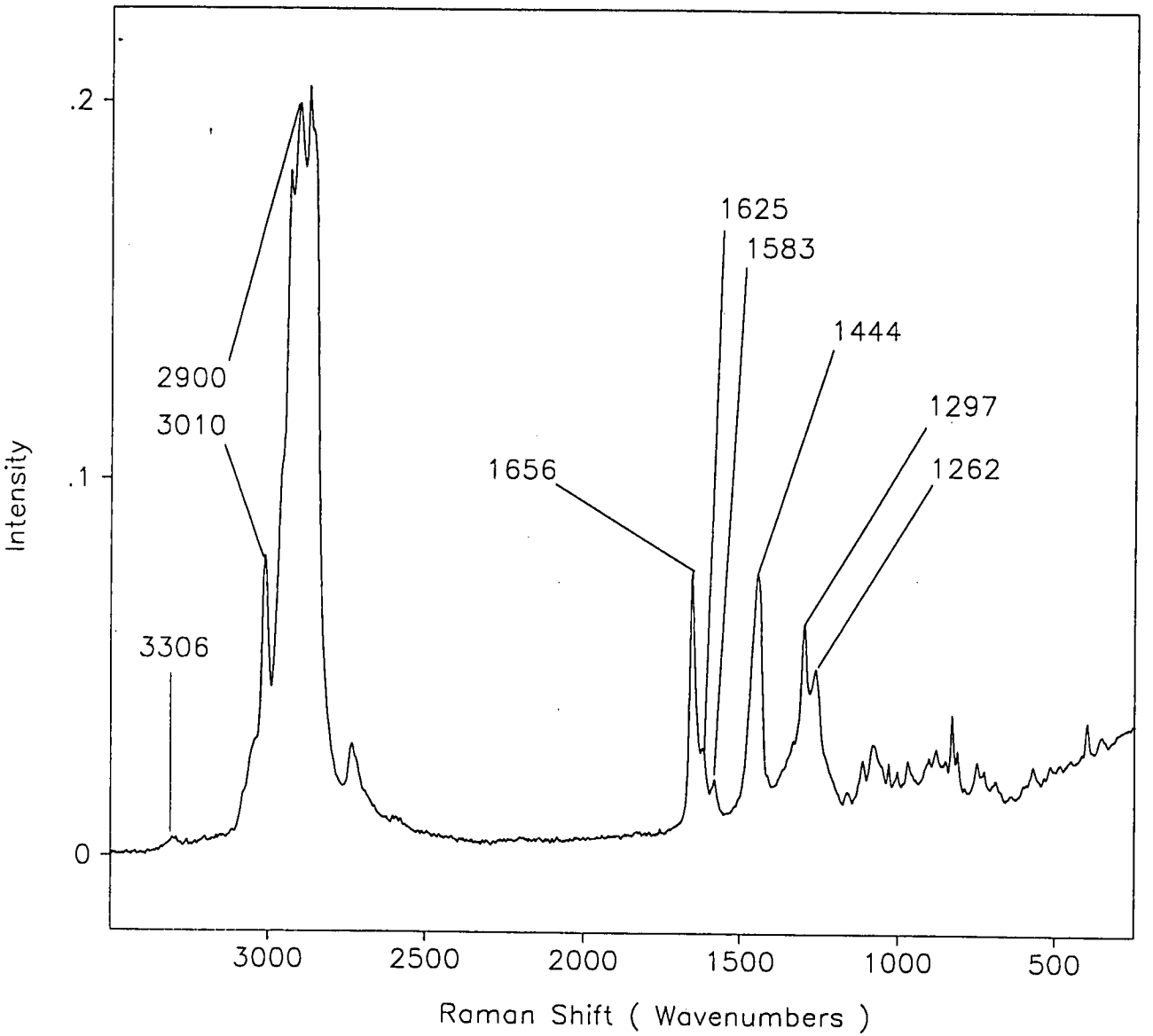

Figure 5.44 – FT–Raman Spectrum of Crosslinker, Cardanol

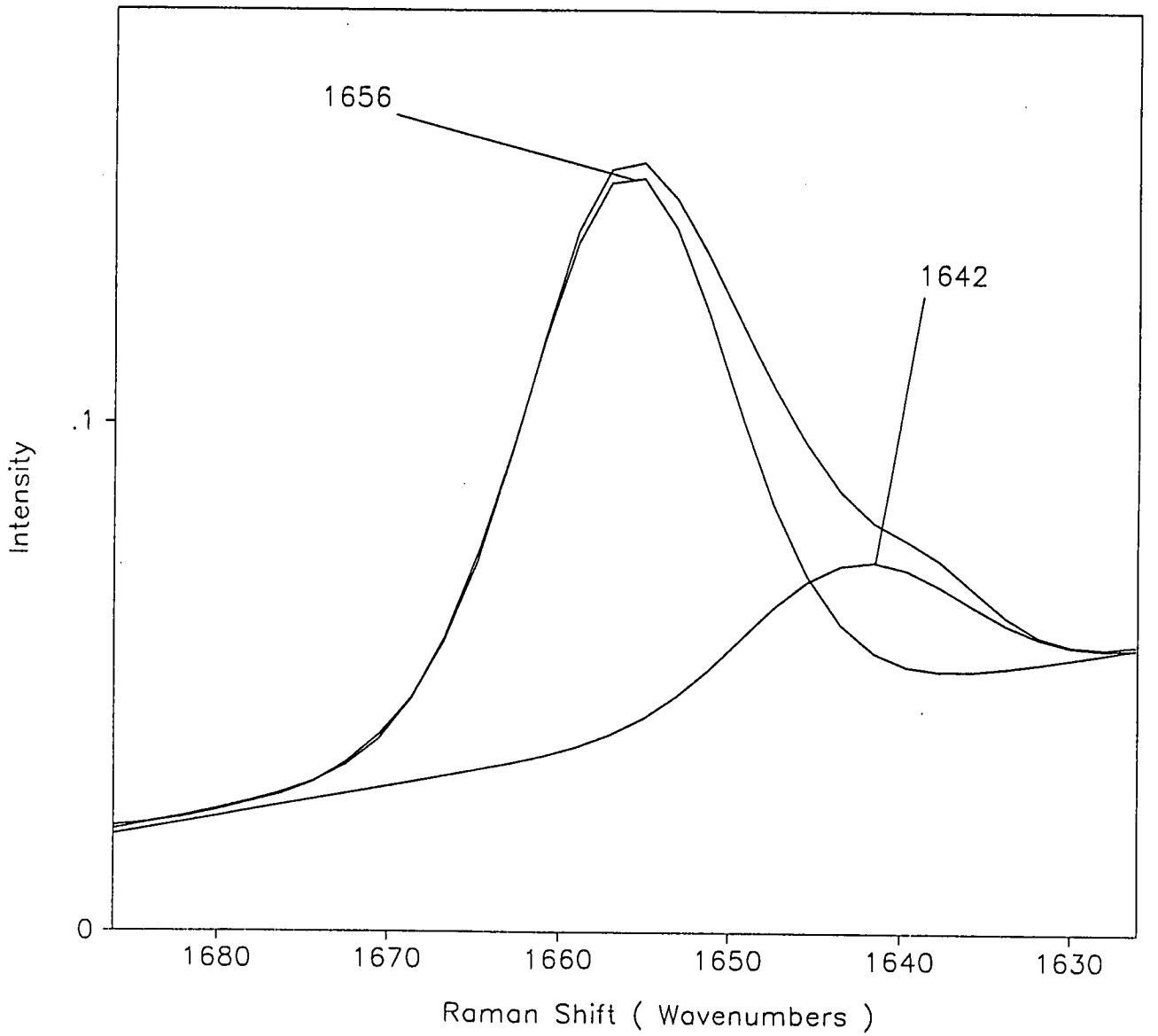

Figure 5.45 – Curfit of cis/trans Spectral Features of Cardanol

3/. Rosin Amine-D.

This aromatic amine is a dark brown constituent of the antifouling system, XK91, discussed above. The structure of this material is shown in Figure 5.46.

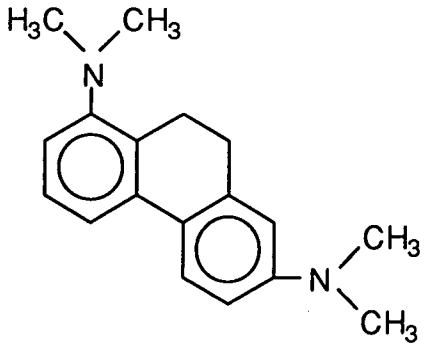

Figure 5.46 - Rosin Amine-D

Figure 5.47 shows the FT-Raman spectrum of this material.

This spectrum is not as would be expected from the structure in Figure 46. The band at 3335 cm^{-1} suggests the presence of NH stretching modes, but none are present in the structure described above. Furthermore, the band at 1680 cm^{-1} is indicative of an amide I carbonyl stretching mode, and the relative strength of this band would tend to suggest a fairly high concentration of amide, as carbonyl stretches are very weak in the Raman spectrum. Furthermore, the bands at 1560 and 1234 cm^{-1} could easily correspond to the frequencies of the amide II and amide III stretching modes, respectively. Hence, it is believed that a high degree of contamination is present, and although there are features in the spectrum which correspond to the above structure, such as the aromatic CH stretching mode seen at 3049 cm^{-1}, it is felt that further assignment is pointless. This reiterates the point made earlier about the purity of materials used at Courtaulds Coatings, and more work is required to investigate this further.

5.6 Concluding Remarks.

This chapter has presented all the work carried out using the waveguide Raman technique during the course of this study. Although the technique theoretically has great potential as a tool for the study of thin polymeric materials and interfaces, the work described above demonstrates the serious limitations of the technique, imposed by purely practical problems. Also demonstrated in the final section is the potential for the study of diffusion processes using WGRS, the possibility of further techniques to examine thin films, and a further indication of the power of the FT-Raman technique to examine previously impossible systems.

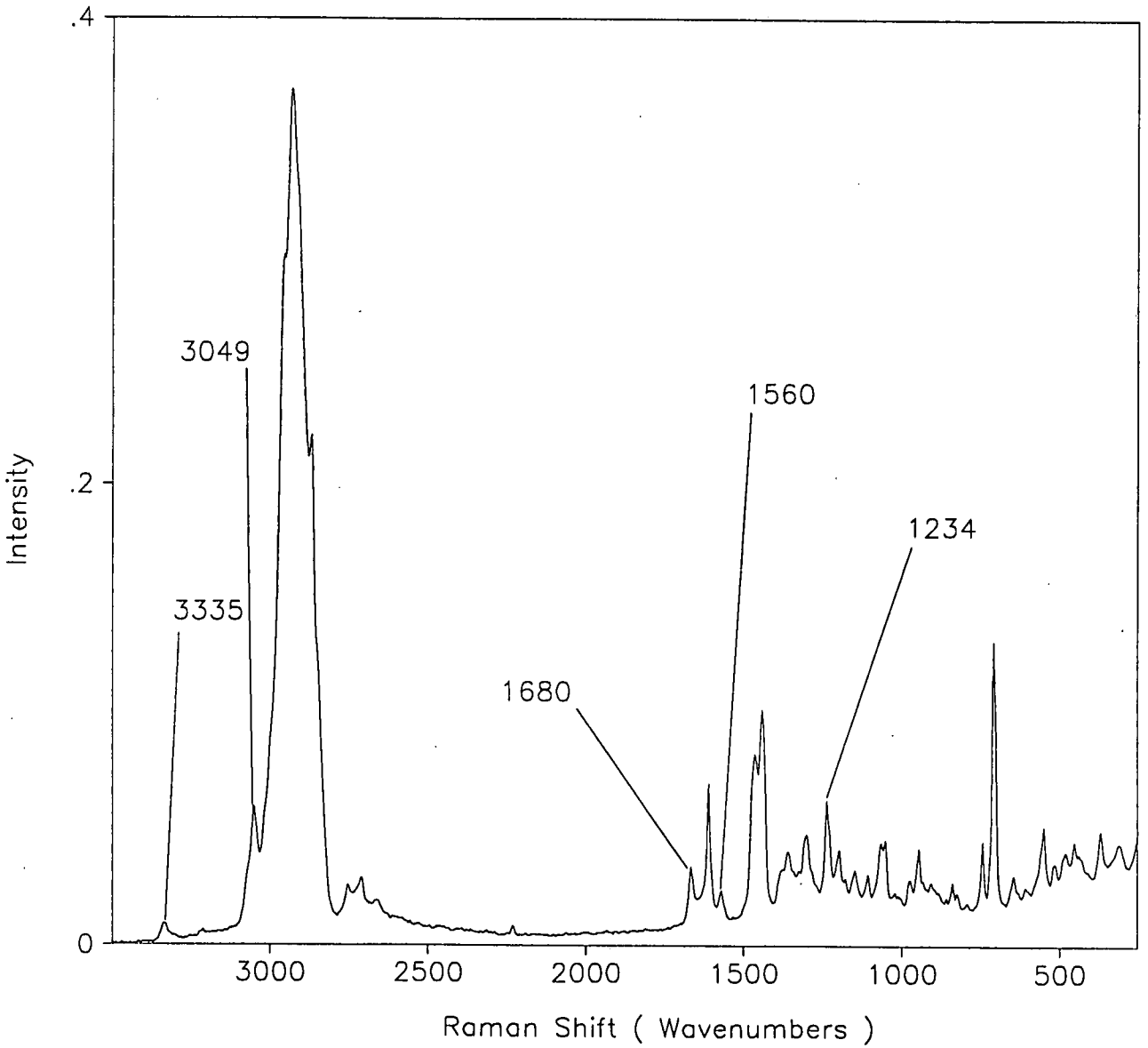

Figure 5.47 – FT–Raman Spectrum of Rosin Amine–D

References.

1/. J.F.Rabolt & J.D.Swalen, "Spectroscopy of Surfaces", Eds. R.J.H.Clark and R.E.Hester, J.Wiley and Sons, London, 1988, Chapter 1.
2/. P.K.Tien & R.Ulrich, J.Opt.Soc.Am., 60, 10, (1970), 1325.
3/. R.Ulrich & R.Torge, Appl.Opt., 12, 12 (1973), 2901.
4/. N.M.Dixon, N.Everall & J.Yarwood, Unpublished work.
5/. © International Business Machines Corporation, 9/11/1990, All rights reserved.
6/. B.Jasse, R.S.Chao & J.L.Koenig, J.Polym.Sci., Polym.Phys.Edn., 16, (1978), 2157.
7/. The Polymer Handbook, Ed. J.Brandrup & E.H.Immergut, J.Wiley and Sons, Publishers, 1989.
8/. Y.Levy, C.Imbert, S.Racine & R.Dupeyrat, Opt.Commun., 11, (1974), 66.
9/. Y.Levy & R.Dupeyrat, J.Physique.Coll.C5, 38, (1975), 253.
10/. F.R.Dollish, W.G.Fateley & F.F.Bentley, "Characteristic Raman Frequencies of Organic Compounds", John Wiley and Sons, (1974), pp's 171, 175 & 179.
11/. Dr. G.Davies (Courtaulds Coatings), Private Communication.
12/. H.H.Landolt & R.Börnstein, Phys.Chem.Tabellen, 1923.
13/. Shell brand-name.
14/. A.S.Michaels, H.J.Bixler & H.B.Hopfenberg, J.App.Polym.Sci., 12, (1968), 991.
15/. D.R.Miller, O.H.Han & P.W.Bohn, Appl.Spectrosc., 41, (1987), 245.
16/. D.R.Miller, O.H.Han & P.W.Bohn, Appl.Spectrosc., 41, (1987), 249.
17/. P.W.Bohn & N.F.Fell, Chemical, Biochemical & Environmental Applications of Fibres, S.P.I.E., 990, Society of Photo-Optical Instrumentation Engineers, Bellingham, Washington, (1988), 130.
18/. D.R.Miller & P.W.Bohn, Anal.Chem., 60, (1988), 407.
19/. N.E.Schlotter, J.Phys.Chem., 94, (1990), 1692.
20/. N.F.Fell, Jr & P.W.Bohn, Appl.Spectrosc., 45, 7, (1991), 1085.
21/. F.R.Dollish, W.G.Fateley & F.F.Bentley, "Characteristic Raman Frequencies of Organic Compounds", John Wiley and Sons, (1974), 144.
22/. J.Cipriani, S.Racine, R.Dupeyrat, H.Hasmonay, M.Dupeyrat, Y.Levy & C.Imbert, Opt. Commun., 11, (1974), 70.
23/. M.Delhaye, M.Dupeyrat, R.Dupeyrat & Y.Levy, J.Ram.Spectrosc., 8, (1979), 351.
24/. R.Iwamoto, M.Miya, K.Ohta & S.Mima, J.Am.Chem.Soc., 102, (1980), 1212
25/. R.Iwamoto, M.Miya, K.Ohta & S.Mima, J.Chem.Phys., 74, (1981), 4780
26/. R.Iwamoto, K.Ohta, M.Miya & S.Mima, Appl.Spectrosc., 35, (1981), 584.
27/. W.Hölzer, O.Schröter & A.Richler, J.Mol.Struct., 217, (1990), 253.
28/. Z.S.Nickolov, J.C.Earnshaw & J.J.McGorvey, Procs. XIIIth ICORS Meeting, Wurzburg, 1992, p.668.
29/. W.Hölzer, O.Schröter & A.Richler, Procs. XIIIth ICORS Meeting, Wurzburg, 1992, p.632.
30/. P.Hendra, C.Jones & G.Warnes, "Fourier Transform Raman Spectroscopy", E.Horwood Ltd., (1991).
31/. C.G.Zimba, V.M.Hallmark & J.F.Rabolt, Abs.Paps.Am.Chem.Soc., 196, Sept, (1988), 49.
32/. C.G.Zimba, V.M.Hallmark, S.Turrell, J.D.Swalen & J.F.Rabolt, J.Phys.Chem., 94, (1990), 939.
33/.J.F.Rabolt, IBM Research Report, RJ8476 (76697), November 11th, 1991.
34/. C.G.Zimba & J.F.Rabolt, Thin Solid Films, 206, 1-2, (1991), 388-393.
21/. F.R.Dollish, W.G.Fateley & F.F.Bentley, "Characteristic Raman Frequencies of Organic Compounds", John Wiley and Sons, (1974), p.63.

Chapter Six - Experimental Fourier Transform Infrared Attenuated Total Reflection Spectroscopy

Chapter Six - Experimental Fourier Transform Infrared Attenuated Total Reflection Spectroscopy.

6.1 Introduction.

This chapter describes the work carried out, during the course of this project, on thin films using Fourier Transform Infrared Attenuated Total Reflection (FT-IR ATR) Spectroscopy. A full theoretical treatment of this technique, along with a review of relevant previous work, is given in Chapter 2. In this chapter, a description of the practical considerations associated with this technique is presented, along with a basic portrayal of the instrumentation involved with an FT-IR spectrometer. The experimental results are then presented, the main substance of which being the examination of diffusion phenomena and subsequent reactions associated with thin epoxy films, along with determination of apparent diffusion and kinetic parameters of these processes. Other brief, inconclusive experiments conducted using the barrier film technique are included for completeness. A full discussion of the major results is presented in Chapter 7, but relevant band assignments are presented in the course of this chapter. Unless otherwise stated, all spectra discussed in this chapter refer to ATR experimental work, and involve 100 scans at 4 cm^{-1} resolution.

It is also worth mentioning here the considerable complexities associated with the systems examined in this study, especially those involved with the diffusion experiments described later on. A full evaluation of these difficulties is considered in Chapter 7, where the impact of these on the actual meaning of the results presented here is fully evaluated. As the work described here was part of an industrially sponsored project, the systems examined were of direct significance to Courtaulds, and the study of simplified systems, which would have been preferable in this kind of project, was of little use to Courtaulds. The relevance of this paragraph will become apparent as this chapter unfolds.

6.2 Practical Considerations.

6.2.1 Film Preparation.

All the films used for experimental measurements described in this chapter were dipped from solutions, and the thickness determined using the alpha-step. Both the dipping equipment and alpha-step are described in Chapter 4.

It is worth reiterating at this juncture an important point regarding film quality, discussed fully in Chapter 4. It is important that the reader is fully aware of the significant structural differences between a so-called poor-quality film (PQF) and a good-quality film (GQF), which arise from the state of solubility of the amine-based crosslinking agent, KH92. The other crosslinking agent used in this project, i.e. Cardanol, produced films of good quality from all the solvent systems used. If KH92 is fully dissolved, a good-quality film results, whereas a poor-quality film results if it is only partially dissolved. Figure 6.1 shows the Scanning Electron Micrographs, taken at Courtaulds Coatings plc, of the different film types, shown in Chapter 4, Figures 4.9 and 4.11.

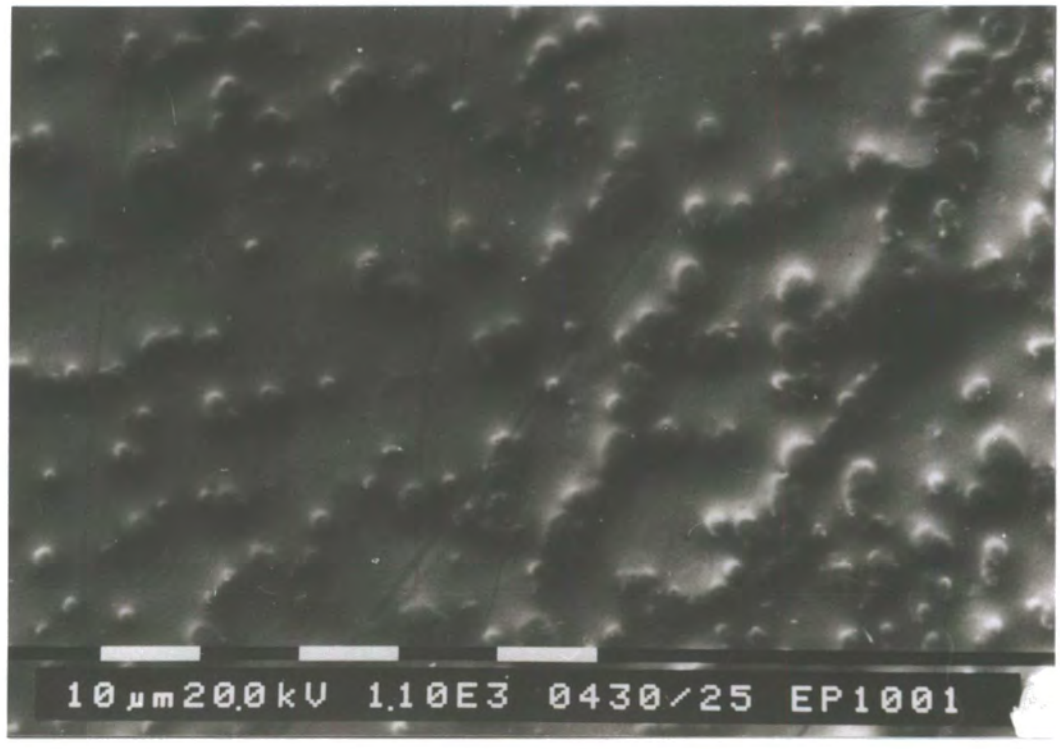

Poor Quality Film

Good Quality Film

Figure 6.1 - SEM Micrographs of Poor and Good Quality Films

The important differences between the two types of film can be summarised thus:-

1/. A PQF is rough and dull, whereas a GQF is smooth and shiny.

2/. A PQF has "particles" of undissolved KH92 (an amine-tipped epoxy molecule, used as a crosslinking agent, see Chapter 1) present, whereas a GQF has none, as satisfactory dissolution of the KH92 occurs.

3/. A PQF is formed from a cloudy solution, in which the KH92 dissolves only sparingly, the undissolved proportion being suspended, whereas a GQF results from a clear solution, where satisfactory dissolution of the KH92 is achieved.

4/. For an *industrial solvent system* (that is a system using low-grade solvents such as those used by Courtaulds Coatings plc) a cloudy solution is formed from blends containing only xylene and butan-1-ol. The important controlling factor which determines film quality in this case is the presence of methanol, which encourages KH92 dissolution, and hence clear solutions, the actual blend being 2 parts xylene, 2 parts butan-1-ol and 1 part methanol. The blend of xylene, butan-1-ol and mesitylene, similar to several formulations used on site at Courtaulds Coatings plc, produces a Poor Quality Film.

5/. For *pure solvent systems*, a similar situation exists, but dissolution can be achieved with a blend of xylene plus either n-butanol or methanol, providing the alcohol is in moderate excess (approximately 1 part xylene to 2.5 parts alcohol). The blend of 2 parts xylene, 2 parts butan-1-ol and 1 part methanol also produces a Good Quality film.

To summarise, a Poor Quality Film arises from an epoxy resin system in which KH92 is used as the crosslinking agent and where a solvent blend of low polarity is used, which allows only sparing dissolution of the KH92. This difference in film quality only applied to systems using KH92 as the crosslinking agent; films produced using Cardanol as the crosslinking agent were always found to be of good quality.

6.2.2 Instrumental Considerations.

Most of the infrared experimental work described in this thesis was carried out in the Surface Spectroscopy Unit (S.S.U.) at Courtaulds Coatings plc, on a Mattson Cygnus FT-IR spectrometer, but some data was also collected using a Mattson Syrius FT-IR in the Raman and Infrared group at Durham University. Figure 6.2 shows the optical arrangement of the Mattson Syrius spectrometer, which has a very similar optical layout to the Cygnus machine at Courtaulds.

The theory concerned with FT-spectroscopy is dealt with adequately in existing literature[e.g. 26-28], and thus a detailed analysis is not presented here. However an overview of the fundamental considerations is presented here, for the sake of completion. This will focus on an FT-IR spectrometer, but will also include pertinent references to FT-Raman machines, such as that used in Chapter 5.

Figure 6.2 - Optical Arrangement of the Mattson Syrius Spectrometer[1]

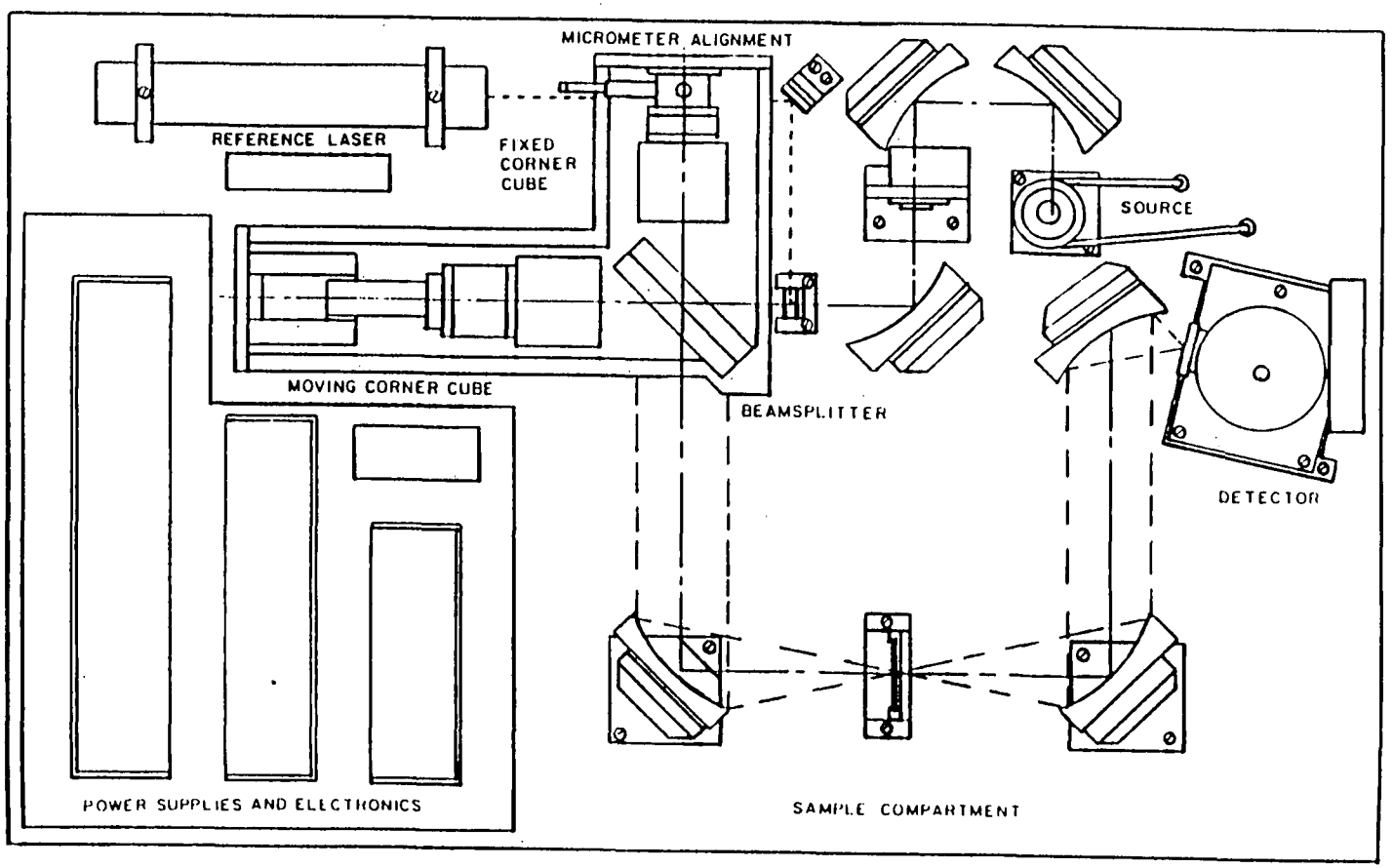

The source of excitation (a black body radiator in an FT-IR spectrometer (polychromatic and incoherent), but a near-infrared (1.064 nm) laser in an FT-Raman (monochromatic and coherent)) produces a beam of electromagnetic radiation, which passes through a variable-size iris, which reduces beam size, into a Michelson (usually) interferometer, which essentially consists of two mirrors and a beam splitter. The beam splitter, usually an alkali-metal/halide disk, coated with a Ge/Si semiconductor, splits the incoming beam into two separate optical paths, each leading to one of two separate mirrors, which reflect the radiation back through the beam splitter, from which it passes through the sample and into the detector (usually a semiconductor device). One of these mirrors is fixed at a known path length from the beam splitter, whereas the other moves backward and forward parallel to the axis of the incoming beam. This movement is such that at the mid-point of travel, the path length from this mirror and the beam splitter is equal to the path length between the fixed mirror and beam splitter, the so-called point of zero path difference. At this point the two beams constructively interfere and a maximum occurs in the detector signal. As the moving mirror moves beyond the point of zero path difference, in the case of a monochromatic source, destructive and constructive interference occurs, plus intermediate points between these two extremes. Thus an interferogram is produced, which takes the form of a cosine wave.

Mathematically, this can be demonstrated by representing the point of zero path difference of the moving mirror travel by x. Thus for monochromatic radiation (e.g. a laser) of wavenumber υ_0, the intensity of radiation reaching the detector is given by[26]:-

$$I(x) = S_{(\bar{\upsilon}_0)}(1+\cos 2\pi\bar{\upsilon}_0 x) \qquad (1)$$

where $S_{(\bar{\upsilon}_0)}$ is the spectral amplitude at wavenumber $\bar{\upsilon}_0$.

$I_{(x)}$ will reach a maximum when:-

$$2\pi\bar{\upsilon}_0 x = 2n\pi, \text{ where } n = 0,1,2..., \text{ or when } x = \frac{n}{\bar{\upsilon}_0} \qquad (2)$$

In the case of a polychromatic radiation source (i.e. the black body radiator in an FT-IR spectrometer), a similar situation is found at the point of zero path difference, i.e. a maximum is produced, termed a centre-burst, but as the mirror moves beyond this point, destructive and constructive interference both occur, due to the presence of numerous waveforms. Mathematically, if we term this range of frequencies as being between ν_L and ν_H, then the radiation intensity reaching the detector can be written:-

$$I/I_{(x)} = \int_{\nu_L}^{\nu_H} S_{(\bar{\nu})}[1+\cos 2\pi\bar{\nu}x].d\nu \qquad (3)$$

For a rapid scanning instrument this can be approximated to:-

$$I'_{(x)} = \int_{\nu_L}^{\nu_M} S_{(\bar{\nu})}[\cos 2\pi\bar{\nu}x].d\upsilon \qquad (4)$$

$S_{(\bar{\nu})}$ (i.e. the spectral amplitude at frequency, $\bar{\nu}$, which is the resulting spectrum) is obtained by Fourier Transformation of $I'_{(x)}$, to give:-

$$S_{(\bar{\nu})} \propto \int_0^{x_{max}} I'_{(x)}\,[\cos 2\pi\bar{\nu}x].dx \qquad (5)$$

Here, x is represented by $x = n\Delta x$, where Δx is the sampling interval and n is the number of samples (sampling occurring during the cycle of the moving mirror). Generally, Δx is of the order of a few microns and thus n can have values up to several thousand, depending on the distance travelled by the moving mirror beyond the point of zero path difference. Thus x_{max} is the maximum mirror travel, which leads to a maximum optical path difference of:-

$$D = 2x_{(max)} \qquad (6)$$

The spectral resolution also depends on $x_{(max)}$.

Two major advantages that an FT-IR spectrometer possesses over a dispersive instrument are:-

1). The Multiplex Advantage.

This arises from the fact that all spectral elements are observed at all times. This leads to a corresponding improvement in signal-to-noise (S/N) ratio over a dispersive machine, since for a dispersive machine, the S/N ratio is described by:-

$$S/N_{(dispersive)} = (\text{Observation Time/Number of Spectral Elements})^{1/2} \qquad (7)$$

whereas for an FT machine, the same ratio is given by:-

$$S/N_{(FT)} = (\text{Observation Time})^{1/2} \qquad (8)$$

Thus, the gain in signal to noise ratio can be termed:-

$$S/N_{(FT)} \,/\, S/N_{(dispersive)} = (\text{Number of Spectral Elements})^{1/2} \qquad (9)$$

2). The Throughput (Jacquinot) Advantage.

This involves the greater proportion of source radiation which passes through an FT instrument. This essentially arises from the fact that a dispersive instrument possesses a narrow entrance slit, which greatly restricts the radiation throughput, whereas an FT instrument is replaced by a circular aperture of larger area.

6.2.3 - ATR Instrumentation.

The ATR apparatus used in this project was, for most of the work carried out, a SPECAC vertical mounting, although some work was carried out using a SPECAC horizontal mounting. The crystal material used was, in the main, zinc selenide, which has a refractive index of 2.4.

A high proportion of the ATR experimental work at Courtaulds was carried out using small, 'recycled' crystals, which are approximately half the length of full crystals. Such crystals are 'made' from broken full crystals, and are used at Courtaulds for routine investigations, although they obviously provide a lower level of sensitivity than 'full', conventional crystals. However, all experiments conducted using these smaller crystals were repeated using full crystals to ensure that experimental observations made were verifiable and were not just some sort of optical artefact arising from the use of these smaller crystals.

6.3 Experimental Measurements.

6.3.1 Initial Investigations.

The initial aim of this study was to examine the interfacial region in a polymeric laminate structure, using Barrier Film FT-IR ATR (ATR) spectroscopy[2-6]. However, little use of the technique was made, due to the potential importance of subsequent discoveries, which emerged during this initial period of investigation. This ATR technique, however, was used to some extent, and is best described with the aid of Figure 6.4.

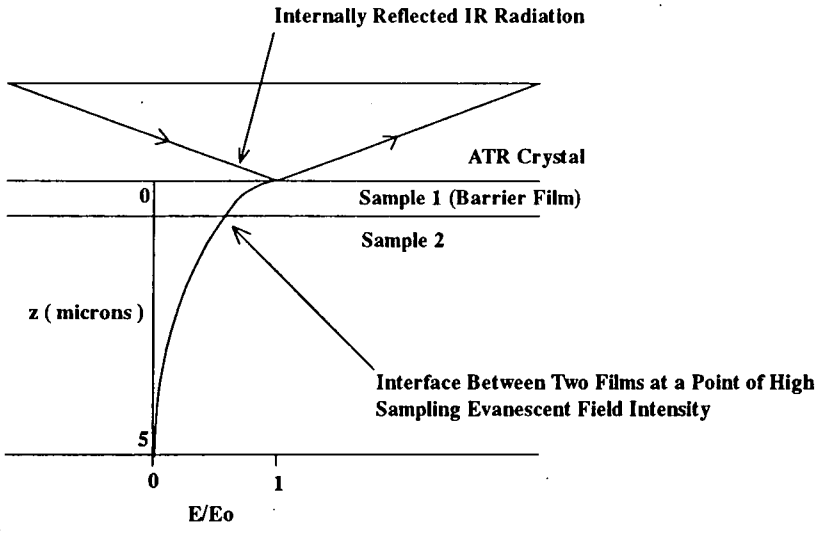

Figure 6.4 - The Barrier Film IR ATR Technique

The evanescent wave, which penetrates into the medium of lower refractive index, decays exponentially with distance into the laminate. The layer in contact with the crystal is termed the barrier layer, the thickness of which must be readily controllable to a fairly accurate degree (in Durham this was achieved using the dipping technique, described in Chapter 4). Thus, it should be possible to position the interfacial region between the barrier film and upper layer, at a position where the intensity of the sampling evanescent field can be accurately estimated. Therefore, it should be possible to position the interfacial region at a point of high evanescent field intensity, which theoretically should enable interfacial interactions to be successfully investigated.

Many paint systems produced by Courtaulds, and indeed other paint manufacturers, are laminate systems, and one important factor needed for a successful system is good adhesion, not only between substrate and paint, but also, in such systems, between the constituent layers. If good adhesion is not achieved, then peeling occurs and the system fails. Obviously, in the rigorous conditions to which marine paints are exposed, such failure is inevitable following a certain period of time - an evil which keeps the marine paint industry in business! However, premature failure of such systems is distinctly undesirable, as system quality, and hence company reputation, is brought into question. At the time of writing, this particular area is of crucial importance, as certain systems have been found to fail under differing climatic conditions, notably in the Far East. Hence, a detailed understanding of adhesion processes in such systems is of

paramount importance, and techniques to investigate such processes are of distinct value.

The barrier layer used in the experimental work carried out in the course of this thesis was generally a crosslinked epoxy resin, in this initial work Epikote[7] 1001, although some work was conducted using polydimethylsiloxane (PDMS) and other relevant substances. The chemistry of these substances is described fully in Chapter One. Throughout this experimental chapter, reference is made to a crude doctor blading method of deposition. This consisted of the spreading of a thin layer of substance by means of a clean spatula, with care being taken not to contaminate the bare crystal area. Although there are reports in the literature regarding the use of FT-IR to examine epoxy resin systems[48-56], there is little on the application of ATR to such systems, the only ones found being Sprouse and Halpin, Jnr.[57], in an army document and Mertzel and Koenig[58], who mention the technique and comment that it is the only FT-IR technique that does not require substantial sample modification.

6.3.1.1 - Epoxy Resin Barrier Layer Work.

1/. Polymeric Acrylic (Water-Based) Top Layer.

This substance is in the form of a water-based suspension, but the exact structure of the acrylic polymer is not known. The functional group, however, is thought to be of the type:-

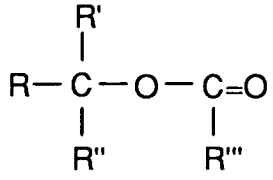

Figure 6.5

This was deposited, using a crude doctor blading method, on a 0.14 μm ± 0.02 μm thick film of Epikote[7] 1001 (structure given in Chapter 1, Page 5), and the resulting laminate examined, the spectrum of which is shown in Figure 6.6 along with the full spectra of the pure epoxy resin and the pure acrylic.

The carbonyl stretching mode, seen in the band at 1727 cm^{-1}, resulting from the acrylic layer, can be clearly seen, which would be expected, as the depth of penetration of the evanescent wave in Epikote[7] 1001 at this frequency is approximately 1.5 μm. Hence a great deal of the evanescent wave will be concentrated within the acrylic layer. This area around the carbonyl band will be the area of interest with regard to interfacial activity, as it is probably the major point of reactivity associated with the acrylic molecule. Figure 6.7 shows the expansion of this area for pure acrylic spectrum, laminate spectrum and the pure epoxy spectrum.

It can be readily seen that in this particular case, a slight shift plus a broadening of the carbonyl band occurs (the halfwidth for the pure acrylic band is 6 cm^{-1} narrower than that seen in the laminate). This is believed to be due to interfacial effects, although it is

Figure 6.6 - Epikote[7] 1001 plus Water Based Acrylic

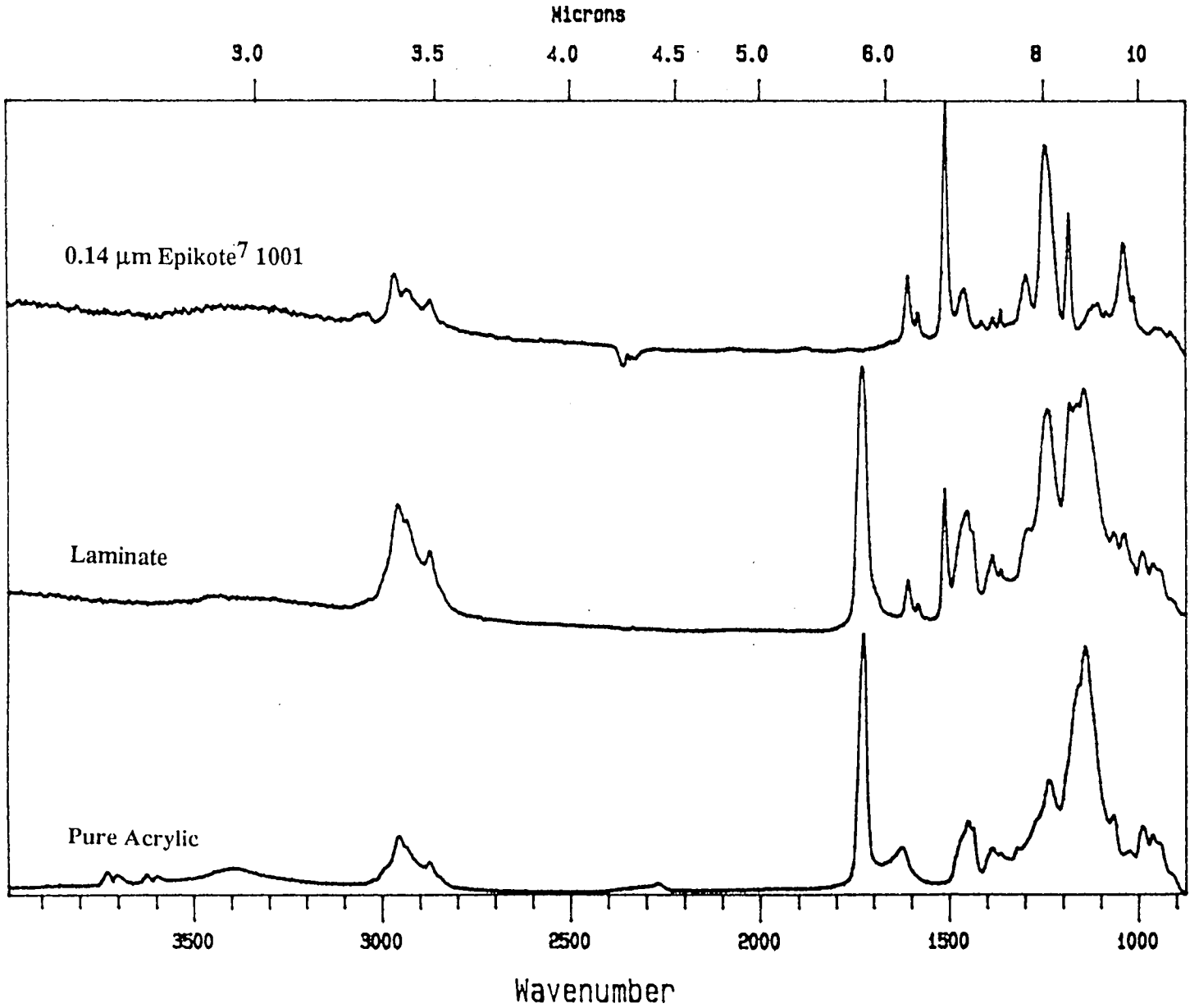

Figure 6.7 - Epikote[7] 1001 plus Water Based Acrylic

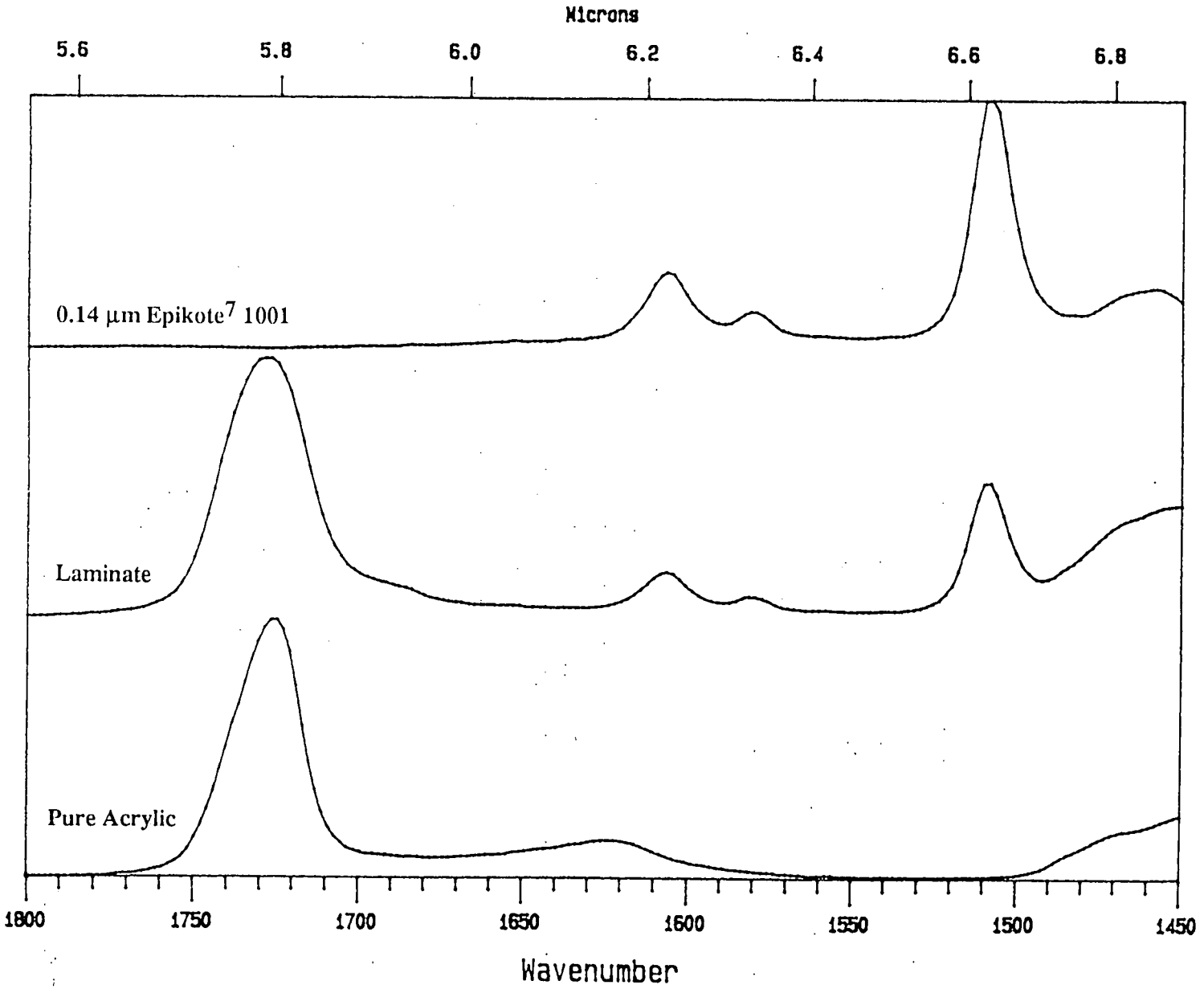

possible it could be a spectral artefact which arises when an ATR spectrum is compared with a transmission spectrum (the spectrum of the pure acrylic was obtained using transmission). However, a further experiment was carried out on this system, using a pure epoxy film of approximate thickness 0.5 μm. The result is presented in Figure 6.8, which shows the carbonyl band in the laminate spectrum, the pure acrylic spectrum and the result of the subtraction of pure acrylic from the laminate acrylic.

Again, the carbonyl band appears to broaden in the laminate, and when the subtraction out of the pure material is conducted, it is believed that the two bands which result are probably indicative of interfacial effects. However, it is not possible to be fully definitive about this, and more work, including obtaining an ATR spectrum of the acrylic, is required.

2/. Acrylic (Solvent-Based) Top Layer.

This material is a solvent-based acrylic polymer, supplied by Cray Valley Chemicals to Courtaulds. Cray Valley have indicated that they do not wish the specific name of this substance to be publicised in this study. Hence, this substance will be referred to as 'solvent-based acrylic' in the remainder of this thesis. It is possible, however, to identify the solvent as the ester, ethyl-3-ethoxypropionate. Figure 6.9 shows the spectra of the 1400-1800 cm^{-1} area produced from a laminate of solvent-based acrylic deposited, using the crude doctor blading method, on the top of approximately 1.7 μm film of Epikote[7] 1001, along with the spectra of the pure resin, the pure solvent-based acrylic and the result of the subtraction of the pure solvent-based acrylic spectrum from the laminate spectrum.

This is of somewhat greater interest. The carbonyl band in the laminate is clearly broader than that arising in the pure solvent-based acrylic, the halfwidth of the band arising from the laminate being 48 cm^{-1}, compared with 31 cm^{-1} for the pure acrylic, plus the central band position shifts to the red, from 1731 cm^{-1} in the pure solvent-based acrylic to 1720 cm^{-1} in the laminate. The result of the subtraction clearly shows a new feature at 1707 cm^{-1}, which is not visible in the pure epoxy spectrum. A shift to the red is indicative of some sort of attractive interaction, and in this case the observation cannot be due to an ATR artefact, similar to that discussed earlier when the water-based system is used, simply because the spectrum of the pure solvent-based acrylic was also obtained using ATR.

It is unclear from the present data whether the presence of solvent plays a role in these observations. It is reported that the acrylic polymer used in both water- and solvent-based systems are the same[47]. Furthermore, the carbonyl band position in the pure materials are also about the same, being 1727 cm^{-1} in the water-based system and 1731 cm^{-1} in the solvent-based system. This slight shift to the blue in the carbonyl band for the solvent based system is probably due to the carbonyl band being a composite feature of both the acrylic and ester (solvent) carbonyl groups. It is thus reasonable to assume that the carbonyl band position for the pure acrylic is 1727 cm^{-1}. However, it is known that diffusion can occur in epoxy resins, and later in this chapter we examine the diffusion of a diisocyanate into similar systems, which consequently interacts within the film, producing a band shift. It thus could be possible that this effect is due to

Figure 6.8 - Epikote[7] 1001 plus Water Based Acrylic

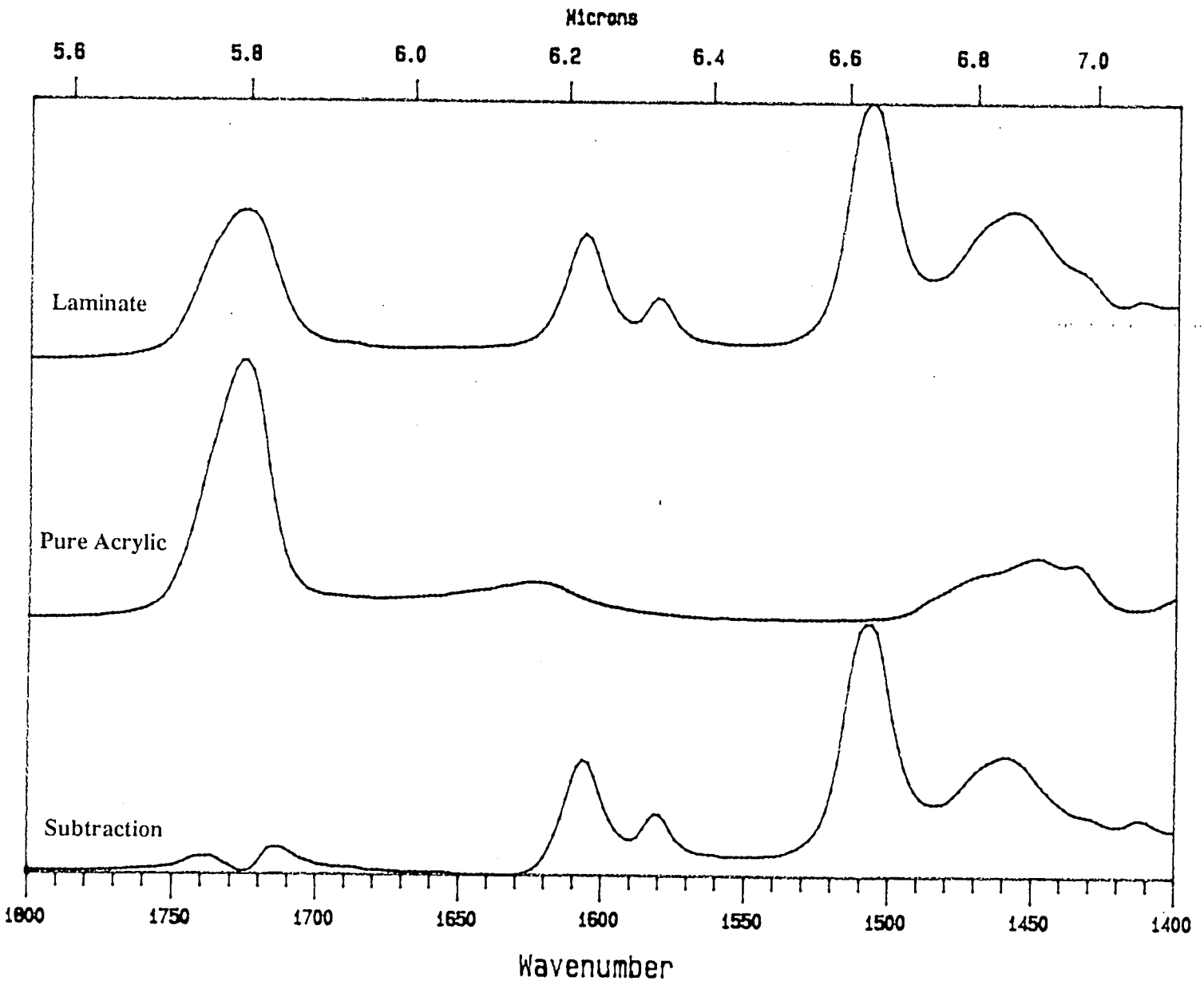

Figure 6.9 - Epikote[7] 1001 plus Solvent Based Acrylic.

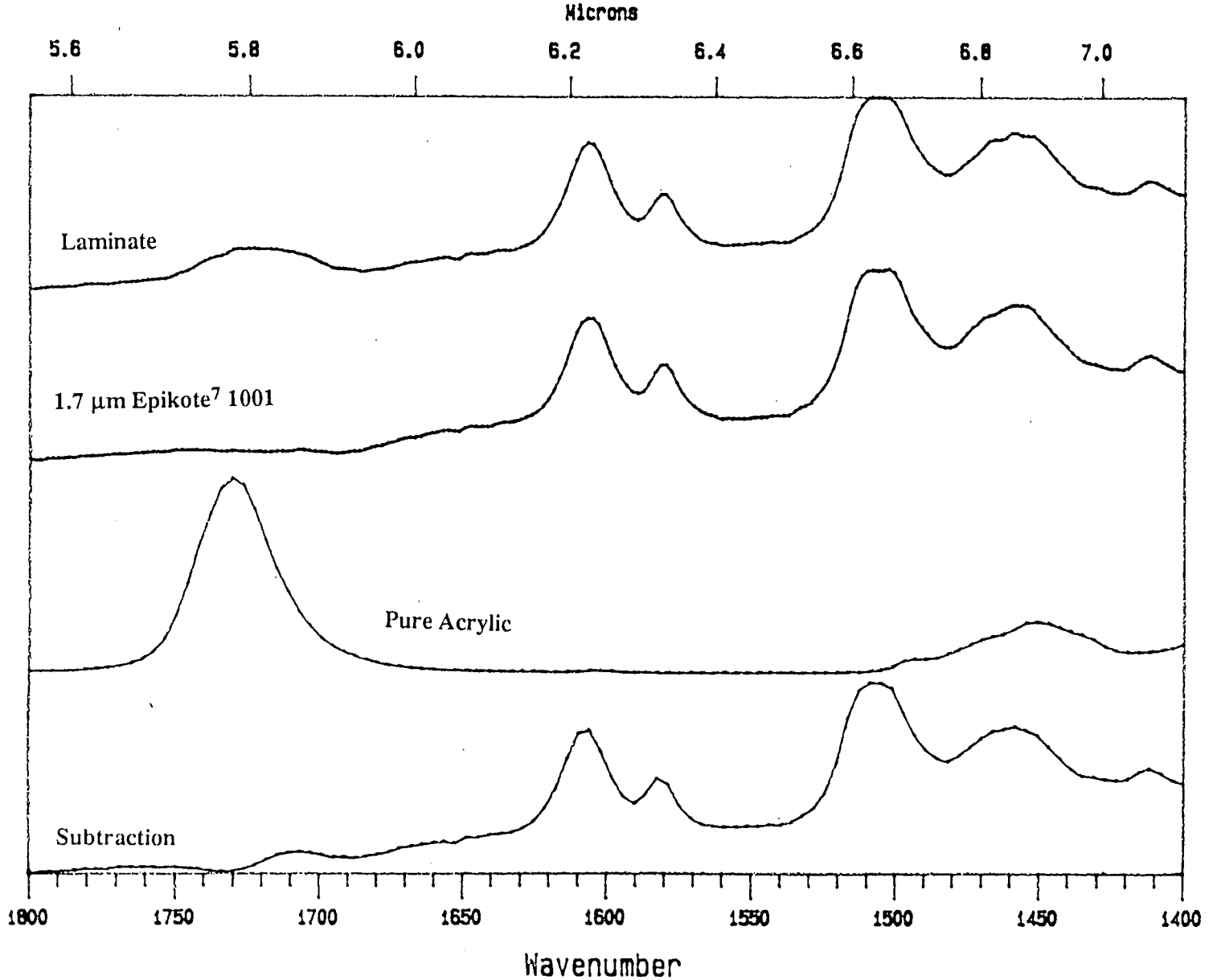

solvent diffusion and consequent interaction, but in the absence of experimental data to prove or disprove this, it is impossible to comment further on this possibility.
Hence, from the available data, it is proposed that the observed shift in position of the carbonyl band is probably due to some interfacial interaction between the two films, most likely originating from hydrogen bonding between the carbonyl group, associated with the acrylic polymer, and the hydroxyl groups, associated with the crosslinked epoxy resin. This is believed to be the first time that this system has been examined using FT-IR ATR spectroscopy.

3/. Alkyd Resin Topcoat.

Alkyd resins are essentially condensation polymers of multi-basic acids and multi-basic alcohols, and have structures similar to that shown in Figure 6.10:-

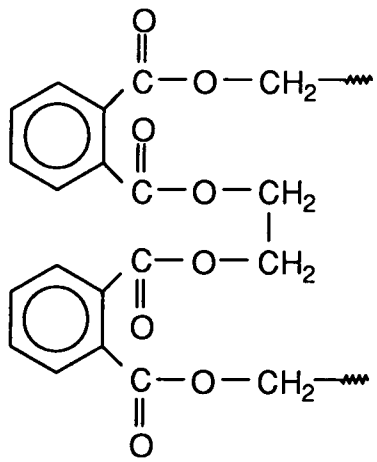

Figure 6.10

Again, this molecule is fairly reactive, with the carbonyl groups providing a site for possible interactions with other molecules. An epoxy film of 0.18 μm ± 0.03 μm thickness was treated with a crudely deposited layer of such an alkyd resin, the precise structure of which is not known. Figure 6.11 shows the spectrum of the 1400-1800 cm^{-1} of the produced laminate, along with the pure epoxy and alkyd resins and the results of a spectral subtraction of the pure alkyd spectrum from the laminate structure.

Again, an interesting result is observed, with a definite shift in the alkyd carbonyl band position. The pure alkyd resin carbonyl frequency is found at 1734 cm^{-1}, whereas the same frequency for the laminated alkyd resin is observed at 1722 cm^{-1}, a shift to the red of 12 cm^{-1}. When the result of the subtraction is examined, a new, residual feature is seen at 1715 cm^{-1}, and the presence of this new feature can be clearly seen in the composite band seen in the laminate spectrum.

Thus, it is believed that an interfacial interaction is being observed between the alkyd resin layer and the crosslinked epoxy layer, which is believed to arise from hydrogen bonding between the carbonyl groups associated with the alkyd resin and the hydroxyl groups associated with the crosslinked epoxy resin. This is believed to be the first time that this system has been examined using FT-IR ATR spectroscopy.

Figure 6.11 - Epikote[7] 1001 plus Alkyd Resin

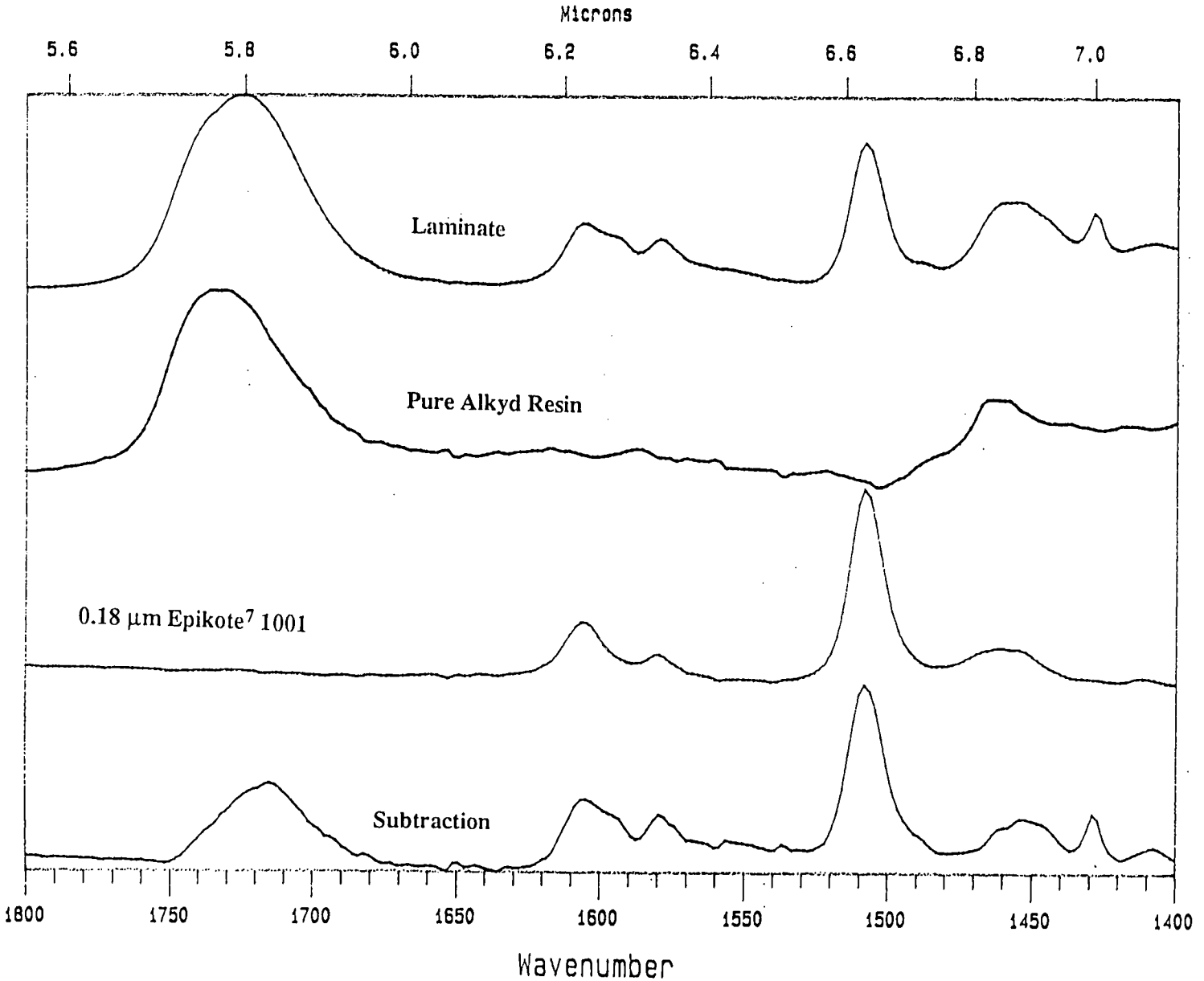

6.3.1.2 - Polydimethylsiloxane (PDMS) Barrier Layer Work.

Polydimethylsiloxane is a rubbery constituent of an anti-fouling paint layer, and thus the mechanism of protein absorption to such a layer is of significant interest to the development of new paint systems. It is known[8] that Bovine Serum Albumin (BSA) forms a layer, approximately 100 Å thick on a layer of PDMS, when the PDMS is treated for 5 minutes with a 1 mg ml^{-1} solution of BSA. To this end, a film of approximately 0.9 μm PDMS was deposited, and treated with BSA solution. The spectra produced are shown, in the 1400-1800 cm^{-1} region in Figure 6.12.

The noise level in the produced spectra is very high, and hence it is impossible to be definitive as to whether there is any spectral evidence for BSA presence. It is possible that we do see some indication of the amide bands in the spectral subtraction, with possible features at approximately 1750, 1655 and 1540 cm^{-1}, which could correspond to protein amide bands, but the evidence produced here is poor, and the experiment clearly requires modification and reproducing.

6.3.1.3 - Other Barrier Layers.

Another constituent of one particular anti-fouling paint system is the polymer XK91, mentioned in Chapter 5. XK91 is essentially a salt, produced from a mixture of 24% polymethylmethacrylate, 56% polyethylmethacrylate and 20% methyl acrylic acid, reacted with Rosin Amine D, which is an aromatic amine the structure of which is given in Figure 46 on Page 86 in Chapter 5. A film of approximately 0.9 μm XK91 was treated with sea-water for approximately 1 week, and the results are shown in Figure 6.13.

If the high frequency side of the amide I carbonyl band (arising from the Rosin amine D) is examined closely, there appears to be some evidence for a new feature under the band, which causes the apparent shoulder. Furthermore, if the spectral subtraction is examined, a weak feature can be seen, which probably corresponds to the band responsible for this shoulder. Also, there is a clear change in the region around 1510 cm^{-1}, which suggests a species has been lost on treatment with sea-water. It is unclear what is occurring here, and further studies are required.

6.3.1.4 - Conclusions.

It is believed that in the experimental studies described above, definitive evidence is presented to substantiate the potential of the barrier film FT-IR ATR technique to the observation of interfacial interactions between polymer films. The results obtained from the use of alkyd resin and solvent-based acrylic topcoats are particularly encouraging. It is further believed that this is the first time all of the above systems have been examined by this technique, and it is a matter of regret that potentially more interesting systems were discovered (described in the remainder of this Chapter), and hence energies were applied elsewhere. However, the potential has been demonstrated, and it is for future workers to realise its fullness.

Figure 6.12 - PDMS plus BSA

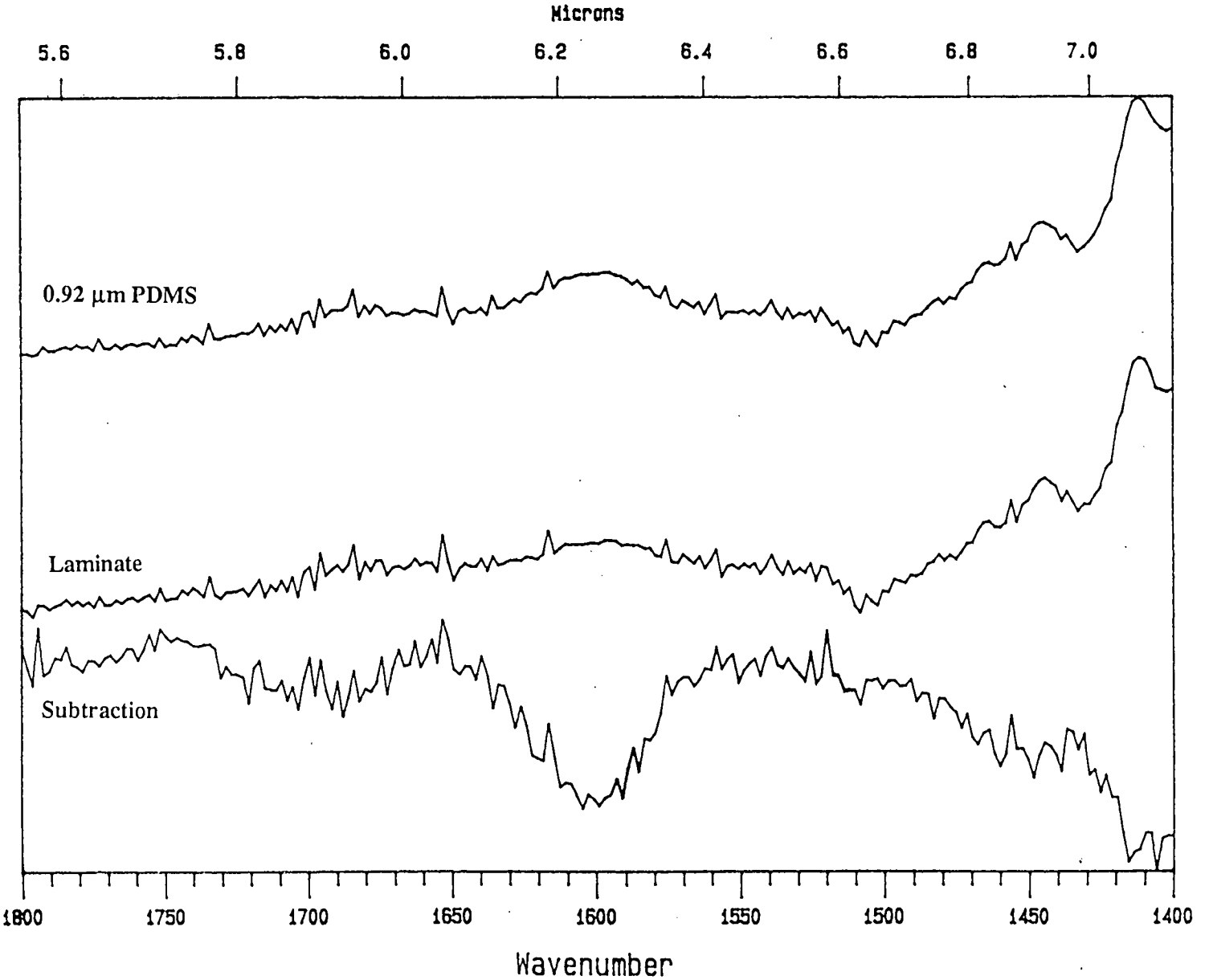

Figure 6.13 - XK91 plus Sea Water

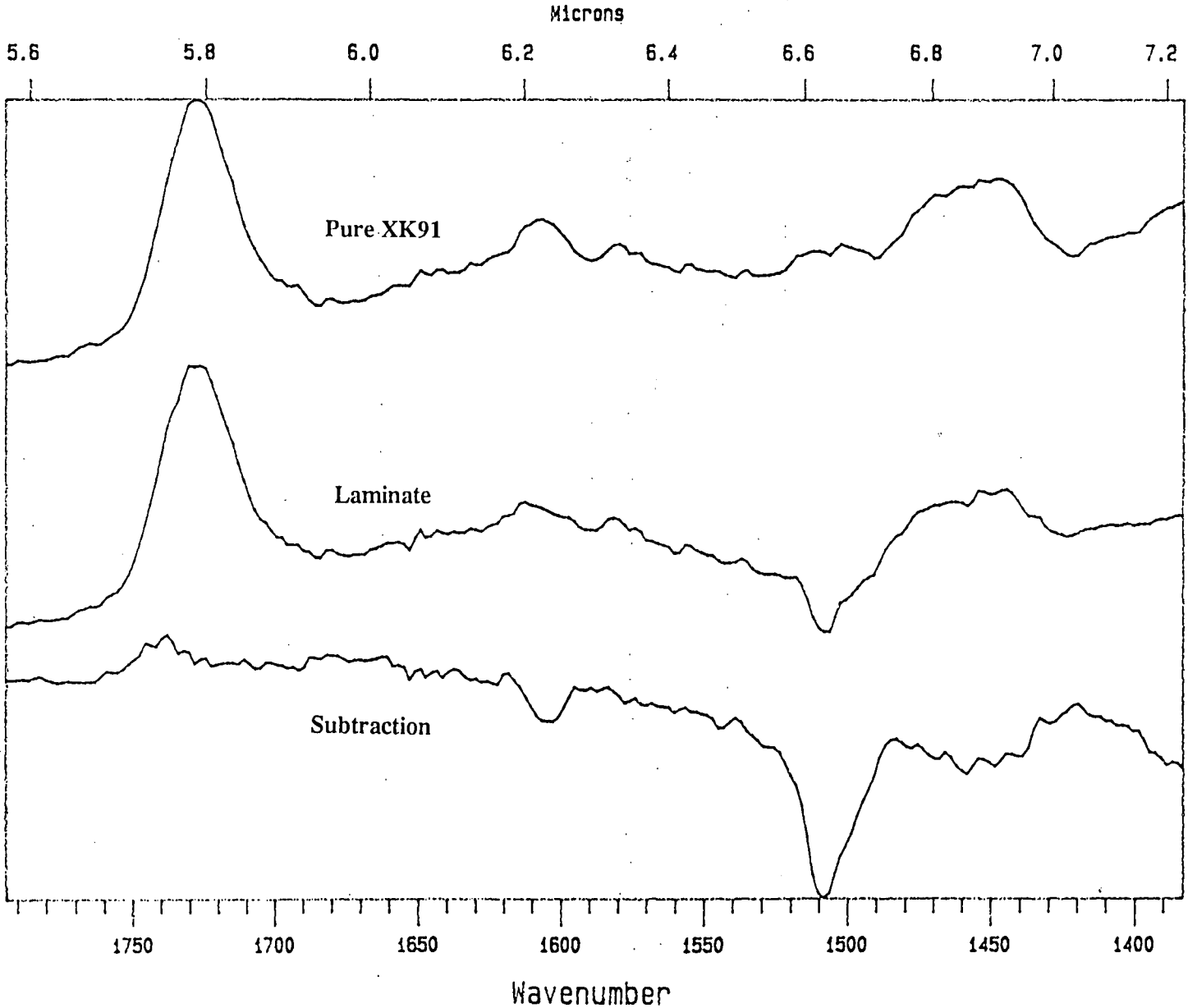

6.3.2 - Diffusion Processes in Epoxy Resins.

6.3.2.1 - Introduction.

The failure of paint systems, as discussed above, is an area of great significance at the time of writing, hence diffusion processes occurring in epoxy resins are of particular importance. Such processes have a direct influence on parameters such as adhesion between layers and paint failure, arising from swelling associated with the diffusing entity. Thus, understanding transport processes in epoxy resins is an area of considerable interest, and is reflected in the literature, a selection of which is briefly reviewed here. The area of predominant interest is the study of water transport in epoxy resins[9-19], which examine the effect of parameters such as chemical structure, degree of crosslinking and the effect of halogens on the diffusion process. There is, however, some disagreement on the actual diffusion mechanism, although there is a consensus towards non-Fickian behaviour. Diffusion of other materials, such as solvents, has also been examined[20-23], and again the processes appear to be non-Fickian.

In this section, the results of experiments conducted to examine the nature of the diffusion of several penetrants into certain epoxy resins is presented, in chronological order, the reason for which will become apparent as the section unfolds. Relevant spectra are presented, along with appropriate diffusion curves and the corresponding calculated diffusion coefficients, but only when enough experimental data was available to make such calculations sensible. The calculated diffusion curves and coefficients have been produced using software developed in Durham[24]. A full discussion of all the diffusion results described in this chapter is given in Chapter 7.

6.3.2.2 - Trimeric Isocyanate Diffusion.

1/. Original Investigations

The investigation into the diffusion processes occurring in epoxy resins began as the result of an accident, when films of the epoxy resin, Epikote[7] 1001, crosslinked with KH92, of the order of 4 μm, were prepared for a barrier film experiment. It was decided that these films would not be discarded, as they would provide additional evidence for the extent of evanescent wave penetration into such systems, by virtue of the fact that any topcoat deposited would be outside the range of the sampling field (about 1.5 μm in the carbonyl region) and thus the topcoat spectrum would not be seen. This was duly accomplished using a solvent-based acrylic topcoat, but when the trimeric isocyanate, CCA315 (see Figure 6.14) was used, unexpected bands were observed in the spectrum at approximately 2260 cm^{-1} and 1680 cm^{-1} (see Figure 6.15). A subsequent experiment, using pure CCA315, confirmed that these bands did indeed arise from this material, with the band at approximately 2260 cm^{-1} arising from the isocyanate, antisymmetric stretching mode, and the band at about 1680 cm^{-1} from the carbonyl stretching mode[25].

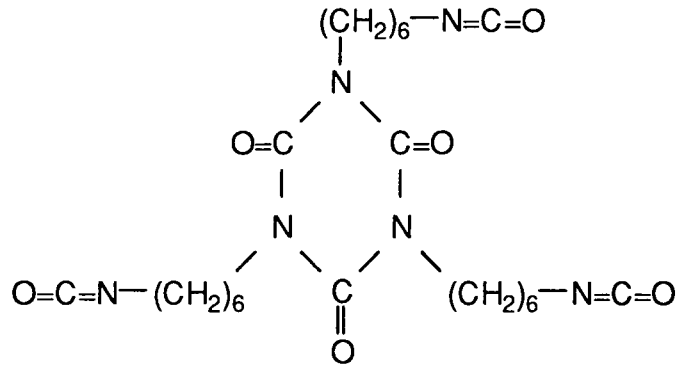

Figure 6.14

Figure 6.15 presents the spectra produced from this initial experiment, and includes the spectrum of the pure isocyanate trimer, the pure resin and the result of a subtraction of pure resin from the laminate spectrum.

The average thickness of this film is 4.2 μm ± 0.2 μm. The depth of penetration (d_p) of the evanescent wave varies with the frequency of the band examined, and at the frequencies of 1680 cm^{-1} and 2260 cm^{-1}, it is calculated (see Chapter 2, Section 2.6.2, page 21) to be 1.52 μm and 0.75 μm respectively. Assuming that the actual depth sampled is generally accepted as being three times d_p, it is conceivable that the 1680 cm^{-1} band arises from evanescent wave penetration into the topcoat, but the band at 2260 cm^{-1} is considerably outside this range, and thus it is believed that it is reasonable to assume that some diffusion of the trimeric isocyanate has occurred. Additionally, a clear broadening of the two bands, plus a red shift was observed, and is clearly evident in both the isocyanate (2260 cm^{-1} shifted to 2238 cm^{-1}) and carbonyl (1680 cm^{-1} shifted to 1658 cm^{-1}) bands in Figure 6.15, when the pure material spectrum is compared to the material which is assumed to have diffused into the epoxy resin. The subtraction confirms this band shift. A red shift tends to imply increased interaction of the material under examination, e.g. hydrogen bonding, and this would be reasonable, as both the isocyanate and carbonyl groups are reactive entities and would hence interact strongly with the hydroxyl groups associated with the crosslinked resin (see Chapter 1).

The need to eliminate the, albeit remote, possibility of the effect being due to extensive evanescent wave penetration was addressed by the use of a very thick film of Epikote[7] 1001, cast from a 60% (solids) solution of the resin, crosslinked with KH92, which yielded a film of thickness 7.6 μm ± 0.4 μm. Five spectra were obtained from this at known times, and the isocyanate region of four of these is shown in Figure 6.16, namely those obtained 5 minutes, 30 minutes and 80 minutes after application, plus the spectrum of the pure isocyanate.

Again, the band corresponding to the trimeric isocyanate is clearly seen, and again a significant red shift is evident, probably indicating hydrogen bonding between the isocyanate groups and the hydroxyl groups associated with the epoxy resin.

Figure 6.15 - Epikote[7] 1001 plus Trimeric Isocyanate

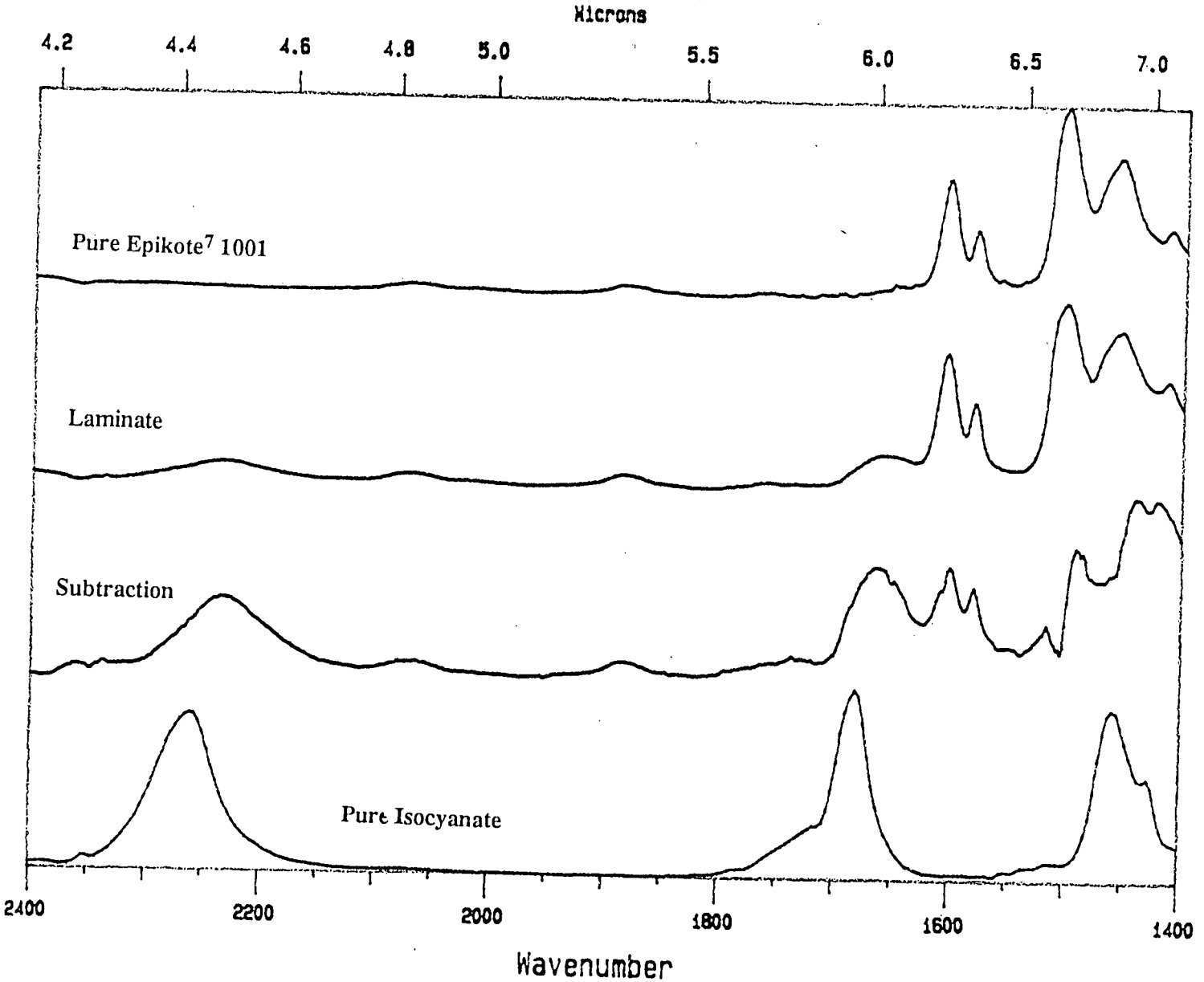

Figure 6.16 - Epikote[7] 1001 plus Trimeric Isocyanate - Isocyanate Region

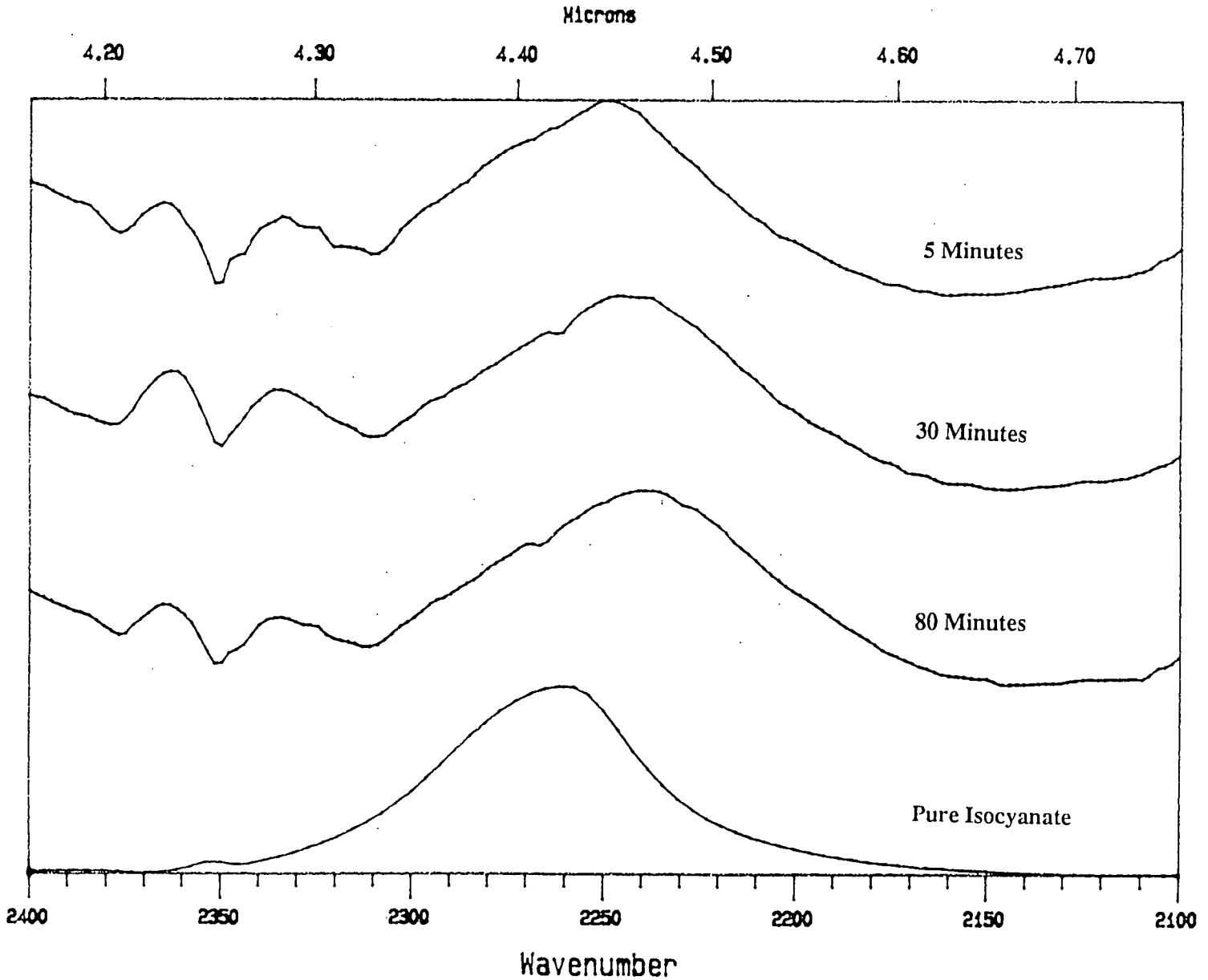

The reaction that occurs between an isocyanate and an alcohol produces a urethane, according to the following reaction:-

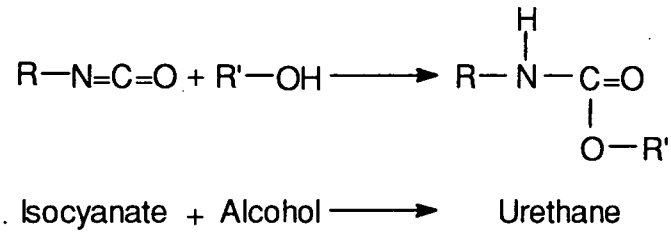

Isocyanate + Alcohol ⟶ Urethane

(Reaction 1)

In the infrared spectrum[31] of a urethane, the carbonyl absorption responsible for the amide I band is seen in the 1730-1720 cm^{-1} range for primary urethanes[34] in dilute solutions in chloroform, but at rather higher frequencies in carbon tetrachloride. A wide range of frequency distributions for this amide I band is observed on passing through secondary to tertiary systems[32-36], with a range between 1705-1739 cm^{-1}, depending on solvent and whether the system is aliphatic or aromatic.

However, a further reaction is also possible, between the isocyanate and any free primary amine groups, resulting from unreacted crosslinking agents. This proceeds as follows:-

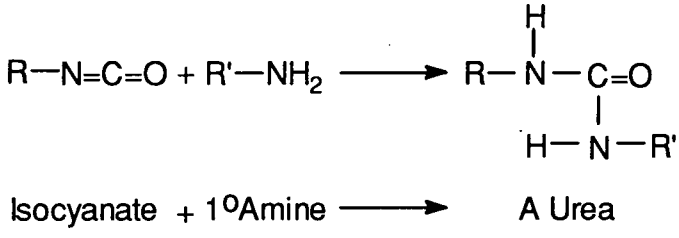

Isocyanate + 1°Amine ⟶ A Urea

(Reaction 2)

Infrared spectra[37-46] of ureas are reported to show three bands in the 1650-1550 cm^{-1} region for a monoalkyl system. These correspond to the carbonyl stretching mode (amide I), and the NH and NH_2 bending modes (amide II). The carbonyl frequency is markedly lower than that found in a 'normal' amide, being in the 1605 cm^{-1} region, with the amide II NH_2 band at 1666-1655 cm^{-1}, and the NH amide II band at 1575-1550 cm^{-1}.

A further experiment was performed to examine whether the band shift and intensity would decrease with time, hence indicating a reaction occuring within the film. Hence an epoxy film was treated with the trimeric isocyanate, and the resulting system left for a known length of time to see if there was any evidence for a reaction occurring, similar to the one described in the reactions above. It was deduced that if such a reaction occurred, two observations should be seen. Firstly, the band at approximately 2260 cm^{-1} would lose the red shift, as all available reaction sites (i.e. OH groups on the crosslinked resin) would be occupied, and thus further isocyanate diffusing into the resin would not have any sites to hydrogen bond with. Secondly, some spectral evidence should be found to support the formation of either or both urethane and urea.

A film of Epikote[7] 1001 was cast, using KH92 as crosslinking agent, which was found to be of thickness 3.7 μm ± 0.5 μm. This was treated with the trimeric isocyanate and examined over a period of approximately one week. Figure 6.17 shows the spectra obtained 30 minutes, 20 hours, 96 hours and 144 hours after isocyanate application. Close inspection of the 2260 cm^{-1} band does indeed indicate that the band appears to lose the red shift, and return towards the position of the band in the pure substance.

This does indeed appear to verify that something is occurring within the film with time. As indicated above, the possible reactions thought to be possible within epoxy films involve the production of both a urea and urethane. However, the spectral region where these bands are expected is heavily obscured by both epoxy peaks and the trimer carbonyl band. Figure 6.18 shows the spectral region 1400-1800 cm^{-1} of the spectrum taken 144 hours after isocyanate application, following subtraction out of both the pure isocyanate and untreated resin.

Unfortunately, the quality of spectra obtained by such multiple subtractions is not very high. There may be some tenuous evidence for features at approximately 1673 cm^{-1} and 1560 cm^{-1}, which could be indicative of urea amide II bands, but it is impossible to be certain. Hence we must rely on the evidence of the decrease in both band intensity and shift, shown in Figure 6.17, for proof of a reaction occurring within the film.

The next step was to try a different epoxy resin, and the resin Epikote[7] 828 was chosen, as this has a smaller repeating unit (n = 1, instead of n = 2.64, as in Epikote[7] 1001, see Chapter 1, Section 1.2.4), and thus, when reacted with KH92, should have a tighter crosslinked matrix, and hence allow both less of the diffusing species to enter plus actual slower diffusion. A film of Epikote[7] 828 was thus prepared, using KH92 as the crosslinking agent, and the film thickness was determined as being 5.0 μm ± 0.8 μ m. This was treated with the trimeric isocyanate, and Figure 6.19 shows the resulting spectra obtained 75 minutes and 20 hours after application, plus the spectra of the pure resin and pure trimeric isocyanate.

It is obvious that in this case, much less of the diffusing species enters the resin, which is consistent with the prediction above, that the crosslinked matrix is tighter, and thus more difficult to access, than in the case of Epikote[7] 1001.

Two further initial experiments were performed using a different crosslinking agent, namely cardanol (see Chapter 1, Section 1.2.4 for structure), which is a far more complex entity. When Epikote[7] 1001 was used, a film was produced which was found to be of thickness 4.9 μm ± 0.5 μm. This was treated with the trimeric isocyanate, and the spectra obtained 10 minutes, 40 minutes and 110 minutes after application are shown in Figure 6.20, along with the spectrum of the pure trimeric isocyanate.

The results from this experiment were clearly different from those shown above as higher band intensities were observed and no band shift was evident. The band seen at 1730 cm^{-1} is due to the trimeric isocyanate solvent, heptyl acetate, and it decreases with time, as the material evaporates. It is likely that this film was in fact cracked, the cracking probably arising from the increased size of the crosslinking agent. The evidence for this is found in both the higher band intensities, which would be consistent

Figure 6.17 - Epikote[7] 1001 plus Trimeric Isocyanate - Isocyanate Region

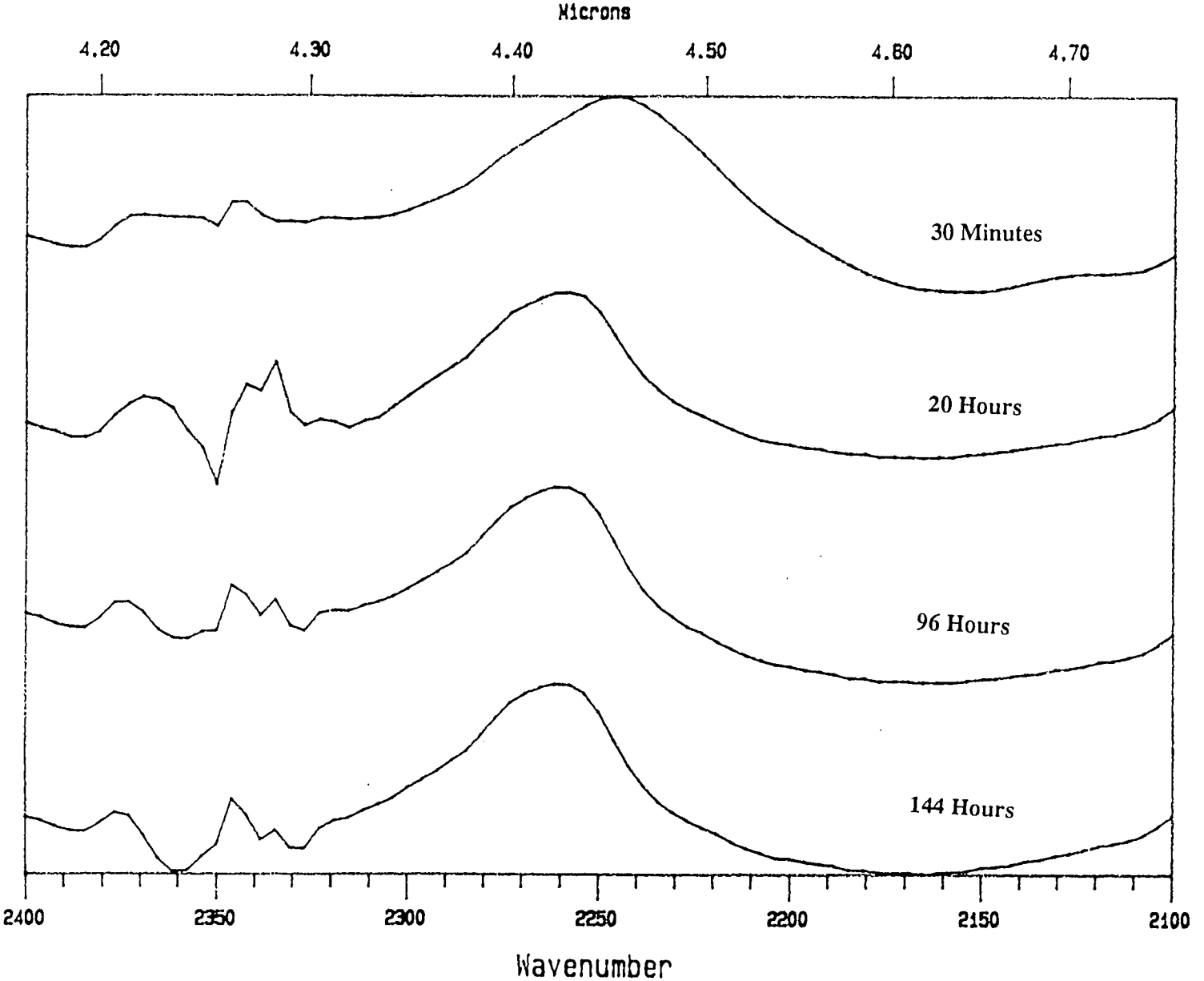

Figure 6.18 - result of Spectral Subtraction

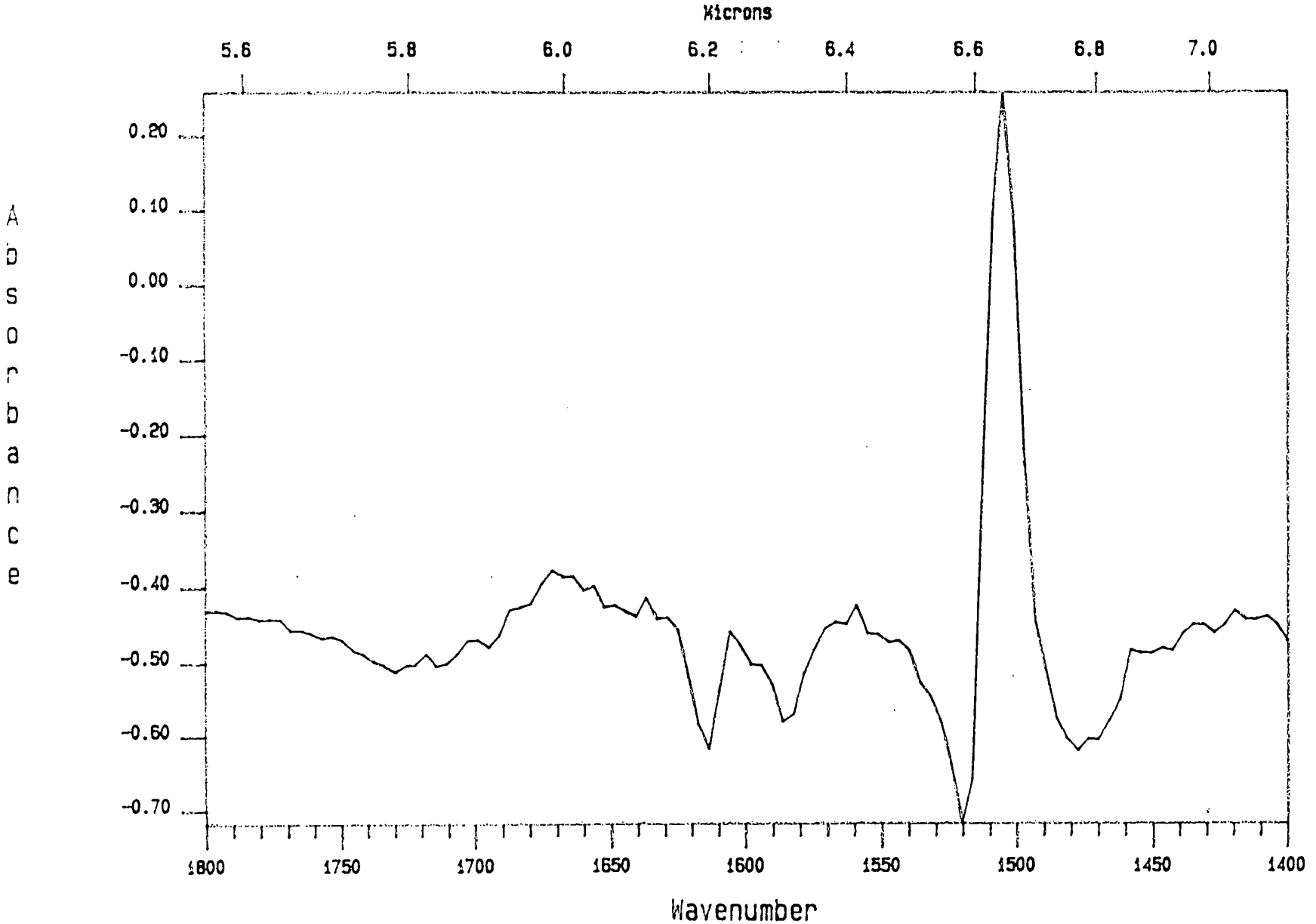

Figure 6.19 - Epikote[7] 828 plus Trimeric Isocyanate

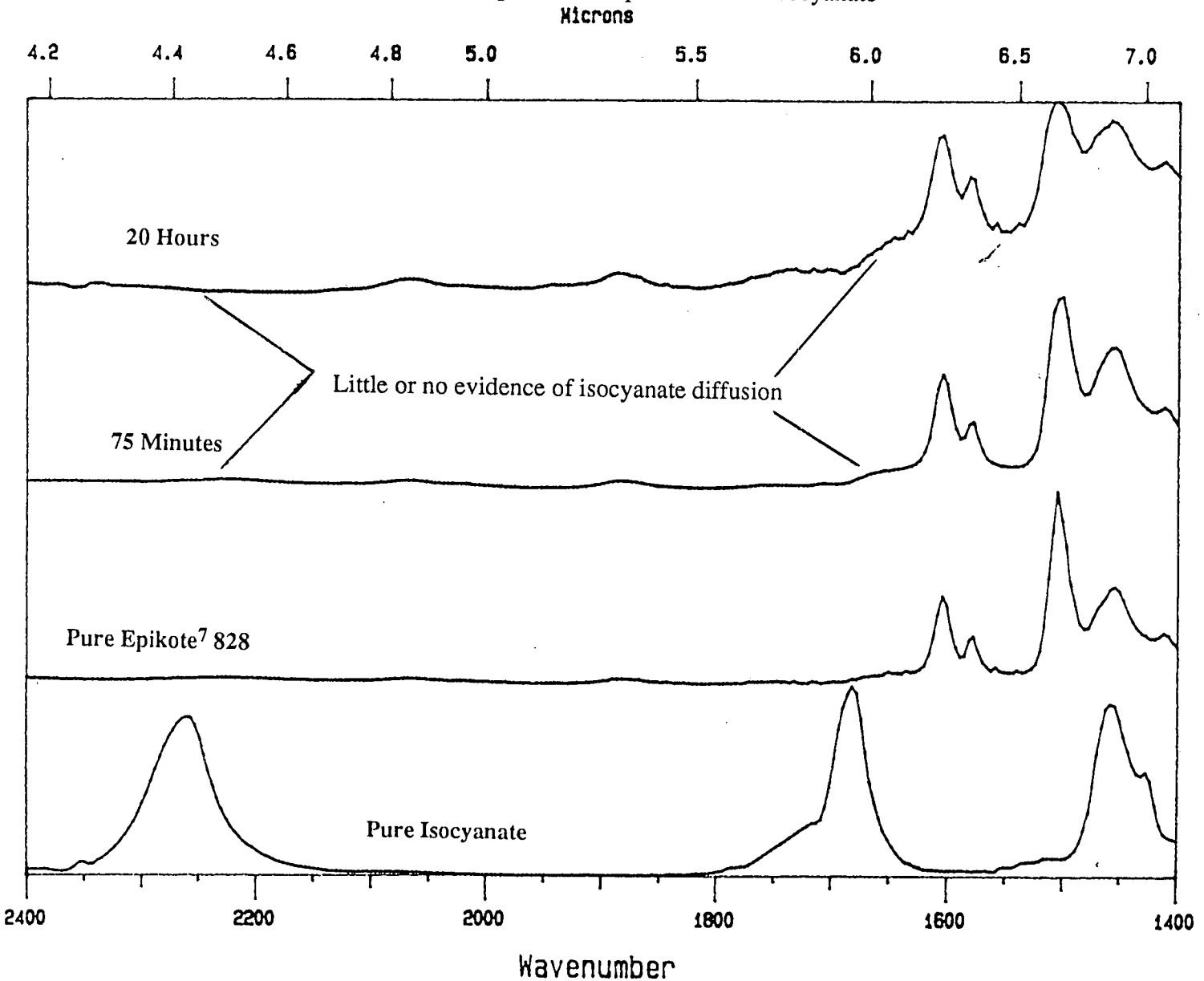

Figure 6.20 - Epikote[7] 1001, Cardanol Crosslinked, plus Trimeric Isocyanate

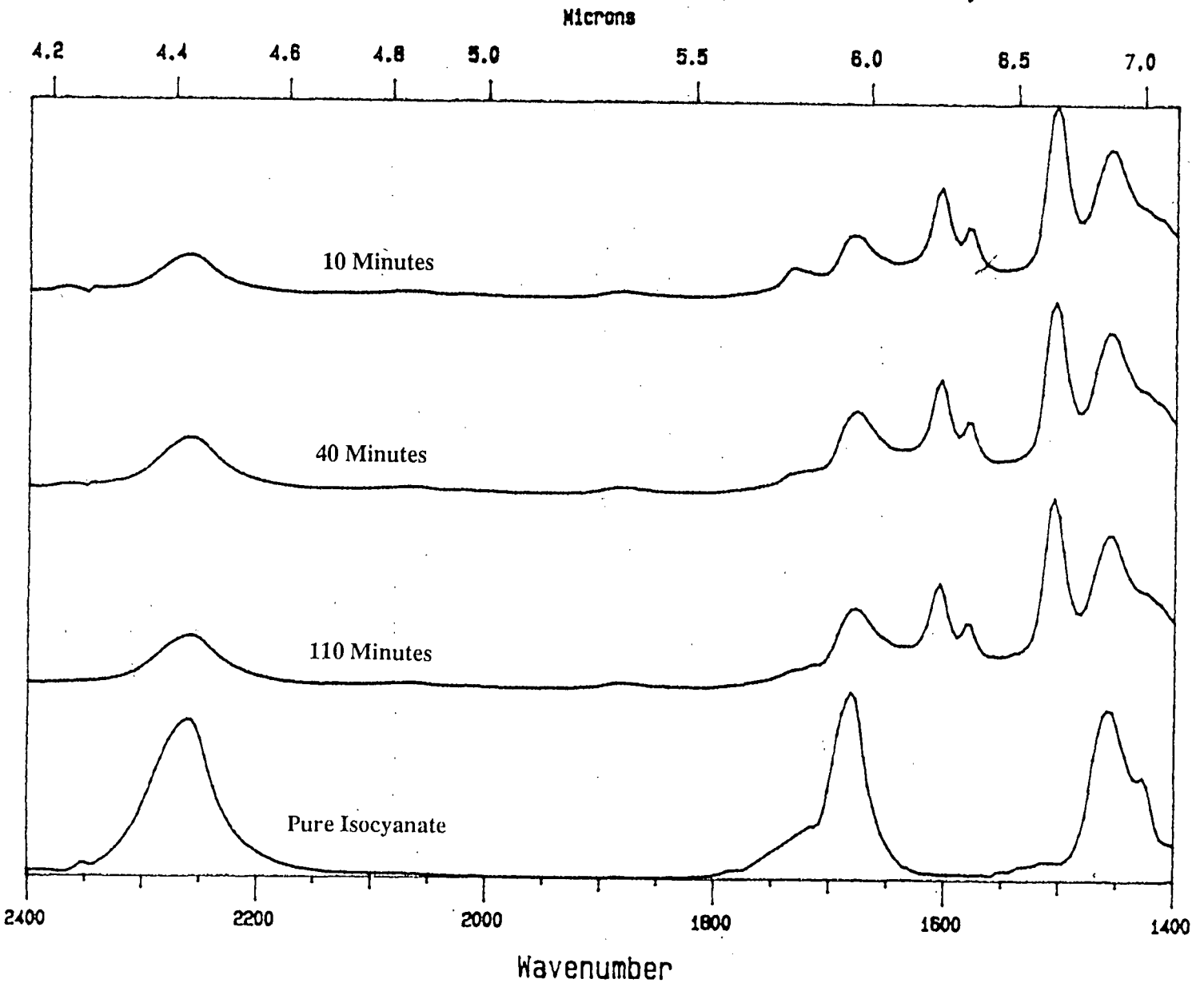

with a material simply running into cracks. Also, the lack of band shift would suggest that the amount of material actually within the epoxy matrix, and thus interacting with the hydroxyl groups, is significantly lower, relative to the material outside the matrix within the cracks. Given that the thickness of the epoxy resin film would appear to preclude the possibility of evanescent wave penetration into the topcoat, the only other sensible explanation is for the film to be cracked. Unfortunately, no S.E.M. pictures were obtained, which possibly would have proved this theory beyond reasonable doubt, although the magnification required may have destroyed the film. However, this is a possibility for future work, because if these films are indeed cracked, then the commercial relevance is clear.

A similar experiment was conducted using Epikote[7] 828 and cardanol, with a film thickness of 4.4 μm ± 0.6 μm. This was also treated with the trimeric isocyanate, but the results obtained were similar to the experiment performed using Epikote[7] 828 with KH92 as the crosslinker, although here there is virtually no evidence for trimer penetration. Figure 6.21 shows the spectra around the isocyanate spectral region produced 15 minutes, 80 minutes and 103 minutes after isocyanate application, along with the spectrum of the pure trimeric isocyanate. It is clear that there is no evidence for any diffusion having occurred in this system.

The trimeric isocyanate used in the above experiments is used as part of a tough, urethane-based topcoat, the other constituents being the solvent based acrylic and a small trace of di-butyl tin dilaurate, which acts as a catalyst for the urethane formation. A final initial experiment was conducted using a film of Epikote[7] 1001, crosslinked with KH92, of thickness 8.1 μm ± 0.5 μm, which was treated with the topcoat mixture. Figure 6.22 shows the isocyanate spectral region, obtained 10 minutes, 30 minutes and 2 hours after the topcoat was applied along with a spectrum of the pure topcoat.

It appears from examination of Figure 6.22 that only a small amount of isocyanate has entered the film. This trace became evident only after subtraction of carbon dioxide. The intensity of the pure isocyanate band does not portray an accurate indication of the amount of material diffused into the film. This can be appreciated if one bears in mind that the part of the band seen at the lower frequency end of the spectrum (part of an overtone feature arising from the epoxy resin) is virtually invisible compared to the fundamental bands of the resin. The fact that little isocyanate has actually diffused into the film is not surprising, as the reaction between the isocyanate and the acrylic hydroxyl groups, in the presence of the catalyst, is reported to be very fast[8].

It was thus decided that the next step was to obtain precise data regarding the diffusion of the trimeric isocyanate into the resin, so that diffusion coefficients and the precise nature of the diffusion could be evaluated. Thus, several long experiments were devised, which were to be carried out on the Sirius 100 at Durham, using a Macro package, which allowed automatic sampling over a specified period of time which was developed there by S. Nunn[29]. However, after several attempts to carry out such a long experiment, it was discovered that no diffusion occurred, and any isocyanate seen resulted from bare crystal contamination. This puzzling observation was re-examined back at Courtaulds Coatings, and further experiments did indeed indicate that the diffusion process reported above was now, for some reason, not taking place.

Figure 6.21 - Epikote[7] 828, KH92 Crosslinked plus Trimeric Isocyanate

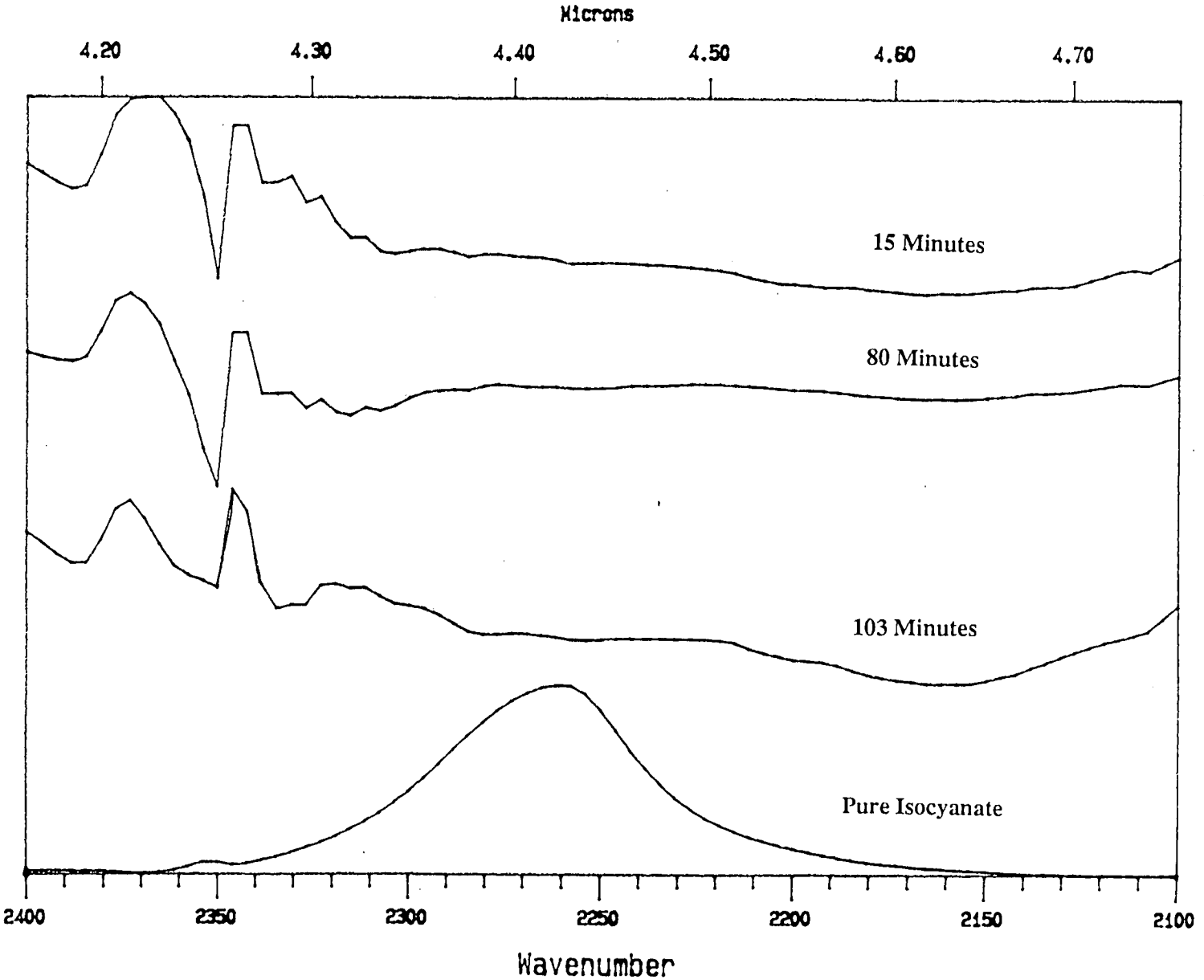

Figure 6.22 - Epikote[7] 1001 treated Trimeric Isocyanate, Solvent Based Acrylic and Tin Catalyst

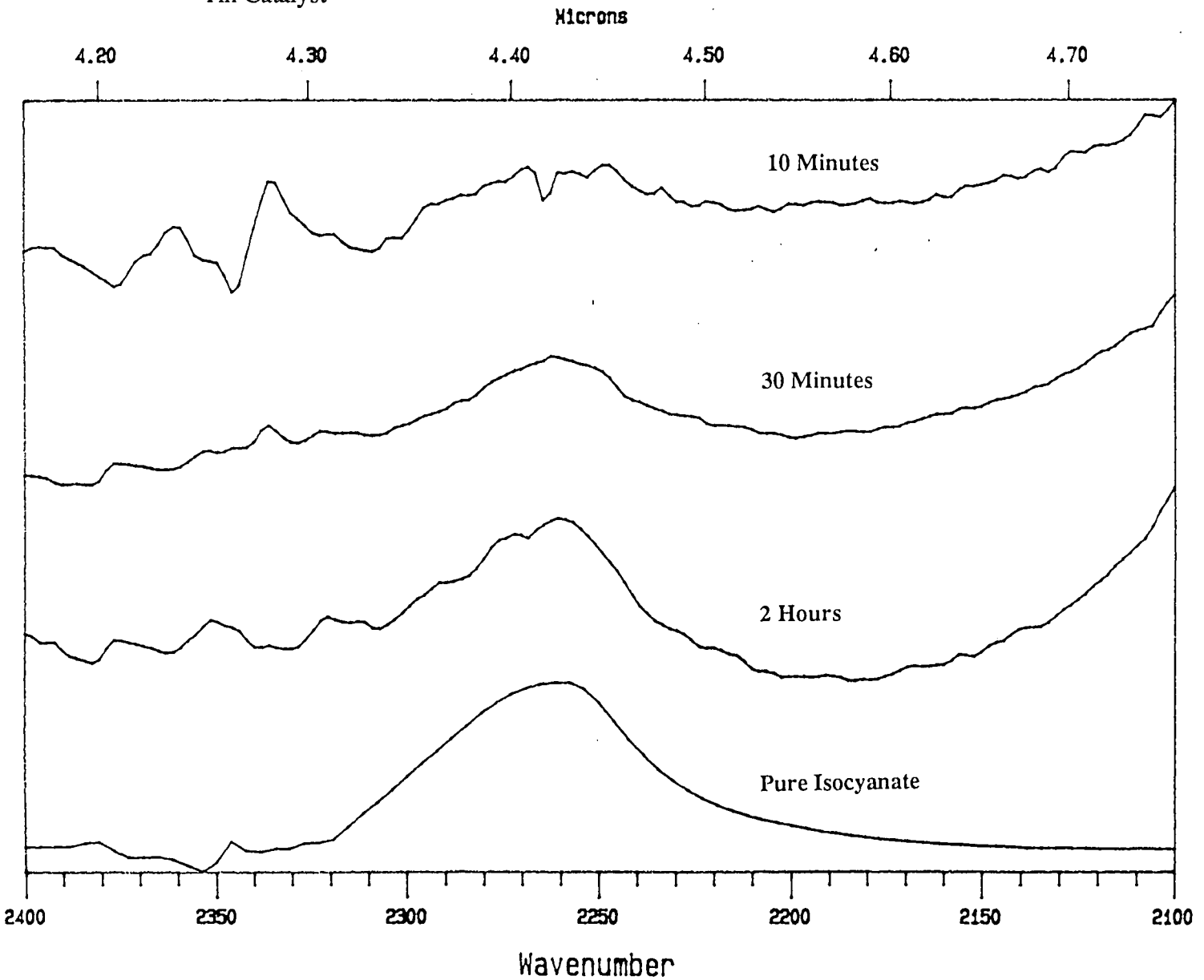

Considerable time was invested in attempts to recover this very interesting diffusion process, as the potential interest to Courtaulds was immense. Early efforts concentrated on the sample of trimeric isocyanate itself, as it is known[8] that the trimer polymerises in the presence of atmospheric water to form a glassy solid polymer, which can be seen around the opening of containers carrying the substance. Thus it was suggested that the same reaction could have occurred, at albeit a slower rate, in the container of isocyanate, and thus the trimer had increased to such a size that it could no longer enter the epoxy matrix. Several samples of pure, unopened trimer were thus obtained and the experiment repeated, but the results were the same.

The next step was a close scrutiny of film preparation. The samples of the epoxy resin and crosslinking agent were the same as those used in the initial experiments. However, the solvent blends and samples had changed several times, so a thorough investigation of the effect of different solvent blends and purity was made. This culminated in the discovery of another diffusion process, namely that involving so-called Poor Quality Films, which is discussed below. However, as discussed below, this process differed from the original diffusion quite markedly and is clearly not the process discovered above.

The original diffusion process described above (Figures 6.15-6.18) was never observed again. In the light of the efforts made to retrieve it, the only possible explanation that can be offered is that a batch of solvent was used, originating from Courtaulds (the purity of which has already been questioned), which contained some contaminant, and that this species affected the crosslinking process and hence the internal structure of the crosslinked resin. Hence, we were dealing with exceptional systems, which allowed the trimeric isocyanate to enter. This is clearly conjecture, but in the light of the observed effect of different blends and solvent quality on film quality, is a credible possibility.

2/. Poor Quality Film Experiments.

The SEM picture of a poor-quality film is shown in Figure 6.1.

As discussed above, a poor-quality film results from a solution in which the crosslinking agent KH92 only dissolves sparingly, with the undissolved majority forming a cloudy suspension. The fact that a limited amount of dissolution does actually occur is demonstrated by the fact that it is possible to obtain solid films of the epoxy resin Epikote[7] 828, which exists as a liquid in the uncrosslinked state. Films dipped from such cloudy solutions contain a mixture of the two separate entities, namely areas of crosslinked resin plus areas of the crosslinking agent, KH92, which is thought to form the wart-like structures apparent in Figure 6.1.

Several instances of diffusion were observed from such films, and Figure 6.24 shows the spectra obtained from a film of 3.2 $\mu m \pm 0.3$ μm of Epikote[7] 1001, taken 8 minutes, 30 minutes and 90 minutes after application, along with the spectrum of the pure trimeric isocyanate.

Both bands arising from the trimeric isocyanate can be clearly seen, and although evanescent wave penetration might explain the appearance of the 1660 cm^{-1} carbonyl

Figure 6.24 - Poor Quality Film of Epikote[7] 1001 plus Trimeric Isocyanate

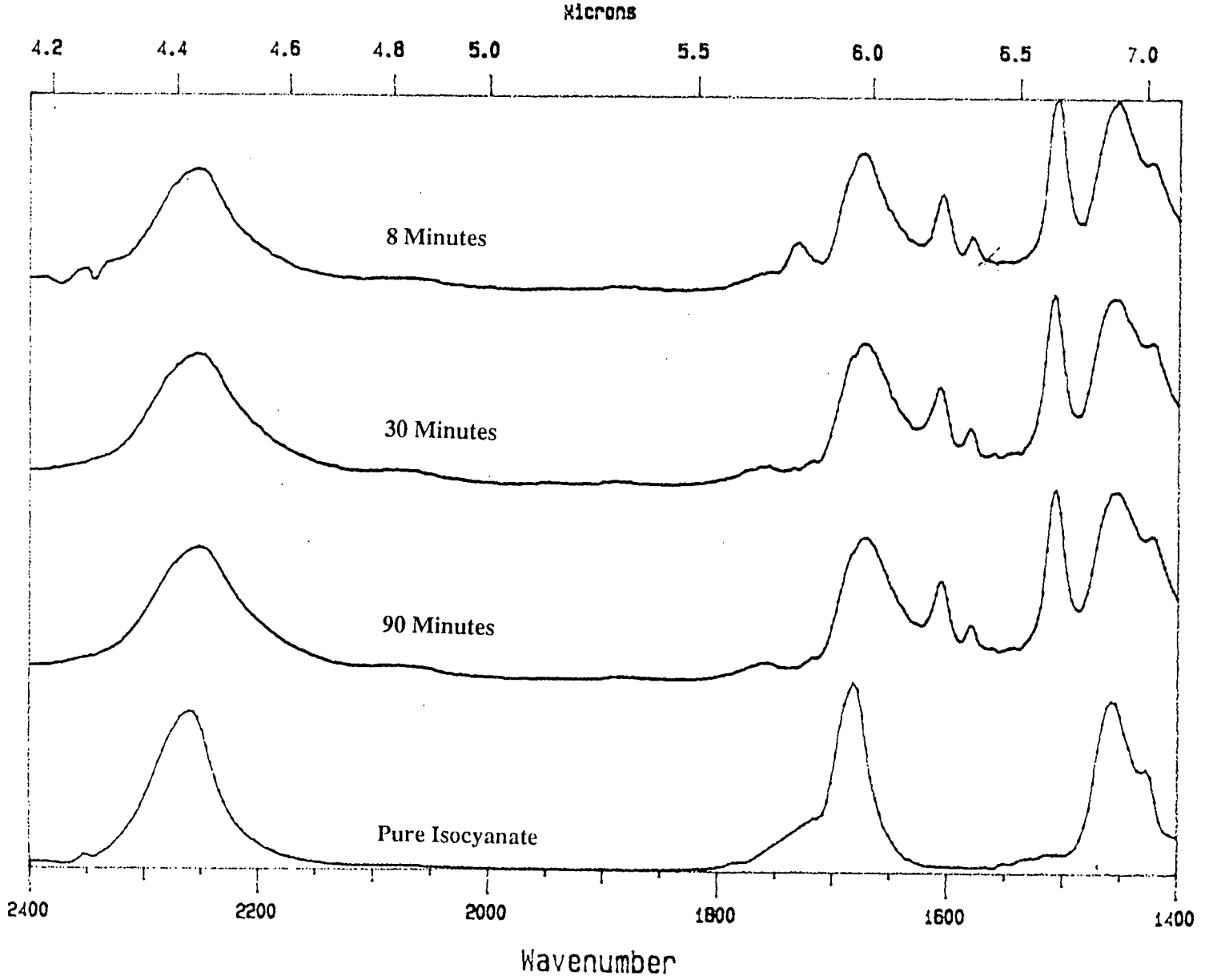

band, the isocyanate band at 2260 cm^{-1} cannot be explained thus. Also a small red shift is evident, with the isocyanate band moving from 2260 cm^{-1} to 2252 cm^{-1} and the carbonyl band shifting from 1680 cm^{-1} to 1671 cm^{-1}. However, this is far less extensive than that seen in the original diffusion experiments, but this does appear to indicate that the films used in the original diffusion experiments might contain some poor charecter. Figure 6.25 shows a comparison of the isocyanate spectral region of the spectrum obtained from this poor-quality film system after 30 minutes, along with that obtained for the original diffusion into a film of 2.9 μm ± 0.2 μm after 45 minutes. Also included is the spectrum of the pure trimeric isocyanate.

It can thus be clearly seen that, although a shift is evident, it is not on the same scale as the original observations.

If Epikote[7] 828 is used instead of Epikote[7]1001, a rather interesting phenomenon is observed. Figure 6.26 shows the spectra obtained when a poor-quality film of Epikote[7] 828 of thickness 3.7 μm ± 0.4 μm is treated with the trimeric isocyanate, at 8 minutes, 20 minutes and 3 hours after application. The spectrum of the pure trimeric isocyanate is also shown.

Here, diffusion is again evident, but the extent of diffusion, measured by the band intensities, is less than that seen in the diffusion into the poor-quality film of Epikote[7] 1001 and, again, there is little or no shifting of the two bands. This is rather interesting, as it follows the trends observed in the original experiments described above, in that it appears to suggest a closer matrix, due to tighter crosslinking.

Table 6.1 below summarises the differences between the two types of diffusion, in the two epoxy resins examined. Only one example is possible for each resin, simply due to the lack of precise data from the original diffusion experiments. These numbers adequately reinforce the above points, regarding the different diffusion processes believed to be occurring.

Table 6.1 - Comparison of Trimer Bands for both Original and Poor Quality Film Data

Time	*Original Experimental Data*				*Poor Quality Film Data*			
	Epikote 1001		Epikote 828		Epikote 1001		Epikote 828	
(mins)	I	cm^{-1}	I	cm^{-1}	I	cm^{-1}	I	cm^{-1}
30	0.39	2241	0.09	2258	0.56	2253	0.37	2259
30	0.26	1657	0.04	1678	0.44	1672	0.32	1678

It is believed that in the poor-quality films the trimeric isocyanate accesses the epoxy resin matrix via the particles of undissolved KH92 in the film, and is seen in the SEM photographs shown in Figure 6.1. The fact that less trimer enters the Epikote[7] 828 systems is believed to be simply due to there being less undissolved KH92 in the film, and hence a higher degree of crosslinking, which thus restricts access into the matrix.

In the case of the Epikote[7] 1001, a small amount of this trimeric isocyanate is near to the resin, at the edge of the KH92 particle. It is thus possible that this could diffuse a little way into the resin, a phenomenon possibly linked to the very low level of

Figure 6.25 - Comparison of Diffusion processes

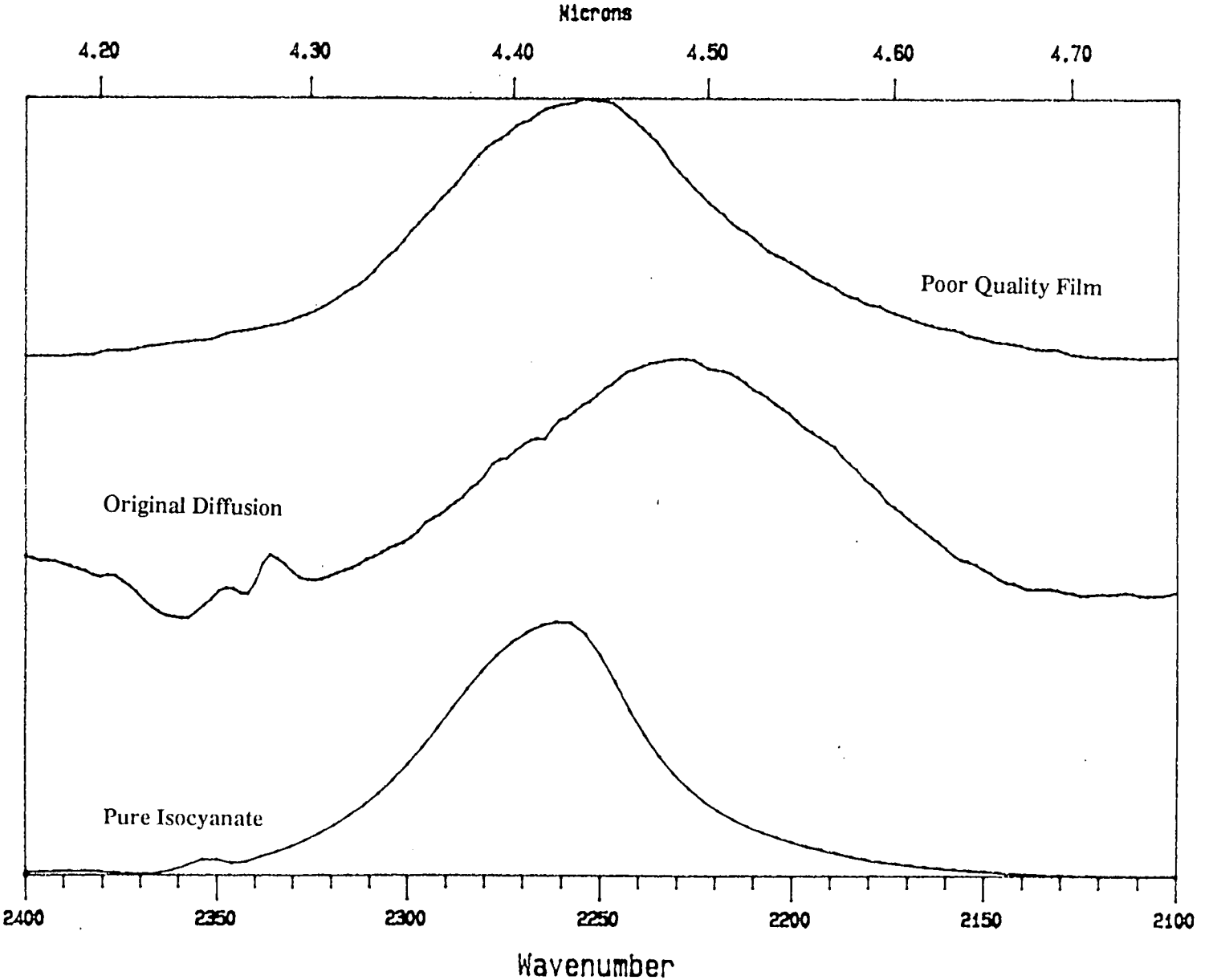

Figure 6.26 - Poor Quality Film of Epikote[7] 828 plus Trimeric Isocyanate

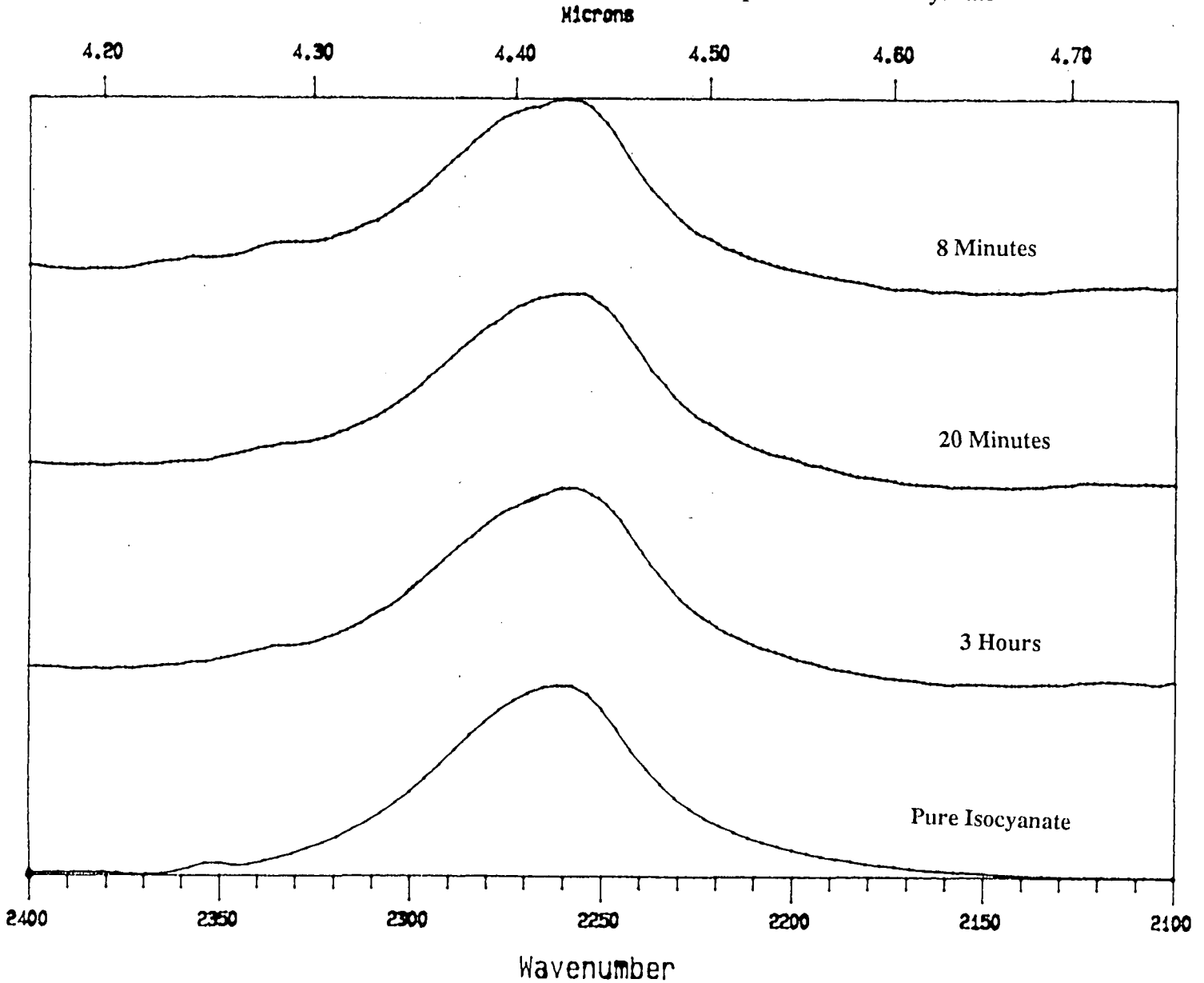

crosslinking within the resin. This isocyanate thus interacts with various functional groups within the resin, thus causing the small shift. This shifted band, arising from the interacted species, is much lower in intensity than that observed in the original diffusion, as much less material is involved with the interaction.

In the case of the Epikote[7] 828, the epoxy resin matrix is crosslinked more tightly (we know that the resin is crosslinked, due to the fact that the resin, in the case of poor-quality films of Epikote[7] 828, has set. Uncrosslinked Epikote[7] 828 is a liquid). The reasons for this lie with the smaller repeating unit, associated with Epikote[7] 828, which leads to smaller distances between crosslinks. Hence the trimer cannot enter the actual Epikote[7] 828 matrix, and hence cannot interact with the resin. Thus no significant band shift is observed.

One final experiment conducted involved a poor-quality film of Epikote[7] 1001, of thickness 5.8 μm ± 0.6 μm, which was treated with trimeric isocyanate, and placed in an oven at 60°C for 18 hours. The purpose of this was merely to attempt to induce a reaction. The resulting spectrum is shown in Figure 6.27.

The isocyanate has clearly entered the range of the evanescent field, and the complicated region around 1650 cm^{-1} suggests that a variety of reactions has occurred. Figure 6.28 shows the result of a curve fit analysis performed using a Gaussian function on the region around 1700 cm^{-1}. The numerical data produced is shown in Table 6.2.

Table 6.2 - Numerical Data

Centre (cm^{-1})	*Amplitude (Abs)*	*Width (cm^{-1})*	*Area (cm^{-2})*
1719	0.47	27.8	13.44
1682	0.94	38.8	37.79
1637	0.24	35.5	9.06
1609	0.32	13.8	4.64

The band at 1719 cm^{-1} is assigned to the urethane carbonyl stretching mode, resulting from the reaction of the isocyanate with the hydroxyl groups associated with the crosslinked resin. The 1682 cm^{-1} feature is believed to arise from the carbonyl group stretching mode associated with the unreacted trimer. The band at 1637 cm^{-1} is thought to arise from the amide carbonyl stretching mode of the urea, resulting from the reaction of the isocyanate with remaining primary amine groups and, finally, the band at 1609 cm^{-1} is probably due to one of the aromatic ring deformation mode of the epoxy resin.

This work, although not replicating the original diffusion process, is nonetheless of significant interest since it demonstrates how different film qualities affect the structure and possibly the efficiency of certain paint systems. The most obvious way forward from this position would be a detailed examination of differences in adhesion between the different types of epoxy film and relevant topcoats. It has also been demonstrated that different solvent blends and quality, along with different crosslinking agents, produce films of variable quality. Thus a future, detailed examination of the qualities of epoxy film produced from all the possible formulations used would be a useful tool towards better understanding of inter-film adhesion.

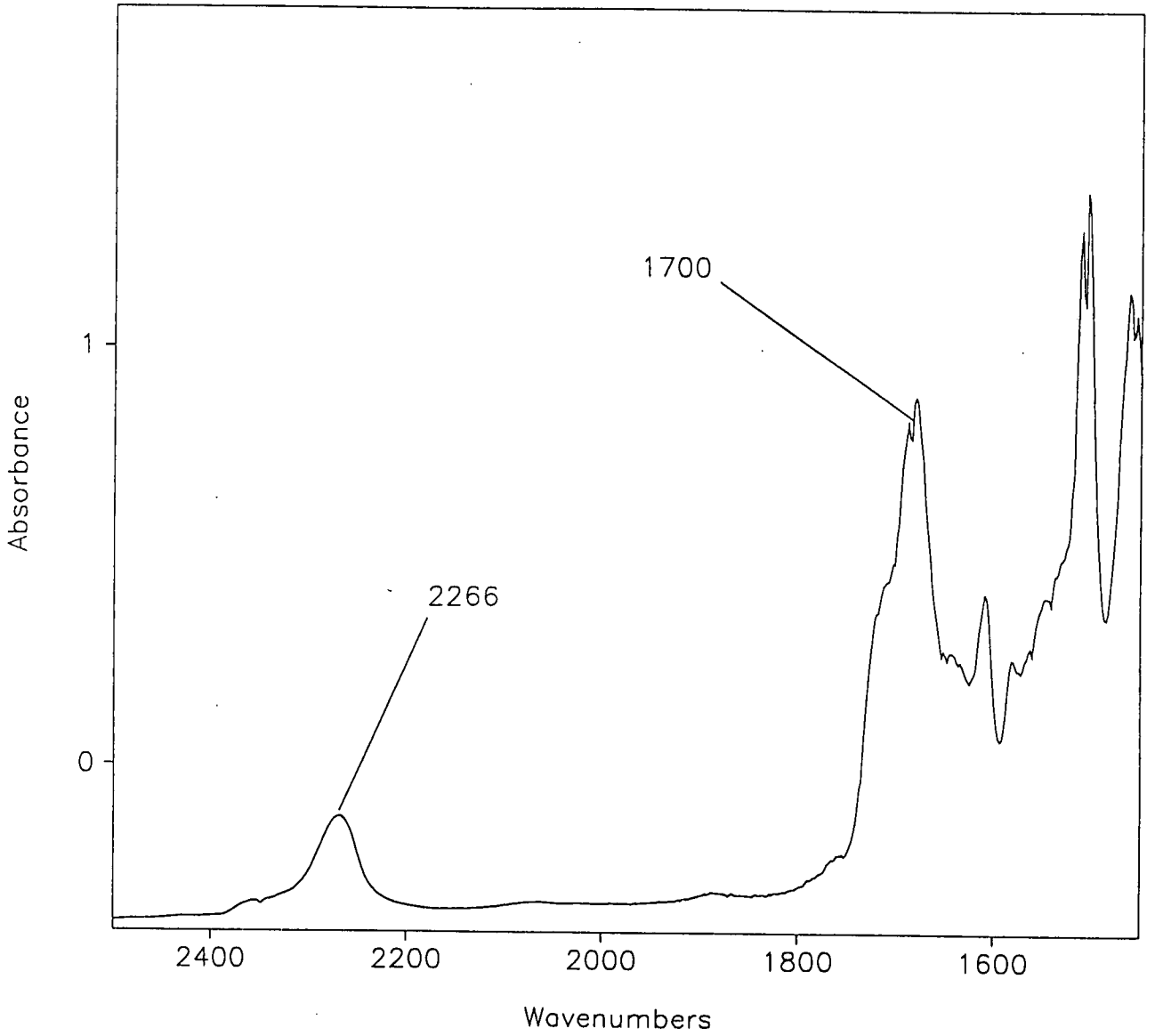

Figure 6.27 – Epikote 1001 + Trimeric Isocyanate after 18 Hours at 60C

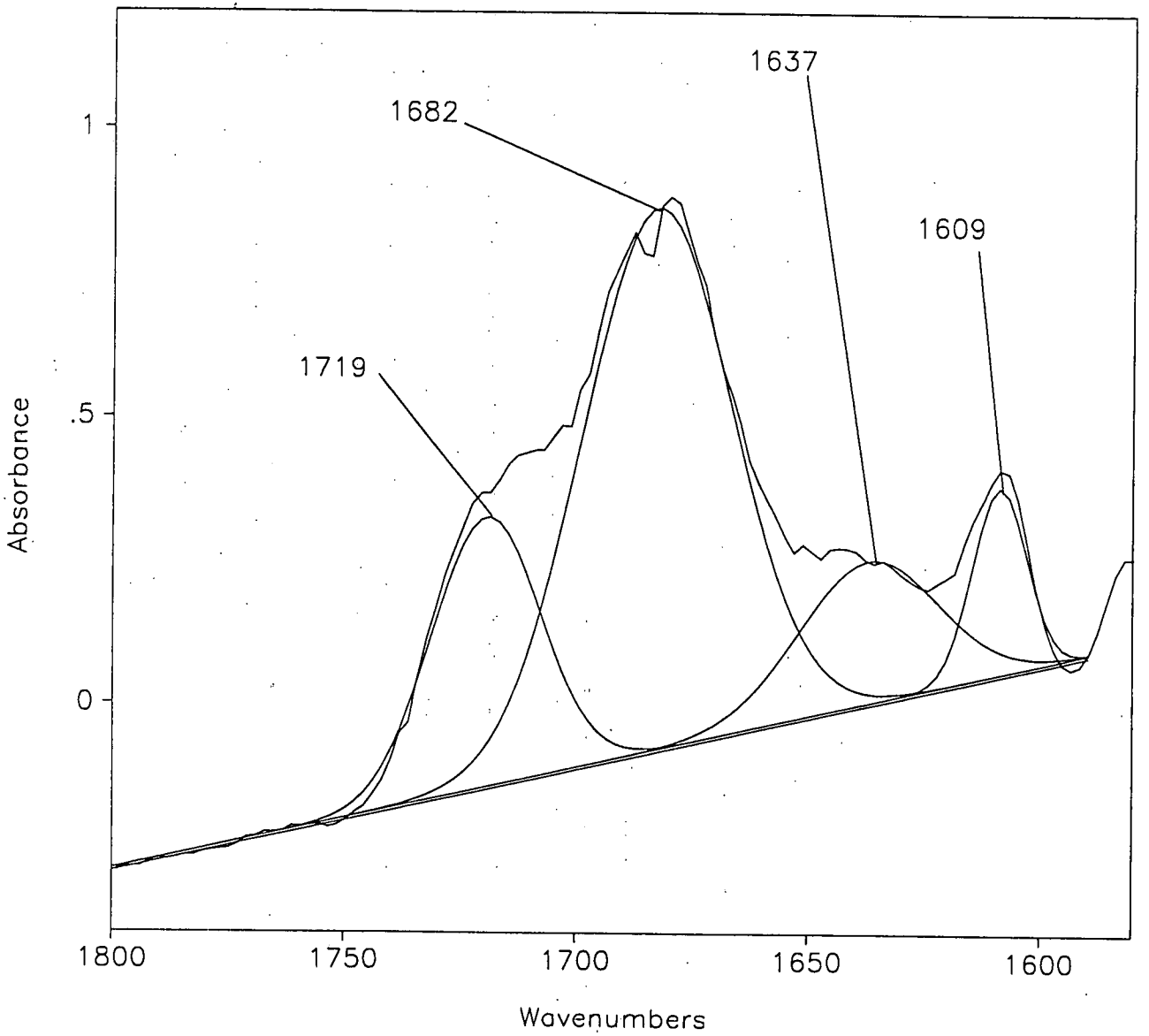

Figure 6.28 – Curvefit of Complex Region from Figure 6.27

6.3.2.3 - Monomeric Isocyanate Diffusion.

The trimeric isocyanate discussed above is prepared by a principal self-addition reaction of hexamethylenediisocyanate (referred to as HMDI in this thesis) shown below:-

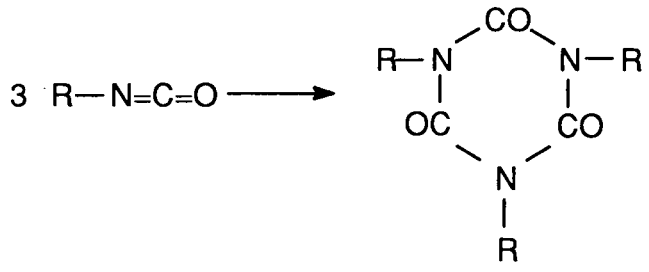

R = $OCN(CH_2)_6$ isocyanurate

(Reaction 3)

As part of a plan conceived during the original trimer diffusion work, some HMDI was obtained, the idea in mind being to attempt to synthesise some cyclic species containing more HMDI groups, in order to find the critical size of diffusing species after which diffusion ceased. With the demise of investigations involving the trimeric isocyanate, it was decided to see if this monomer (HMDI) would diffuse into the matrix. Thus, an experiment was performed whereby HMDI was put on top of a good-quality film of Epikote[7] 1001 and examined. It was discovered that the monomer did indeed diffuse into such films, and it was decided to examine this diffusion process.

In the course of this work, a further interesting discovery was made. The monomeric isocyanate appeared to react within the film, in a similar, although more prominent manner, to that seen with the trimeric isocyanate work. It is believed that the isocyanate reacts with both the hydroxyl and amine groups, associated with the crosslinked epoxy resin, and forming a urethane and urea respectively. This reaction is demonstrated by the appearance of a new feature, believed to originate from the urethane carbonyl, at approximately 1715 cm^{-1}. As the new band appeared, and increased in intensity, the HMDI band at approximately 2260 cm^{-1} was observed to decrease in intensity. The nature of the reaction is considered fully in the subsequent section, which deals with the reaction kinetics.

This section on the diffusion data is divided into two parts. The first considers the diffusion data, with the second, much shorter section, tentatively dealing with some kinetic aspects regarding the reaction occurring within the film. Two types of epoxy resin were used in this study, Epikotes[7] 828 and 1001, which were both crosslinked with KH92 in the pure solvent blend of 2 parts xylene, 2 parts n-butanol and 1 part methanol, which always produced films of Good Quality. Obviously only a selection of the spectral data obtained is presented below, but all relevant diffusion curves, diffusion coefficients and kinetic parameters are listed in full.

The number of experiments described here is not sufficient to provide a full, detailed account either of the diffusion processes occurring or the kinetics and nature of the

consequent reactions. Also, we had the additional problem of the complexity of the actual system we were attempting to examine. This has been mentioned earlier in this Chapter and will be evaluated further in Chapter 7. The data presented here, however, provides a reasonable basis for tentative explanations and observations, plus ideas for possible future work. These, again, are discussed fully in Chapter 7.

6.3.2.3.1 - Diffusion Data.

All diffusion curves shown here include the mathematically predicted curves arising from Fickian and Case II analysis of the data obtained. The software used in these manipulations was produced by M.R. Pereira at Durham University[24]. The experimental data used in these calculations are the spectral intensities (corrected to baseline) of the isocyanate band. It is accepted that this band is a composite species, including both the free and associated molecular species, but most of the data presented here was obtained using the instrument at Courtaulds Coatings, which does not possess any curve fitting software. Some subtraction techniques were attempted on the Courtaulds data, but the results from this were of such poor quality that they were meaningless and was thus discarded. Some of the data listed below was carried out at Durham, using the Mattson Sirius FT-IR machine, which functions using the more sophisticated FIRST™ software. This allowed the use of Macro packages, developed by Simon Nunn at Durham[29], which allowed continual monitoring of the processes occurring. It is the data from these experiments which form the basis for the kinetic speculations discussed later in this Chapter.

The diffusion data is given in separate tables in this Chapter, but in one table in Chapter 7, when the data is discussed fully. The calculated diffusion coefficients are divided into two sections, Fickian and Case II, depending on the model used. Both items of software calculate diffusion coefficients from the entered data, and generate a set of calculated data points from this calculated coefficient. Thus, on most plots shown here there are three curves, representing the experimental data, Fickian curve and Case II curve. In the case of the Fickian evaluation, only one coefficient is produced, which is indicative of the one-step process associated with Fickian diffusion.

However, in the Case II calculation, two coefficients are produced, which refer to the early pseudo-Fickian process and the second, slower diffusion, which is typical of a Case II process. However, a further weighting term, X_A, is also produced by the Case II calculation. This is referred to[24] as the fraction of molecules partially immobilised on the absorption sites, and gives an indication of which of the two processes associated with Case II diffusion is dominant. A high value of X_A indicates that the diffusion is dominated by the quicker, pseudo-Fickian initial process, and thus D_1 is the term of greater significance. Conversely, a low value of X_A, indicates that the second, slower phase is dominant, and thus D_2 is the term of greater importance. This is reiterated at the relevant point in Chapter 7, where the significance of the calculated data is evaluated.

1/. Epikote[7] 1001.

Three sets of experiments were conducted on this epoxy resin system, at different cure times.

(i). 24 Hour Cure.

Of the two experiments conducted using this cure time, only one produced data of use for evaluation of diffusion parameters. This involved a film thickness of 5.4 μm ± 0.4 μm and Figure 6.29 shows the diffusion curve obtained for this experiment.

The diffusion coefficients obtained for this experiment are shown in Table 6.3.

Table 6.3 - Diffusion Coefficients for 24 Hour Cured 1001

	Fickian	Case II		
Thickness (μ m)	*D* $cm^2\ sec^{-1}$	D_1 $cm^2 sec^{-1}$	D_2 $cm^2 sec^{-1}$	X_A
5.4±0.4	2.76×10^{-10}	2.61×10^{-10}	2.05×10^{-10}	0.99

(ii). 48 Hour Cure.

Two experiments were carried out with this cure time, using thicknesses of 4.0 μm ± 0.6 μm and 4.0 μm ± 0.3 μm. The diffusion curves obtained for these experiments are shown in Figures 6.30 and 6.31.

The diffusion coefficients obtained from these experiments are given in Table 6.4.

Table 6.4 - Diffusion Coefficients for 48 Hour Cured 1001

	Fickian	Case II		
Thickness (μ m)	*D* $cm^2 sec^{-1}$	D_1 $cm^2 sec^{-1}$	D_2 $cm^2 sec^{-1}$	X_A
4.0±0.6	8.59×10^{-11}	1.01×10^{-9}	5.18×10^{-11}	0.24
4.0±0.3	8.27×10^{-11}	2.23×10^{-10}	2.69×10^{-11}	0.51

(iii). 72 Hour Cure.

Only one experiment was performed with this cure time, namely on a film of thickness 5.0 μm ± 0.7 μm. The duration of this experiment was 120 hours, and Figure 6.32 shows the spectra obtained 30 minutes, 2 hours, 24 hours and 120 hours after isocyanate application. The small feature seen in the spectrum obtained after 30 minutes is due to contamination by MIBK (methylisobutylketone), used to clean the end of the crystal before sampling commenced. Figure 6.33 shows the resulting diffusion curves.

The diffusion coefficients obtained are given in Table 6.5.

Figure 6.29 - HMDI Diffusion into 24 Hour Cured Epikote 1001

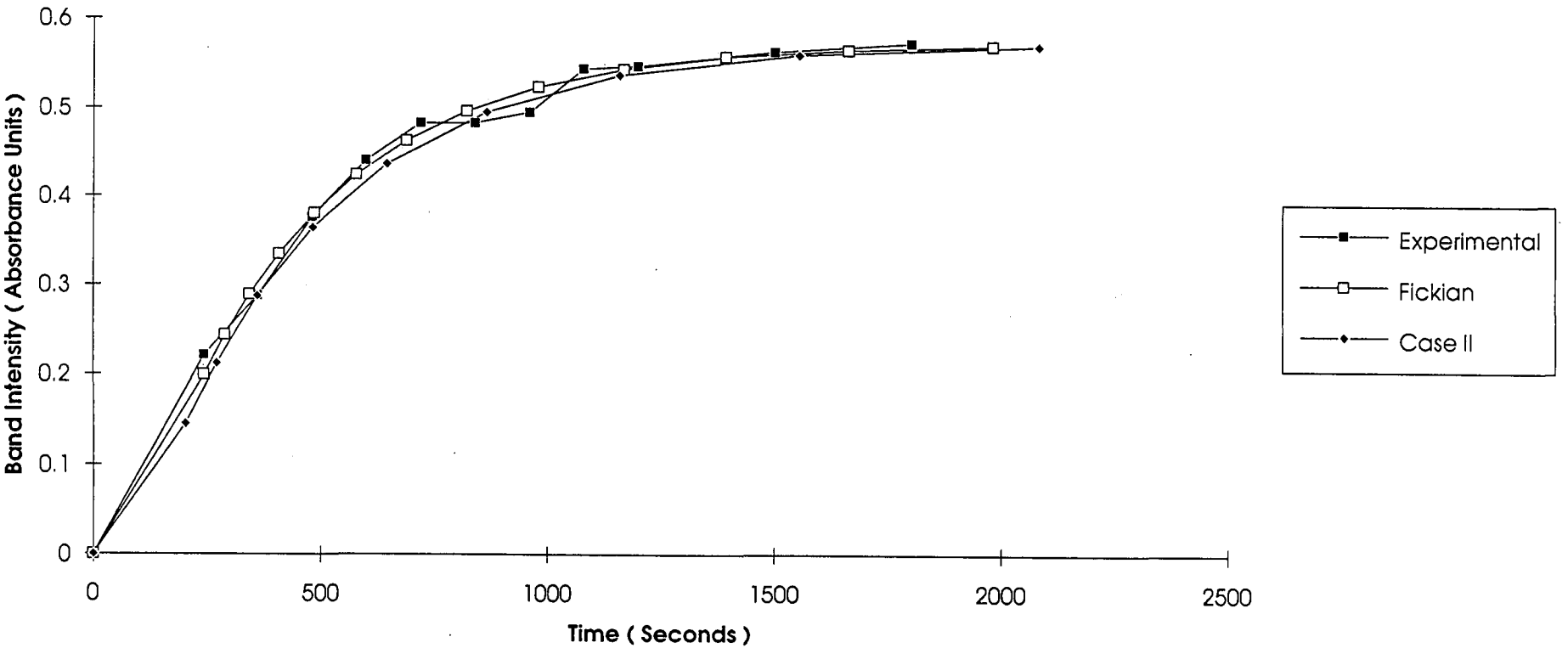

Figure 6.30 - HMDI Diffusion into 48 Hour Cured Epikote 1001

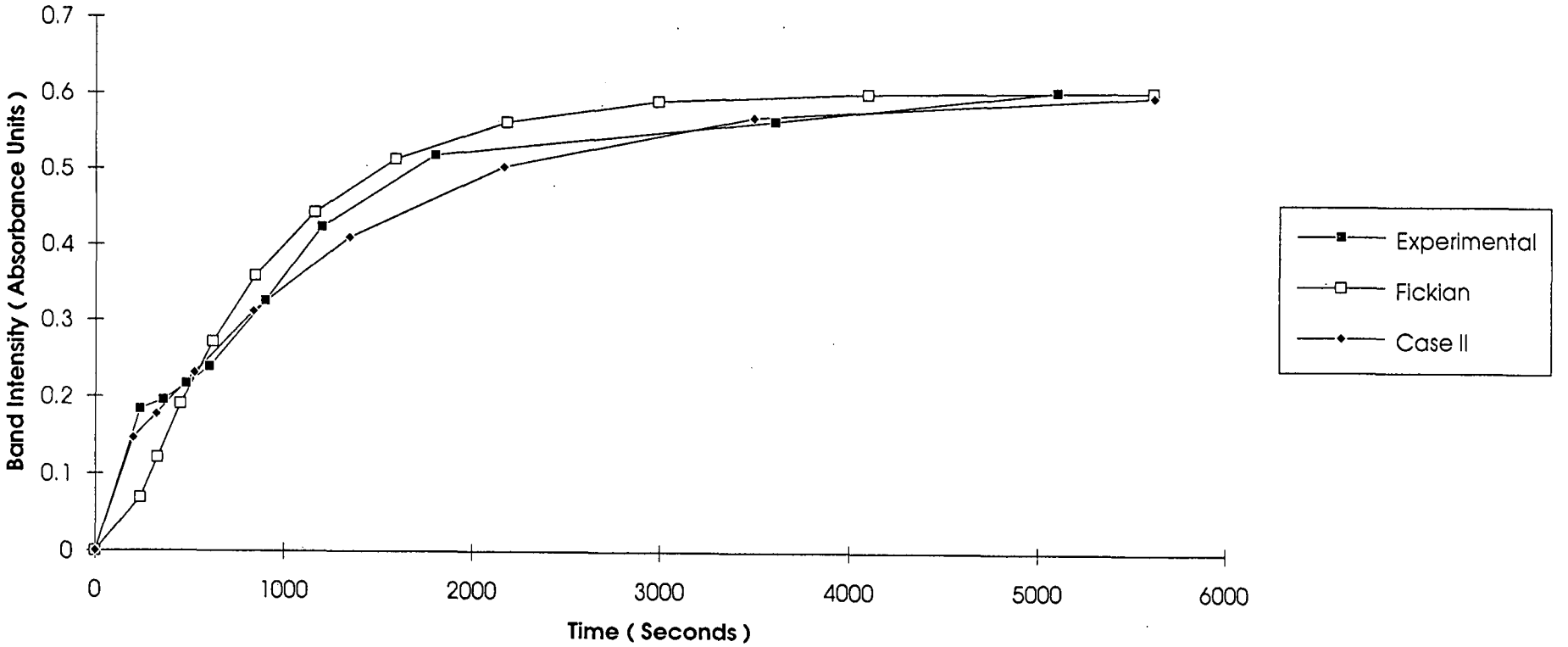

Figure 6.31 - HMDI Diffusion into 48 Hour Cured Epikote 1001

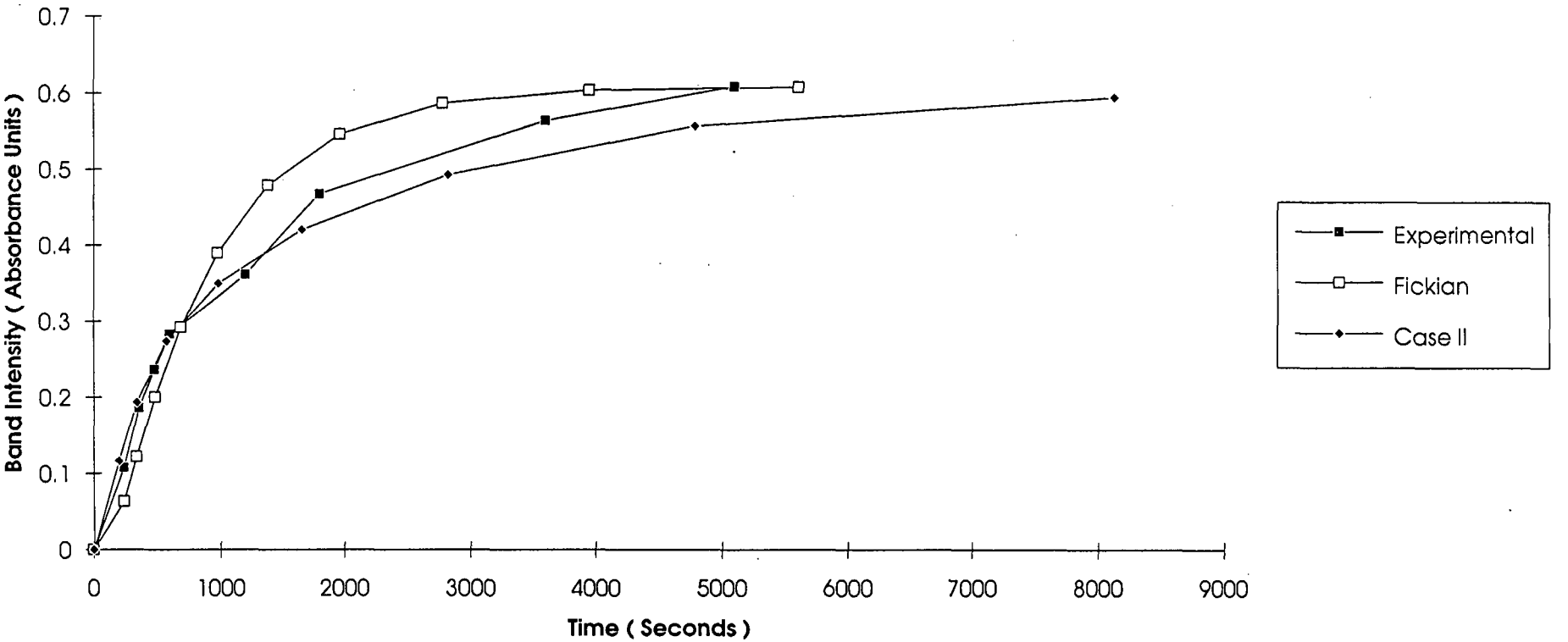

Figure 6.32 - 72 Hour Cured Film of Epikote[7] 1001 plus Monomeric Isocyanate.

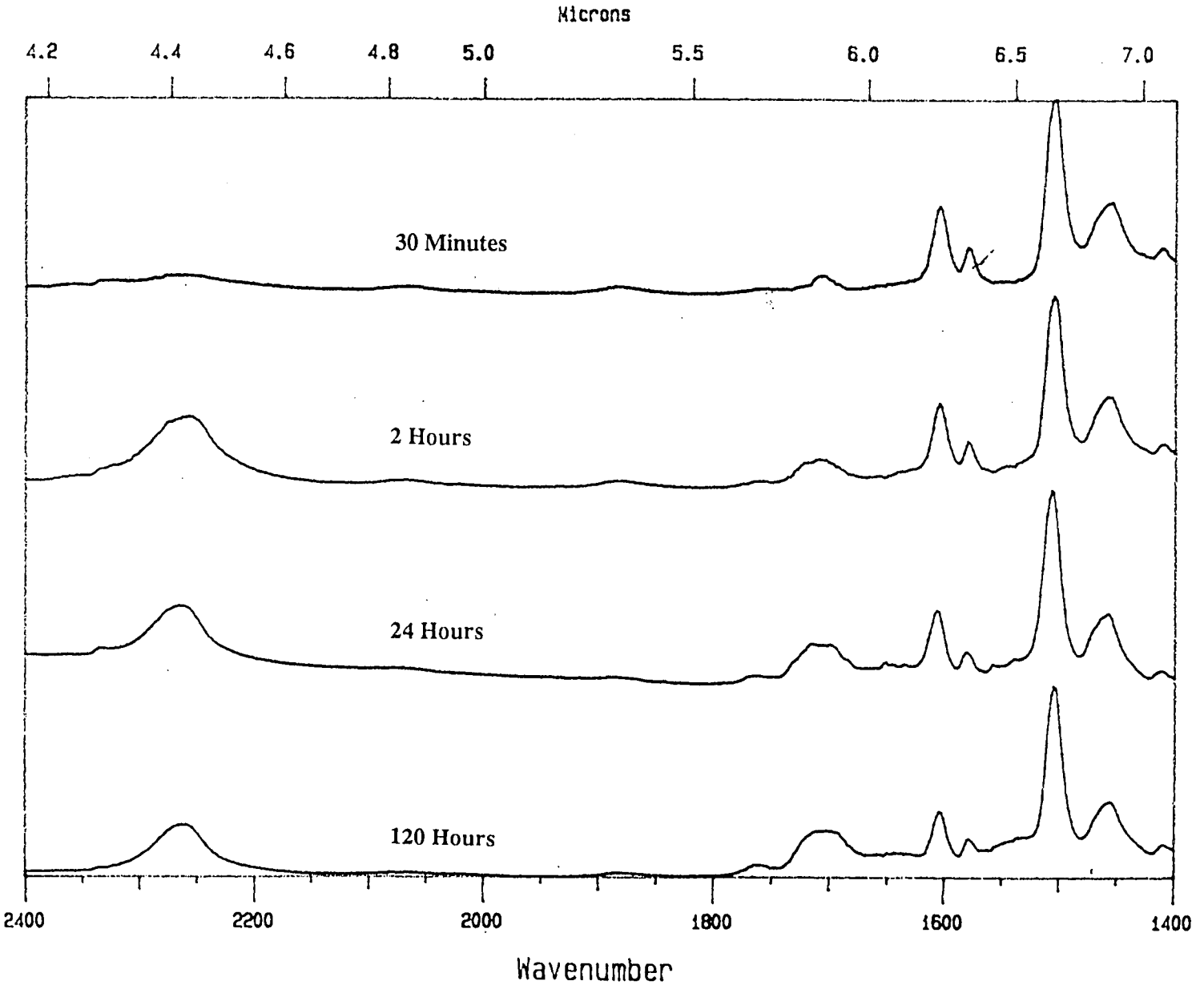

Figure 6.33 - HMDI Diffusion into 72 Hour Cured Epikote 1001

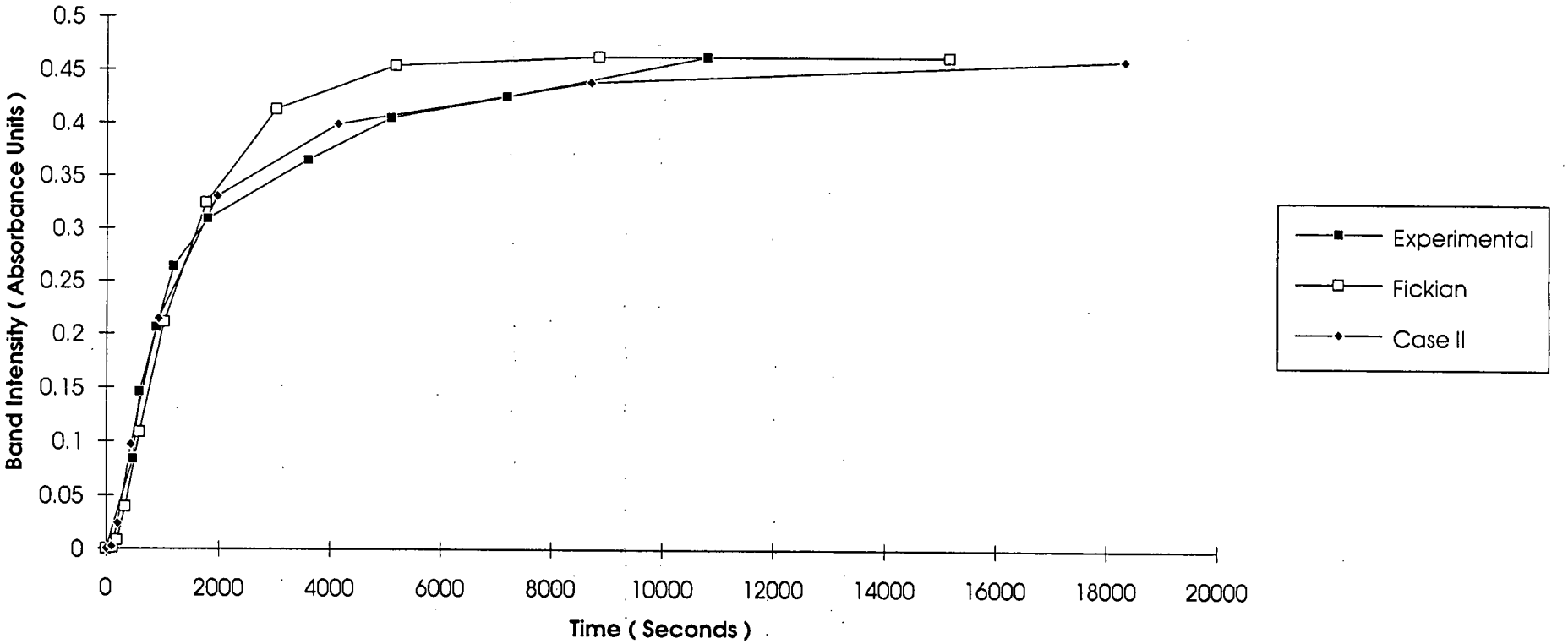

Table 6.5 - Diffusion Coefficients Obtained for 72 Hour Cured 1001

	Fickian	Case II		
Thickness (μ *m*)	D cm^2sec^{-1}	D_1 cm^2sec^{-1}	D_2 cm^2sec^{-1}	X_A
5.0±0.7	8.47×10^{-11}	1.18×10^{-10}	1.3×10^{-11}	0.8

2/. Epikote[7] 828.

Two sets of experiments were conducted using this resin, again at different cure times.

(i). 24 Hour Cure.

Three experiments were performed using this cure time, on films of thickness 2.4 μm ± 0.3 μm, 3.5 μm ± 0.6 μm and 5.0 μm ± 0.4 μm. Figure 6.34 shows some of the spectra obtained 15 minutes, 30 minutes, 1 hour and 2 hours after isocyanate application using the film of thickness 3.5 μm ± 0.6 μm, and Figure 6.35 shows the diffusion curve obtained from this experiment. The feature at approximately 1715 cm^{-1} is again believed due to MIBK contamination.

Figure 6.36 and 6.37 show the diffusion curves for the other two experiments.

The diffusion coefficients obtained for these experiments are given in Table 6.7.

Table 6.7 - Diffusion Coefficients Obtained from 24 Hour 828

	Fickian	Case II		
Thickness (μ *m*)	D cm^2sec^{-1}	D_1 cm^2sec^{-1}	D_2 cm^2sec^{-1}	X_A
2.4±0.3	3.28×10^{-9}	1.07×10^{-10}	5.51×10^{-12}	0.58
3.5±0.6	9.09×10^{-11}	8.65×10^{-11}	8.08×10^{-11}	0.99
5.0±0.4	7.08×10^{-11}	2.01×10^{-10}	7.92×10^{-12}	0.54

(ii). 48 Hour Cure.

Two experiments were conducted at this cure time, using a thickness of 5.4 μm ± 0.7 μm and 2.0 μm ± 0.4 μm. Figure 6.38 shows spectra resulting from the experiment performed over a total duration of 15 hours on the film of thickness 5.4 μm ± 0.7 μm, obtained 30 minutes, 5 hours, 10 hours and 15 hours after isocyanate application. Figure 6.39 shows the resulting diffusion curve for this experiment.

The resulting diffusion curve for the other experiment is shown in Figure 6.40.

The diffusion coefficients obtained are shown in Table 6.8.

Figure 6.34 - 24 Hour Cured Film of Epikote[7] 828 plus Monomeric Isocyanate.

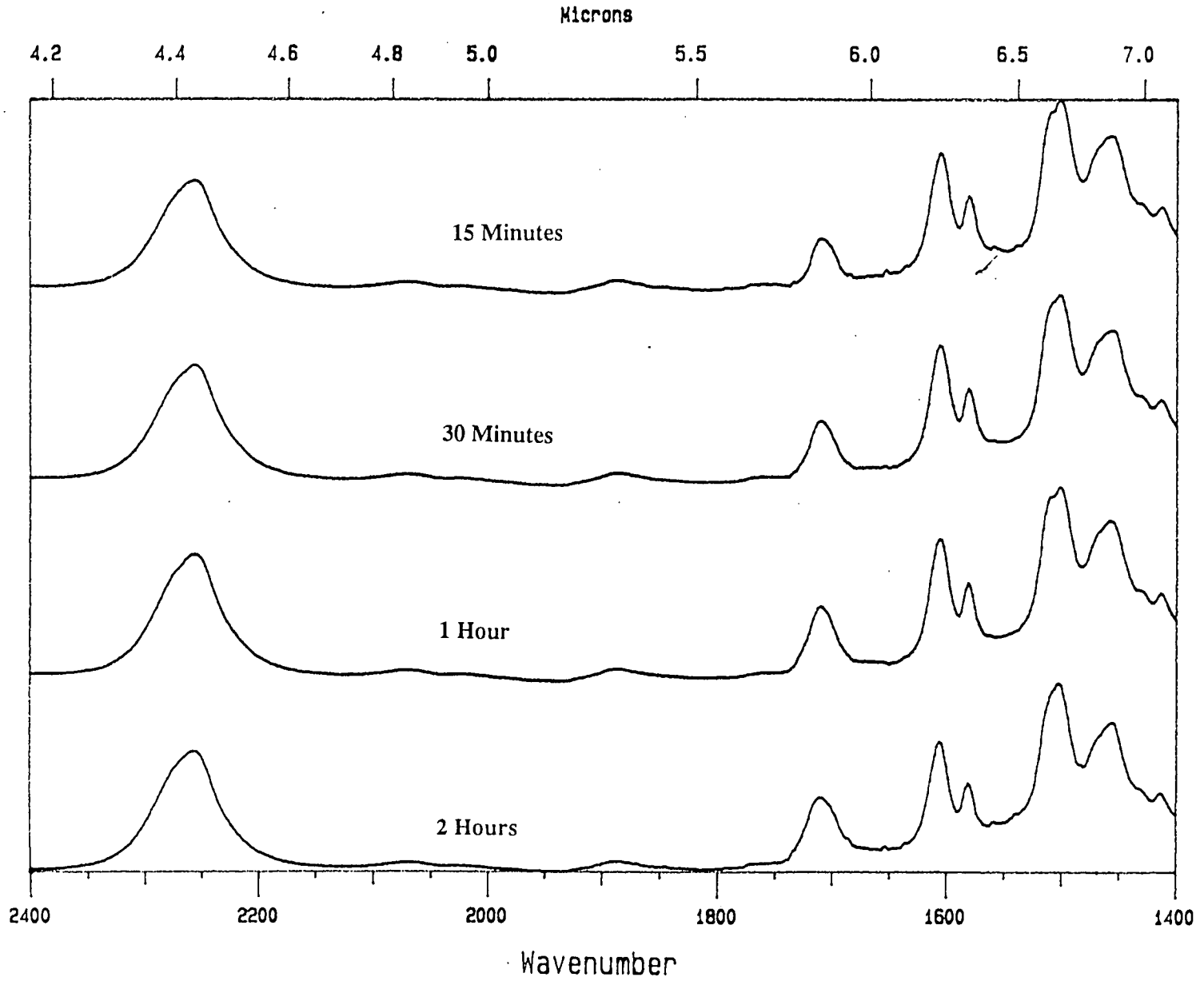

Figure 6.35 - HMDI Diffusion into 24 Hour Cured Epikote 828

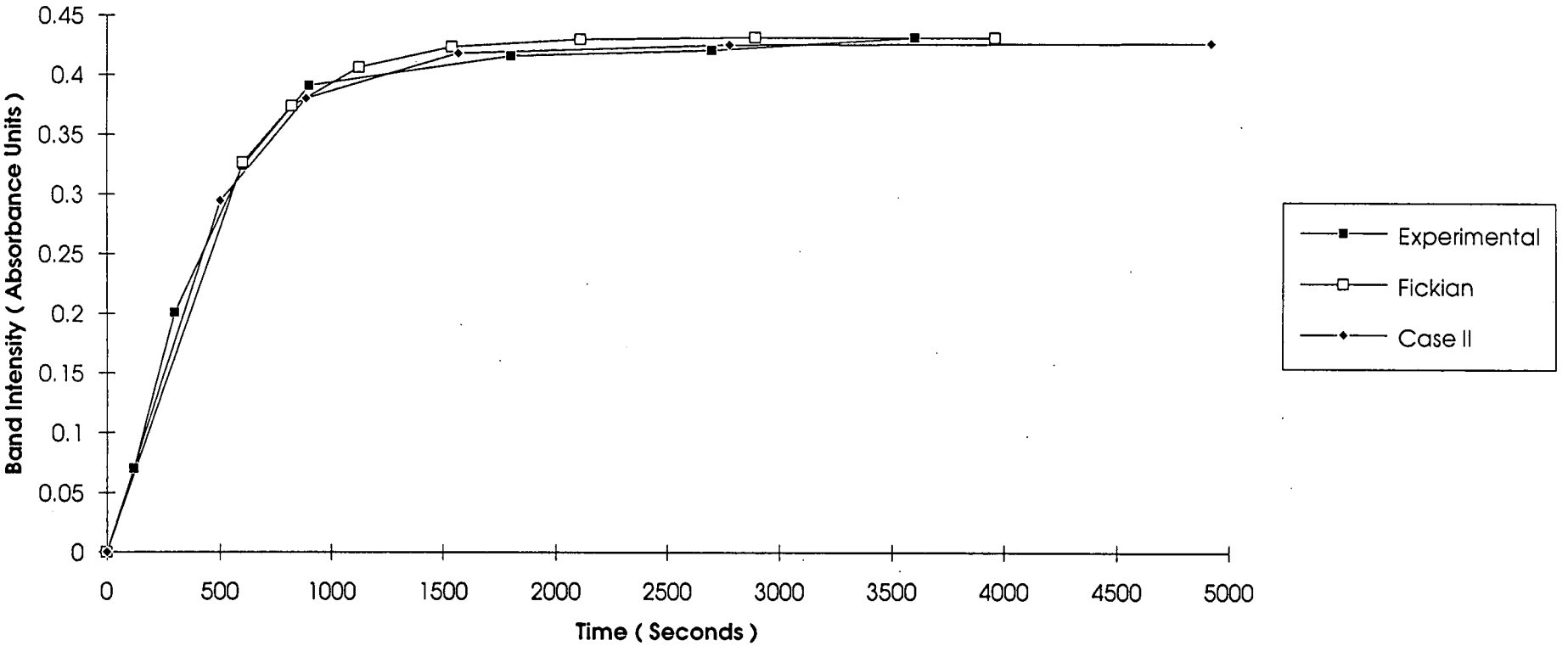

Figure 6.36 - HMDI Diffusion into 24 Hour Cured Epikote 828

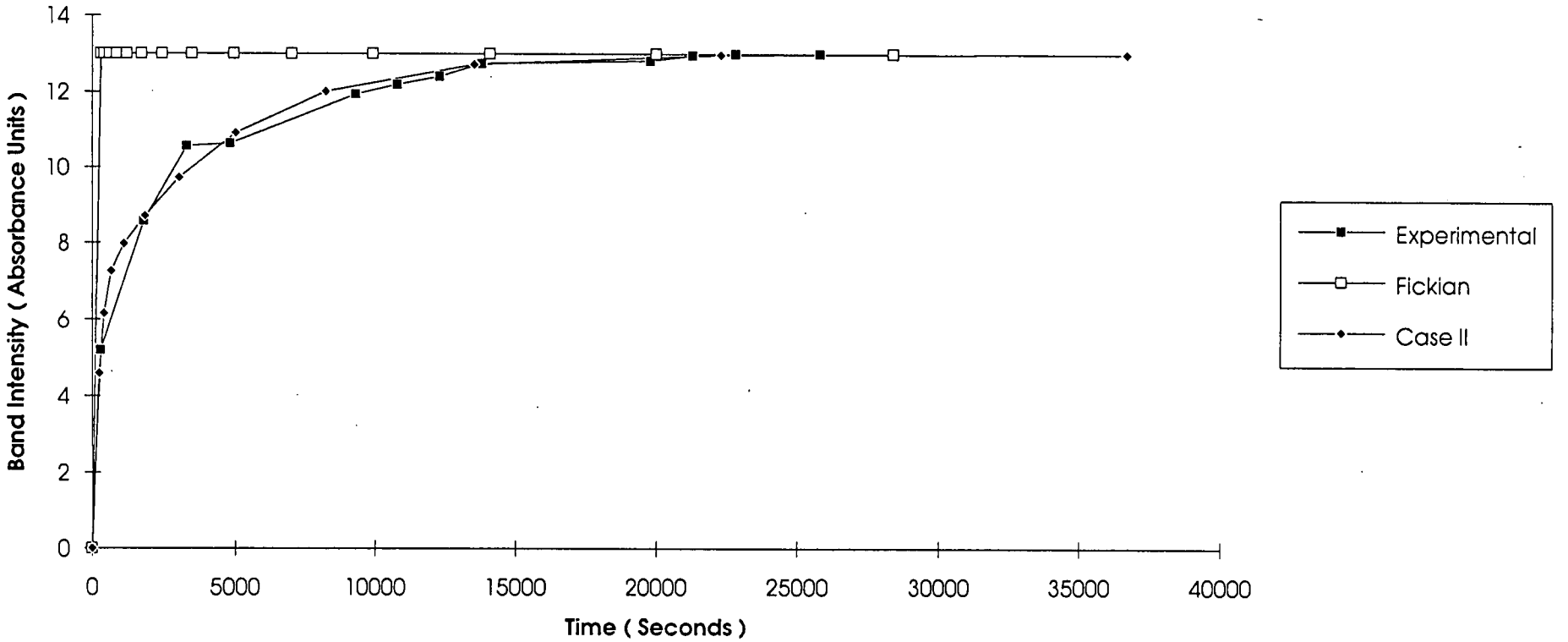

Figure 6.37 - HMDI Diffusion into 24 Hour Cured Epikote 828

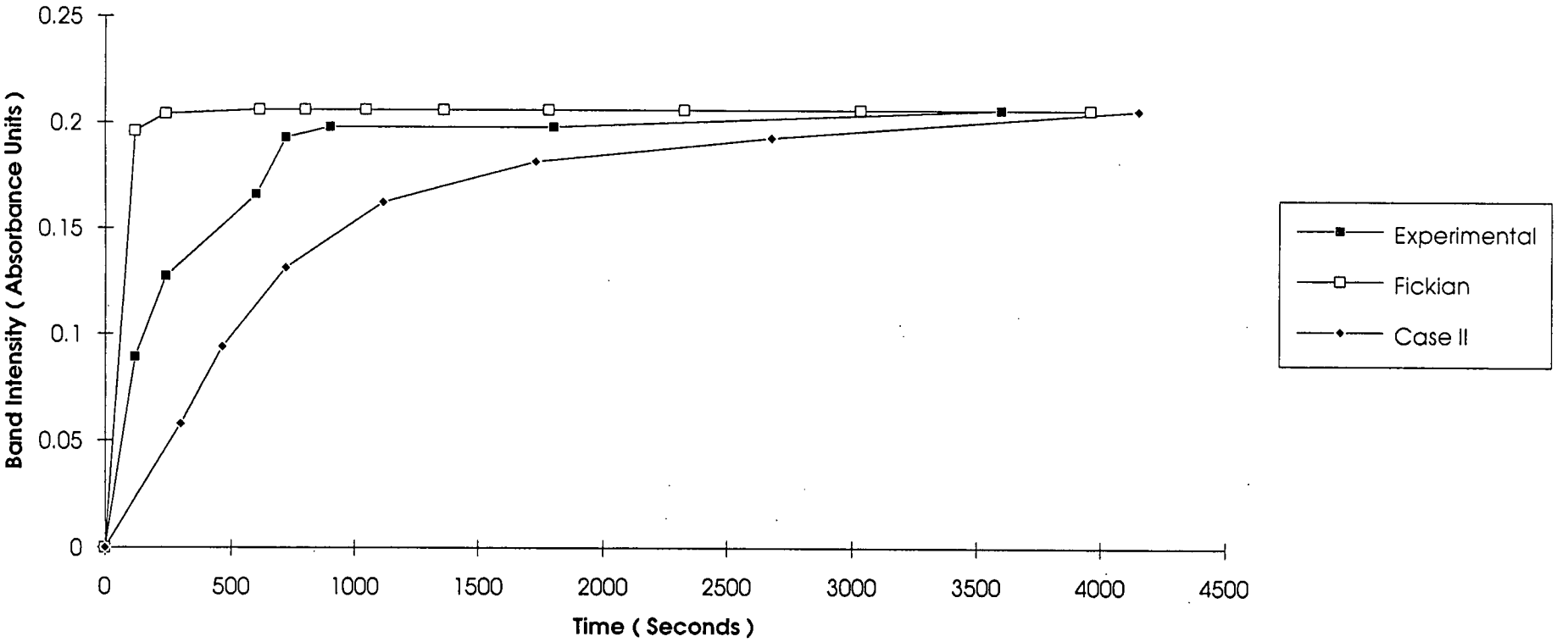

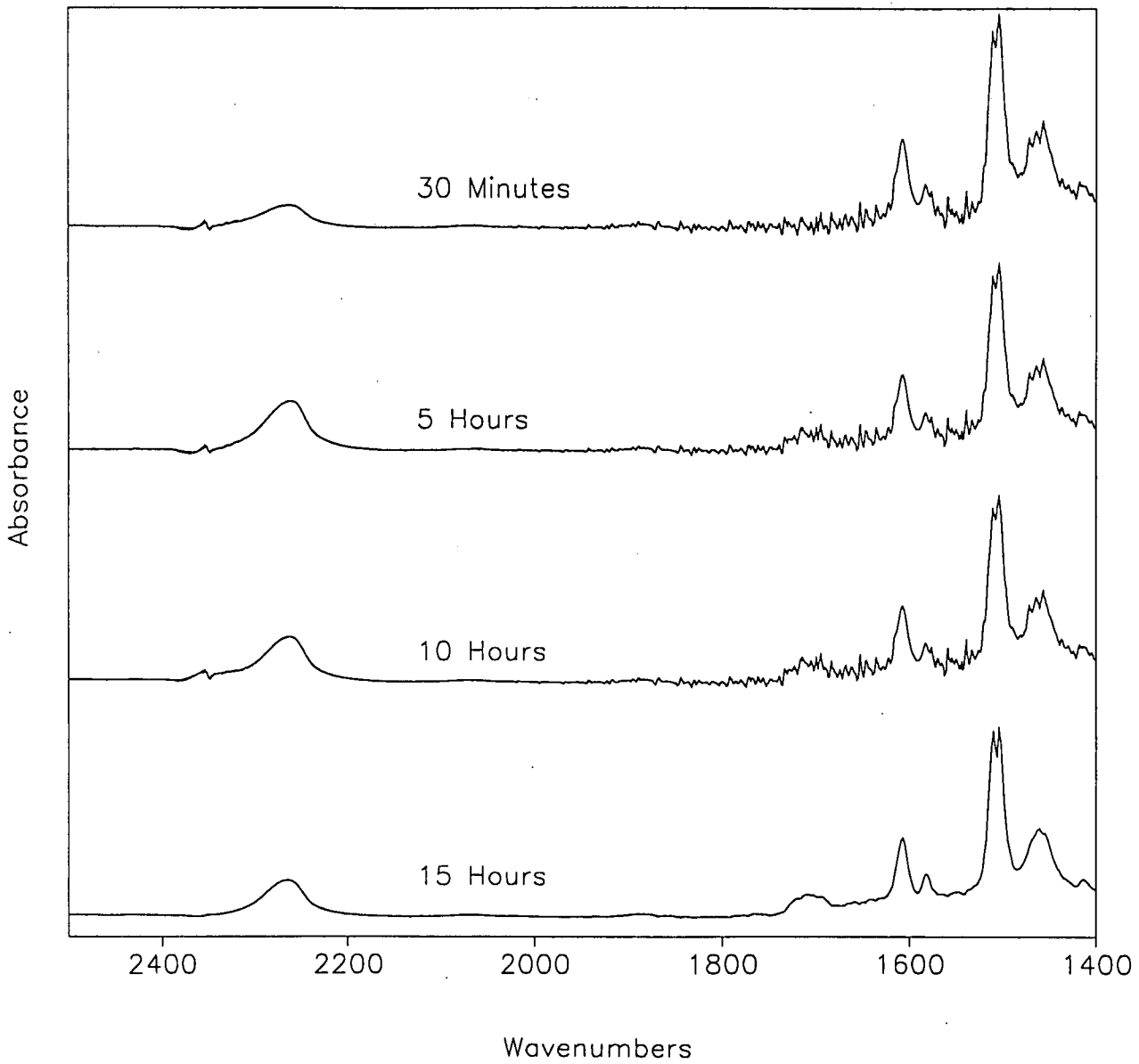

Figure 6.38 - 48 Hour Cured Film of Epikote[7] 828 plus Monomeric Isocyanate.

Figure 6.39 - HMDI Diffusion into 48 Hour Cured Epikote 828

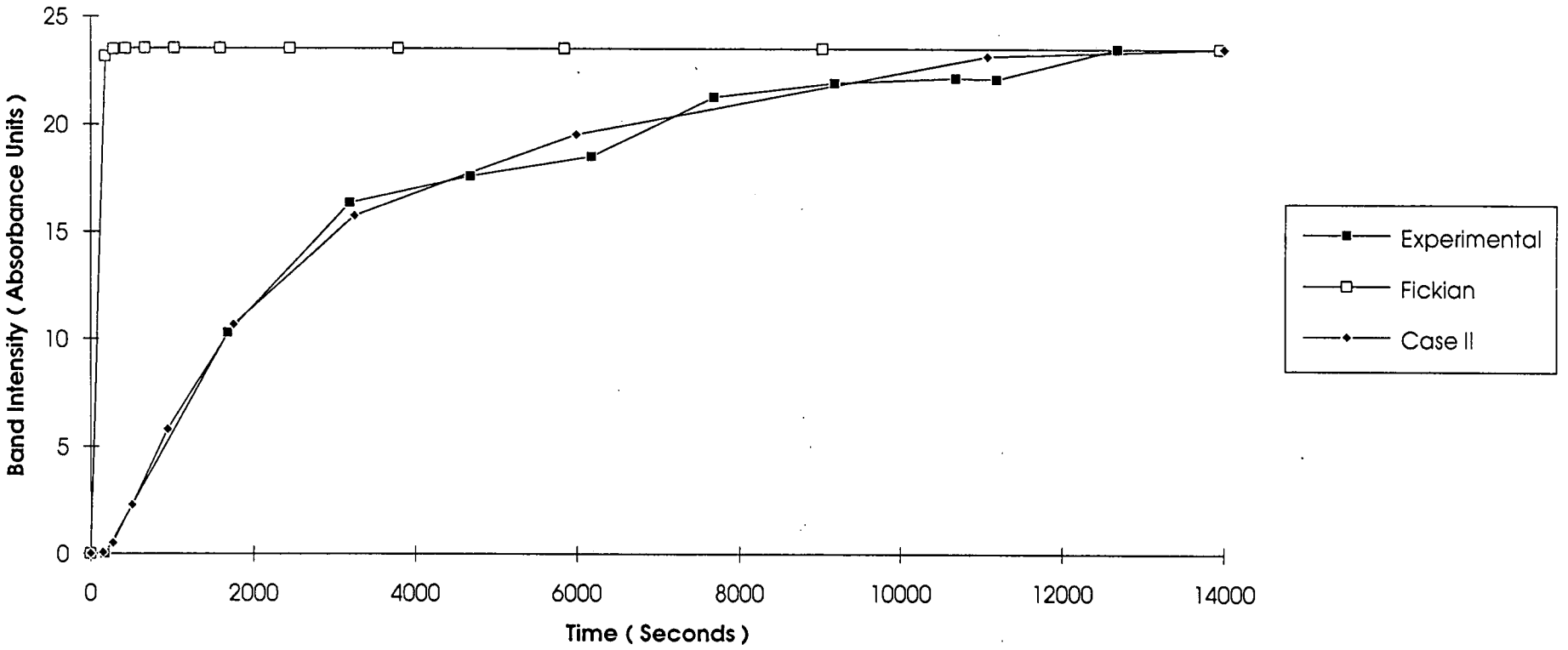

Figure 6.40 - HMDI Diffusion into 48 Hour Cured Epikote 828

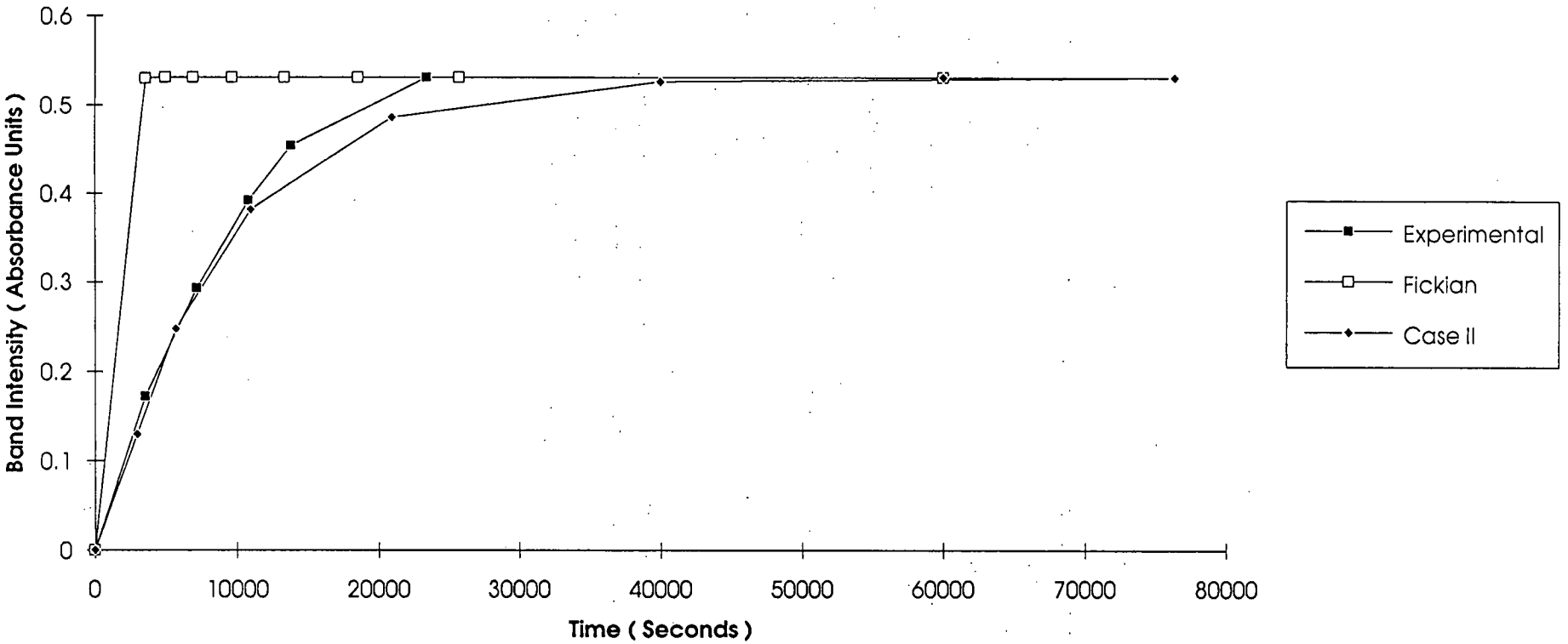

Table 6.8 - Diffusion Coefficients obtained from 48 hour old Epikote[7] 828

	Fickian	Case II		
Thickness (μ *m*)	*D* cm^2sec^{-1}	D_1 cm^2sec^{-1}	D_2 cm^2sec^{-1}	X_A
5.4±0.7	2.91×10^{-9}	8.90×10^{-11}	2.12×10^{-11}	0.63
2.0±0.4	1.99×10^{-10}	7.39×10^{-12}	1.94×10^{-12}	0.12

All the data presented in the above section will be discussed fully in Chapter 7.

6.3.2.3.2 - Kinetic Data.

1/. Introduction.

The calculation of reaction kinetics parameters from the spectral data produced from the FT-IR experiments encountered several major difficulties, associated with the complexity of the system under examination. In order to produce a sensible report, these problems are discussed fully here, rather than in Chapter 7, where their impact on the data produced is more readily appreciated. One important consequence of this reaction was that the reacted epoxy layer appeared to adhere much more firmly to the ATR crystal. Further experiments using a mild steel substrate also produced this effect, and the effect was noticed irrespective of epoxy resin used and cure time. This important observation, and its possible consequences, are discussed fully in Chapter 7.

During experiments described above, where an epoxy resin was treated with HMDI, a new spectral feature was observed at approximately 1715 cm^{-1}. As explained earlier in this section, this was attributed to some sort of reaction occurring within the film. There are two major reactions which are thought to occur within the epoxy film. Firstly, there is that involving the isocyanate and the hydroxyl groups (these are formed as a result of the crosslinking process of the epoxy resin with an amine - see Chapter 1, page 5). This reaction is already described above, but is reproduced here for convenience.

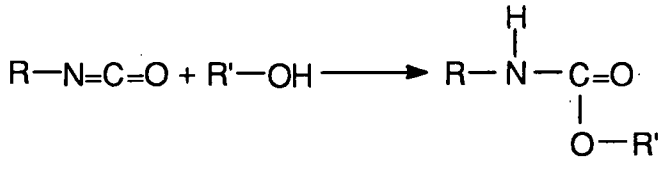

Urethane

In the infrared spectrum[31] of a urethane, the carbonyl absorption responsible for the amide I band is seen in the 1730-1720 cm^{-1} range for primary urethanes[34] in dilute solutions in chloroform, but at rather higher frequencies in carbon tetrachloride. A wide frequency distribution is observed on passing through secondary to tertiary systems[32-36], with a range between 1705-1739 cm^{-1}, depending on solvent and whether the system is aryl or alkyl.

The second major reaction thought to occur in epoxy films, crosslinked with an amine, is the reaction between the residual amine groups, which results from incomplete usage of the available crosslinking agent. This is described in Reaction 2 above, but is reproduced for convenience.

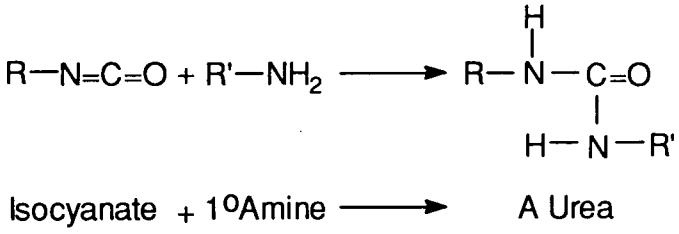

Infrared spectra[37-46] of ureas are reported to show three bands in the 1650-1500 cm^{-1} region for a monoalkyl system. These correspond to the carbonyl (amide I), NH and NH_2 bending modes (amide II). The carbonyl frequency is markedly lower than that found in a 'normal' amide, being in the 1605 cm^{-1} region, with the amide II NH_2 band at 1666-1655 cm^{-1}, and the NH amide II band at 1575 - 1550 cm^{-1}.

The most obvious band resulting from the reaction within the epoxy film, in the spectral data presented, is centred at approximately 1715 cm^{-1}. As the infrared data for a urea is concentrated at a lower frequency, it is reasonable to assume that this observed band must originate wholly from a urethane structure. However, the reaction to form a urea does occur. Figure 6.41 shows the data obtained from the experiment conducted on a 5.4μm film of 48 hour cured Epikote[7] 828. The three spectra shown are those of the pure epoxy film, the spectrum taken at the conclusion of the experiment (over 15 hours after the monomeric isocyanate was applied), plus the result of a spectral subtraction of the pure epoxy spectrum from the final spectrum.

It can be clearly seen from the subtraction that three bands are in evidence at approximately 1710, 1641 and 1541 cm^{-1}. The band at 1710 cm^{-1} is undoubtedly the urethane amide I carbonyl band, with the bands at 1641 and 1541 cm^{-1} being attributable to the NH_2 and NH amide II carbonyl bands, respectively. The amide I carbonyl band arising from the urea is not visible, due to the presence of a phenyl ring band, arising from the epoxy resin, which is located at approximately 1605 cm^{-1}. This will effectively obliterate any trace of the urea band, and will also mean that evidence for this urea band will be subtracted out with the epoxy resin.

This introduces an immediate dilemma, when attempting a kinetic analysis of this data, namely that the isocyanate is being consumed in two processes, one to form the urethane and one to form the urea. Where two reactions are competing for the same reactant, kinetic data produced cannot be a true reflection of either of the actual processes. Hence, any kinetic information available from the obtained spectra for the appearance of both urea and urethane entities, plus the consumption of the isocyanate, will be somewhat inaccurate.

Furthermore, the presence of water vapour in the spectral region around 1700 cm^{-1} also makes quantitative measurement of the intensity of the urethane band very difficult. Various methods were employed to minimise the interference, such as subtraction of both pure water vapour and the early spectra from the same experiment,

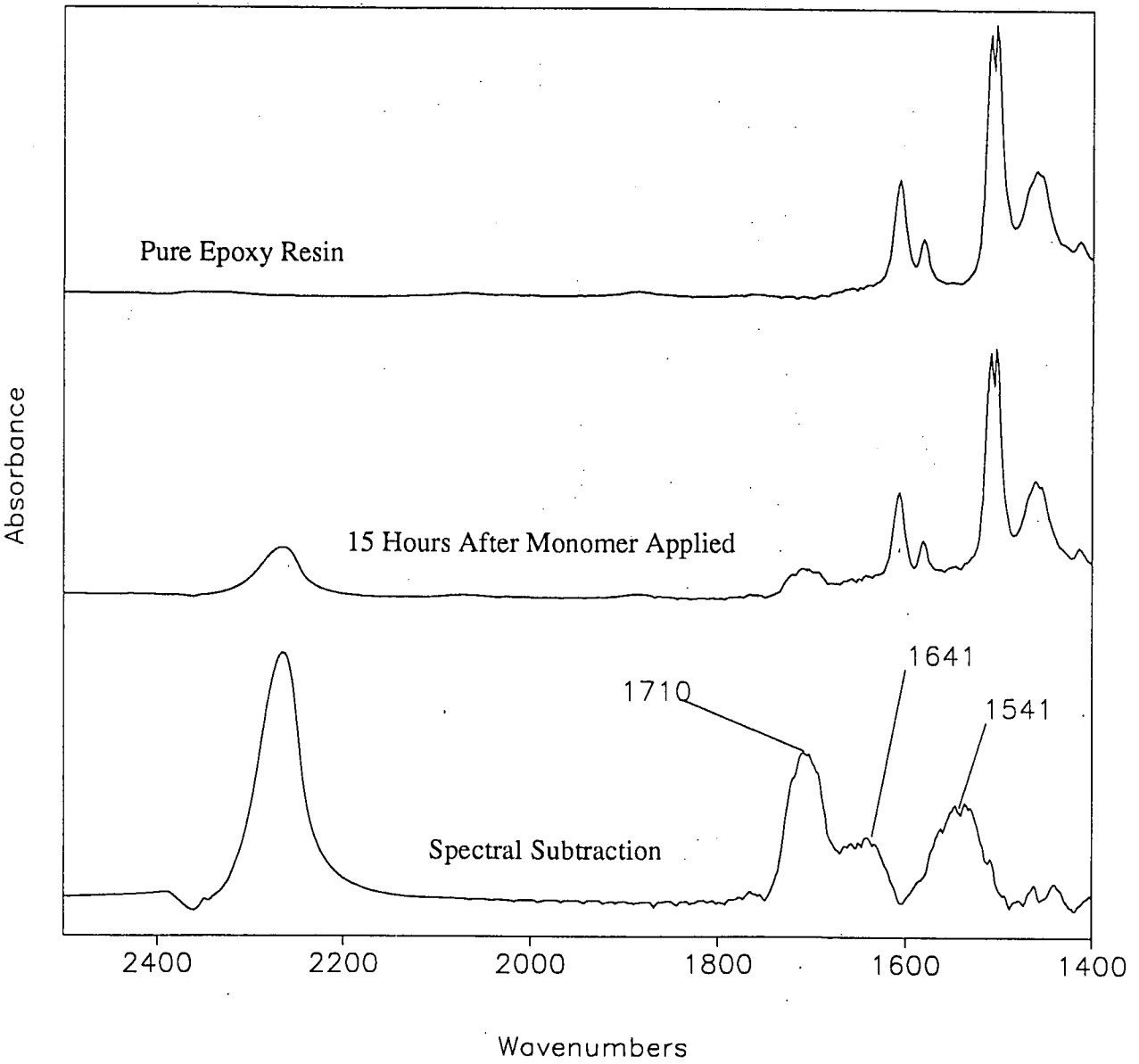

Figure 6.41 - 48 Hour Cured Film of Epikote[7] 828 plus Monomeric Isocyanate.

and ratioing against spectra obtained early in the experiment, but none produced data of quantitative potential. In addition, the data produced for the urea bands, following subtraction out of the epoxy bands, was completely meaningless.

It is not possible, to the best of my knowledge, to completely overcome these problems. With the added complexities of water vapour interference and subtraction difficulties, the data produced from the spectral intensity of the urethane and urea bands were not considered further.

Finally, it is also not possible to observe the disappearance of the hydroxyl group, associated with the crosslinked resin, as the OH region of the infrared spectrum (3200 - 3500 cm^{-1}) is also obscured by the broad vibrational mode of the water vapour. A further water-related problem is also introduced here, in that the MCT detectors used for this investigation have to be cooled with liquid nitrogen. Hence, there is an ongoing problem of the detector icing as atmospheric water vapour freezes.

Thus, consideration of the kinetics of this reaction is restricted to a limited quantitative examination of the decrease in the intensity of the isocyanate band seen at approximately 2260 cm^{-1}. As discussed above, the fact that this reacts in two ways within the film means that the true significance of this evaluation is unclear. However, as it is believed that this is the first time that this reaction has been studied by such methods, it is surely a worthwhile exercise, if only to provide an tentative indicator to future workers.

2/. Kinetic Theoretical Considerations.

A simple rate law, describing the consumption of the isocyanate occurring here, with respect to time, may be written thus:-

$$-d[NCO]/dt = k[NCO]^x[Epoxy]^y \qquad (1)$$

where x and y describe the order of the reaction with respect to isocyanate and epoxy resin concentrations. It has already been discussed above that we were not able to measure the kinetics of the epoxy band decrease, or the urethane band increase. Hence the remainder of this section will concentrate on the kinetics of the consumption of the isocyanate band.

The first order rate law, for the disappearance of the isocyanate, can be expressed thus.

$$-d[NCO]/dt = k[NCO]^x \qquad (2)$$

which may be rearranged to give:-

$$\ln\left([NCO]_t/[NCO]_0\right) = -kt \qquad (3)$$

Thus, if ln $[NCO]_t/[NCO]_0$ is plotted against time, then a first order reaction will give a straight line, the gradient of which will produce a value for -k, with respect to the isocyanate band consumption.

3/. Experimental Data.

The data used in this tentative evaluation is that data obtained on the Mattson Sirius instrument at Durham University, using the Macro package, developed by Simon Nunn[29]. This data was accumulated at half-hourly intervals over a long period of time, and thus data was available which referred to the decrease in the intensity of the isocyanate band, which occurred later on in the process.

For the purposes of this evaluation, $[NCO]_0$ was assumed to be the intensity of the isocyanate band immediately before the slope turned downwards, thus indicating that the reaction had begun. Clearly, this is not totally accurate, as the spectra show a plateau region, where the continuing diffusion of the isocyanate into the film and the rate of the reaction effectively cancel each other out, and hence the band intensity remains constant. It is thus appreciated that the real value of $[NCO]_0$ would be at some earlier point, but for the purposes of tentative evaluation, presented here, this problem is not considered. However, this is a further example of the complexity of this system.

The data produced from Durham was evaluated using a first order rate law, and Figure 6.42 shows the resulting graph of this data obtained for 24 hour cured Epikote[7] 828. It can be seen that this data appears to fit a first order rate law fairly precisely. Thus, the remaining data was also evaluated using the first order rate law. Figures 6.43, 6.44 and 6.45 show the resulting graphs of the data obtained from 48 hour cured Epikote[7] 1001, 24 hour cured Epikote[7] 1001 and 48 hour cured Epikote[7] 828, respectively.

Table 9 gives a summary of the values of the first order rate constant, k, evaluated from these graphs.

Table 9 - Summary of Rate Constant Data

Resin	*Cure Time*	*Rate Constant (sec^{-1})*
Epikote[7] 828	24 Hours	1.31×10^{-5}
Epikote[7] 828	48 Hours	1.82×10^{-5}
Epikote[7] 1001	24 Hours	2.11×10^{-5}
Epikote[7] 1001	48 Hours	1.25×10^{-5}

Thus it appears that we can write a modified rate law for the consumption of the isocyanate:-

$$-d[NCO]/dt = k[NCO]^1 \qquad (4)$$

where $k = 1.62 \times 10^{-5} \pm 0.43 \times 10^{-5}$ sec^{-1}.

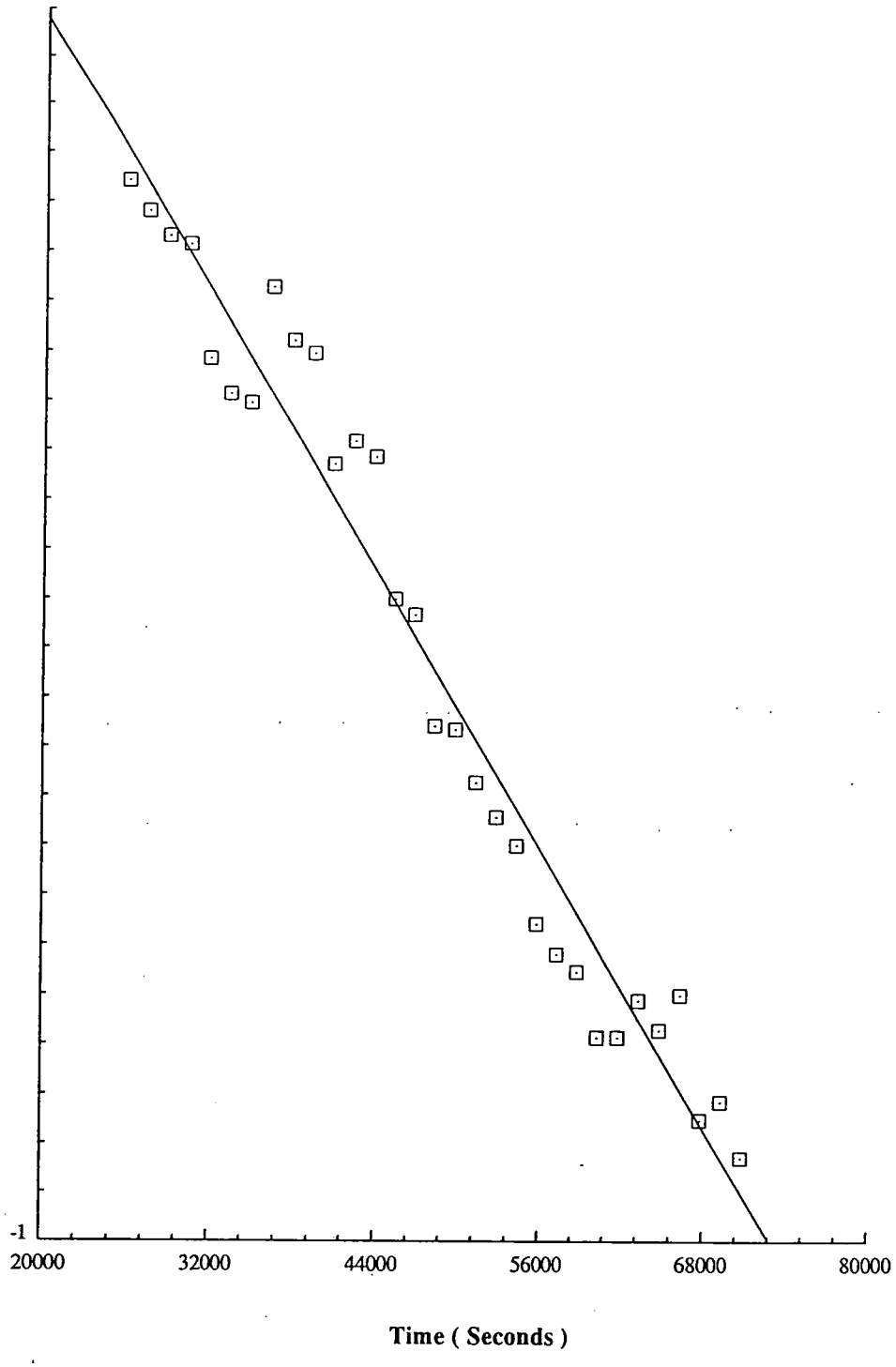

Figure 6.42 - First Order Plot of HMDI Reaction With 24 Hour Cured Epikote 1001

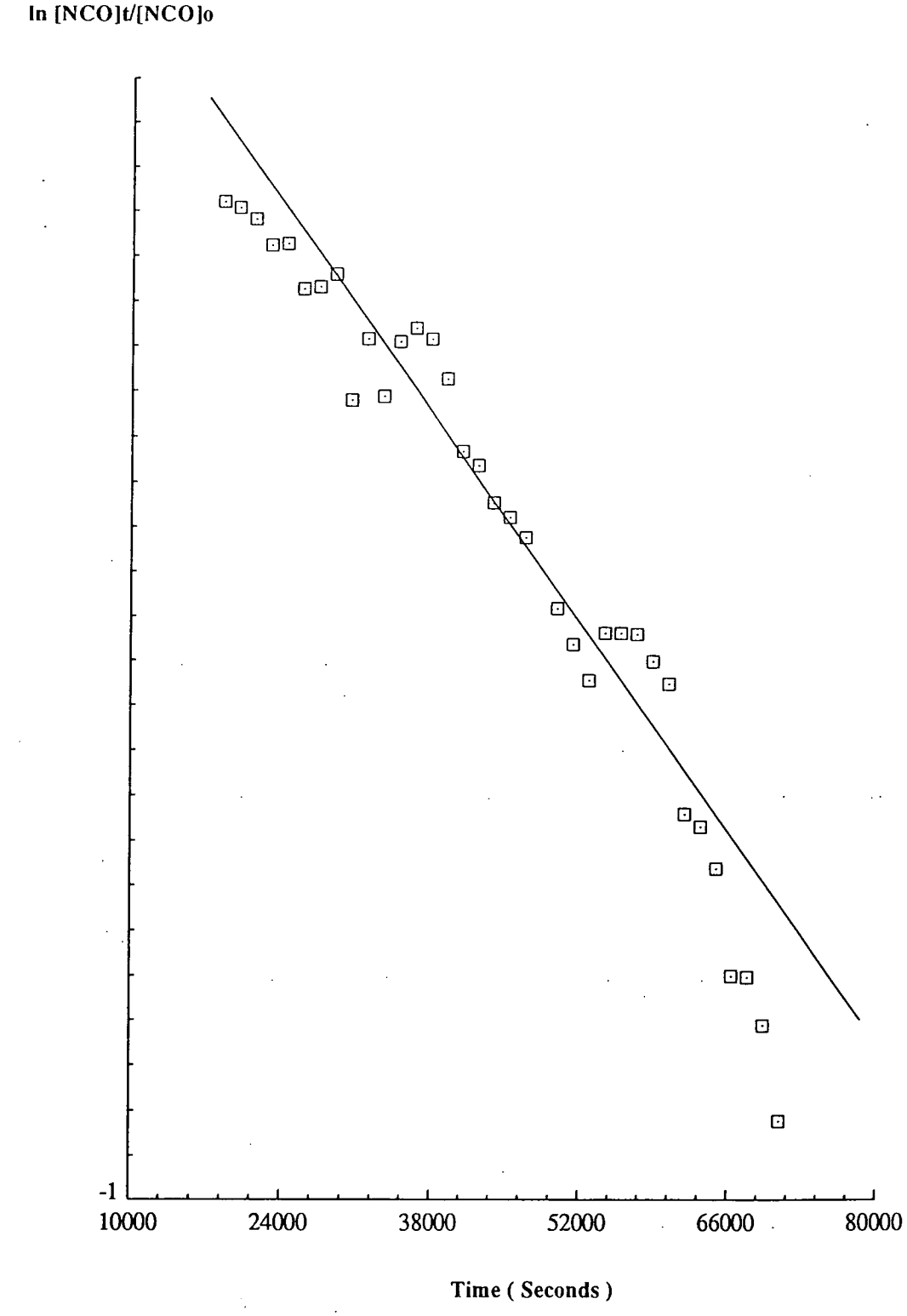

Figure 6.43 - First Order Plot of HMDI Reaction

With 48 Hour Cured Epikote 1001

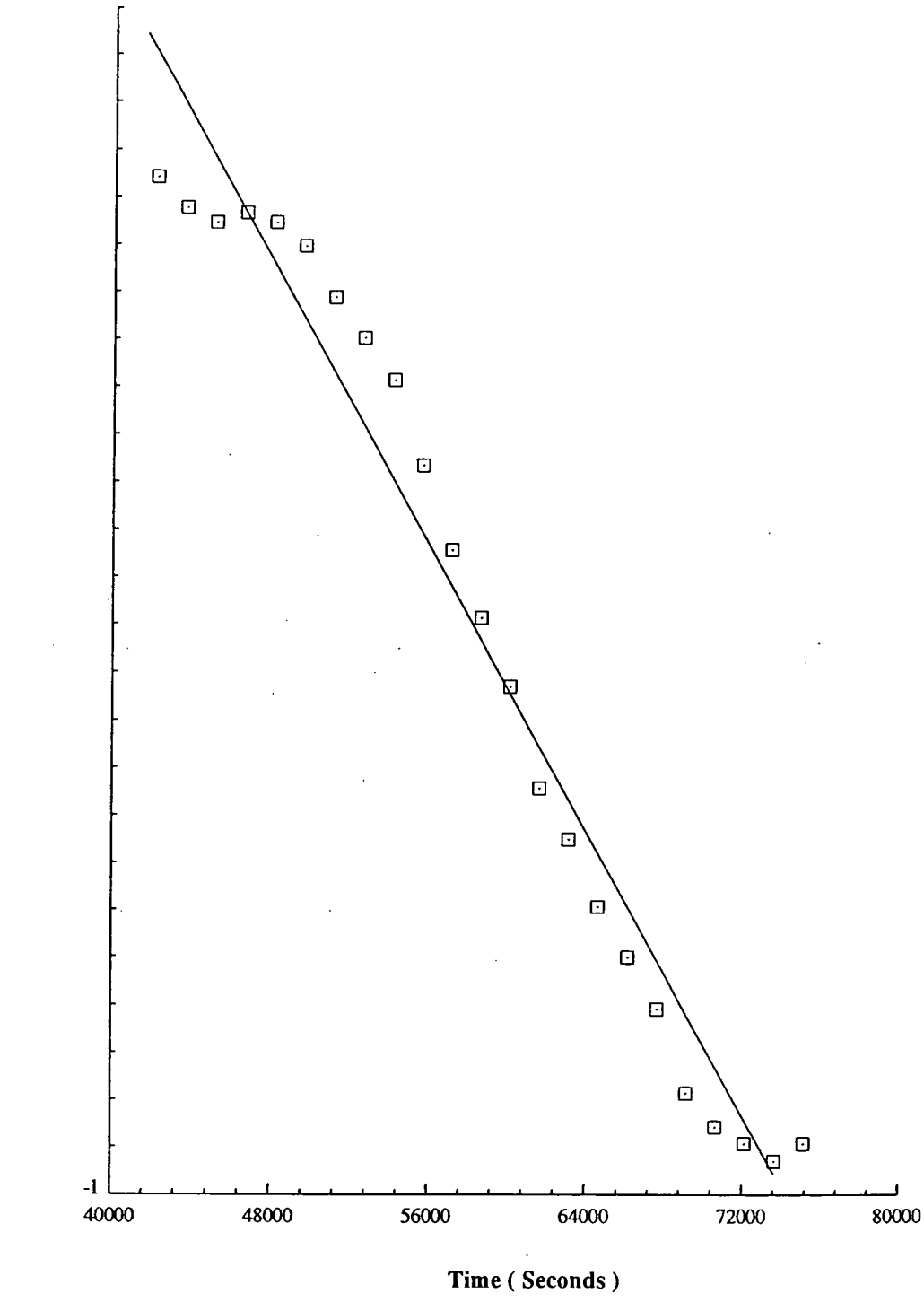

Figure 6.44 - First order Plot of HMDI Reaction

With 24 Hour Cured Epikote 828

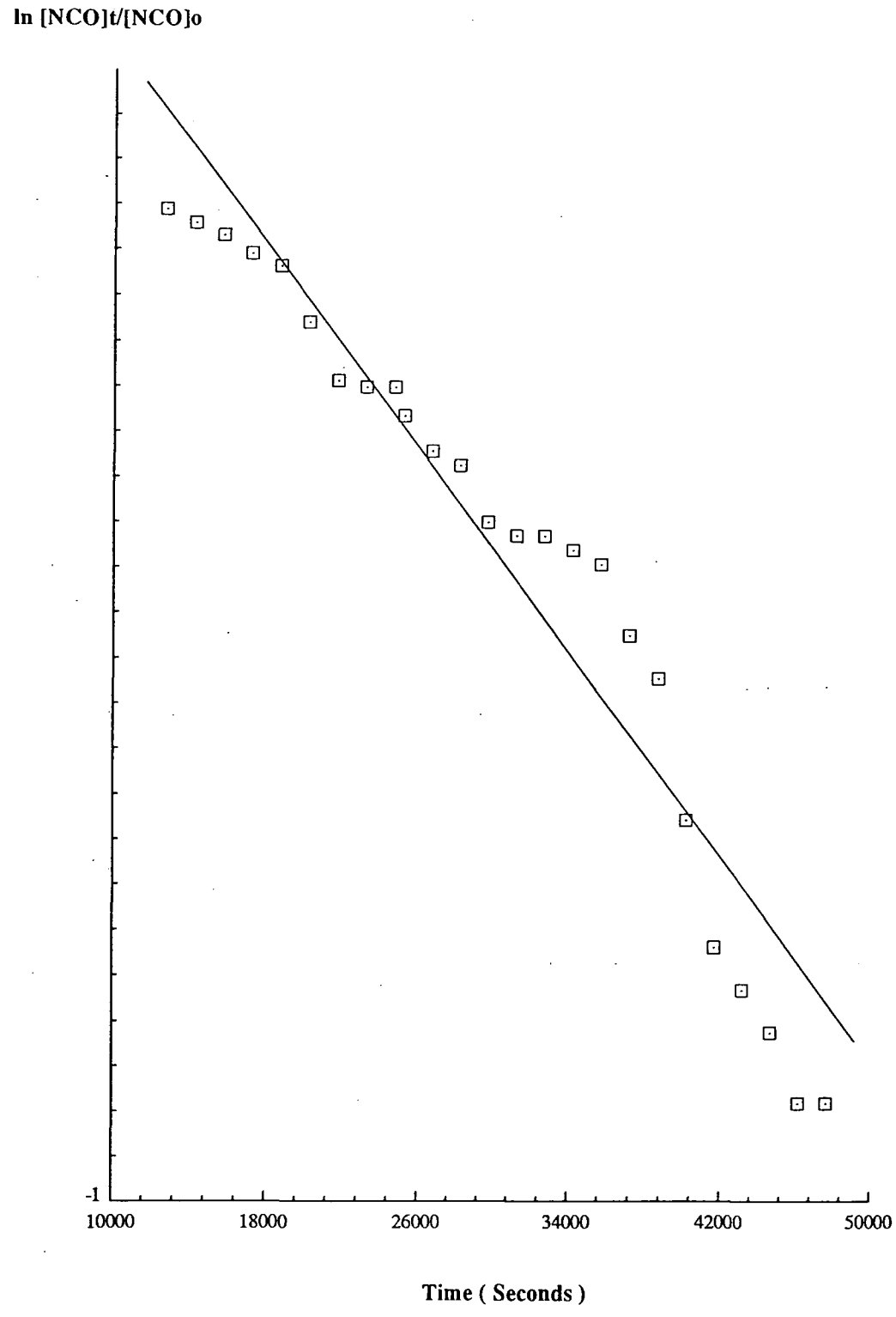

Figure 6.45 - First Order Plot of HMDI Reaction

With 48 Hour Cured Epikote 828

6.4 - Concluding Comments.

The above chapter provides an indication of the power of evanescent wave (ATR) spectroscopy, in that different chemical processes occurring in the same system can be evaluated in situ using a single technique. The main aim of this side of the project, to observe interfacial interactions, has, in the barrier film work, been achieved, and the scope for future such experiments has been clearly demonstrated. In addition to this, however, the diffusion of isocyanates in epoxy resins has been studied, it is believed for the first time by FT-IR ATR spectroscopy, and both this process mechanism plus the consequences of the diffusion have, I believe, far reaching possibilities for Courtaulds.

References.

1/. M.H.Greenhall, Ph.D. thesis, University of Durham, 1992.
2/. F.M.Mirabella, J.Polym.Sci., Polym.Phys.Ed., 21, (1983), 2403.
3/. C.S.P.Sung & C.B.Hu, Adv.Chem.Ser. (Multiphase Polym.), 176, (1979), 69.
4/. C.S.P.Sung, C.B.Hu & E.W.Merrill, A.C.S.Div.Polym.Chem., Polym.Prepr,.19, 1, (1978), 20.
5/. C.S.P.Sung, C.B.Hu, E.W.Merrill & E.W.Saltzman, J.Biomed.Mater.Res., 12, (1978), 791.
6/. C.B.Hu & C.S.P.Sung, A.C.S. Div. Polym. Chem., Polym. Prepr., 21, 1 (1980), 156.
7/. Shell brand-name.
8/. Dr.G.Davies (Courtaulds Coatings), Private Communication.
9/. Y.Diamant, G.Marom & L.J.Broutman, J.App.Polym.Sci., 26, 9, (1981), 3015.
10/. T.C.Wong & L.J.Broutman, Plastics Engineering, 39, 3 (1983), 52.
11/. T.S.Ellis & F.E.Karasz, Abs.Paps.Am.Chem.Soc., 185, Mar, (1983), 154.
12/. M.T.Aronhime, J.K.Gillhan & R.D.Small, Abs.Paps.Am.Chem.Soc., 186, Aug, (1983), 127.
13/. M.A.Grayson & C.J.Wolf, Abs.Paps.Am.Chem.Soc., 187, Apr, (1984), 34.
14/. J.A.Barrie, P.S.Sagoo & P.Johncock, J.Memb.Sci., 18, Mar, (1984), 197.
15/. T.C.Wong & L.J.Broutman, Polym.Eng.& Sci., 25, 9, (1985), 529.
16/. J.A.Barrie, P.S.Sagoo & P.Johncock, Polymer, 26, Aug, (1985), 1167.
17/. T.C.Wong & L.J.Broutman, Polym.Eng & Sci., 25, 9, (1985), 521.
18/. A.Tson & N.A.Peppas, Abs.Paps.Am.Chem.Soc., 195, June, (1988), 212.
19/. M.C.Lee & N.A.Peppas, Abs.Paps.Am.Chem.Soc., 199, Apr, (1990), 54.
20/. T.K.Kwei & H.M.Zupko, J.Polym.Sci., Part A-2, 7, (1969), 867.
21/. H.L.Firsch, J.Polym.Sci., Part A-2, 7, (1969), 879.
22/. J.J.Sahlin & N.A.Peppas, Ind. & Eng.Chem.Res., 30, 1, (1991), 211.
23/. P.Kalenda, J.App.Polym.Sci., 45, 12, (1992), 2235.
24/. M.R.Pierra, University of Durham, 1992.
25/. Y.Taguchi, I.Shibuya, M.Yasumoto, T.Tsuchiya & K.Yoremoto, Bull.Chem.Soc.Jap., 63, 12, (1990), 3486.
26/. C.N.Banwell, "Fundamentals of Molecular Spectroscopy", McGraw-Hill: London, (1983).
27/. P.R.Griffiths, "Transform Techniques in Chemistry", Plenum, New York, (1978).
28/. J.Michael Hollas, "Modern Spectroscopy", 2nd Edition, Wiley & Sons, (1992).
29/. N.S.Nunn, University of Durham, 1992.
30/. Dr.G.Davies (Courtaulds Coatings), Private Communication.
31/. L.J.Bellamy, "The Infrared Spectra of Complex Molecules", Volume 1, (3rd Edition), Chapman and Hall, London (1975), Chapter 12, pp. 248 & 249.
32/. J.Renema, Ph.D. Thesis, University of Utrecht, 1972.
33/. R.A.Nyquist, Spectrochim. Acta., 19, (1963), 509.
34/. S.Pinchas & D.Ben-Ishai, J.Am.Chem.Soc., 79, (1957), 4099.
35/. A.R.Katritzky & R.A.Jones, J.Chem.Soc., (1960), 676.
36/. M.Sato, J.Org.Chem, 26, (1961), 770.
37/. L.J.Bellamy, "The Infrared Spectra of Complex Molecules", Volume 1, (3rd Edition), Chapman and Hall, London (1975), Chapter 12, p. 250.

38/. H.M.Randall, R.G.Fowler, N.Fuson & J.R.Dangl, "Infrared Determination of Organic Structures", Van Nostrand, 1149.
39/. H.W.Thompson, D.L.Nicholson & L.N.Short, Discuss.Faraday Soc., 9, (1950), 222.
40/. H.J.Becher & J.Griffel, Naturweiss, 43, (1956), 467.
41/. H.J.Becher, Chem.Ber., 89, (1956), 1593.
42/. J.L.Boivan & P.A.Boivan, Can.J.Chem., 32, (1954), 561.
43/. P.A.Boivan, W.Bridgeo & J.L.Boivan, Can.J.Chem., 32, (1954), 242.
44/. C.I.Jose, Spectrochim. Acta, 25A, (1969), 111.
45/. Y.Mido, Spectrochim.Acta, 28A, (1972), 1508.
46/. D.F.Kutepov & S.S.Dubov, J.Gen.Chem.(Moscow), 30, 92, (1960), 3448.
47/. Cray Valley Chemicals, Private Communication.
48/. R.E.Smith, F.N.Larson & C.L.Long, J.App.Polym.Sci., 29, 12, (1984), 3713.
49/. P.A.Sanderson & R.O.Allen, Abs. Paps. Am. Chem. Soc., 193, Apr, (1987), 186
50/. T.Nguyen, W.E.Byrd & D.P.Bentz, Abs. Paps. Am. Chem. Soc., 196, Sept, (1988), 97.
51/. R.O.Allen & P.A.Sanderson, App. Spectrosc. Revs., 24, 3-4, (1988), 175.
52/. R.O.Allen, R.Miller, P.A.Sanderson & E.Bartick, Abs. Paps. Am. Chem. Soc., 200, Aug, (1990), 19.
53/. F.Gaillard, A.Bonnard & H.Hocquaux, Surf. and Int. Anal., 17, 7, (1991), 537.
54/. U.Meyer, R.Salzer & J.Radditz, Makromolekulare Chemie-Macromolecular Symposia, 52, Dec, (1991), 261.
55/. C.J.Debakker, N.A.StJohn, G.A.George, Abs. Paps. Am. Chem. Soc., 203, Apr, (1992), 175.
56/. M.Abbate, E.Martuscelli, P.Musto, G.Ragosta & G.Scarinzi, J.Polm.Sci, Part B - Polym. Phys., 32, 3, (1994), 395.
57/. J.F.Sprouse & B.N.Halpin Jnr., Army Materials and Mechanics Research Centre, Watertown, Massachusetts, U7917, Ref. No. AMMRC-TR-78-45, Nov. 1978.
58/. E.Merzel & J.L.Koenig, Adv.Polym.Sci., 75, (1986), 73.

Chapter Seven - Discussion of Results and Conclusions

Chapter Seven - Discussion of Results and Conclusions.

7.1 - Introduction.

In this chapter, the results reported in the previous two chapters are evaluated and discussed. The chapter is split into two sections, each dealing with the results arising from both the Raman and infrared experiments reported in Chapters 5 and 6.

7.2 - Waveguide Raman Spectroscopy.

7.2.1 - Introduction.

Many of the results presented in Chapter 5 concentrate on actual Waveguide Raman spectra of polymeric films, and the assignments of the bands involved, and thus are discussed fully during the course of that chapter. In the following section, however, certain more unusual features arising from this study are considered more carefully, with a view to understanding the, at times, puzzling effects observed. Thus, this section is divided into three parts. The first considers the issue of the substrate peaks, with the second dealing with the apparent contradiction of the results of attempted diffusion experiments with those reported in the literature. Finally, concluding comments are made regarding both the achievements made in this aspect of the project, along with the apparent usefulness of the technique as a whole, based on the experiences of this project.

7.2.2 - Substrate Features.

There are several references in the literature to the observation of substrate features in waveguide Raman experiments. Two of these arose from some of the very first waveguiding experiments conducted by Levy et al.[1,2], in which broad features around 500 cm^{-1} are attributed to the substrate. Rabolt and Swalen[3] also indicate a Pyrex band in the at approximately 500 cm^{-1} in the difference spectra from the m=2 mode of a PVA/PMMA laminate, but do not mention it further. Levy and Dupeyrat[2], however, do discuss the appearance of the substrate band, but merely comment that it arises when penetration of the evanescent wave into the substrate is sufficient to give an 'easily detectable Raman signal'. Further work has concentrated on the complications arising from increased penetration of the evanescent tail into substrate materials during FT-Raman experiments[4-7]. This study considers increased Rayleigh scattering, but does not mention, or show any spectral evidence of Raman scattering.

At the outset of this project, and in the work carried out at Durham previous to this project[8], substrate bands were not observed. However, when the dipping procedure began to be used for film preparation purposes, peaks have been regularly observed, in certain systems which we have demonstrated as arising from the substrate (see Chapter 5, Figure 5.13). The substrate bands observed in this project, however, are notably different to those reported in the literature, in that the literature reports one broad band at approximately 500 cm^{-1}, whereas work described in Chapter 5 repeatedly produces 2 bands at approximately 800 cm^{-1} and 1000 cm^{-1}. All the experiments above were performed using quartz as the substrate, due to its lower refractive index properties, whereas Rabolt and Swalen[3] used Pyrex. The exact nature of the substrate used by

Levy et al[1,2] is not clear, but bearing in mind the similarity of the bands observed by them to those reported by Rabolt and Swalen, it is reasonable to assume that they also used Pyrex.

Single Film Systems.

Table 7.1 shows a comprehensive list of all the single film systems used in this project, and includes relevant electric field calculations for not only the polymer film, but also residual fields predicted in the substrate. It is assumed that most of the waveguiding streaks examined arose from the m=0 waveguiding mode, which is generally reported to be the most intense[3,7] and was hence usually examined in single film systems.

Table 7.1 - Electric Field Data for Single Film Systems

Polymer Examined	Film Thickness (μm)	Mode Angle (From normal)	% Ef‡ in Film	% Ef‡ in Substrate
PS	2.78	11.32°	99.87	0.13
PVAc	3.00	-3.73°	88.34	11.65
PVC	3.50	4.32°	99.90	0.09
PVA*	1.95	1.16° (m=1)	94.46	5.22
PMMA*	1.60	-1.00°	75.76	23.81
PVP	5.60	2.84°	99.90	0.04
PDMS†*	7.60	-1.65°	88.74	10.91

† - Phenylated PDMS.
* - indicates substrate peaks observed.
‡ - Electric Field.

Neither AF137 or Epikote[18] 1001 (see Chapter 5) could be analysed for electric field distribution, as the refractive index of AF137 remained unknown and the film of Epikote[18] 1001 was so thick that mode identification was impossible, an effect that is reported[3] to occur in very thick films.

In all three cases where substrate peaks were in evidence, the electric field calculation showed a significant evanescent wave tail into the substrate, which would produce significant Raman scattering, and hence satisfactorily explains the presence of such peaks. Also, in all but one case where such peaks are not observed, little penetration of evanescent wave into the substrate is theoretically predicted, which again is satisfactory.

However, one anomaly is observed, namely the poly(vinylacetate) system, where a significant penetration of evanescent wave into the substrate is predicted, but little, if any, evidence can be seen of such substrate peaks in the spectrum (see Figure 5.10, Chapter 5). Furthermore, only one waveguiding mode was observed for the system, which is consistent with the theoretical calculations, which also predict just the one mode. The most feasible explanation for this observation is that it could just be a simple case of experimental error, in that the film thickness might not have been determined accurately. This is reasonable, as this film was prepared by horizontal flow, and the thickness determined by passing the alpha step over a small section cut out of

the film, which was the early method of alpha-step analysis, and which did not indicate the non-uniformity of film thickness discovered through longer scans. Hence the accuracy of the film thickness determination would be unsafe.

Laminate Systems.

Of the three successful systems examined, only two were scanned fully. The PS/PVP system was never examined fully, as the region of interest occurred between 850 cm^{-1} and 1100 cm^{-1}, so it is difficult to state definitively whether or not substrate bands were seen in the spectrum. However, the other two systems were examined fully, and produced some very interesting results.

(A). Poly(vinyl alcohol) (PVA, n=1.52)/Polymethylmethacrylate (PMMA, n=1.4893).

All three of the systems discussed in Chapter 5 showed strong evidence of substrate peaks in every spectrum. The electric field data is displayed in Tables 7.2, 7.3 and 7.4 for each system separately.

Table 7.2 - System One; 0.575 μm PMMA under 2.205 μm PVA

Mode Number	Mode Angle from Normal	% Field in PMMA film	% Field in PVA film	% Field in Substrate
0	2.86°	1.37	98.65	0
2	-0.24°	27.16	72.69	0

Table 7.3 - System Two; 2.75 μm PMMA under 1 μm PVA

Mode Number	Mode Angle from Normal	% Field in PMMA film	% Field in PVA film	% Field in Substrate
1	-0.56°	86.56	12.43	0.41
2	-1.13°	72.39	24.69	1.75

Table 7.4 - System Three; 0.5 μm PMMA under 1.5 μm PVA

Mode Number	Mode Angle from Normal	% Field in PMMA film	% Field in PVA film	% Field in Substrate
0	2.5°	3.33	99.63	0
1	0.5°	19.91	79.95	0

The spectroscopic observations from System Two tie in with the theoretical predictions, as substrate bands are indeed observed. However, the other two systems are not so simple, with substrate bands observed, but not predicted theoretically. Furthermore, the spectra obtained seem to agree with these theoretical predictions, in as much as the fields do indeed seem largely concentrated within the top layer, and hence away from the substrate area. These are very puzzling observations.

The only plausible explanation is simply experimental error, arising from the non-uniformity of film thickness produced by the dipping procedure (discussed fully in Chapter 4). As explained above, all error evaluations used in this thesis arise from this non-uniform problem, and thus the calculations performed use a mean average of film

thickness, whereas the actual thickness is, in the main, very variable. Thus, such calculations can never be more than an educated estimate, and the true cause of these bands is the penetration of evanescent field into the substrate.

It would be a worthwhile exercise for future workers in waveguide Raman spectroscopy to repeat the above experiments, possibly using spin casting, which is reported as giving good uniformity of film thickness.

(B). Polystyrene/Poly(vinylalcohol).

Table 7.5 shows the electric field distribution in both polymers and the substrate.

Table 7.5

Mode Number m	Mode Angle (from Normal)	% Field in PS	% Field in PVA	% Field in Substrate
0	9.96	96.41	3.43	0
1	5.43	78.69	20.66	0
2	0.75	33.74	57.33	5.34
3	-2.52	27.48	57.85	13.01

This predicts that no substrate peaks should be visible in modes m=0 and m=1, but that they should be seen in modes m=2 and m=3. This is not the case, with substrate peaks being clearly evident in all four spectra. When the field is concentrated in the PS layer, the substrate peaks do decrease in intensity, which is probably an effect arising from the particularly high Raman scattering cross-section associated with PS. However, the substrate peaks are still clearly visible.

Again, it is not easy to explain this observation in any way, apart from suggesting experimental error, arising from the non-uniformity of films produced by the dipping procedure and hence the above calculation is also not accurate, and that penetration of the evanescent wave into the substrate does indeed occur.

It is evident from the literature that such substrate peaks have indeed been seen before, but this is the first time (also published[9]), to the best of my knowledge, that substrate peaks arising from a quartz substrate have been either reported or discussed fully. It is hoped that the above observations will form the basis for a future, more detailed work on these interesting features.

7.2.3 - Diffusion Experiments.

Waveguide Raman spectroscopy (WGRS), along with other integrated optical techniques, has been reported as being a useful tool for examining diffusion processes in polymeric materials[10-16]. Schlotter[15]describes a method which uses WGRS as a tool to monitor, in situ, by use of a liquid flow cell, the diffusion of a binary mixture of ethanol and perdeuterotoluene into polystyrene waveguides of thickness between 1-2 μm. Spectra are produced to verify the claim and show the diffusion of this mixture to be an unidentified non-Fickian process. Fell and Bohn[16] adopt a method by which analysis of film thickness and refractive index is used, followed by optical

modelling to determine the time dependence diffusion processes. This is reported as indicating that n-hexane diffuses into polystyrene films of thicknesses 1-7 μm via a Case II mechanism, but with a leading Fickian edge.

As mentioned towards the end of Chapter 5, all attempts made in the course of this project to study diffusion mechanisms by waveguide Raman Spectroscopy failed due to the waveguide streak disappearing when the diffusant entered the system. A variety of systems were examined, and the relevant data is presented in Table 7.8.

Table 7.8

Film	Diffusant	Film R.I.	Diffusant R.I.	Film Thickness
Epikote 1004	HMDI.*	1.581	Unknown	3.8 ± 0.6μm
Epikote 1004	MIBK‡	1.581	~1.38	~ 4μm
Epikote 1004	Acetone	1.581	~1.35	~ 4μm
Polystyrene	MIBK‡	1.583	~1.38	2.8 ± 0.1μm
Polystyrene	Acetone	1.583	~1.35	~ 3 μm
Polystyrene	Nitrate†	1.583	~1.33#	~ 3.3μm

* hexamethylenediisocyanate.
‡ methylisobutylketone.
† From an aqueous solution of potassium nitrate.
# Assumed to be similar to the refractive index of water.

As already stated, it was not possible to study any of these systems once the diffusant had been applied, as the waveguide streak faded completely.

However, in the course of this project, we have shown that it is possible spectrally to detect the presence of other materials in the film. The three spectra shown in Figure 5.15, Chapter 5, show evidence for residual toluene (the solvent used) in a film of polymethylmethacrylate (PMMA). The other two spectra show pure toluene and a PMMA film deposited from a xylene solution, which does not possess such solvent peaks. Such a system resembles one in which a diffusion process has occurred, with some of the diffusant remaining in the film. Hence we have proved that diffusion processes should, theoretically, be possible, in agreement with the observations cited in the literature.

The possible explanations for this effect, relate directly to the relative refractive indices of the polymer film and the diffusant. Before discussing these, however, it is worthwhile focusing on the actual diffusion process occurring.

As the diffusion process proceeds, the liquid diffusant infiltrates through the voids (ie. unoccupied areas) in the polymer matrix. Hence, there will be distinct areas within the matrix, namely the areas of polymer chain and areas of void filled with diffusant.

One of the most important criteria relating to successful waveguiding is that the medium in which waveguiding is to occur must be of a higher refractive index than both substrate and superstrate. If this criterion is not satisfied, then propagation will

not occur, as predicted by the relevant Fresnel coefficients (See Chapters 2 and 5, plus Reference 3), and waveguiding will not proceed. It is obvious from Table 7.8 above that all the known refractive indices of the diffusants used are well below the refractive index of quartz (1.457), and thus could not support a waveguide. This will obviously affect the waveguiding properties of the film in an adverse fashion[3], in that the voids occupied with diffusant will not satisfy this criterion for waveguiding. Thus a laser beam entering an area of polymer could theoretically begin waveguiding, but once the beam encounters an area of low refractive index diffusant, it should cease. Such negative results have been clearly demonstrated in the experiments conducted.

In the case of the residual toluene in the PMMA film, the refractive index of toluene is estimated[17] to be approximately 1.5, the higher refractive index, relative to those of the solvents discussed above, being undoubtedly due to the presence of the phenyl ring. In this case, as the diffusant refractive index is above that of the quartz, then waveguiding is able to proceed. It must, however, be noted at this juncture that the toluene peaks seen arise from residual solvent remaining from the deposition of the film.

Schlotter[15] uses a binary mixture of perdeuterotoluene and ethanol, and reports refractive indices for these as being 1.507 and 1.366 respectively. The binary mixtures used range from 2-12% perdeuterotoluene, so the combined refractive index of the mixture will be closer to 1.366. For waveguiding to occur, according to accepted theory[e.g. 3], this binary mixture should possess a higher refractive index than the substrate. In this publication, however, Schlotter makes the very curious remark that the solvents in the binary mixture are of a lower refractive index compared with the film, which is a necessary criterion for the maintenance of a guided wave in a polymer film. He makes no reference to any theoretical substantiation for this remark, and this is the first and only reference that I have encountered to this criterion.

A further puzzle is the solvent system under examination. Toluene is a well-known solvent for polystyrene, and Schlotter refers to this ability, and also states that he believes that the film does indeed eventually dissolve to some extent. Thus it is unclear whether the process studied is indeed diffusion or dissolution, despite the low levels of toluene used.

Spectra, however, are produced to substantiate his claims, and they do indeed show an increase in the ethanol band as time progresses, so it is evident that waveguiding can be used to examine diffusion, but it is curious why it was never possible to examine diffusion in the experiments conducted in this project. It would be worthwhile for future workers possibly to repeat Schlotter's work.

Thus, it is evident that waveguide Raman spectroscopy may be used to study diffusion processes, but, for successful experimentation, the refractive index of the diffusant must allow waveguiding to occur. To the best of my knowledge, the question of diffusant refractive index has never before been discussed in print, although it clearly must be recognised by other workers.

7.2.4 - Concluding Remarks.

Waveguide Raman Spectroscopy has useful theoretical potential, but the difficulties associated with getting good, reliable information from the technique are immense. Throughout this project, although some good results were obtained, a great deal of time and energy was expended on attempting feats which, at present levels of film preparation and Raman detection limits, were not possible. There are many laminate systems which theoretically would provide excellent chances of detecting interfacial interaction, but which simply cannot be prepared due to solvent difficulties. Such problems underline the frustration that can result from this technique.

It has been stated in previous studies[3] that interfacial analysis using this technique is at least feasible, but the difficulties associated with concentrating the electric field over an area, quite often less than one percent of the total area, is to say the least difficult. However, Rabolt and Swalen[3], provide corroborating spectral evidence, and although noise levels are high in the subtracted spectra (as would be expected), there is clear evidence of new features. I believe that they were fortunate indeed; obtaining such evidence appears very difficult and was not once observed in this project.

We have also proved that certain conditions for successful waveguiding are not quite as rigorous as originally stated. Rabolt and Swalen[3] also report this, in relation to film thickness uniformity. We have demonstrated that all films prepared using the dipping procedure, which accounts for at least two thirds of those studied here, are not of uniform thickness, and contain a prominent slope from one end of the film to the other. In some cases, this caused a thickness difference of well over a micron, and yet the system managed to support a waveguide. As stated earlier, this has quite far-reaching implications toward a complete re-working of the present theoretical basis to waveguiding, but this is outside the scope of this project.

To conclude, a number of previously unreported waveguide Raman spectra have been seen during the course of this project, along with the observation and explanation of seemigly new substrate bands. Speculations on how diffusion processes can be followed using waveguide Raman spectroscopy have been made, and hopefully future workers will be able to confirm or refute these suggestions. Also demonstrated here has been how different solvents affect film quality, and thus waveguiding properties all but one (spin coating) of the readily available film preparation methods have been evaluated. Finally, it has been clearly demonstrated, in agreement with other workers observations[3], that uniformity of film thickness in waveguiding systems is not a rigorous demand, and that certain systems which do not produce smooth, uniform films may be able to be examined using this technique.

7.3 - Fourier Transform Infrared Attenuated Total Reflection Spectroscopy.

7.3.1 - Introduction.

Unlike the work carried out using waveguide Raman spectroscopy which is a description of simply how the technique was utilised to obtain spectra of polymeric films, the work carried out using FT-IR ATR spectroscopy is rather more an expression of the application of a spectroscopic technique to the evaluation of chemical processes occurring within thin films. Important spectral assignments are dealt with adequately in Chapter 6. This section is split into three subsections. The first tentatively examines the small amount of diffusion data obtained from the penetration of the monomeric isocyanate (hexamethylenediisocyanate, HMDI) into good-quality films of Epikotes[7] 1001 and 828. Other diffusion processes are not considered in any detail, as the data produced was not reproducible and is thus somewhat tenuous, and has been included merely to identify the process that led to the examination of monomer diffusion. The second subsection considers the actual reaction process occurring in the film, along with a speculation as to the actual kinetics, and the third considers the important results which have emerged from this study, regarding film quality and adhesion.

However, before we concentrate on the actual numerical data, it is worth reiterating the difficulties associated with the systems examined. As with most industrially funded work, problems of interest to the sponsors tend to involve actual industrial systems, which, by their very nature, tend to be somewhat complex. The systems studied here are no exception, and hence before examining the science produced from these systems, it is worth defining exactly what we have been studying and listing the associated complexities.

1/. Films of industrial grade epoxy resins are treated with an isocyanate, which diffuses into the polymer matrix.

2/. This diffusion appears to be affected by i). polymer structure, ii). solvent system used and iii). time of cure.

3/. The diffusing isocyanate, once inside the polymer, is capable of two types of reaction, namely i). with hydroxyl groups to form a urethane, and ii). with amine groups to form a urea.

4/. The combination of the reactions and diffusion produces a distorted view of both processes, i.e. the diffusion process does not reach its full extent, due to the reaction removing some of the penetrant; the reaction beginning earlier than that indicated from the spectral results, but is distorted by more isocyanate diffusing into the system.

These four brief points indicate the complexity of the system involved, and must be taken into account during the following discussion, when they will be iterated and expanded on where necessary. Thus this section is necessarily based equally on speculation and experimental observation.

7.3.2 - Diffusion Data.

The diffusion data presented in this thesis is calculated using the spectral intensity of the isocyanate band at 2260 cm^{-1}, until the intensity reaches a plateau, in the graph of time vs. intensity. Clearly, this plateau will be lower than what would be achieved if no reaction occurred, and thus the data, and comments relating to it, cannot be fully quantitative.

Furthermore, with so little experimental data, it is very difficult to be accurately quantitative about this process, and until more work is carried out, comments must be limited to speculations, based on the acquired data, and curves shown in Chapter 6. The reason so little data is reported was simply due to the discovery of this interesting process, in the final stages of the experimental work, which allowed only a very restricted study. However, this is believed to be the first time that this particular diffusion process has been studied.

Table 7.9 shows all the diffusion data obtained from experiments described in Chapter 6.

Table 7.9 - Summary of Diffusion Data Obtained

			Fickian	Case II		
Resin	CureTime (Hours)	Thickness (μm)	D $cm^2\ sec^{-1}$	D_1 $cm^2\ sec^{-1}$	D_2 $cm^2\ sec^{-1}$	x_A
1001	24	5.4	$2.76x10^{-10}$	$2.61x10^{-10}$	$2.05x10^{-10}$	0.99
1001	48	4	$8.59x10^{-11}$	$1.01x10^{-9}$	$5.18x10^{-11}$	0.24
1001	48	4	$8.27x10^{-11}$	$2.23x10^{-10}$	$2.69x10^{-11}$	0.51
1001	72	5	$8.47x10^{-11}$	$1.18x10^{-10}$	$1.3x10^{-11}$	0.8
828	24	2.4	$3.28x10^{-9}$	$1.07x10^{-10}$	$5.51x10^{-12}$	0.58
828	24	5	$7.08x10^{-11}$	$2.01x10^{-10}$	$7.92x10^{-12}$	0.54
828	24	3.5	$9.09x10^{-11}$	$8.65x10^{-11}$	$8.08x10^{-11}$	0.99
828	48	5.4	$2.91x10^{-9}$	$8.90x10^{-11}$	$2.12x10^{-11}$	0.63
828	48	2	$1.99x10^{-10}$	$7.39x10^{-12}$	$1.94x10^{-12}$	0.12

The X_A term is explained in Chapter Six, page 107.

In the literature[19-32] examined, there is some disagreement on the actual diffusion mechanism, although there appears to be a consensus towards a non-Fickian process, with chemical structure, degree of crosslinking, temperature increase and the inclusion of halogens into the epoxy structure all being reported as influencing the actual process.

If the diffusion curves obtained in this study are examined, it is evident that most of the data fits the Case II model more accurately than the Fickian. This can be seen if Figures 6.30, 6.31, 6.33, 6.36, 6.39 and 6.40, given in Chapter 6, are examined. Some of the curves on these diagrams appear to be similar, but close examination reveals the experimental curve follows the Case II curve more closely than it does the Fickian curve. Thus, from the small amount of evidence obtained, it seems we can reasonably

assume that the diffusion of HMDI into epoxy resins appears to be non-Fickian, which is in agreement with the literature. There are exceptions to this rule, seen in Figures 6.29 and 6.35. In these, the two curves are exceptionally similar and cannot be clearly differentiated. This is thought to be due to experimental error, arising from both the complexities of this rather difficult system, discussed at various points in this thesis, plus a simple lack of data.

Having determined that the process appears to be non-Fickian, and if we assume the process is Case II the values given in Table 9 can be examined, to see which of the two processes associated with the Case II diffusion is predominant. Thus the X_A term is examined, as discussed above, and the value considered with the chemistry of the films in mind.

There is a considerable lack of consistency with many of the values calulated here. Very tentatively, the data appears to suggest that diffusion into the 24 hour cured resin appears to be dominated by the initial pseudo-Fickian process, whereas diffusion into the 48 hour cured resin, appears to be dominated by the slower, non-Fickian process. This is actually reasonable. As the cure time increases, a higher proportion of the resin will be crosslinked, and hence the polymer matrix will be a tighter, less accessible system with regards to penetrants. The data obtained for the 72 hour resin, however, appears to contradict this hypothesis, but as only one data point is available, until further work is carried out, it is possible to explain this by simple experimental error. There are, however, two further contradictions to this proposal in the data available for 48 hour cured resins, namely two values of X_A which are greater than 0.5. In the case of 48 hour cured Epikote[18] 1001, the value calculated is 0.51, which is only marginally over 0.5 and hence can be accounted for as being well within the bounds of experimental error. However, the value of 0.63, calculated for the 48 hour cured Epikote[18] 828, is not so easy to explain in this manner, especially as it is very far removed from the other value of 0.12.

It is believed this is the first time that the diffusion of HMDI in epoxy resin systems has been observed, and from the tentative experimental exercise carried out above, it is believed that this is a non-Fickian process, which appears to be affected by the length of cure time of the resin. However, this study gives only a semi-quantitative indication of the process parameters, and until more work is carried out it shall remain so.

7.3.3 - Kinetic Data and the Effect of Reaction on Film Adhesion.

Table 7.10 shows a summary of the reaction rate data produced in Chapter 6, which fits the data produced for the consumption of the isocyanate band to a first order rate law. To the best of my knowledge, this is the first time that the reaction of hexamethylenediisocyanate with an amine cured epoxy resin has been observed by FT-IR ATR spectroscopy.

Table 7.10 - Summary of Kinetic Information

Resin	*Cure Time*	*Rate Constant (sec^{-1})*
Epikote[7] 828	24 Hours	1.31×10^{-5}
Epikote[7] 828	48 Hours	1.82×10^{-5}
Epikote[7] 1001	24 Hours	2.11×10^{-5}
Epikote[7] 1001	48 Hours	1.25×10^{-5}

From the data in this table, we can write an apparent rate law for the consumption of the isocyanate by the reactions which occur in the film:-

$$-d[NCO]/dt = k[NCO]^1 \quad (1)$$

where $k = 1.62 \times 10^{-5} \pm 0.43 \times 10^{-5}$ sec^{-1}.

The complications which have made the kinetic analysis of the data so difficult have been adequately dealt with in the salient part of Chapter 6, and it is worthless repeating them here. However, one important consequence of this reaction is that the epoxy resin film is observed to adhere more strongly to the substrate. It is proposed that this important observation be discussed here, as the meaning of the kinetic data presented has been adequately described by expression (1) above.

The question of adhesion between polymer layers, and indeed between polymer layers and substrates, is of crucial importance to the success of paint systems. If good adhesion is not achieved at any level within the laminates, which form many paint systems, then simply the system fails and the paint peels. It is inevitable that paint systems will eventually fail, and this is an accepted fact of life. Premature failure of such systems is, however, obviously undesirable. Hence, a detailed understanding of adhesion processes, along with possibilities of enhancement of such adhesion characteristics, is of crucial importance to continuing success in maintaining or improving both the performance of paints and the competitive edge in the market place.

The enhanced adhesion of the epoxy resin film, following treatment with hexamethylene diisocyanate, to a metallic substrate has not, to the best of my knowledge, been observed before. The literature reported on the subject is considerable, dealing mostly with adhesion to carbon fibres and other organic films, but some is available regarding adhesion to metal[34-44]. Schmidt and Bell[40] mention methods used to increase the durability of metal/epoxy species, but concentrate on silane compounds. No mention, to the best of my knowledge, is made in the literature of the enhancement of adhesion brought about by isocyanate reaction within the film, although Kamon and Furukawa[45] describe the actual curing of epoxy resins by diisocyanates, reporting the formation of trimeric isocyanate bridges of identical form to the trimeric isocyanate used in this project. It is reported[45] that resins cured in this way are highly heat-resistant.

The specific adhesion enhancement reported here is not of substantial use to Courtaulds, as the isocyanate involved is of a highly toxic nature. However, the fact

that this has been observed opens the way to future work, to investigate the possibility of producing another reagent which imparts the same enhancements to the film. In addition, if a treated film exhibits a considerable enhancement in adhesion to a metallic substrate, will it adhere in a similar enhanced fashion to other layers? If so, this observation could have immense, far-reaching importance.

The exact mechanism of the enhanced adhesion is obviously due to increased interaction between the film and the substrate. In an untreated crosslinked epoxy resin, the only group which enable significant interaction with the substrate is the hydroxyl group. However, after such a film is penetrated with the isocyanate, such groups react to form both urea and urethane amide groups. Furthermore, it is feasible with the di-isocyanate penetrant that one isocyanate group on a molecule will react, but the other may not, thus offering the highly interactive isocyanate group for possible further interaction, if it is in the vicinity of the substrate. Thus the interactive capabilities of the treated film are increased significantly and hence it adheres much more firmly to the substrate.

Clearly, further work is required to quantify the extent and potential of this effect and this will be discussed in the section on future work below.

7.3.4 - Epoxy Resin Film Quality.

In this project we have defined a very important parameter, i.e. the issue of the quality of epoxy resin film. It has been shown that this is directly influenced by both solvent blend and solvent quality. Table 7.11 summarises this important matter, although the parameter of solvent quality in an industrial environment appears to be in such a state of flux that, in that category, observations are probably no more than a generalisation. Certainly, in the case of the blend of 1 part n-butanol to 1 part xylene, although the table suggests that Poor Quality Films result, this was sometimes not the case, with good films being produced from industrial solvents.

Table 7.11

	Industrial Grade Solvents		Analar Grade Solvents	
Solvent Blend	Epikote 1001	Epikote 828	Epikote 1001	Epikote 828
2B:2X:1M	Good	Good	Good	Good
1B:1X	Poor	Poor	Poor	Poor
X	Won't dissolve	Won't dissolve	Won't dissolve	Won't dissolve
B	Won't dissolve	Won't dissolve	Won't dissolve	Won't dissolve
2B:2X:>1M	Medium	Medium	Medium	Medium
2B:2X:1Mes	Poor	Poor	Poor	Poor

Key to Table.

B = n-butanol; X = xylene; M = methanol; Mes = Mesitylene (Shellsol).

References.

1/. Y.Levy, C.Imbert, J.Cipriani, S.Racine & R.Dupeyrat, Opt.Commun., 11, (1974), 66.
2/. Y.Levy & R.Dupeyrat, J.Physique, Coll.C5, 38, (1975), 253.
3/. J.F.Rabolt & J.D.Swalen, "Spectroscopy of Surfaces", Eds. R.J.H.Clark and R.E.Hester, J.Wiley and Sons, London, 1988, Chapter 1.
4/. C.G.Zimba, V.M.Hallmark, J.F.Rabolt & J.D.Swalen, Thin Solid Films, 160, (1988), 311.
5/. C.G.Zimba, V.M.Hallmark, S.Turrel, J.D.Swalen & J.F.Rabolt, J.Phys.Chem., 94, (1990), 939.
6/. C.G.Zimba & J.F.Rabolt, Thin Solid Films, 206, 1-2, (1991), 388-393.
7/. J.F.Rabolt, IBM Res.Journal, RJ 8476 (76697), (1991).
8/. N.M.Dixon, N.Everall & J.Yarwood, Unpublished work.
9/. J.K.F.Tait, N.M.Dixon, N.Everall, G.Davies, R.McIntyre & J.Yarwood, J.Raman.Spec., 24, (1993), 511-518.
10/. A.S.Michaels, H.J.Bixler & H.B.Hopfenberg, J.App.Polym.Sci., 12, (1968), 991.
11/. D.R.Miller, O.H.Han & P.W.Bohn, Appl.Spectrosc., 41, (1987), 245.
12/. D.R.Miller, O.H.Han & P.W.Bohn, Appl.Spectrosc., 41, (1987), 249.
13/. P.W.Bohn & N.F.Fell, Chemical, Biochemical & Environmental Applications of Fibres, S.P.I.E., 990, Society of Photo-Optical Instrumentation Engineers, Bellingham, Washington, (1988), 130.
14/. D.R.Miller & P.W.Bohn, Anal.Chem., 60, (1988), 407.
15/. N.E.Schlotter, J.Phys.Chem., 94, (1990), 1692.
16/. N.F.Fell, Jr & P.W.Bohn, Appl.Spectrosc., 45, 7, (1991), 1085.
17/. Chemistry Data Book, Eds. J.G.Stark and H.G.Wallace, 2nd Edition, 1982.
18/. Shell brand-name.
19/. Y.Diamant, G.Marom & L.J.Broutman, J.App.Polym.Sci., 26, 9, (1981), 3015.
20/. T.C.Wong & L.J.Broutman, Plastics Engineering, 39, 3 (1983), 52.
21/. T.S.Ellis & F.E.Karasz, Abs.Paps.Am.Chem.Soc., 185, Mar, (1983), 154.
22/. M.T.Aronhime, J.K.Gillhan & R.D.Small, Abs.Paps.Am.Chem.Soc., 186, Aug, (1983), 127.
23/. M.A.Grayson & C.J.Wolf, Abs.Paps.Am.Chem.Soc., 187, Apr, (1984), 34.
24/. J.A.Barrie, P.S.Sagoo & P.Johncock, J.Memb.Sci., 18, Mar, (1984), 197.
25/. T.C.Wong & L.J.Broutman, Polym.Eng.& Sci., 25, 9, (1985), 529.
26/. J.A.Barrie, P.S.Sagoo & P.Johncock, Polymer, 26, Aug, (1985), 1167.
27/. T.C.Wong & L.J.Broutman, Polym.Eng & Sci., 25, 9, (1985), 521.
28/. A.Tson & N.A.Peppas, Abs.Paps.Am.Chem.Soc., 195, June, (1988), 212.
29/. M.C.Lee & N.A.Peppas, Abs.Paps.Am.Chem.Soc., 199, Apr, (1990), 54.
30/. T.K.Kwei & H.M.Zupko, J.Polym.Sci., Part A-2, 7, (1969), 867.
31/. H.L.Firsch, J.Polym.Sci., Part A-2, 7, (1969), 879.
32/. J.J.Sahlin & N.A.Peppas, Ind. & Eng.Chem.Res., 30, 1, (1991), 211.
33/. M.R.Pierra, University of Durham Internal Report, 1993.
34/. A.Coury, A.Jevne & P.Cahalan, J.Electrochem.Soc., 128, 3, (1981).
35/. J.M.Park & J.P.Bell, J.Electrochem.Soc., 128, 3, (1981).
36/. A.J.Denicola & J.P.Bell, Abs.Paps.Am.Chem.Soc., 183, Mar, (1982), 104.
37/. A.J.Denicola & J.P.Bell, ACS Symposium Series, 221, (1983), 119.
38/. J.F.Watts & J.E.Castle, J.Mat.Sci., 19, 4, (1984), 2259.
39/. P.J.Hine, S.Elmuddarris & D.E.Packham, J.Adhes., 17, 3, (1984), 207.
40/. R.G.Schmidt & J.P.Bell, Adv.Polym.Sci., 75, (1986), 33.
41/. D.P.Sheih & J.L.Massingill, J.Coat.Tech., 59, 752, (1987), 42.
42/. R.G.Schmidt & J.P.Bell, J.Adhes., 25, 2, (1988), 85.
43/. R.G.Schmidt & J.P.Bell, J.Adhes., 27, 3, (1989), 135.
44/. P.S.Shieh & J.L.Massingill, J.Coat.Tech., 62, 781, (1990), 25.
45/. T.Kamon & H.Furukawa, Adv.Polym.Sci., 80, (1986), 173.

Achievements reported in this thesis.

To the best of my knowledge, the following achievements have been reported for the first time in this thesis.

(A) - Raman Spectroscopic Work.

Reports of the first known waveguide Raman spectra of polyvinyl chloride, phenylated polydimethylsiloxane, Epikotes[18] 1001 & 1004, and AF137.

The first report of the conventional Raman spectrum of the trimeric isocyanate, CCA315.

Reports of the first known FT-Raman spectra of the epoxy resin crosslinking agents KH92 & Cardanol. It has also been reported that the cis-trans ratio associated with the pentadec-8-enyl, present in the cardanol polymeric system, appears to be cis:trans, 1:4. The FT-Raman spectrum of Rosin amine D is also presented, although the spectrum and the reported structure do not correlate.

The first observation via waveguide Raman spectroscopy of the two broad features attributed to quartz, the first report of a total internal reflection (TIR) spectrum of quartz, and the first comprehensive examination and explanation of this phenomenon.

The first tentative explanation of the difficulties associated with attempts to study diffusion processes using waveguide Raman spectroscopy.

(B) - Infrared Spectroscopic Work.

It is believed that, apart from the presented spectra of pure epoxy resins and hexamethylenediisocyanate, all the FT-IR ATR spectroscopic studies carried out in this section have been reported for the first time in this thesis.

The first report of FT-IR ATR spectroscopically observed interfacial interactions between the solvent-based acrylic and an epoxy resin, and between an alkyd resin and an epoxy resin.

The first FT-IR ATR spectroscopic report of the diffusion process of the trimeric isocyanate, CCA315 into epoxy resin films, and the subsequent reaction within those films with both hydroxyl and amine groups both at room temperature and at elevated temperature.

The first FT-IR ATR spectroscopic report of the diffusion of hexamethylenediisocyanate into films of epoxy resins, along with the first tentative evaluation of the diffusion parameters associated with this process.

The first FT-IR ATR spectroscopic report of the reaction of hexamethylenediisocyanate with the hydroxyl and amine groups present within the film, along with the first tentative evaluation of part of the kinetics associated with this system.

(C) - Miscellaneous.

The first report of the increased adhesion of the epoxy resin layer to both ATR crystal and mild steel substrates, following the reaction of hexamethylene diisocyanate within the film.

The first report of the role of solvent on produced film qualities of epoxy resins, along with the first definition of poor and good quality films plus the first SEM pictures of the two different types of film.

Future Work Suggestions.

(A) - Waveguide Raman Spectroscopy.

With the current considerable interest in this technique, there is no shortage of research workers who are keen to grapple with the associated difficulties. It would be a worthwhile exercise to pursue the work conducted using laminates, and to examine a wide range of structures which have the potential for interfacial activity. The solvent problem is the major difficulty, as this limits the possibilities considerably, but future work should also be conducted on the possibilities of constructing laminates for waveguide experiments via other methods, such as pressing and casting from the melt. Another area which would be interesting to pursue would be further work on diffusion into waveguiding systems, in order fully to establish the refractive index relationship required. This could be a potentially very useful application of the technique, if the difficulties could be overcome. The area of FT-waveguide Raman is one in which first tentative steps have been taken, and the difficulties associated with near infrared excitation are considerable. However, in relation to the systems we have attempted to study, further work in this area would be useful, as it could remove the fluorescence problem. Also, attempts could be made to use dye lasers also to combat the fluorescence problems.

(B) FT-IR Work.

It would be very interesting to pursue all the work described in the FT-IR section of this thesis, especially the barrier-film experiments and the diffusion of isocyanates into epoxy films, and the subsequent reaction. The problems of water vapour contamination, which introduced difficulties in evaluating the kinetics, could be overcome by using a TGS uncooled detector and a very dry sampling environment. This should allow the urethane band to be evaluated fully, and possibly also allow the hydroxyl and amine bands associated with the epoxy resin to be examined. For the diffusion process to be understood fully, the diffusion experiments need to be repeated and increased in number considerably. It may also be useful to examine the diffusion of other materials into such systems.

(C) Other Work.

The issue of increased adhesion of the epoxy film to metallic substrates is one which could be followed up, with actual measurements of the adhesion, along with a search for other less toxic materials which could replace the HMDI. Further work would also be useful into the question of the role of solvent in quality of film produced. It would be interesting to compare the adhesion of other materials to good- and poor-quality films, to see if there is any notable difference.

Appendices

Appendix I - Structures of Polymeric Materials.

This appendix lists the structures of the simple polymers described during the course of this thesis.

1/. Polystyrene.

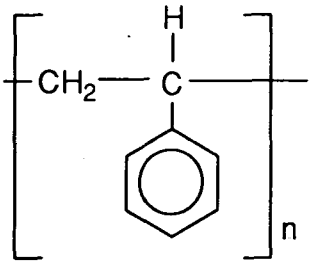

2/. Poly (vinylacetate).

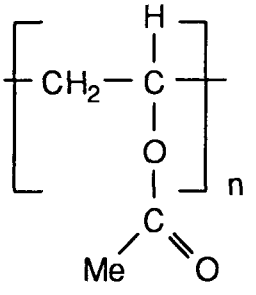

3/. Poly (vinylchloride).

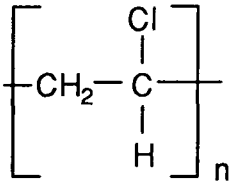

4/. Poly (vinylalcohol).

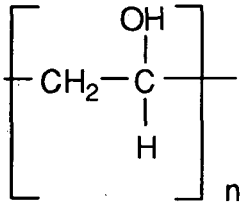

5/. Polymethylmethacrylate.

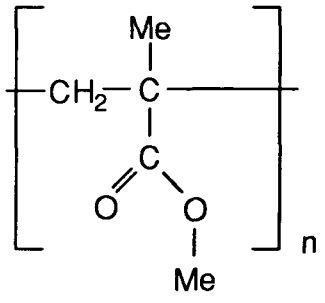

6/. Poly (vinylpyrrolidone).

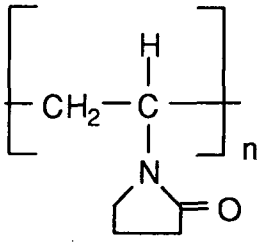

7/. Polyethylene.

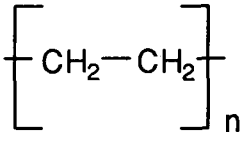

8/. Polyethylmethacrylate.

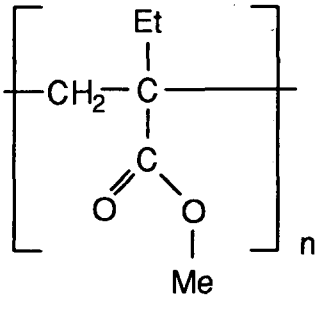

All other polymeric systems discussed in this thesis, are either of unknown structure, eg. the acrylics used in Chapter 5, or the structures are described at another point during this thesis, eg. the Epoxy resins used.

Appendix II - Colloquia, Lectures and Seminars given by Invited Speakers, Attended by the Author.

1/. 1990.

7-XI-1990; Dr. D. Gerrard (British Petroleum); 'Raman Spectroscopy for Industrial Analysis'.

8-XI-1990; Dr. S. K. Scott (Leeds University); 'Clocks, Oscillations and Chaos'; DUCS lecture.

14-XI-1990; Prof. T. Bell (SUNY, Stony Brook, U.S.A.); 'Functional Molecular Architecture and Molecular Recognition'.

28-XI-1990; Dr. B. J. Whittaker (Leeds University); 'Two-Dimensional Velocity Imaging of State-Selected Reaction Products'.

2/. 1991.

15-I-1991; Prof. B. J. Alder (Lawrence Livermore Labs., California); The Boys-Rahman Lecture: 'Hydrogen in all its Glory'.

17-I-1991; Dr. P. Sarre (Nottingham University); 'Comet Chemistry'; DUCS lecture.

23-I-1991; Prof. J. Higgins; 'Rheology and Molecular Structure of Ionomer Solutions'.

24-I-1991; Dr. P. J. Saddler (Birkbeck College, London); 'Design of Inorganic Drugs: Precious Metals, Hypertension and H.I.V.'. DUCS lecture.

30-I-1991; Prof. E. Sinn (Hull University); 'Coupling of Little Electrons in Big Molecules, Implications for the Active Sites of (Metalloproteins and other) Macromolecules'.

6-II-1991; Dr. R. Bushby (Leeds University); 'Biradicals and Organic Magnets'.

20-II-1991; Prof. B. L. Shaw (Leeds University); 'Synthesis with Coordinated, Unsaturated Phosphine Ligands'.

6-III-1991; Dr. C. M. Dobson (Oxford University); 'N.M.R. Studies of Dynamics in Molecular Crystals'.

The following 10 lectures we given as part of an International Polymer Science Conference, held at Durham University.

22-VII-1991; Prof. D. L. Allara; 'Vibrational Spectroscopy of Polymer Surfaces'.

22-VII-1991; Prof. C. J. van-Oss; 'Acid/Base Effects at Polymer Interfaces'.

22-VII-1991; Dr. M. J. Miles; 'S.T.M. of Polymers at Surfaces'.

23-VII-1991; Prof. D. Phillips; 'Time Resolved Evanescent Wave Induced Fluorescence Spectroscopy as a Probe of Polymer Surfaces'.

23-VII-1991; Dr. M. Stamm; 'Charecterisation of Polymer Surfaces by Reflectivity and Interference Techniques'.

23-VII-1991; Prof. R. J. Young; 'Polymer Surface and Interface Charecterisation using Raman Microscopy'.

23-VII-1991; Prof. J. C. Earnshaw; 'Laser Light Scattering from Polymer Thin Films'.

24-VII-1991; Dr. M. C. Davies; 'Aspects of the Surface Chemistry of Bio-materials'.

25-VII-1991; Dr. M. C. Cater; 'Theoretical Aspects of Polymers Attached to Surfaces'.

25-VII-1991; Prof. P. A. Pincus; 'Polymer Surfaces and Interfaces - Their Relevence and Importance'.

31-X-1991; Dr. R. Keeley (Metropolitan Police Forensic Science Unit); 'Modern Forensic Science'. DUCS lecture.

6-XI-1991; Prof. B. F. G. Johnson (Edinburgh University) 'Cluster - Surface Analogues'.

20-XI-1991; Dr. R. More O'Ferrall (University College, Dublin); 'Some Acid-Catalysed Rearrangements in Organic Chemistry'.

28-XI-1991; Prof. I. M. Ward (IRC in Polymer Science, University of Leeds); The S.C.I. Lecture: 'The Science and Technology of Orientated Polymers'

6-XII-1991; Prof. R. G. Snyder; 'Microphase Seperation in Crystalline Binary n-Alkane Solutions'.

11-XII-1991; Dr. W. D. Cooper (Shell Research); Colloid Science: Theory and Practise'.

1992.

22-I-1992; Dr. K. D. M. Harris (St. Andrews University); 'Understanding the Properties of Solid Inclusion Compounds'.

12-II-1992; Dr. D. E. Fenton (Sheffield University); 'Polynuclear Complexes of Molecular Clefts as Models for Copper Biosites'.

26-II-1992; Dr. M. L. Hitchman (Strathclyde University); 'Chemical Vapour Deposition'.
11-III-1992; Dr. S. E. Thomas (Imperial College, London); 'Recent Advances in Organoiron Chemistry'

Thirteenth International Conference on Raman Spectroscopy; Wurzburg, Bavaria; September 1992. Numerous lectures and seminars attended.

15-X-1992; Dr. M. Glazer & Dr. S. Tarling (Oxford University and Birkbeck College, London); 'It Pays to be British ! - The Chemist's Role as an Expert Witness in Patent Litigation'. DUCS lecture.

22-X-1992; Prof. A. Davies (University College, London); The Ingold-Albert Lecture: 'The Behaviour of Hydrogen as a Pseudometal'

18-XI-1992; Dr. R. Nix (Queen Mary College, London); 'Characterisation of Heterogeneous Catalysts'.

9-XII-1992; Dr. A. N. Burgess (ICI Runcorn); 'The Structure of Perfuorinated Ionomer Membranes'.

1993.

20-I-1993; Dr. D. C. Clary (University of Cambridge); 'Energy Flow in Chemical Reactions'.

10-II-1993; Dr. D. Gillies (University of Surrey); 'N.M.R. and Molecular Motion in Solution'.

24-II-1993; Prof. C. J. M. Stirling (University of Sheffield); 'Chemistry on the Flat- Reactivity of Ordered Systems'.

13-V-1993; Prof. J. A. Pople (Carnegie - Mellon University, Pittsburgh, U.S.A.); The Boys - Rahman Lecture: 'Applications of Molecular Orbital Theory'.

17-VI-1993; Prof. O. F. Nielson (H. C. Ørsted Institute, University of Copenhagen); 'Low - Frequency IR and Raman Studies of Hydrogen Bonded Liquids'.

Appendix III - Publications, Posters and Seminars Resulting from the Studies Described in this Thesis.

(A). Posters and Seminars.

June 1991; Seminar given to the Infrared and Raman Group, University of Durham Chemistry Department, entitled 'Waveguide Raman Spectroscopy of Thin Polymer Films and Interfaces'.

September 1991; Poster Presented to an Internal Conference of the IRC in Polymer Science (Bradford, Durham and Leeds), entitled 'Waveguide Raman Spectroscopy of Thin Polymer Films and Interfaces'.

December 1991; Seminar given to the Surface Spectroscopy Unit of Courtaulds Coatings, plc, at Felling, Gateshead, entitled 'Waveguide Raman Spectroscopy of Thin Polymer Films and Interfaces.

December 1991; Poster Presented at the Department of Chemistry, University of Durham Internal ICI Poster Competition, entitled 'Waveguide Raman Spectroscopy of Thin Polymer Films and Interfaces'. This Poster was awarded Third Prize in the Competition.

May 1992; Seminar given to the Infrared and Raman Group, University of Durham Chemistry Department, entitled 'ATR Infrared and Waveguide Raman Studies of Thin Polymer Films'.

September 1992; Prize Winning Poster Presented at The Thirteenth International Conference on Raman Spectroscopy, Wurzburg, Bavaria, entitled 'Waveguide Raman Spectroscopy of Thin Polymer Films and Interfaces'.

May 1993; Seminar given to the Infrared and Raman Group, University of Durham Chemistry Department, entitled 'ATR Infrared Spectroscopy of Diffusion Processes in Thin Polymer Films'.

June 1993; Seminar given to the Department of Chemistry, University of Durham, entitled 'ATR Infrared and Waveguide Raman Spectroscopy of Thin Polymer Films'.

(B). Publications.

'Waveguide Raman Spectroscopy of Thin Polymer Films and Interfaces', G.Davies, N.M.Dixon, N.Everall, R.M^{c}Intyre, J.K.F.Tait & J.Yarwood, ICORS'92 Conference Proceedings, Page 632.

'Waveguide Raman Spectroscopy of Polymers and Polymer Laminates'; Jonathan K.F.Tait, N.Michael Dixon, Neil Everall, Gerald Davies, Robert M^{c}Intyre and Jack Yarwood; Journal of Raman Spectroscopy, **24**, (1993), 511-518.